National Library
of Canada

Bibliothèque nationale
du Canada

Canadian Theses Service

Service des thèses canadiennes

Ottawa, Canada
K1A 0N4

NOTICE

The quality of this microform is heavily dependent upon the quality of the original thesis submitted for microfilming. Every effort has been made to ensure the highest quality of reproduction possible.

If pages are missing, contact the university which granted the degree.

Some pages may have indistinct print especially if the original pages were typed with a poor typewriter ribbon or if the university sent us an inferior photocopy.

Reproduction in full or in part of this microform is governed by the Canadian Copyright Act, R.S.C. 1970, c. C-30, and subsequent amendments.

AVIS

La qualité de cette microforme dépend grandement de la qualité de la thèse soumise au microfilmage. Nous avons tout fait pour assurer une qualité supérieure de reproduction.

S'il manque des pages, veuillez communiquer avec l'université qui a conféré le grade.

La qualité d'impression de certaines pages peut laisser à désirer, surtout si les pages originales ont été dactylographiées à l'aide d'un ruban usé ou si l'université nous a fait parvenir une photocopie de qualité inférieure.

La reproduction, même partielle, de cette microforme est soumise à la Loi canadienne sur le droit d'auteur, SRC 1970, c. C-30, et ses amendements subséquents.

NL-339 (r. 88/04) c

Canada

CONCRETE
SPILLWAY-EARTHFILL
INTERFACE FOR LARGE DAMS

A Parametric Study on Soil-Structure Interaction

RICHARD D. LALONDE

A thesis
Submitted under the supervision of
Dr. Vinod K. Garga
Associate Professor

in partial fulfillment
of the requirements for the degree of
Master of Applied Science

Department of Civil Engineering
Faculty of Engineering
University of Ottawa

ISBN 0-315-68110-1

Dedication

This degree is dedicated to Arthur and Doris. This work has only been possible due to their love, understanding and patient support. To them my love.

Acknowledgements

The author wishes to thank the Natural Sciences and Engineering Research Council for financial assistance to Professor Garga, through which this study was made possible.

Thanks is owed to Professor M. J. Duncan of Virginia Polytechnical Institute for providing the SSTIPN finite element program.

Special thanks are also due to my colleagues and friends whose valuable advice have contributed to the work presented here. I would like to thank some of them individually.

To H. Hachem who spent endless hours helping me organize and apply my thoughts in a creative fashion. His 'What If...' approach has focused my mixed ideas into logical patterns.

To Tiziano Mastrangelo, P.Eng, whose down-to-earth perspective and initiative I find quite motivating. His friendship is unforgettable and indestructible.

To L. Newton, her loyal support and belief in me has made this all worthwhile. She is truly my sunshine. To Lise ...

Summary

Ever since earth dams have been constructed, engineers are faced with the problems of interfaces within or adjacent to the impervious core material.

The design approach to these interfaces are based on engineering judgement and empirical procedures of which their implementation is largely left to the discretion of the site engineers.

Although the design of such interfaces is important to the safety of the dam, very little is reported on this subject in the technical literature.

A parametric study was conducted to determine the influence of wall inclination, wall roughness, foundation compressibility and various backfill materials on the stresses and deformations developed in the region of the soil-structure interface.

Using a non-linear finite element program (SSTIPN), the results show that the normal stress distribution, although approximating at-rest conditions, has larger magnitudes than anticipated in the lower region of the wall if a compressible foundation is present. The large settlements observed in the soil mass due to the compressible foundation, combined with a rough interface at the spillway/earthfill junction, may cause large deformations. problems. Based on these findings and the behaviour of the interface when varying the parameters being studied, a recommendation for the selection of the materials is presented.

Notations

B	Bulk Modulus	(kN/m^2)
c'	Cohesion	(kN/m^2)
c'_c	Factored Cohesion	(kN/m^2)
c_a	Wall Adhesion	(kN/m^2)
e	Void Ratio	(—)
E	Young's Modulus	(kN/m^2)
E_i	Initial Tangent Modulus	(kN/m^2)
E_t	Tangent Modulus	(kN/m^2)
E_{ur}	Unloading-Reloading Modulus	(kN/m^2)
F	Safety Factor	(—)
F_o	Degree of Shear Mobilized for At-Rest Condition	(—)
h	Final Overburden Head	(m)
h_o	Surcharge Head Removed	(m)
H	Height of Wall	(m)
K	Modulus Number	(—)
K_A	Active Earth Pressure Coefficient	(—)
K_b	Bulk Modulus Number	(—)
K_I	Shear Stiffness Coefficient	(—)
K_{Iur}	Unloading-Reloading Shear Stiffness Coefficient	(—)
K_n	Normal Stiffness	(kN/m^2)
K_o	At-Rest Earth Pressure Coefficient	(—)
K'_o	Compacted At-Rest Earth Pressure Coefficient	(—)
K_P	Passive Earth Pressure Coefficient	(—)

K_s	Shear Stiffness	(kN/m^2)
K_{st}	Tangent Stiffness	(kN/m^2)
K_{si}	Initial Tangent Stiffness	(kN/m^2)
K_{ur}	Unloading-Reloading Modulus Number	(—)
$K_{1,\phi'}$	K_1 Parameter	(—)
K_1	Limiting At-Rest Earth Pressure Coefficient	(—)
m	Bulk Modulus Exponent	(—)
p_a	Active Earth Pressure	(kN/m^2)
p_o	At-Rest Earth Pressure	(kN/m^2)
p_p	Passive Earth Pressure	(kN/m^2)
P_a	Atmospheric Pressure	(kN/m^2)
P_A	Total Active Thrust	(kN)
P_{Af}	Active Earth Pressure at Failure	(kN/m^2)
P_{AH}	Horizontal Active Thrust	(kN)
n	Modulus Exponent	(—)
N_{cAH}	Horizontal Thrust Parameter	(—)
N_{cAV}	Vertical Thrust Parameter	(—)
$N_{\gamma AH}$	Horizontal Thrust Parameter	(—)
$N_{\gamma AV}$	Vertical Thrust Parameter	(—)
R_f	Failure Ratio	(—)
W	Weight of Soil Wedge	(kN)

α	Inclination of the Wall w.r.t the Vertical	(Radian)
α	Unloading Coefficient	(—)
α_e	Angle of Slip Surface at Equilibrium	(Degree)
α_f	Angle of Slip Surface at Failure	(Degree)
β	Intermediate Active State Factor	(—)
δ	Wall Friction Angle	(Degree)
Δ	Wall Movement Required for Active Condition	(m)
Δ_s	Shear Displacement	(m)
Δ_n	Normal Displacement	(m)
$\Delta\phi'$	Reduction in ϕ' with Confining Pressure	(Degree)
ϵ	Strain	(—)
γ'	Buoyant Unit Weight of Soil	(kN/m^3)
γ_w	Unit Weight of Water	(kN/m^3)
γ_z	Unit Weight of Soil at Depth z	(kN/m^3)
ν_t	Tangent Poisson's Ratio	(—)
ϕ'	Angle of Internal Friction of Soil	(Degree)
ψ	Flow Rule Material Angle	(Degree)
ψ	Direction of Force **R**	(Degree)
σ_n	Normal Stress Acting on the Wall	(kN/m^2)
σ'_{ho}	Initial Active Lateral Pressure	(kN/m^2)
σ'_{hm}	Maximum Horizontal Compacted Stress	(kN/m^2)
σ'_{h1}	Active Lateral Earth Pressure Under Loading	(kN/m^2)
$\sigma'_{h,r}$	Residual Lateral Earth Pressure	(kN/m^2)
σ'_v	Vertical Effective Stress	(kN/m^2)
σ_1	Major Principal Stress	(kN/m^2)
σ_3	Minor Principal Stress	(kN/m^2)

$\tan\phi_e$	Factored Angle of Internal Friction of Soil	(—)
τ	Mobilized Shear Stress	(kN/m^2)
τ'_e	Shear Stress at Equilibrium	(kN/m^2)
τ_f	Shear Strength of the Interface	(kN/m^2)
τ_{ult}	Ultimate Shear Stress	(kN/m^2)
τ_w	Shear Stress Along the Wall	(kN/m^2)
θ_w	Inclination of the Wall w.r.t the Horizontal	(Degree)

Contents

List of Tables

List of Figures

Chapter 1

Introduction

1.1 General

Since early times, the study of lateral earth pressures has been considered a common and important problem in soil mechanics. Earth pressures acting against a typical concrete surface is a consequence of the stresses that occur on the interface between the soil mass and structure. Its magnitude, direction, and distribution is dependent upon the soil and structure properties, the characteristics of the interface and the displacements or deformations of the structure relative to the soil mass. Typical engineering projects such as retaining walls, gravity walls, sheetpiling, timbered cuts, bridge abutments, crib walls and earth dams incorporating concrete spillways all require the estimation of lateral earth pressures.

The earliest theories, put forward by Coulomb in the 18th Century and by Rankine in the 19th Century, estimated the lateral earth pressure distribution. Coulomb's theory accounted for the presence of wall friction, whereas Rankine's considered smooth walls only. The lateral earth pressure at any given depth was proposed to be equal to the overburden effective stress multiplied by a coefficient of lateral earth pressure. The coefficient was chosen so that the formulation reflected the active, at-rest, or passive state of the soil.

Typical embankment dams consist of an inner impervious core section contained within coarser shoulder material and appropriately designed filter transition zones. The dam extends along its axis to meet the valley abutments on either side. A portion of the dam length may incorporate a concrete spillway structure to regulate the volume of water contained in the reservoir and the discharge of water downstream. The impervious core material in the earthfill embankment is compacted directly against the side of the spillway as successive lifts of core material are placed (Figure 3.14). The embankment slopes are widened near the contact zone so as to allow the earthfill to wrap around both the upstream and downstream side of the spillway thereby ensuring a competent interface between soil and concrete. The spillway section will generally be placed on a rock foundation whereas this is not required for the embankment fill.

Due to the massive and unyielding nature of typical spillways incorporated in large earth dams, it is perceivable that its interaction with an adjacent soil mass will not develop an active soil state. The spillway interface, as with the valley abutments, are assumed to have such negligible deformations as to warrant a new approach in determining stresses and strains in the soil mass and along the interface. With the numerous geometric and material property variations to be studied, it is necessary to ensure that a simplistic yet repeatable method of analysis be implemented. The results of this analysis would also be applicable to interaction problems at the interface of the valley abutments as well as for bridge abutments and retaining walls.

1.2 Statement of the Problem

The theories developed by early researchers have been widely used for the calculation of lateral earth pressures and have generally proven reliable. Many designs were based on the assumption that the soil mass adjacent to the wall had reached the active state.

However, after Terzaghi's investigations in 1934, engineers realized that the structure must yield outward a small amount in order for the pressure to be reduced to the active state. Since most retaining structures yield a sufficient amount to induce the active state in the soil mass, designs based on active earth pressures are still acceptable. However, some soil-structure projects, such as bridge abutments and concrete spillways, are considered rigid and have limited movement thereby developing lateral earth pressures which are greater than the active case.

Lateral earth pressures are influenced by the compaction of the backfill, the types of soils used for backfill, temperature, ground-water fluctuations, induced wall movements such as rotation or translation, and vibrations due to earth tremors, traffic or wave action.

Questions remain concerning the overall performance of the interface when faced with the possibility of differential settlements between soil and structure when combined with any combination of wall inclination and surface roughness.

1.3 Objectives of the Investigation

The objectives of this research were to conduct a parametric study on the influence of:

- wall inclination
- the effects of wall roughness
- a compressible foundation material
- varying backfill properties

and the significance of the above parameters on the deformations and lateral earth pressures developed at the soil-structure interface between the concrete spillway wall and the adjacent earth embankment.

1.4 Scope of the Study

A literature review on lateral earth pressure was undertaken to ensure a substantial background to commonly used theories. Large scale laboratory and field tests related to this subject were also examined.

A non-linear finite element program (SSTIPN) was used to run the numerous meshes and parametric variations. The model simulated the placement of layers as typical of a construction sequence.

The analysis consisted of three individual spillway interfaces where the wall inclination varied between 80 to 90 degrees. For each of these situations, three parametric studies were made. The first study consisted of varying the compressibility of the foundation in order to investigate the effect of differential settlement. In the second series of cases, the interface wall roughness and its effects were studied by varying the wall roughness from a smooth to a rough surface. Finally the third group of runs attempted to simulate the effects of using various backfill materials such as soft clay or stiff clay and noting their effect on the soil-structure interface.

1.5 Outline of the Report

The following is an outline of the topics covered in this report.

- Literature review of major contributions to earth pressures including existing theories, large-scale tests, field studies.

- The non-linear hyperbolic stress-strain model, its parameters and limitations.
- The Finite Element Program SSTIPN.
- The meshes used in the analysis and the choice of parameters used in the study.
- Parametric analysis of the SSTIPN results.
- Analysis and discussion of the results obtained.
- Conclusions and suggestions for future research.

Chapter 2

Literature Review

2.1 General

Theoretical and analytical methods of determining lateral earth pressures and deformations in a soil mass adjacent to a rigid wall have been included hereunder. These findings are supported by data taken from field monitoring, large scale testing, laboratory and model studies which are currently available. Compaction and its effects on the lateral stresses is also commented on.

2.2 Existing Theories

2.2.1 Coulomb (1776)

Coulomb's theory takes into account the friction between the wall and the adjacent soil. The wall friction angle δ is most easily determined by direct shear tests. The shear strength τ_f at any point along the wall will be:

$$\tau_f = c_a + \sigma_n \tan\delta \tag{2.1}$$

where: c_a denotes the wall adhesion (if cohesion exists)
σ_n denotes normal stress acting on the wall

Coulomb's theory assumes a minimum deformation condition for the wall such that the state of shear failure will either be active or passive and the slip surface of the wedge of soil will pass through the heel of the wall. This slip surface will invariably be curved near the bottom of the wall in both active and passive cases due to wall friction, but Coulomb simplified the analysis by assuming the failure surface to be plane. In the active state the curvature is slight and the error is therefore negligible. For the passive state, with ϕ' denoting the soil's angle of internal friction, when δ exceeds $\phi'/3$ the error becomes large and the analysis involves consideration of the stability of the soil wedge between the wall and the trial plane. The method is not exact as only force equilibrium is analyzed, and moment equilibrium is not being considered. The analysis is usually performed graphically using the force polygon method. Observing Figure 2.1, it is noted that **R**, being the resultant of the normal and shear forces on the failure plane, is considered to act in the direction ϕ' with respect to the normal of the failure plane when fully mobilized. Since the direction and the magnitude of the forces **W**, $\mathbf{C}_a$ and **C** are known, the force polygon can be drawn and the magnitude of **P** determined. The maximum value of **P** found from a number of trial wedges indicates the total active thrust. The point of application of the total active thrust is not given directly by Coulomb's theory but can be obtained from the pressure distribution on the wall. This distribution can be deduced by constructing a family of failure surfaces over various depths along the height of the wall.

Coulomb's theory can be adapted as well to the passive case if the failure surfaces are assumed to be plane i.e. when δ is less than $\phi'/3$. In the passive case the reaction **P** acts at an angle δ above the normal to the wall surface and the reaction **R** at an angle ϕ' above the normal to the failure plane. In the passive state the minimum value of **P** must be determined.

2.2.2 Rankine (1857)

The Rankine theory assumes a soil mass with a horizontal surface and having a vertical boundary formed by a smooth wall surface. The soil is assumed to be homogeneous and isotropic. The vertical and horizontal stresses in the soil mass are considered the principal stresses.

Rankine's theory considers the stresses in a mass of soil when it reaches a state of plastic equilibrium, i.e. shear failure is imminent. The stress conditions at failure can be described using a Mohr-Coulomb diagram such as one shown in Figure 2.2. The relevant shear strength parameters are c'

and ϕ'. Shear failure occurs along a plane oriented at an angle of $(45^\circ+\phi'/2)$ to the major principal plane. The soil mass however must have sufficient deformation so that the limiting state can be reached.

If there is a movement of the wall away from the soil, the decrease in the horizontal stress is related to the amount of lateral strain in the soil. If the expansion is sufficient enough, the value of the horizontal stress will decrease to its minimum value such that the active state develops.

The relationship between σ_1' and σ_3' at this stage can be derived from the Mohr circle:

$$\mathrm{K}_A = \frac{1-\sin\phi'}{1+\sin\phi'} \tag{2.2}$$

$$\mathrm{p}_a = \mathrm{K}_A\sigma_1' - 2\mathrm{c}'\sqrt{\mathrm{K}_A} \tag{2.3}$$

The active pressure $\mathbf{p}_a$ which corresponds to the lateral stress is due directly to the weight of the soil. Given sufficient movement of the wall away from the soil, the horizontal stress becomes equal to the active pressure, and the soil is said to be in the active Rankine state.

The force, per unit width of wall, due to the active pressure distribution is referred to as the total active thrust $\mathbf{P}_A$. This force is easily determined by a force equilibrium method.

In the above derivation, a wall deformation away from the soil was considered. If, on the other hand, the wall moved against the soil mass there would be a lateral compression of the soil and the value of the horizontal stress will increase until a plastic equilibrium is reached such that:

$$\mathrm{K}_P = \frac{1+\sin\phi'}{1-\sin\phi'} \tag{2.4}$$

$$p_p = K_P \sigma'_1 + 2c'\sqrt{K_P} \tag{2.5}$$

When the horizontal stress becomes equal to the passive pressure the soil is said to be in the passive Rankine state.

Since the theory assumes that the wall surface is smooth whereas in practice considerable friction may be present, this assumption results in an overestimation of the active pressure and an underestimation of the passive pressure to an extent which depends on the magnitude of the wall friction.

2.2.3 Janbu (1970)

Janbu's theory, using a simple limit equilibrium concept, differentiates between classical earth pressure theories, which are failure theories, and actual design, which must be based on equilibrium conditions. A safety factor concept is incorporated in the formulation to ensure that the stress state in the soil will not reach the active or passive pressure and hence to large deformations due to imminent failure. The development of design charts and selection of safety factors enable the evaluation of shear stresses that may act along the interface.

Earth pressures at failure, estimated by Coulomb or Rankine, and at equilibrium for a plane strain and perfectly smooth wall are shown in Figure 2.3. Failure values are supplied an additional subscript f i.e. P_{Af}.

Since smooth walls are rarely encountered in practice, the theory introduces shear stresses along the wall. If τ_f is the shear strength of the interface then

τ_e, the shear stress at equilibrium is given by:

$$\tau_e = \frac{\tau_f}{F} = \frac{c' + \sigma' \tan\phi'}{F} \tag{2.6}$$

The global factor of safety in the above equation can also represent the degree of shear mobilization at equilibrium. The safety factor F can also be integrated into the soil parameters c′ and ϕ' as partial factors of safety such that:

$$c'_e = \frac{c'}{F} \tag{2.7}$$

and:

$$\tan\phi'_e = \frac{\tan\phi'}{F} \tag{2.8}$$

We can then rewrite the shear stress equation in the following form:

$$\tau_e = c'_e + \sigma' \tan\phi'_e \tag{2.9}$$

At limit equilibrium the shape and location of the critical shear surface will invariably be different from the failure surface:

$$\alpha_f = 45^\circ + \frac{\phi'}{2} \tag{2.10}$$

and:

$$\alpha_e = 45^\circ + \frac{\phi'_e}{2} \tag{2.11}$$

The major principal stress is expressed as:

$$\sigma'_1 = N_e \sigma'_3 + 2c_e\sqrt{N_e} \tag{2.12}$$

in which:

$$N_e = \tan^2\alpha_e \tag{2.13}$$

and:

$$\tan\alpha_e = \tan\phi'_e + \sqrt{1 + \tan^2\phi'_e} \tag{2.14}$$

The earth pressure at rest can be considered as a limit equilibrium corresponding to a degree of shear mobilization of $1/F_o$ and F_o can be evaluated using:

$$F_o = \frac{1}{\sqrt{1+\sin\phi'}} \tag{2.15}$$

which, in its derivation, makes use of Jaky's formulae for the determination of the at-rest earth pressure coefficient:

$$K_o = 1 - \sin\phi' \tag{2.16}$$

The coefficient of pressure at-rest K_o can then be evaluated using the following:

$$K_o = \frac{1}{N_o} - \frac{c'}{\sigma_1'}\frac{2}{F_o\sqrt{N_o}} \tag{2.17}$$

Where N_o can be determined using Equation 2.13 and 2.14 by substituting ϕ_c' for ϕ_o'.

Janbu has expressed these equations in a design chart shown in Figure 2.4. The top part of this figure shows calculated F_o values based on measured or evaluated K_o and $\tan\phi'$. The same portion of the graph also shows a theoretical curve using Equation 2.15. The lower graph of Figure 2.4 presents curves for K_o for various values of c' as obtained from Equation 2.15 and 2.17.

2.2.4 Lee & Herington (1972)

Traditional methods for determining earth pressures assume that the shear strength along a failure surface could be expressed by the constants c and ϕ. Those methods also required the determination of wall adhesion c_a and wall friction angle δ, which were assumed to lie between the smooth and rough interface conditions.

The validity of these assumptions can be studied by the use of the theory of plasticity. From consideration of the velocity field it was shown that c_a and δ are less than c and ϕ, and are defined by a kinematic soil-wall boundary condition. These two wall parameters were found to be dependent variables, unlike traditional analyses. For any soil state, the relationships for the Coulomb type parameters for the interface can be established by statics to be:

$$c_a = \frac{c\cos\phi\sin 2(\phi_w - \alpha)}{1 - \sin\phi\cos 2(\phi_w - \alpha)} \tag{2.18}$$

and:

$$\tan\delta = \frac{\sin\phi\sin 2(\phi_w - \alpha)}{1 - \sin\phi\cos 2(\phi_w - \alpha)} \tag{2.19}$$

where:

$$\phi_w = \alpha - \frac{\pi}{4} + \frac{\psi}{2} \tag{2.20}$$

The associated flow rule has restrictions that $c_a = c$ and $\delta = \phi$ whereas the nonassociated flow rule requires that $c_a < c$ and $\tan\delta < \tan\phi$. For associated flow rule materials use $\psi = \phi$ while nonassociated materials which have zero incremental volume change use $\psi = 0$. The angle α denotes the inclination of the wall with respect to the vertical.

The authors also derived an expression for the horizontal active thrust which can be represented for practical purposes by:

$$P_{AH} = H(cN_{cAH} + \frac{\gamma H}{2}N_{\gamma AH}) \tag{2.21}$$

in which N_{cAH} and $N_{\gamma AH}$ are dimensionless thrust parameters analogous to bearing capacity factors, and dependent on ϕ and the geometry of the problem.

From the statics along the soil-wall interface, the relationships between the vertical thrust factors N_{cAV}, $N_{\gamma AV}$ and the corresponding horizontal thrust factors N_{cAH} and $N_{\gamma AH}$ for the active state can be established as:

$$N_{cAV} = \frac{c_a}{c}(1 + \tan^2 \alpha) - N_{cAH} \tan \alpha \tag{2.22}$$

and:

$$N_{\gamma AV} = N_{\gamma AH} \frac{\tan \delta \cos \alpha + \sin \alpha}{\tan \delta \sin \alpha - \cos \alpha} \tag{2.23}$$

The values of N_{cAH} and $N_{\gamma AH}$ can be obtained from Figure 2.5 for a range of wall slopes ranging from 0° to 20° and the specific backfill slopes are 0° and ±20°. The numerical differences between the values for the associated and nonassociated flow rule materials are very small and not detectable on these plots. For associative flow rule materials, the values of c_a and δ are equal to c and ϕ respectively, but for nonassociative flow rule materials $c_a <$c, and $\tan \delta < \tan \phi$.

2.2.5 Bang (1985)

Free standing retaining walls with cohesionless backfill soils are typically designed based on the active lateral pressure theories due to the tendency of outward tilting of the wall. Special cases do exist however, where movement is restricted such as bridge abutments or concrete spillways, such that the lateral earth pressures developed could be greater than the active lateral earth pressures.

A method is described that estimates the magnitude of the lateral earth pressure during the transition between **initial active** state when only the soil element at the ground surface experiences sufficient lateral movement to achieve an active condition and **full active** state when the entire soil mass from the ground surface to the base of the wall are in active condition. The **intermediate active** state exists between both extremes.

In Figure 2.6 a free body diagram of an active wedge is shown with a vertical wall, horizontal backfill and cohesionless material. The active thrust $\mathbf{P}_A$ can be obtained by force equilibrium:

$$\mathrm{P}_A = \frac{\mathrm{W}\tan(45^\circ - \psi/2)}{1 - \tan\delta\tan(45^\circ - \psi/2)} \tag{2.24}$$

in which:

$$\mathrm{W} = \frac{1}{2}\gamma z^2 \tan(45^\circ - \psi/2) \tag{2.25}$$

The angle ψ representing the direction of force **R**, is equal to the internal angle of friction of the soil, ϕ, when the soil mass is in fully active condition.

Therefore we may express the active thrust $\mathbf{P}_A$ as:

$$\mathrm{P}_A = \frac{1}{2}\gamma z^2 \frac{\mathrm{A}^2}{\mathrm{B}} \tag{2.26}$$

in which:

$$\mathrm{A} = \tan(45^\circ - \psi/2) \tag{2.27}$$

$$\mathrm{B} = 1 + \frac{\mathrm{m}}{2} - (1 - \mathrm{A}^2) \tag{2.28}$$

$$\mathrm{m} = \frac{\tan\delta}{\tan\psi} \tag{2.29}$$

The angle ψ, however, may be less than the soil friction angle ϕ, when the soil mass is yet to be in fully active condition. Therefore at any intermediate active state, the variation of the angle ψ, could be assumed as:

$$\psi = \phi - \phi(1 - \beta)\frac{z}{\mathrm{H}} \tag{2.30}$$

This gives values of ψ for various depths depending on the intermediate active state factor β:

- initial active state $\beta = 0$
- full active state $\beta = 1$
- intermediate active state $0 < \beta < 1$

In Figure 2.7 the resulting calculation of the lateral earth pressures at various values of β are shown. The results are compared with Jaky's equation.

2.3 Large Scale Tests and Field Studies

2.3.1 Introduction

There exist many published reports on large scale tests and instrumented field data. However, relatively few reports have reliable findings on lateral earth pressures. The difficulty arises in obtaining accurate measurements of earth pressures due to the introduction of a rigid inclusion in a deformable media. Even with recent advances in pressure cells, the precision of these instruments is still somewhat lacking. Data cited in literature is often not reliable due to poorly defined measurement procedures, more specifically, the type of instrument, its calibration and installation. It is also common for reports to neglect a mention of significant variables such as geometry, soil properties and backfilling procedures.

2.3.2 Retaining Wall Tests: Terzaghi (1934)

Many researchers have reported Terzaghi's large scale tests conducted at M.I.T. The apparatus consisted of a 2.13 m deep, 2.13 m wide and 4.27 m long bin. The 4.27 m long 2.13 m wide high wall could be made to translate or rotate about its base. Load cells were installed on the movable wall. A series of four tests were performed using an angular, medium, uniform sand to backfill the bin. The backfill was placed loosely in the box for one test and compacted in 15.2 cm (6 in) lifts for the other three tests. The coefficient of earth pressure corresponded well with the at-rest condition in the loosely dumped sand, but the pressures in compacted sand were appreciably higher. Terzaghi experimentally investigated the magnitude of displacement which was needed to reach the state of plastic equilibrium. Terzaghi concluded that it was about H/1000 for dense sandy soils and slightly more for cohesive-frictional materials.

2.3.3 Highway 922: Broms & Ingelson (1972)

Broms and Ingelson described earth pressure measurements and wall displacements for an abutment of a 110 m long reinforced concrete bridge.

The backfill material consisted of uniform sand placed upon well graded sandy gravel. The backfill was placed in layers of approximately 60 cm in thickness. A 3 ton vibratory roller compacted each lift.

The earth pressure distribution on the abutment wall was measured by four instrumented rigid steel plates, which in turn were connected to load cells behind the wall. During compaction, the measured lateral earth pressures corresponded to an earth pressure coefficient of K_o=0.4.

The changes of the lateral earth pressures were measured after the placement of the backfill from June 1968 to November 1970. The highest pressures were, as a rule, measured during the summer when the bridge expanded and the abutment walls were pushed against the backfill. The lowest earth pressures were measured during the winter periods when the bridge contracted. The pressures in the upper portion of the wall decreased to zero indicating that the abutment wall separated from the backfill during winter.

During freezing and thawing, it was believed that the backfill probably compacted itself more and the material could also have dropped into the open crack between slab and the backfill. This then would have explained the higher pressures recorded in the spring of 1970 when the earth pressure increased sooner and with less required wall movements than in the previous years. This indicates that, with time, the maximum earth pressures may approach passive earth pressures due to self-compaction of the backfill.

The authors recommend placing a compressible layer of insulation behind the front wall. This layer would limit the gradual increase in lateral pressures, reduce frost penetration, decrease the heave of the soil and decrease the compaction-induced stresses during construction stage.

2.3.4 Cow Green Dam: Vaughan & Kennard (1972)

A study was undertaken at the Cow Green Dam, monitoring the interface between a concrete dam and an embankment dam. The transition was achieved by wrapping the embankment around the end of the concrete dam. The junction between the core and the concrete section was formed mainly by placing the core against the end face of the concrete and by extending the core to overlap the upstream face of the concrete section.

The risk of the formation of cracks, either at the interface between the concrete and the core zone of the embankment dam or even within the core adjacent to the contact, can be evaluated using the earth pressure readings. Two mechanisms by which cracks may form have been identified. If, during the construction or after impounding, the total stress on the interface between the core and the concrete drops to zero, a crack will open on the interface. A similar argument applies within the soil mass adjacent to the interface when tensile stresses occur. The second mechanism is that of hydraulic fracture. If, after impounding, the total pressures against and near the wall remain compressive but are lower than the seepage pressure, then the effective stress may become zero or tensile as pore pressures increase during the reservoir filling. Cracks may then open suddenly.

As shown in Figure 2.8, the two contact faces were kept vertical to above top water level and were given a vertical batter of 1 in 9. The end face was also inclined in plane at an angle of 1 in 9 to the upstream-downstream direction. No keyways or seepage collars were used. The concrete was smooth to provide a sound surface and minimize large stress concentrations along the interface. Boxouts permitted the installation of earth pressure cells and piezometers which would be in the plane of the interface.

Four cells were installed in the end face of the junction and one on the upstream face. At the end of construction, the cells measured total pressures and pore pressures substantially greater than the anticipated maximum reservoir pressure. Thus no risk of cracking was predicted after reservoir filling. The earth pressure coefficient at the end of construction averaged a value of 0.69. See Table 2.1.

A slight decrease in earth pressure had been observed since the end of construction, which is attributed to the consolidation of the clay. The rate of reduction of the earth pressure was not considered to be of concern for future cracking.

2.3.5 Basement Walls: Rehnman & Broms (1972)

Load tests were carried out on a 6 m long and 2.5 m high heavily reinforced concrete wall constructed in Stockholm Sweden. The wall was built on a 10 cm thick-reinforced slab as shown in Figure 2.9. The wall was instrumented with twelve hydraulically operated earth pressure cells of the Glötzl type. Hinged at the bottom, the wall was able to rotate about its base by two hydraulically operated rams.

The concrete wall was coated with asphalt in the same way as an ordinary basement wall. For some of the tests the surface was covered by 50 mm thick Rockwool insulation mats so as to study how a compressible layer affected the magnitude and distribution of the lateral earth pressure on a rigid wall.

Two different backfill materials were used, namely a gravelly sand and a silty sand. Each was either placed loosely behind the wall without compaction or compacted in layers. For the test series with compacted backfills the soil was compacted in layers by either a 400 kg or 140 kg vibratory plate compactor with four passes per layer. The lateral earth pressure developed by large concentrated loads on the surface of the fill was investigated by driving heavy wheeled front loaders on the surface of the completed backfill close to the wall.

The earth pressures for the loosely placed backfill (both gravelly sand and silty fine sand) were found to increase approximately linearly with depth and an earth pressure coefficient equal to 0.35 for the gravelly sand and 0.31 for the silty fine sand as shown in Figures 2.10 and 2.11 respectively. No appreciable difference in the measured earth pressures was observed for the tests where insulation was placed behind the wall, although the earth pressures were slightly higher. This contradicts the findings of the Highway 922 project by Broms & Ingelson (1972).

The overburden pressure was measured by five earth pressure cells installed in the floor slab under the backfill. The measured overburden near the wall was 75% lower than the calculated overburden. These results indicate that part of the weight of the fill was carried by friction along the wall.

The compacted backfill had an approximately triangular distribution of lateral earth pressure with depth. The measured earth pressures were somewhat lower than those in the loosely placed material partly due to a small displacement of the wall during compaction of the backfill. The insulation mats did not appreciably affect the earth pressures either. The silty fine sand when compacted had lateral earth pressures decreasing with depth due to a small lateral displacement of the wall.

The increase in lateral earth pressures due to driving a front end loader close to the wall was large in the loosely placed material while in the compacted material the increase was smaller. Relatively high pressures (60 to 70% increase) remained after removal of concentrated loads from the wheel loaders.

When the wall was rotated away from the backfill, the lateral earth pressures were reduced considerably. The results indicate that it is possible to support basement walls with struts during construction and the high lateral earth pressures can then be released by allowing the wall to move a few millimeters after the struts are removed.

The effect of rainwater increased the lateral earth pressures as water seeped through the backfill and decreased to their initial value after a period of time. The watering caused the loosely placed granular backfill to settle approximately 5% of the height of fill.

Loosely placed silty fine sand was observed to increase its lateral earth pressure with time. The earth pressures increased considerably for the uninsulated parts when the backfill froze. settlements were observed in the spring season (10% of fill height) but earth pressures had decreased below their initial value. This was probably due to a small deflection in the wall.

2.3.6 Highway 290: Coyle & Bartoskewitz (1976)

In September 1970, a 5-yr. study was undertaken to measure lateral earth pressures on full-scale retaining walls supporting highway fills, and to compare with computed pressures by Coulomb and Rankine theories.

A precast panel retaining wall was instrumented with nine Terra Tec pneumatic earth pressure cells and four force transducers between the end pillasters and the panel in order to measure the total thrust of the wall. The pillasters were founded on piers 0.91 m in diameter, 6.10 m deep and 3.65 m on centers. The 3.05 m high panel was supported by a 0.91 m by 0.61 m square cap on each pier. The interface between the cap and the wall base had neoprene rubber pads.

The backfill was placed in 15.2 cm (6 in) compacted lifts and compaction was accomplished with small hand operated vibratory rollers. The backfill consisted of uniformly graded fine sand.

Movement of the wall was recorded throughout the test. The movement of the panel during the backfilling operation was essentially translational. After completion of the backfilling, the panel experienced both translational and rotational movements.

A comparison of the measured and theoretical pressure distribution on the panel was computed by the traditional theories for the fully active case. The computed earth pressure coefficients were 0.29 and 0.31 for the Coulomb and Rankine theories respectively. Although good rapport between theoretical and observed earth pressures existed near the top of the wall, with time the earth pressures against the bottom of the wall increased substantially. Wall movements were not considered enough to develop the totally active case since although the wall did yield gradually during backfilling, only those movements occurring after backfilling were thought to contribute to the development of the totally active case. Using at-rest coefficient of earth pressure of K_o=0.8 correlation with pressures at the lower level of the wall indicated that at-rest case existed at the bottom of the retaining walls.

2.3.7 Retaining Wall Field Test: Matsuo et al. (1978)

The authors describe the measured results of the earth pressure acting on a large scale prototype retaining wall. The retaining wall for testing was made of concrete, 10 m in height. The lowest end on the retaining wall was supported by a hinge and a set of three oil jacks behind the wall. The wall was instrumented with concrete plates 2 m in height and 1 m in width, which in turn were attached to four load cells per plate. A total of five plates were installed through the depth of the wall and two additional load cells were placed under the lowest end of the pressure receiving plate in order to investigate the total wall friction.

The silty sand and two slags produced in the process of iron manufacture were used as the backfill materials. Slag A consisted of a well-graded gravelly sand while slag B was a uniform gravel.

The retaining wall was set up with support by the oil jacks which were installed between the test wall and the wall of an existing building. As backfilling progressed the pressure plates were set up until the backfill reached 10 m in height.

After completion of the backfill, the retaining wall was kept in the at-rest state for a period till the earth pressures became stabilized. A tilting deformation away from the backfill was then given to the wall by the use of the oil jacks to achieve the active state.

For the active state, the displacements required to bring the whole backfill into a state of active plastic equilibrium was found to be (6-8)H/1000 for the silty sand and (3-5)H/1000 in the case of the slags. The difference in magnitude of critical displacement depended on the difference in deformation characteristics between silty soils and granular slags. The wall friction angle was observed to reach twice the angle of friction of the silty sand i.e. $\delta = 2\phi$ and $\delta = \phi$ for the slags. The earth pressure gradually increased again when the wall was left in the active state. It was observed that, given time, the recovery of earth pressure can reach over half of its initial at-rest pressure. The practice of assuming the wall friction angle as $\delta = 2/3\phi$, commonly adopted in design, is therefore questionable.

2.3.8 São Simão Dam: Viotti & De Avila (1979)

The São Simão hydroelectric dam, located in South-Central Brazil, was instrumented with a set of earth pressure cells and piezometers along the interface between the left earth embankment and the concrete spillway. The concrete at the transition zone had smooth surfaces which were thought to be an improvement from the use of irregularities since it tended to make the compaction of the core difficult and provided stress concentrations.

Instruments were installed to monitor the behaviour of the contact zone and to investigate the possibility of crack development in the impervious core.

The instruments were of the pneumatic type and were activated by the circulation of nitrogen. Block-outs were left in the concrete structure for the installation of the instruments. Seven earth pressure cells were installed, four of them about 50 m below crest elevation and three about 20 m below crest. Cell N°1 and N°4 were installed at the lower elevation, N°1 on the upstream face and cell N°4 in the transverse face. Cell N°2 and N°3 were installed at the same elevation, being N°2 in the downstream filter contact and N°3 inside the core. The upper cells, 5, 6 and 7 were installed respectively in the upstream, transverse and downstream faces. Cell N°5 and N°6 are in the core contact and N°7 in the filter. In order to provide effective stress measurements piezometers were coupled with earth pressure cells 1, 2, 4, 5 and 6. Four more piezometers were installed in the contact between the fill and the concrete in order to give a complete picture of the piezometric levels in it. Besides, a set of seven piezometers was installed in a cross-section about 18 m apart from the contact to get piezometric levels unaffected by the contact.

At the end of construction the cells were reading total pressures of the order 20% of the calculated overburden stress, except for cell N°2 and N°3 which were reading pressures of the order of 35% of overburden stress. Although smaller than expected, these values correlated well with the data on Cow Green Dam, as reported by Vaughan & Kennard (1972).

The readings of the instruments and overburden pressures are summarized in Table 2.2 for conditions during construction until one year after reservoir impounding.

The variations in water level also caused changes in the earth pressure readings, but since many effects occur simultaneously such as pore pressure changes, movements of concrete structure and earthfill, it is difficult to understand the behaviour thoroughly. Cell N°1 showed an effective stress close to zero, leading to the conclusion that hydraulic fracturing may have occurred and indicates that the upstream face of the transition wall has an ineffective contact in comparison with the transverse face.

2.3.9 Shaker Table Experiment: Sherif et al. (1982)

Despite extensive earlier studies, there still remained conflicting opinions regarding the nature and magnitude of stresses exerted on retaining structures. Also, the location of the total thrust and effect of wall movement were problems that had not yet been resolved.

A rigid soil box 2.4 m long, 1.8 m wide and 1.2 m deep was attached to a shaking table 3 m long and 2.4 m wide. The sides of the box were made of 6.4 mm thick transparent plexiglass such that deformations and internal soil movement could be monitored. The table was mounted on a track and bearing system which would ensure low friction during operation.

The model was designed such that it could remain stationary, translate as a rigid body or rotate at the base or at the top. The wall was instrumented with three horizontal load cells in the face of the wall and one vertical load cell at the base of the wall.

Dry Ottawa silica sand was used throughout the investigation. The sand was first gently placed in the soil box by means of a flexible tube for the loose cases. For dense cases, the loosely placed soil was densified by shaking 15.2 cm (6 in) lifts at a frequency of 6 Hz for five seconds. For medium-dense cases the loose soil was placed up to full height of the wall and subjected to the same vibrations as for the dense case. When testing began, at-rest lateral pressure data was recorded, without wall movements, and active lateral pressure data was acquired when sufficient wall displacements away from the soil was imposed. A second series of tests, studying the effect of ground acceleration or dynamic excitation was also performed but will not be discussed herein since it is beyond the scope of this thesis.

The data acquired for the at-rest conditions are summarized in Figure 2.12 and Figure 2.13. The values in Figure 2.12 demonstrates the increase in at-rest earth pressures as the soil density increases. This behaviour arises from the fact that densification locks in lateral stresses and can actually reverse the principal stress direction such that lateral stresses exceed the overburden pressure. The at-rest earth pressure coefficient was also observed to reach a nearly constant value of 0.5, indicating that following strong vibrations, the horizontal earth pressures can attain 50% of the overburden pressure. From Figure 2.13 it can be shown that the point of application of the total lateral thrust, $(h/H)_{so}$, is independent of soil density and appears to be slightly higher than the expected centroid of a linear pressure distribution i.e. (0.36H as opposed to 0.33H).

Once the at-rest conditions were attained, the wall was slowly moved translationally away from the fill at a rate of 3.81×10^{-4}mm/s. During wall movement, data was recorded from the instrumentation. Results show, as presented in Figure 2.14, that although it was not obvious when the soil entered active plastic state, the value of $\tan\delta$ reached its maximum after a certain wall displacement. The point of application also seemed to reach it's highest point when the peak value of $\tan\delta$ was achieved. Tests showed that this maximum $\tan\delta$ was reached with less wall displacement if the soil density increased, as shown in Figure 2.15. When the peak value of $\tan\delta$ was achieved, the active earth pressure coefficient was higher than the values given by the Coulomb solution by about 30%, as shown in Figure 2.16.

These results can be explained by the fact that $\tan\delta_{max}$ occurred when the wall displacements were about H/6000, whereas the active earth pressure coefficient is defined at a wall displacement of H/1000. Both coefficients seemed to agree well if the choice of H/1000 was used as the criteria for active plastic state. The average wall translation required for $\tan\delta_{max}$, to permit full active state, can be expressed as a function of the soil friction angle ϕ (in degrees), and wall height H:

$$\Delta = \mathrm{H}(7.0 - 0.13\phi)10^{-4} \tag{2.31}$$

This implies that the active case actually develops under much lower wall deformations than previously believed. The point of application of active thrust, defined at $\tan\delta_{max}$, which was seen to increase slightly with soil density, is suggested to act at 0.42H from the base of the wall when the wall is believed to move translationally.

2.3.10 Dickson Dam Embankment: Brandt (1985)

The test facility, located within the reservoir of Dickson Dam in Alberta, Canada, comprised of a 6 m high and 6 m wide reinforced concrete wall. The fill was placed in 5 cm thick layers and compacted using a sheepsfoot roller. The fill was classified as a fine sandy silt with clay.

The test wall was instrumented with three contact pressure cells, six shear displacement devices and three shear stress devices. The instruments were installed in a four column and three row matrix fashion with two shear displacement devices at each depth. In addition to wall instrumentation, instruments were placed within the fill to monitor displacements and stresses. These included eight magnetic extensometers in seven vertical lines and two clusters of five earth pressure cells. The position of all instruments is shown in Figure 2.17. The wall movements were monitored using a slope indicator installed parallel to the interface and three settlement points along the crest of the wall.

Wall instrumentation data shows that normal stresses measured near the bottom of the wall are greater than the at-rest lateral earth pressure. These findings are consistent with published data taken from contact cells (Vaughan & Kennard, 1972 and Coyle et al., 1974). A typical profile of the normal stresses are shown in Figure 2.18 for the last three days of monitoring the instrumentation. These curves do not however, follow the general linearly increasing trend as depicted on the same graph as the at-rest and active theoretical earth pressure distributions.

The development of shear displacement with height of the wall is represented in Figure 2.19. The maximum shear displacements appear to occur at the center of the wall.

The shear stresses developed along the height of the wall had a similar trend to that of the shear displacement. Typical shear stress distributions are shown in Figure 2.20. This is expected since an increase shear stress is normally associated by an increase in shear displacement. The shear stresses at both the top and toe of the wall would likewise be reduced to zero.

The settlement profile in Figure 2.21 was plotted for several periods during the fill construction. It can be seen that there appeared to be no time-dependent behaviour of the fill and that excessive settlements were observed a small distance away from the wall. It was believed that softening of the foundation due to weathering and movement of the wall away from the fill during construction explains the unusual increase in settlement near the wall. It was thought that a soil wedge between the wall and the remaining backfill formed a load transfer towards the remaining fill and towards the wall. See Figure 2.22.

Based on the settlement profiles of the fill it follows that high wall adhesion and foundation settlement may generate larger settlements than anticipated and thus increase the tendency for longitudinal cracking. It may hence be noted that such defective behaviour can occur within the adjacent soil mass and not exactly at the interface.

2.4 Compaction-Induced Stresses

2.4.1 General

The earth pressure distribution and magnitude behind retaining structures is not that which can predicted by classical earth pressure theories. This could be attributed to the stresses induced by compaction which, even after removal of the surficial loading, remain in the soil mass as 'locked-in' stresses. However, only limited information is available on the magnitude of pressures developed on a retaining wall and its corresponding yielding, due to a transient load condition. The following section presents an introduction to a few advancements on the evaluation of compaction-induced stresses.

2.4.2 Rowe (1954)

Rowe stipulated a theory for the calculation of lateral pressures exerted by cohesionless soils. Although his work was directed toward the study of intermediate states between at-rest and fully active or passive, his work did lead to an early postulate for the effects of compaction on lateral pressures.

Rowe's theory was based on the hypotheses that the degree of mobilization of the soil friction angle ϕ' and the wall friction angle δ depends upon the degree of movement of the shear planes which in turns was primarily due to the amount of interlocking of the soil grains. Conventional limiting equilibrium methods using the fractional ϕ' and δ were acceptable.

The theory was supported by performing a series of direct shear tests on several different sands and recording the friction angle developed at various levels of slip strain. He noticed that removal of a surcharge pressure resulted in a very small relaxation of the peak lateral pressures. It was suggested that the final earth pressure coefficient could be expressed as:

$$K_o' = K_o(1 + \frac{h_o}{h}) \tag{2.32}$$

Where h_o is the surcharge head removed and h the final overburden head.

Schmidt (1967) later proposed a similar equation which allowed for some degree of relaxation of lateral stresses following surcharge removal:

$$K_o' = K_o(1 + \frac{h_o}{h})^{\alpha} \tag{2.33}$$

where: $\alpha = 0.3$ to 0.5 for most sands
$\alpha = 1.2 \sin\phi'$ for initially NC clays.

2.4.3 Broms (1971) & Ingold (1979)

Broms proposed a stress path theory to explain lateral earth pressures induced by compaction on rigid, non-yielding structures. Later, Ingold extended the theory to cases where structural deflections were permissible but had not modified the theory appreciably.

Considering an element of dry cohesionless soil at some depth z, then for the active case the lateral pressure will be:

$$\sigma_{ho}' = K_a \gamma z \tag{2.34}$$

If the vertical effective stress is now increased by an amount $\Delta\sigma'_v$, then:

$$\sigma'_{h1} = \mathrm{K}_a(\gamma z + \Delta\sigma'_v) \tag{2.35}$$

If the increase in vertical effective stress is transitory then when it is removed, the vertical effective stress should recover its original value.

In the proposed model, it was assumed that below a critical depth z_c, there was no reduction in the horizontal effective stress since the increase in vertical effective stress $\Delta\sigma'_v$ induced some plastic lateral strains which were irrecoverable.

The change in vertical effective stress with depth could be obtained by Boussinesq for a line load p:

$$\Delta\sigma'_v = \frac{2\mathrm{p}}{\pi z} \tag{2.36}$$

The expression for $\Delta\sigma'_v$ in Equation 2.36 may be substituted into Equation 2.35 and letting $\Delta\sigma'_v \gg \gamma z$:

$$\Delta\sigma'_{h1} = \frac{2\mathrm{p}\mathrm{K}_a}{\pi z} \tag{2.37}$$

The critical depth is defined as:

$$z_c = \mathrm{K}_a\sqrt{\frac{2\mathrm{p}}{\pi\gamma}} \tag{2.38}$$

The maximum value of the horizontal effective stress that can be sustained is that which is developed at the critical depth and can be obtained by combining Equation 2.37and 2.38:

$$\sigma'_{hm} = \sqrt{\frac{2\mathrm{p}\gamma}{\pi}} \tag{2.39}$$

It should be noted that as the height of the fill is increased, there may occur a depth h_c at which the conventional active pressure exceeds the compaction-induced pressure:

$$h_c = \frac{1}{K_a \sqrt{\frac{2p\gamma}{\pi}}} \tag{2.40}$$

The resulting pressure distribution is shown in Figure 2.23.

2.4.4 Seed (1983)

Seed presents a new model and analytical procedure for the calculation of peak and residual compaction-induced stresses against a vertical, non-deflecting structure. The noncompaction-related stresses result from K_o conditions and the major and minor principal stresses are oriented horizontally and vertically.

The model accomplishes the compaction of leveled fill layers by an incremental cyclic application and removal of a uniform, vertical surcharge loading. The development of a multi-cycle K_o loading/unloading hysteretic behaviour model allows the evaluation of compaction-induced stresses. The formulation is unfortunately complex but can be readily incorporated into a finite element program.

Five material property parameters are required for the model and are shown in Table 2.3. The K_o-unloading coefficient, α, proposed by Schmidt (1967), is related to $\sin\phi'$ by a function described in Figure 2.24. This function is shown along with its standard deviation curves.

The frictional component parameter $K_{1,\phi'}$ and the cohesion c' together determine the limiting coefficient of at-rest lateral earth pressure K_1:

$$K_1 = K_{1,\phi'} + \frac{2c'}{\sigma'_v}\sqrt{K_{1,\phi'}} \tag{2.41}$$

A full discussion of the formulation is presented in Seed's doctoral thesis. A simple hand calculation procedure approximates the behaviour quite closely. The simplified method requires a similar $\Delta\sigma'_v$ profile with depth as with the rigorous incremental approach and is shown in Figure 2.25. This profile is then multiplied by a factor F ($0 \leq F \leq 1$) determined as:

$$F = \frac{5^\alpha}{4} - 0.25 \tag{2.42}$$

A new profile should be drawn by adding the resulting scaled $F\Delta\sigma'_v$ to the at-rest lateral earth pressure profile $K_o\sigma'_v$ to obtain the final residual lateral stresses $\sigma'_{h,r}$ versus depth:

$$\sigma'_{h,r} = K_o\sigma'_v + F\Delta\sigma'_v \tag{2.43}$$

The near surface portion of the residual lateral stresses profile should then be reduced such that:

$$\sigma'_{h,r} \leq K_1\sigma'_v \tag{2.44}$$

Below the depth of the maximum remaining residual lateral stress the profile should be modified to increase linearly with depth at a rate:

$$\sigma'_h = K_o(1 - F)\Delta\sigma'_v \tag{2.45}$$

until the K_o lateral earth pressure is intersected at greater depths.

2.5 Determination of At-Rest Coefficient K_o

It has been shown that the active pressure is associated with lateral expansion of the soil and is a minimum value, whereas the passive pressure is associated with lateral compression and is a maximum value. If the soil has experienced no lateral straining, then the corresponding lateral earth pressure is called the earth pressure at-rest such that:

$$p_o = K_o \sigma'_v \tag{2.46}$$

The value of K_o, the at-rest earth pressure coefficient, can be evaluated experimentally by means of the triaxial K_o-test, where the lateral strain of the specimen is maintained at zero.

The strain required to mobilize the passive pressure is considerably higher than that required to mobilize the active pressure. For any condition intermediate to the active and passive states, the value of the horizontal stress is unknown.

If an outward deformation of the wall does not satisfy the minimum deformation condition for the development of the active state, the soil adjacent to the wall remains in a state of equilibrium and the lateral pressure will be between the at-rest and active values. In practice, the magnitude of the wall deformation is unknown. The soil is normally backfilled near the wall after the structure has been partially or fully constructed. Some degree of outward wall deformation will take place during backfilling. Since cumulative displacements result in a reduction of lateral pressure towards the active value, some designers feel retainings wall need be built to withstand at-rest pressures such that yielding of the wall will be minimized.

For sands and NC clays, with a vertical wall and horizontal backfill, the value of K_o can be approximated by several formulas proposed by a few authors:

Jaky (1944):

$$K_o = 1 - \sin\phi' \tag{2.47}$$

Rymsza (1979):

$$K_o = \tan^2(45^\circ - \frac{\phi'}{3}) \tag{2.48}$$

Mayne & Kulhawy (1982):

$$K_o = (1 - \sin\phi')\left[\left(\frac{OCR}{OCR_{max}^{(1-\sin\phi')}}\right) + \frac{3}{4}\left(1 - \frac{OCR}{OCR_{max}}\right)\right] \tag{2.49}$$

Hendron (1963):

$$K_o = \frac{1}{2}\left[\frac{1 + \sqrt{\frac{6}{8}} - \sqrt[3]{\frac{6}{8}}\sin\phi'}{1 - \sqrt{\frac{6}{8}} + \sqrt[3]{\frac{6}{8}}\sin\phi'}\right] \tag{2.50}$$

Brooker & Ireland (1965):

$$K_o = 0.95 - \sin\phi' \tag{2.51}$$

Alpan (1967):

$$K_o = 0.19 + 0.233\log(PI) \tag{2.52}$$

2.6 Wall Movements to Mobilize Active State

Previous observations indicating the minimum required displacements of the wall have been summarized. The values seem to vary considerably in order of magnitude but tend to emphasize the fact that very little wall movement is required to achieve the active state:

$\Delta = \frac{H}{1000}$	Terzaghi (1940)
$\Delta = \frac{H}{3000}$	Jansson et al. (1948)
$\Delta = \frac{H}{500}$	Rowe (1969)
$\Delta = \frac{H}{1200}$	Matteotti (1970)
$\Delta = \frac{H}{320}$	Clough & Duncan (1971)
$\Delta = \frac{H}{2000}$	Rehnman & Broms (1972)
$\Delta = \frac{(6-8)H}{1000}$	Matsuo et al. (1978)
$\Delta = \frac{H}{500}$	Ingold (1979(a))
$\Delta = H(7 - 0.13\phi_{deg})10^{-4}$	Sherif et al. (1982)

2.7 Conclusions

The findings presented above show that lateral earth pressures measured in large scale field studies are observed to be very dependent on construction practice, installation of instrumentation, and data analysis. The variability of the results obtained in this literature review may be attributed to specific site conditions. The fluctuation of the ground water table, compaction method and effort, vibrations and soil temperature contribute unique effects to lateral earth pressure distribution. Although the assumption that earth retaining structures do yield a sufficient amount to initiate active earth pressure, it is recommended that structures designed for small deformations, or structures constrained from yielding, should use the at-rest earth pressure coefficient to estimate the pressure along the soil-structure interface.

Chapter 3

Finite Element Simulation

3.1 General

Computational methods, such as finite elements, provides a means to analyse stresses and deformations in a soil mass. The ease given to the user to supply the geometry, boundary conditions and material properties allows many complex problems to be resolved. Many of these situations are not readily studied using conventional methods. In order that soil deformations be realistic, a reasonable stress-strain relationship is required. Most soils exhibit a nonlinear, inelastic and stress dependent behaviour which is difficult to model. The hyperbolic model (Duncan et al., 1978) was developed to meet these requirements.

3.2 Hyperbolic Model

3.2.1 Introduction

The hyperbolic model (Duncan et al., 1978), an incremental stress-strain relation, was formulated directly as a simple extension of the isotropic, linear elastic model but incorporated variable tangential moduli which replaced the elastic constants. In each increment, the stress-strain behaviour is treated as being linear and the generalized Hooke's Law of elastic deformations governs. This incremental approach makes the model well suited for implementation to finite element programs. The material parameters are easily obtained from standard laboratory tests.

3.2.2 Formulation

Three important characteristics in the stress-strain behaviour of soils must be reproducible in the incremental model. These are nonlinearity, stress-dependency and inelasticity. The choice of model parameters accounts for these characteristics.

Stress-strain curves have been found (Duncan et al., 1978) to be approximated reasonably well with hyperbolas (Figure 3.1). The hyperbola represents the nonlinear component and is formulated as:

$$(\sigma_1 - \sigma_3) = \frac{\epsilon}{\frac{1}{E_i} + \frac{\epsilon}{(\sigma_1 - \sigma_3)_{ult}}} \tag{3.1}$$

The value of the initial tangent modulus E_i and the ultimate deviatoric stress $(\sigma_1 - \sigma_3)_{ult}$ can be determined easily by transforming the stress-strain curve such as shown in Figure 3.2.

Most soils exhibit steeper initial stress-strain curves and higher strength when confining pressure is increased. This in turn affects E_i and $(\sigma_1 - \sigma_3)_{ult}$. This stress dependency is accounted by the empirical relation:

$$E_i = KP_a \left(\frac{\sigma_3}{P_a}\right)^n \tag{3.2}$$

The modulus number K and modulus exponent n are both dimensionless while E_i and the atmospheric pressure P_a are in the same system of units. The parameters K and n can be determined by plotting $\log(E_i/P_a)$ against $\log(\sigma_3/P_a)$ as shown in Figure 3.3.

The variation of $(\sigma_1 - \sigma_3)_{ult}$ with σ_3 is related to the stress difference at failure $(\sigma_1 - \sigma_3)_f$ by introducing a failure ratio R_f:

$$(\sigma_1 - \sigma_3)_f = R_f(\sigma_1 - \sigma_3)_{ult} \tag{3.3}$$

Because $(\sigma_1 - \sigma_3)_{ult} \geq (\sigma_1 - \sigma_3)_f$ the value of R_f is always smaller than unity (usually 0.5 to 0.9). The stress difference at failure $(\sigma_1 - \sigma_3)_f$ is represented by the Mohr-Coulomb strength relationship:

$$(\sigma_1 - \sigma_3)_f = \frac{2c' \cos\phi' + 2\sigma_3 \sin\phi'}{1 - \sin\phi'} \tag{3.4}$$

The tangent modulus E_t is defined as the instantaneous slope of the stress-strain curve. Its expression is derived by differentiating Equation 3.1 with respect to ϵ and using Equation 3.2, 3.3 and 3.4 to form:

$$E_t = \left[1 - \frac{R_f(1 - \sin\phi')(\sigma_1 - \sigma_3)}{2c' \cos\phi' + 2\sigma_3 \sin\phi'}\right]^2 KP_a \left(\frac{\sigma_3}{P_a}\right)^n \tag{3.5}$$

If the values of the parameters K, n, c', ϕ', and R_f are known then the tangent modulus can be calculated for any stress condition.

The inelastic behaviour of the soil is represented by the use of a different modulus number K when the specimen is unloaded at some stage during a test. Since the stress-strain curve followed during unloading is steeper than the curve followed during primary loading, Figure 3.4, the soil behaviour is inelastic and the strains are only partially recoverable. The unloading-reloading modulus E_{ur} is related to the unloading-reloading modulus number K_{ur} by an expression similar to Equation 3.2:

$$E_{ur} = K_{ur} P_a \left(\frac{\sigma_3}{P_a}\right)^n \tag{3.6}$$

The value of K_{ur} is always larger than the value of K, and n is assumed to remain constant during unloading/ reloading.

The nonlinearity in the volume change characteristic of a soil can be accounted for by using a variable bulk modulus. According to the theory of elasticity, the value of bulk modulus is defined by:

$$B = \frac{\Delta\sigma_1 + \Delta\sigma_2 + \Delta\sigma_3}{\Delta\epsilon_v} \tag{3.7}$$

The value of B however, is seen to increase with increasing confining pressure and thus a stress dependent relation such as presented earlier is applied:

$$B = K_b P_a \left(\frac{\sigma_3}{P_a}\right)^m \tag{3.8}$$

The bulk modulus number K_b and the bulk modulus exponent m are dimensionless parameters while B and P_a are expressed in the same system of units. The values of K_b and m are easily determined from a graph similar to Figure 3.5.

The tangent Poisson's ratio ν_t is defined in terms of the tangent modulus and bulk modulus as:

$$\nu_t = \frac{\mathrm{B} - \mathrm{E}_t}{6\mathrm{B}} \tag{3.9}$$

In order to ensure that the Poisson's ratio remains within its limits of $0 \leq \nu_t \leq 0.5$, restrictions on the range of values of B are imposed. This is accomplished by setting limits to the bulk modulus of:

$$\frac{\mathrm{E}_t}{3} \leq \mathrm{B} \leq 17\mathrm{E}_t \tag{3.10}$$

The Mohr envelopes for cohesionless soils is curved to some extent and makes it difficult to select a single value of ϕ'. The values of ϕ' are found to decrease logarithmically with confining pressure as:

$$\phi' = \phi'_0 - \Delta\phi' \log\left(\frac{\sigma_3}{\mathrm{P}_a}\right) \tag{3.11}$$

In this equation ϕ'_0 is the value of ϕ' when the confining pressure is at atmospheric pressure and $\Delta\phi'$ is the reduction in ϕ' for a tenfold increase in σ_3.

3.2.3 Selection of Hyperbolic Parameters

A total of nine parameters are needed to represent soil behaviour using the hyperbolic model. These parameters are listed in Table 3.1.

The parameter values can be obtained from the results of conventional triaxial compression tests. The relationships outlined previously can be used for effective stress analyses (using data from drained tests) or total stress analyses (using data from unconsolidated-undrained tests).

A data base containing parameter values for many different types of soils is available (Duncan et al., 1978) in order to estimate reasonable values of these parameters. This information is useful for assessing soil parameters when insufficient data is given, for situations when laboratory facilities are unavailable, or for checking the reliability of test results obtained in the laboratory.

3.2.4 Parameter Sensitivity

Each hyperbolic parameter has a unique effect on the stress-strain relationship or on the volumetric strain. An evaluation of their sensitivities were conducted on each parameter when individually isolated. Figures 3.6 to 3.12 inclusive show the variation in the behaviour of the stress-strain and volumetric strain curves in response to changes in certain parameters. Unless noted in each respective legend, the hyperbolic variables are taken as representative of the Oroville Dam Shell material (Duncan et al., 1978):

PARAMETER	VALUE
K	1320
n	0.4
R_f	0.73
K_b	1030
m	0.15
$c'(KN/m^2)$	0.0
ϕ'	55
$\Delta\phi'$	8.5

Each parameter studied had a pronounced effect on the material behaviour when subjected to increasing stress level. Although these variations are visually conclusive in the figures cited previously, a summary of each parameter and their role in the soil's response when subjected to increasing deviatoric stress is discussed hereunder:

PARAMETER	OBSERVATION	FIGURE
K	Influences initial rise of stress-strain curve Deviatoric stress at failure remains constant No change in volumetric straining	3.6
K_b	Principal variable for volume compressibility No changes in stress-strain behaviour Decreases volumetric straining	3.7
c'	Linearly increases asymptotic failure value Shape of stress-strain curve remains constant Increases volumetric straining slightly	3.8
ϕ'	Increases asymptotic failure value Shape of stress-strain curve remains constant Very little effect on volumetric straining	3.9
n	Dependent on magnitude of confining pressure Increases initial portion of curve accordingly Does not affect deviatoric stress at failure	3.10–3.12
m	Dependent on magnitude of confining pressure No influence on stress-strain relationship As m increases, volume curves become singular	3.10–3.12

3.2.5 Limitations

The hyperbolic model, a seemingly more refined approach at soil modelling, is not without its limitations. The restrictions denote the extent of the models applicability to all the soil types generally encountered. A summary of these limitations is presented:

- The model is valid for analyses prior to failure and is useful for predicting movements in soil masses with stresses not exceeding 60-70% of the ultimate value.
- The hyperbolic relationships do not include volume changes due to shear (second-order) dilatancy and are limited in predicting deformations in loose or dense sands under low confining pressures.
- The hyperbolic parameters are not fundamental soil properties but are empirical coefficients derived from laboratory tests. These parameters depend on the density of the soil, its water content, the pressure range used in testing and the drainage conditions.
- The hyperbolic relations are hypoelastic formulation stating that the soil behaviour is governed by the instantaneous variable moduli at the current state of stress. Hypoelastic models, however, are not thermodynamically founded and may generate energy for certain loading-unloading cycles. (Chen and Baladi, 1985)
- Although an unload-reload modulus is incorporated in the model, it is advised to keep loading monotonically increasing. The model includes only one stress path, whereas the loading and/or unloading

could cause a wide range of stress paths. The unloading-reloading modulus concept cannot acceptably model plastic work and cyclic straining.

- The hyperbolic model cannot represent the strain softening behaviour since the deviatoric stress attempts to reach an asymptotic value at failure.

3.3 Interface Elements

3.3.1 Introduction

In conventional finite element theory, two adjacent elements are required to have equal displacements along their common boundary. This ensures that no gaps may open or that no relative displacements will occur between the two elements. However, relative displacements do occur at soil-structure interfaces and should be so represented. This interface behaviour can be modelled adequately using a one-dimensional slip element. The element is placed along the boundary between soil and structure elements wherever relative movements are anticipated.

3.3.2 Goodman's Interface

Goodman (Goodman et al., 1968) developed a joint element having zero thickness, for use with the finite element method. Although originally designed for the analysis of joints and seams on the behaviour of rock masses, the model is applicable to any discontinuities and composite materials.

The stress vector may be expressed in terms of a product of unit joint stiffness and displacements:

$$\begin{bmatrix} \tau \\ \sigma_n \end{bmatrix} = \begin{bmatrix} K_s & 0 \\ 0 & K_n \end{bmatrix} \begin{bmatrix} \Delta_s \\ \Delta_n \end{bmatrix} \tag{3.12}$$

where: K_s denotes shear stiffness
K_n denotes normal stiffness
Δ_s denotes shear displacement
Δ_n denotes normal displacement

The shear strength of the joint element is given by the Mohr-Coulomb failure criteria:

$$\tau_f = c_a + \sigma_n \tan\delta \tag{3.13}$$

Relative movements may occur at interfaces between soil masses and structures due to various loadings. There are three basic deformation modes that an interface element may experience at any stage of loading:

- During loading the joint element experiences compression and until the shear strength of the joint is reached the interface element has no shear displacements. This stick or no-slip stage has a very large value of K_n $(10^9 - 10^{10}\text{kN/m}^2)$ to prevent significant overlapping on the adjacent element. The value of K_s is determined by a procedure developed in the following section.

- After the element has failed in shear, Equation 3.13, with the interface still in compression, the value of K_s is reduced to a negligible value to allow for sliding or slip mode. The value of K_n remains large.
- After tensile conditions, an opening of a gap between the structure and backfill occurs. K_s and K_n are assigned very low stiffness values to model the separation or debonding mode.

3.3.3 Interface Behaviour

The results of direct shear tests (Goodman et al., 1968) on interface materials (soil and concrete) indicate that nonlinear stress-displacement curves can be approximated using a hyperbolic relationship (Figure 3.13). The shear stress values reach asymptotic limits with increasing displacement. The steepness of the stress-displacement curve and the peak shear stress values also increase with increasing confining pressure. This interface behaviour may be conveniently expressed by means of equations similar to those developed to model the stress-strain of soils. The curves shown in Figure 3.13 have an equation of the form:

$$\tau = \frac{\Delta_s}{\frac{1}{a} + \frac{\Delta_s}{b}} \tag{3.14}$$

The coefficient a is the initial slope of the stress-displacement curve (analogous to the initial tangent modulus E_i). This slope is referred to as the initial tangent stiffness K_{si}. The coefficient b is the asymptote value, τ_{ult}. The relationship between this ultimate shear stress τ_{ult} and the peak shear stress of the interface τ_f introduces the failure ratio R_f:

$$\tau_f = R_f \tau_{ult} \tag{3.15}$$

The values of R_f for the curves shown in Figure 3.13 varied from 0.82 to 0.95.

Both the initial tangent stiffness K_{si} and the shear strength of the interface τ_f (Equation 3.13) depend on the normal stress on the interface:

$$K_{si} = K_I \gamma_w \left(\frac{\sigma_n}{P_a}\right)^n \tag{3.16}$$

The use of γ_w is to ensure that the equation is of a dimensionless form. The shear stiffness coefficient K_I should be replaced by the unloading-reloading shear stiffness coefficient K_{Iur} when appropriate.

Hence, the variation of shear stress with displacement may be expressed as:

$$\tau = \frac{\Delta_s}{\frac{1}{K_I \gamma_w \left(\frac{\sigma_n}{P_a}\right)^n} + \frac{R_f \Delta_s}{c_a + \sigma_n \tan\delta}} \tag{3.17}$$

For incremental nonlinear analyses, it is convenient to define a tangent stiffness value K_{st} which is representative of the slope of the shear stress-displacement curve at the beginning of each increment. Differentiating Equation 3.17 with respect to Δ_s, the tangent stiffness value may be expressed as:

$$K_{st} = \left[1 - \frac{R_f \tau}{c_a + \sigma_n \tan\delta}\right]^2 K_I \gamma_w \left(\frac{\sigma_n}{P_a}\right)^n \tag{3.18}$$

Thus with values of σ_n and τ at the beginning of the increment and the parameters K_I, n, R_f, c_a, and δ, the tangent stiffness K_{st} may be calculated.

3.4 Finite Element Program SSTIPN

3.4.1 Introduction

The finite element method has been established as a powerful research tool in studying earth retaining structures. Recent advances in the development of constitutive models and the incorporation of interface elements have made it possible to analyse soil-structure interaction problems more reliably. Its ability to predict both stresses and deformations with a minimum of simplifying assumptions and its versatility are key advantages. The theoretical basis for numerical modelling has been well established and will not be repeated in this thesis. The finite element program SSTIPN and its implementation to soil-structure analysis are discussed in the following section.

3.4.2 SSTIPN Capabilities

The program SSTIPN "Soil-Structure Interaction Program, Nonlinear" is a general finite element program which incorporates the hyperbolic model to account for it's nonlinear constitutive laws. The program follows the general programming concepts and solution techniques of the programs SAP, ISBUILD and LSBUILD developed at the University of of California, Berkeley. The solution procedure is coded for incremental analysis.

An increment may consist of the placement of a layer of fill, the placement of a structure or the application of loads to the current structure or soil mass. Structural materials are assumed to behave as linear elastic. This flexible approach can simulate actual construction sequences. It has also been shown that this gradual mesh development tends to yield better results than the programs which are restricted to analyzing completed meshes only.

The placement of a layer of fill is simulated by applying forces to represent the weight of the added layers. The newly placed layer is assigned very small modulus values to model the soil's low stiffness after placement. The layer is assigned stresses reflecting the overburden pressure at its center and lateral stresses using the at-rest earth pressure coefficient. The program assigns zero displacements to the surface nodal points such that the top layer will not show any settlement or deformations unless a loading condition is subsequently imposed.

If the loads being applied to the soil-structure system have very large magnitudes, it is recommended that these loads be applied in several increments to improve the accuracy of the hyperbolic model.

Each increment is analyzed twice, the first time using soil modulus values based on the initial stresses at the beginning of the increment, and the second time using the soil modulus values based on the average stresses during the increment.

Many types of elements have been implemented in this finite element program. This version includes, aside from the basic elements, structural elements (bars and beams), nodal links, interface elements, and pre-existing soil elements. The pre-existing soil elements may have their initial stresses generated by the user in the input if so desired. The program is capable of handling the placement of fill or structures on rigid or compressible foundations. Fill layers need not be horizontal and the surface of the wall can be given any geometric shape desired.

The program SSTIPN incorporates a new procedure from that of its predecessors for imposing desired boundary conditions. Although it greatly reduces computational time, it is not always possible to impose non-zero displacements to nodal points.

3.5 Parametric Study

3.5.1 Introduction

The contact zone between a spillway and the core of an embankment dam has always been an area of considerable concern in dam designs. The soil-concrete interaction, with such differing modulus values, as well as potential cracking and seepage, indicates the need to ensure a good transition zone. Many existing dams have based their design on precedence using:

- wide soil-concrete contact areas to ensure adequate stress distribution along the interface. Widening the core width and/or the spillway section would create this effect.
- smooth concrete surfaces to reduce localized stress concentrations due to irregularities on the wall. It also makes for better compaction of

the soil against the wall.

- no wingwalls or lateral walls are normally used for seepage measures. These walls hinder compaction of soil and can be compensated by adequate filter placement in the transition zone.
- wrap around of spillway wall using shoulders of the embankment section. This increases the seepage path and gives added contact between soil and structure.
- adequate filters downstream of the central core and along the downstream face of the spillway wall.
- near-vertical batters for better compaction near the wall and better soil-structure contact.

A typical spillway/embankment transition zone is shown in Figure 3.14. The section labelled A-A is representative of the type of profile being studied in the finite element meshes. The wall height is assigned a vertical height of 100 m throughout the analysis.

Although the interface being studied was actually a 3-Dimensional problem, the analysis was conducted using a 2-Dimensional plane strain finite element program. Due to time constraints and non-availablility of a more sophisticated program, the SSTIPN program was used. For a qualitative analysis, this was considered an adequate model. It is believed that the results would still be applicable to retaining wall problems.

3.5.2 Wall Inclination

To study the effect of the wall inclination, a few meshes (Figure 3.15 to 3.17) were used in the numerical analysis. Each of the meshes have been designed to resemble each other with respect to the elements and their overall geometry. A few of their common aspects are:

- 250 backfill elements in 10 construction layers.
- 50 foundation elements in 2 layers.
- 10 interface elements along the spillway-backfill contact.

The distance between the outer soil boundary and the base of the wall at the foundation level was kept constant in all meshes. Its length was assigned two and a half times the height of the wall to ensure that the outer boundary would not affect the stress state in the region near the wall.

The concrete structure is assumed completely unyielding, rigid and, since its internal stress distribution is not required in this analysis, only the interface boundary will be incorporated in the meshes.

The mesh simulates a construction sequence beginning with only the foundation material and adding a layer of backfill material in successive layers until the full height of the wall is reached. The interface elements is also placed progressively as each layer is added.

The nodal points along the mesh boundaries are not restricted from moving along their boundaries but are restrained from any movement normal to the boundary. This is analogous to having rollers at each of these nodal points. The ground surface (top nodal points) are not restricted in any way. Both bottom corners are fixed completely since they belong to both the vertical as well as the bottom boundary.

The nodal points along the interface, however, are an exception. Each of these points have actually two nodes, one attached to the soil element while the other belongs to the structure element. Both these nodes are linked together by the interface element. The structural nodes are fixed from all movement, whereas the soil elements have been given complete freedom of movement.

3.5.3 Interface Roughness

To observe the effect of wall roughness on the stresses and deformations in the soil mass adjacent to the concrete structure, three analyses were performed. The interfaces were assigned values regarding the characteristics of the interface as shown in Table 3.2. These values describe three distinct interfaces, I1, I2, and I3, ranging from perfectly smooth to perfectly rough. These parameters have been carefully selected as representative of these types of wall surfaces and compare well with parameter selections from similar studies. (Goodman et al., 1968; Clough and Duncan, 1971).

3.5.4 Foundation Compressibility

Three cohesionless materials have been selected to model the compressibility of the foundation. The hyperbolic parameters used to model the three compressibilities, F1, F2, and F3 are shown in Table 3.2. The parameters have been chosen such that the volumetric straining of each material differed in magnitude under compressive loading. These materials were selected to correlate well with cohesionless material parameters published (Clough and Duncan, 1971). The at-rest earth pressure coefficient K_o was calculated using Jaky's formulae. Typical stress-strain curves for these three materials are shown in Figure 3.18. These graphs were generated using a program which was developed to analyse a one element mesh subjected to increasing axial strains and incorporated an iterative procedure to calculate the corresponding stresses.

3.5.5 Backfill Materials

Silty clay materials were used for representing the earth embankment impervious core section. The hyperbolic parameters for materials B1, B2, and B3 are listed in Table 3.2 and their stress-strain curves are shown in Figure 3.19.

Chapter 4

Finite Element Results

4.1 General

The meshes detailed in Chapter 3 specified the geometry of the soil mass for use in the finite element simulation. The material properties of the interface, foundation, and backfill were given sets of numerical values as were indicated in Table 3.2.

Each possible combination of material selection was run through the finite element program. Since each of the four variables studied (e.g. foundation compressibility) has three sets of parameters to allow its material properties to vary slightly (e.g. F1, F2, F3), eighty-one different permutations resulted. In order to visualize the effect of various wall angles (e.g. W1, W2, W3), the interface, backfill, and foundation properties remained constant (e.g. I2, F2, B2) such that the three runs W1-I2-F2-B2, W2-I2-F2-B2, W3-I2-F2-B2 were compared. These runs can be abbreviated to 1222, 2222, and 3222 respectively. The figures presented hereunder contain three curves corresponding to each set of a particular variable while using the average values W2, I2, F2, or B2 for the remainder of the variables. The discussion which follows is merely to clarify the figures provided.

4.2 Soil-Structure Interface

4.2.1 Normal Stress

The normal stress is the stress component taken perpendicular to the wall surface. The distribution of normal stress is often considered linearly increasing with depth. The results shown in Figures 4.1 to 4.4 follow this general trend. The stress distribution does however have greater concentrations near the toe of the wall due to the proximity and influence of the foundation, and negligible stress magnitudes near the upper portion of the wall due to the newly placed layer's low overburden and stiffness. All the distributions seem to be greater than the K_o-line. This is probably due to the nonyielding nature of the wall, the presence of a compressible foundation material, and the rotation of the principal plane in the vicinity of the interface.

Variations in wall inclination (Figure 4.1) produces minor changes in the normal stress distribution and are distinguished by the slight increase in the normal stress associated with wall inclinations that present a gentler slope to the soil mass. Nonetheless, their distributions all have similar trends.

Figure 4.2 depicts the increase in the normal stress when the interface is given very low strength as in interface I1. This is due to the high displacements that occurs along the wall surface due to slipping when the shear stress reaches the ultimate strength of the interface.

The compressibility of the foundation seems to have insignificant influence on the normal stress, except close to the base of the wall. The very soft foundation (F1) tends to increase the normal stress in the lower portion of the wall as shown in Figure 4.3.

The use of different materials to be placed as backfill against the wall results in higher normal stresses when the soil being used has a low friction angle (Figure 4.4) These soils with low angles of internal friction develop high at-rest earth pressure coefficients and subsequently larger normal stresses.

4.2.2 Shear Stress

The shear stress, acting tangential to the wall surface, is presented in Figures 4.5 to 4.8. Their distributions should resemble a linearly increasing function where the maximum shear stress occurs near the lower center of the wall and the shear stress is negligible at the top as well as the bottom of the wall. An exception occurs when the shear stress acting along the interface exceeds the strength of the interface. In this instance, the shear stress on the wall takes the value of the shear strength at that particular wall height since the interface cannot support larger mobilized stresses than its ultimate strength. Slippage occurs so as to alleviate this excess stress.

As with the normal stress component, the differences in shear stress distribution due to variations in wall angles is negligible (Figure 4.5).

The influence of interface roughness does however demonstrate the failure of interface I1 in Figure 4.6. This interface was conceived to fail due to its low strength assigned to it. Large displacements along the interface due to the full strength mobilization when using interface I1 is anticipated.

Due to the relationship between normal and shear stresses, the increase in normal stresses at the toe of the wall due to a compressible foundation F1, as observed in Fig 4.3, induces a corresponding increase of shear stresses in this region as well (Figure 4.7).

The low friction angles of particular backfill materials decreases the magnitude of shear stresses since the wall friction angle is dependent of the soil's angle of internal friction. (i.e. $1/3\phi$ for I2). This is observed in Figure 4.8.

4.2.3 Principal Stress Rotation

The major principal stresses σ_1 and σ_3 usually act in the vertical and horizontal directions respectively for geostatic states of stresses with a horizontal ground surface. A progressive rotation of principal stresses does however occur through the soil mass as the soil element approaches the wall interface. The principal stress rotations shown in Figures 4.9 to 4.12

are representative of the principal stress inclination in the soil elements adjacent to the rigid concrete wall.

In Figure 4.9, the rotation of the principal planes tends to increase when the wall becomes vertical. Inclined walls reduce the rotation of the principal stresses near the interface.

The smooth interface I1 in Figure 4.10 clearly shows the lack of rotation due to the slippage near the interface. The slip state at the interface must suppress the stress rotations due to its friction free and roller type movement.

As with normal and shear stresses at the toe of the wall, soft foundations, such as F1, tend to increase the principal stress rotation in the lower wall regions. Figure 4.11 demonstrates the toe effect associated with compressib foundations.

Figure 4.12 demonstrates the lower stress rotations that result when using stiffer backfill materials (B2 and B3). Softer materials are considered more deformable and hence can develop large principal stress rotations.

4.2.4 Shear Displacements

The distribution of shear displacement along the interface is dependent on many factors. Its general shape however, remains constant throughout Figures 4.13 to 4.16. There are negligible displacements at the top and near the toe of the wall. Although very small displacements are apparent in the figures, noticeable movements occur only when the interface fails.

The inclination of the wall reduces shear displacements slightly; the 90° wall facilitates movement along the wall due to its vertical surface (Figure 4.13).

Figure 4.14 denotes the larger shear movements occurring when the smooth interface I1 is used. The relative displacements of an interface in slip mode reaches eight to ten times the displacement of a rough non-yielding interface.

Compressible foundations such as F1 do increase the shear displacements as shown in Figure 4.15 but their magnitudes are still rather negligible.

Stiff backfill materials have larger shear displacements than very soft silty clay soils (Figure 4.16) due to the higher shear stresses mobilized near the interface. This is also due to the higher cohesion allocated to the stiff backfill material B3.

4.3 Soil Mass Profile

4.3.1 Mobilized Shear Stress

Shear stresses develop in the soil mass adjacent to the wall due to the distribution of forces in the backfill and the deformations of the soil near the wall interface. The maximum shear stress value attainable at any point in the backfill is largely dependent on the normal pressure. The magnitude of the shear stress at any point can be stated as a fraction of the maximum achievable shear stress. The mobilized shear stress is defined as the ratio of the shear stress over the maximum shear stress and expressed as a percentage. Figures 4.17 to 4.20 show a typical profile through the soil mass taken at the mid-height of the wall. Although the mobilized shear stress magnitudes vary with depth, the general trend remains similar. Generally, large mobilized shear stresses are observed near the wall and are reduced to negligible values at distances greater than half to one full wall height away from the wall.

Variations in wall inclination (Figure 4.17) demonstrates the slight increase of mobilized shear stress for the vertical wall W3 than for inclined walls. Steep wall interfaces have larger shear displacements and larger mobilized shear stresses near the wall.

The smooth interface I1 in Figure 4.18 has very low mobilized shear stress near the wall surface due to the wall's inability to generate large shear stresses along the interface before slipping.

Compressible foundations such as F1 allow for larger strains to be present in the backfill and induce larger shear stresses through the soil mass as shown in Figure 4.19.

Figure 4.20 indicates the increase in shear stresses apparent in soft backfill materials due to the soil's smaller stiffness value.

4.3.2 Elastic Settlement Profile

The addition of successive uniform layers of fill increases the overburden pressure throughout the soil mass and induces settlement. Figures 4.21 to 4.24 illustrate the effects of having a rigid structure adjacent to a fill. The profiles were taken at the mid-height of the wall. The settlement of the fill increases with depth due to the overburden. There is no settlement on the surface of the fill and the deformations of the soil at the toe of the wall is due only to the compression of the foundation.

There is no appreciable settlement difference due to the variation in wall inclination (Figure 4.21). The displacements increase gradually from very small values near the wall to constant magnitudes a half to one full wall height away from the wall.

The smooth interface I1 allows an almost uniform settlement throughout the soil mass due to the slip state of the interface (Figure 4.22).

Foundation compressibility (Figure 4.23) demonstrates a major influence on settlement. The compressible foundation F1 substantially increases the settlement in the soil mass.

Figure 4.24 illustrates that the backfill material B1 has proportionately larger settlements than the stiffer backfills B2 or B3 due to the deformation properties of the fill material.

4.3.3 Principal Stress Ratio

The principal stress ratio σ_1/σ_3 is an indication of the magnitude of shear stresses and varies according to depth as well as distance away from the wall interface. The ratio is greatest at the concrete surface due to the presence of a rigid structure and the rotation of the principal plane near the wall. The ratio reduces rapidly to a constant value less than one full wall height away from the structure. Very little effect is produced by varying the wall inclination (Figure 4.25); however the very smooth interface I1 in Figure 4.26 reveals a very low ratio near the wall surface. Very compressible foundations, such as F1, vary the principal stress ratio from very large magnitudes near the interface to very low values with increasing distance from the wall (Figure 4.27). The use of different backfill materials yields wide variations in the principal stress ratio curves which can be associated primarily with the different initial K_o values of the materials (Figure 4.28).

4.3.4 Rotation of Principal Plane

The existence of a rigid structure adjacent to a deformable medium influences the state of stress in the soil mass near the soil-structure junction. This trend is noticeable up to half a wall height distance away from the concrete surface. The rotation of the principal plane throughout the soil mass profile is represented in Figures 4.29 to 4.32. Only the roughness of the interface (Figure 4.30) seems to influence the rotations to any significant effect. Due to the slip nature of the interface I1, the concrete wall leaves no impression upon the soil mass and the boundary condition along the wall surface is virtually nonexistent.

Chapter 5

Analysis & Discussion

5.1 General

Due to the nonlinearity of the soil and interface, the proximity of a compressible foundation, and the observed earth pressures resulting in magnitudes larger than K_o, an analysis conducted using the existing earth pressure theories is not feasible. A study examining the consequences of the results will be presented.

5.2 Shear Stiffness Coefficient

A study on the choice of the shear stiffness coefficient K_I was undertaken. Figures 5.1 to 5.4 show the influence of K_I. For these graphs, the run type

W2-I2-F2-B2 was used, but allowing K_I to vary according to the values stated in the legends. The normal stress is not affected by K_I (Figure 5.1). The increase shown for the low values of shear stiffness is due to the failure of the interface. Figure 5.2 clearly demonstrates the increase in shear stress mobilized due to the increasing friction. Figure 5.3 denotes the increase of principal stress rotations due to the increase in roughness of the interface elements. Figure 5.4 describes the progressively larger shear displacements associated with very low stiffness coefficients.

5.3 Zone of Influence

The finite element meshes developed for the parametric study extends the backfill material two and half wall heights from the toe of the wall to the farthest most boundary conditions implemented on the far wall. This ensures that the area near the concrete interface is not affected by the far wall and that the monitored behaviour represents only the effects of a rigid wall surface adjacent to a soil mass. Evidently, the concrete interface will not affect the soil mass at any large distance away from the interface but the extent of its influence zone remains unknown. Figures 5.5 to 5.8 show the zone of backfill influenced by the proximity of a rigid non-yielding concrete structure. The curves delineate an area in the adjacent soil that is affected by the presence of the wall. These curves trace points in the backfill which correspond to elements that have no shear stresses. These elements have no rotation of the principal plane and as such the major and minor principal stresses coincide with the vertical and horizontal stresses respectively.

Aside from a few exceptions, the influence zone can be contained within one wall height distance away from the wall interface. It is believed that a finite element mesh encompassing these influence zones would yield similar results as the observations obtained with the larger mesh. The far wall boundary conditions, however, would need to be considered.

5.4 Strain Vectors

The deformation behaviour of a soil mass near a concrete interface is shown in Figure 5.9. This profile is typical for most of the parametric materials used. The section shown was taken from the run type W2-I2-F2-B2. The major factor involved in the soil deformation is from the settlement of each layer due to the addition of consecutive layers of fill being placed in a construction type sequence. Notice the relatively small deformations near the top and bottom of the backfill profile. The largest displacements are observed near the center of the fill height and far away from the influence of the wall. The soil mass near the wall has very small displacements. In addition, there is a gradual rotation pattern developing in the direction of straining of the soil mass as it nears the wall and the foundation region. The effect of the wall is noticeable up to a full wall height distance away from the interface. Figure 5.10 shows the deformation pattern for the smooth interface I1 in the soil mass. It is evident that the friction free surface of the soil-concrete interface allows a more uniform settlement to take place in the soil mass with minimal rotations of these vectors.

5.5 Major Principal Stress Contours

To illustrate further the behaviour of the backfill near the wall, Figure 5.11 shows the contour levels of the major principal stress σ_1 in the soil mass. The effect is also noticeable up to one full height in distance away from the wall surface and more pronounced at lower depths. The reduction in the major principal stress near the wall is due to the rotation of the principal axis close to the wall.

5.6 90^o Wall Analysis

Figure 5.12 shows the comparison between the classical lateral earth pressure coefficients and the actual normal stress acting against the concrete interface. It is observed that the pressure against the wall surface is greater than the at-rest state estimate and tends towards the passive pressure. The lateral earth pressure coefficients for each normal stress distribution is listed in the legend. These coefficients take into account the wall friction angle. It is believed that the high normal stress near the wall surface is due to the characteristics of the concrete wall. The rigid non-yielding nature of the wall may be associated with the intermediate passive state of the backfill. Note the reduction in normal stress near the toe of the wall for the case when a completely rigid foundation is used instead of a compressible medium.

5.7 Application of Resultant Thrust

For homogeneous soils with the ground water table at the surface, the lateral earth pressures have, in theory, a linearly increasing distribution. The resultant force applied to the wall is determined by the area of the triangle. This resultant thrust acts through the centroid of the triangle, located at H/3 from the base of the wall.

The location and magnitude of the resultant thrust for each run type are tabulated in Table 5.1. The very low centroids for all runs is readily apparent. The low normal stresses at the top of the wall due to the low straining after the placement of the final fill layer and its low stiffness value assigned, as well as the large stresses at the base of the wall due to the proximity of the foundation contribute to the low centroid for the application of the thrust force.

Inclined walls have larger thrust magnitudes due to the addition of a component of the weight of soil directly upon it. Smooth interfaces and compressible foundations allow settlement and compaction near the wall surface, thus increasing the lateral earth pressure. The difference in resultant forces for the backfill materials is due to their respective initial K_o values.

5.8 Summary of Parametric Study

The findings reported in Chapter 4 based on the finite element results are briefly summarized in Table 5.2. The synopsis indicates the increasing or decreasing trends that are apparent in response to variations in the parameters examined. The review allows the reader in essence to note the trend in soil-structure interaction when a specific parameter is altered.

Steeper wall inclinations do not benefit the contact zone with any appreciable advantages. A slight inclination is preferable to insure proper compaction near the wall surface and also increases the the normal stresses slightly.(Figure 4.1)

Very rough interface surfaces provide a decrease in deformations near the wall (Figure 4.14) and increase the shear stresses in this region thus ensuring a competent bonding of the soil to the wall interface. (Figure 4.6)

Incompressible foundations improve settlement problems in the soil mass (Figure 4.23) and along the interface (Figure 4.15) so as to reduce crest deformations.

Stiff impervious materials used in the core section of the embankment would certainly decrease the overall settlement in the soil mass (Figure 4.24) but will contribute large displacements along the soil-concrete interface (Figure 4.16). A silty clay material of medium stiffness is advised so as to develop proper adhesion of the soil to the interface and allowing for slightly larger settlements in the core material adjacent to the concrete surface.

Figures 5.13 to 5.20 are intended to demonstrate the difference between the most deformable case when using W3-I1-F1-B1 and its counterpart the least deformable soil medium with W1-I3-F3-B3. This comparison delineates the limits of maximum and minimum deformations possible in this analysis. Although all results are plotted, there is notable variations in shear displacements along the interface (Figure 5.16) due to the slip state of interface I1 and Figure 5.18 which shows the large settlements associated with the very deformable soil materials. The diverse curves shown on Figure 5.19 are representative of the various K_o values assigned to each respective backfill material.

5.9 Influence of Compaction

As discussed in Section 2.4, compaction-induced stresses remain in the soil mass as residual stresses due to a 'lock-in' mechanism. Although the finite element program SSTIPN cannot model transient loads, the effects of compaction on the normal stresses at the interface should be investigated. Figure 5.21 shows the difference in the normal stress distribution when taking the soil compaction in account. For this example, run 3222, with a vertical wall, was plotted along with the increase in normal stresses anticipated at the interface by using Seed's simplified bi-linear model presented in Section 2.4.4. The material property parameters required for this model were based on the information given for the backfill material B2 and are as follows:

$$\begin{aligned} K_o &= 0.455 \\ K_1 &= 2.98 \\ \alpha &= 0.56 \\ F &= 0.288 \\ K_3 &= 0.288 \end{aligned}$$

The peak compaction pressure profile was taken from Figure 2.25 using $X = 0.5$ feet with no foundation effects.

The observed increase in the normal stress distribution only affects the upper portion of the wall since in the lower portion the at-rest pressures exceed the compaction-induced stresses.

5.10 Hyperbolic Model Verification

In order to verify that the hyperbolic stress-strain relationship implemented in the finite element program actually modelled the soil behaviour as intended, the following test was performed.

A one cell element mesh with a given set of hyperbolic parameters, as presented in Section 3.2.4, was run on the finite element program.

The program output was used to plot the resulting stress-strain curve shown in Figure 5.22. For comparison and verification purposes, a short non-linear hyperbolic relationship was programmed on an IBM micro computer and, given the same hyperbolic parameters, yielded a stress-strain relationship which agreed well with the finite element program results. (Figure 5.22)

5.11 Case Study: Clough & Duncan (1971)

To validate the results obtained using the finite element program SSTIPN, an attempt was made to compare results with the findings of another finite element study conducted by Clough & Duncan (1971). A number of analyses were performed using the rigid wall and backfill system shown in Figure 5.23.

In the original paper, three analyses of walls rotating about their bases were studied, using the following assumptions regarding the characteristics of the interface bewteen the wall and the backfill:

	smooth	rough	perfectly rough
δ	0.1	24	35
K_I	1	40000	75000
n	0.0	1.0	1.0
R_f	1.0	0.9	0.9

The properties of the backfill used in the analyses were chosen to be representative of a medium dense sand. The values of the parameters assigned to the backfill were published as follows:

	backfill
γ (lb/ft^3)	100
K	720
n	0.5
R_f	0.8
c′(lb/ft^2)	0
ϕ'	35
K_o	0.43

Although each case investigated the rotation of the wall about its base, the graphs published also give results for the horizontal wall pressure for no outward deflection of the wall.

Using the same mesh as shown in Figure 3.17, without incorporating the foundation elements, the results for each case were plotted in Figures 5.24 to 5.26 along with the results by Clough & Duncan. For each wall interface, good correlation between runs produced by SSTIPN and the findings reported by the authors can be observed.

The apparent reduction in normal stresses observed for rough walls agrees well with the SSTIPN results in the thesis (Figure 4.2). The lack of variation in the curves reported by the authors may be attributed to the simplification of data points when assuming a straight line relationship for the at-rest cases.

Chapter 6

Conclusions

6.1 General

This parametric study of rigid non-yielding soil-concrete interfaces has lead to a number of interesting conclusions. Some of the most prominent of these results will be discussed in more detail in the section that follows. Techniques and analyses which were beyond the scope of the thesis will be mentioned later as a reference for readers attempting to research this problem further.

6.2 Conclusions

1. The presence of a compressible foundation affects the normal stresses only in the lower region of the wall but does however have a large influence on shear stresses and settlements in the soil mass adjacent to the interface.

2. The gradual inclination gradient of the principal stresses observed within one wall height of the concrete surface results in normal stresses greater than in the case when the major and minor principal stresses coincide with the vertical and horizontal directions respectively. Classical theories do include procedures for frictional wall cases but do not have any provisions for the increase apparent for the rotation of the principal plane.

3. The normal stress distributions obtained in the analyses closely follows the at-rest earth pressure coefficient for the upper half of the wall. In the lower regions of the wall, the earth pressure coefficients were greater than the at-rest value. The intermediate passive pressures apparent in the bottom half of the wall is believed to be attributed to the nonlinear stress-strain behaviour of the soil.

4. The location of the total thrust on the wall is found to be lower than expected. This is due to the large normal stresses near the toe of the wall caused by the presence of a compressible foundation and the intermediate passive earth pressures acting on the lower wall. The substantial increase in thrust can be accounted by the same reasons.

5. The zone of influence can be said to encompass a locale up to one wall height in distance away from the interface. In-situ measurements of the core material for pertinent information concerning the monitoring of the soil-concrete interface should be conducted in this region.

6. The use of a slightly inclined wall surface is advised so as to allow for proper compaction near the interface. A frictional concrete finish with an even surface will ensure proper bonding of the soil and reduce any local stress concentrations due to an irregularly shaped contact face. An incompressible and competent foundation is recommended to minimize the settlement in the core material of the dam. A fairly stiff clay material is advised for the central core selection.

7. The compaction stresses only affect the upper region of the wall whereas in the lower section of the wall the K_o distribution governs.

8. The hyperbolic relationship implemented on an IBM micro was found predict exactly the response from the finite element program SSTIPN.

9. The results between two finite element programs yielded comparable normal stresses, their differences being anticipated. The interface roughness has been shown to vary the normal stress distribution in the parametric study as well as the case study.

6.3 Recommendations for Future Research

1. Research incorporating a model for the development of compaction-induced stresses resulting from repeated loading and unloading can

be implemented. The progressive locked-in stresses would be induced by a hysteresis lateral earth pressure model.

2. The use of a 3-dimensional program to study the effect of seepage forces which act normal to the dam axis should be undertaken.

3. Finite elements can be used to evaluate the optimal shape of the concrete interface. The surface would not be required to be planar.

References

AGGOUR, M. S., and BROWN, C. B., 1974. **The Prediction of Earth Pressure on Retaining Walls due to Compaction**, Geotechnique, Vol. 24, No. 4, pp. 489–502.

ALPAN, I., 1967. **The Empirical Evaluation of the Coefficient K_O and K_{OR}**, Soils and Foundations, Japanese Soc. of SMFE, Vol. 7, No. 1, pp. 31–40.

ARTHUR, J. R. F., CHUA, K. S., DUNSTAN, T., and RODRIGUEZ, J. I., 1980. **Principal Stress Rotation: A Missing Parameter**, Journal of Geotech. Eng., Proc. ASCE, Vol. 106, No. GT4.

BANG, S., 1985. **Active Earth Pressure Behind Retaining Walls**, Journal of Geotech. Eng., Proc. ASCE, Vol. 111, No. 3, pp. 407–418.

BAUER, G. E., 1967. **Stresses and Deformations on Braced Cuts in Sand**, PhD Thesis, University of Ottawa, Ottawa.

BEIER, H., SCHADE, D., and LORENZ, W., 1979. **Penetration of Impervious Earth Cores by Structures.** 13th International Congress on Large Dams, New Delhi, pp. 221-232.

BRANDT, J. R., 1985. **Behaviour of Soil-Concrete Interfaces.** PhD Thesis, University of Alberta, Edmonton.

BROMS, B. B., 1971. **Lateral Earth Pressures Due to Compaction of Cohesionless Soils**, Proc. 2nd Budapest Conf. SMFE, pp. 373-384.

BROMS, B. B., and INGELSON, I., 1972. **Lateral Earth Pressure on a Bridge Abutment**, Proc. 5th European Conf. SMFE, Madrid, Vol. 1, Theme 1, pp. 117-123.

BROOKER, E. W., and IRELAND, H. O., 1965. **Earth Pressures at Rest Related to Stress History**, Canadian Geotech. Journal, Vol. 2, pp. 1-15.

Canadian Foundation Engineering Manual, 1985., 2nd Edition, Canadian Geotechnical Society.

CARTER, M., 1981. **Geotechnical Engineering Handbook**, Pentech Press.

CAQUOT, A., and KERISEL, J., 1966. **Traite de Mecanique des Sols**, 4th Edition, Gauthier-Villars.

CASAGRANDE, L., 1973. **Comments on Conventional Design of Retaining Structures**, Journal of Soil Mechanics and Foundations Div., Proc. ASCE, Vol. 99, No. SM2, pp. 181–198.

CHEN, R., 1986. **Finite Element Modelling of Interface Behaviour in Geologic Media**, PhD Thesis, University of West Virginia, Morgantown.

CHEN, W. F., and BALADI G. Y., 1985. **Soil and Plasticity: Theory and Implementation**, Elsevier Science Publishers.

CLOUGH, G. W., and DUNCAN, J. M., 1971. **Finite Element Analyses of Retaining Wall Behaviour**, Journal of Soil Mechanics and Foundations Div., Proc. ASCE, Vol. 97, No. SM12, pp. 1657–1673.

COOKE, J. B., 1984. **Progress in Rockfill Dams**, Journal of Geotech. Eng., Proc. ASCE, Vol. 110, No. 10.

COYLE, H. M., and BARTOSKEWITZ, R. E., 1976. **Earth Pressure on Precast Panel Retaining Wall**, Journal of Geotech. Eng., Proc. ASCE, Vol. 102, No. GT5, pp. 441–456.

CRAIG, R. F., 1978. **Soil Mechanics**, 2^{nd} Edition, Van Nostrand Reinhold (UK) Co. Ltd.

DE MELLO, V. F. B., 1977 **Reflections on Design Decisions of Practical Significance to Embankment Dams**, Geotechnique, Vol. 27, No.

3, pp. 279–355.

DESAI, C. S., and CHRISTIAN, J. T., 1977. **Numerical Methods in Geotechnical Engineering**, McGraw-Hill.

DESAI, C. S., and SARGAND, S., 1984. **Hybrid FE Procedure for Soil-Structure Interaction**, Journal Geotech. Eng., Proc. ASCE, Vol. 110, No. 4, pp. 473–486.

DESAI, C. S., and SIRIWARDANE, H. J., 1984. **Constitutive Laws for Engineering Materials**, Prentice-Hall Inc., New Jersey.

DRNEVICH, V. P., 1975. **Constrained and Shear Moduli for Finite Elements**, Journal of Geotech. Eng., Proc. ASCE, Vol. 101, No. GT5, pp. 459–473.

DUNCAN, J. M., BYRNE, P., WONG, K. S., and MABRY, P., 1978. **Strength, Stress-Strain and Bulk Modulus Parameters for Finite Element Analyses of Stresses and Movements in Soil Masses**, National Science Foundation, Report No. UCB/GT/78-02, University of California, Berkeley.

DUNCAN, J. M., and SEED, R. B., 1986. **Compaction-Induced Earth Pressures Under K_o-Conditions**, Journal of Geotech. Eng., Proc. ASCE, Vol. 112, No. 1, pp. 1–23.

EISENSTEIN, Z., and BRANDT, J. R. T., 1985. **Soil-Concrete Interaction Test Facility**, 15th International Congress on Large Dams, Lausanne.

GOODMAN, R. E., TAYLOR, R. L., and BREKKE, T. L., 1968. **A Model for the Mechanics of Jointed Rocks**, Journal of Soil Mechanics and Foundations Div., Proc. ASCE, Vol. 94, No. SM3, pp. 637–659.

GUDEHUS, G., 1977. **Finite Elements in Geomechanics**, John Wiley and Sons, London.

HANDY, R. L., 1985. **The Arch in Soil Arching**, Journal of Geotech. Eng., Proc. ASCE, Vol. 111, No. 3, pp. 302–318.

HARDIN, B. O., and DRNEVICH, V. P., 1972. **Shear Modulus and Damping in Soils: Measurement and Parameter Effects**, Journal of Soil Mechanics and Foundations Div., Proc. ASCE, Vol. 98, No. SM6, pp. 603–625.

HARDIN, B. O., 1983. **Plane Strain Constitutive Equations for Soils**, Journal Geotech. Eng., Proc ASCE, Vol. 109, No. 3, pp. 388–407.

HENDRON, A. J., 1963. **The Behaviour of Sand in One-Dimensional Compression**, PhD Thesis, Dept. of Civil Eng., University of Illinois.

HOLTZ, R. D., and KOVACS, W. D., 1981. **An Introduction to Geotechnical Engineering**, Prentice-Hall Inc., New Jersey.

INGOLD, T. S., 1979(a). **Retaining Wall Performance During Backfilling** Journal of Geotech. Eng., Proc. ASCE, Vol. 105, No. GT5, pp. 613–626.

INGOLD, T. S., 1979(b). **The Effects of Compaction on Retaining Walls**, Geotechnique, Vol. 29, No. 3, pp. 265–283.

JAKY, J. 1944. **The Coefficient of Earth Pressure at Rest**, Journal for Society of Hungarian Architects and Engineers, Budapest, Hungary, pp. 355–358.

JAMES, R. G., SMITH, I. A. A., and BRANSBY, P. L., 1972. **The Prediction of Stresses and Deformations in a Sand Mass Adjacent to a Retaining Wall**, Proc. 5th European Conf. SMFE, Madrid, Vol. 1, Theme 1, pp. 39–46.

JANSSON, H., WICKERT, A., and RINKERT, A., 1948. **Earth Pressures Against Retaining Walls**, Proc. 2nd Int'l Conf. on Soil Mech., Rotterdam, Vol. 2, pp. 71–76.

JANBU, N., 1972. **Earth Pressure Computations in Theory and Practice**, Proc. 5th European Conf. SMFE, Madrid, Vol. 1, Theme 1, pp. 47–54.

JAPPELLI, R., BALDOVIN, G., BERTI, P., DOLCIMASCOLO, F., and MUSSO, A., 1979. **Behaviour of a Core-Spillway Block Contact During Construction and Operation**, 13th International Congress on

Large Dams, New Delhi, pp. 1107–1120.

JIN, B. I., and LEE, S. Y., 1979. **Design of Interface in Composite Type Dam,** 13^{th} International Congress on Large Dams, New Delhi, pp. 823–846.

JONES, C. J. F. P., 1975. **Earth Pressures Against the Abutments and Wing Walls of Standard Motorway Bridges,** Geotechnique, Vol. 25, No. 4, pp. 731–742.

KEZDI, A., 1972. **Earth Pressure Measurements,** Proc. 5^{th} European Conf. SMFE, Madrid, Vol. 1, Theme 2, pp. 157–162.

LEE, I. K., and HERINGTON, J. R., 1972. **Effect of Wall Movement on Active and Passive Pressures,** Journal of Soil Mechanics and Foundations Div., Proc. ASCE, Vol. 98, No. SM6, pp. 625–640.

MATSUO, M., KENMOCHI, S., and YAGI, H., 1978. **Experimental Study on Earth Pressure of Retaining Wall by Field Tests,** Soils and Foundations, Japanese Soc. of SMFE, Vol. 18, No. 3, pp. 27–41.

MATTEOTTI, G., 1978. **Some Results of Quay-Wall Model Tests on Earth Pressure,** Proc. Institute of Civil Eng., 47, pp. 185–204.

MAYNE, A. M., and KULHAWY, FRED H., 1982. **K_o-OCR Relationship in Soil,** Journal of Soil Mechanics and Foundations Div. Proc. ASCE, Vol. 108, No. GT6, pp. 851–872.

MICHELS, V. S., and DICKSON, R. S., 1979. **Dam Abutment and Core-Filter Interfaces Dartmouth Dam, Australia**, 13^{th} International Congress on Large Dams, New Delhi, pp. 563–590.

NAKAI, T., 1985. **Finite Element Computations for Active and Passive Earth Pressure Problems of Retaining Wall**, Soils and Foundations, Japanese Soc. of SMFE, Vol. 25, No. 3, pp. 98–112.

PALMERTON, J. B., and LEFEBVRE, G., 1972. **Three-Dimensional Behaviour of a Central Core Dam.**, U.S. Army Engineer Waterways Experiment Station, Research Report S-72-1, Vicksburg, Mississippi.

PANT, B., 1979. **Fundamental Aspects of Dam-Foundation Interface Problems in Relation to some Gravity Dams in India**, 13^{th} International Congress on Large Dams, New Delhi, pp. 895–912.

PENMAN, A. D. M., and CHARLES, J. A., 1979. **The Influence of Their Interfaces on the Behaviour of Clay Cores In Embankment Dams**, 13^{th} International Congress on Large Dams, New Delhi, pp. 695–714.

QUIGLEY, D. W., and DUNCAN, J. M., 1978. **Earth Pressures on Conduits and Retaining Walls**, U.S. Army Engineer Waterways Experiment Station, Report No. UCB/GT/78-06, University of California, Berkeley.

RADUKIC, V., 1979. **Observed Behaviour of Embankment Dams at some Typical Interfaces**, 13th International Congress on Large Dams, New Delhi, pp. 1005–1022.

REHNMAN, S. E., and BROMS, B. B., 1972. **Lateral Pressures on Basement Wall. Results from Full-scale Tests**, Proc. 5th European Conf. SMFE, Madrid, Vol. 1, Theme 2, pp. 189–197.

ROWE, P. W., 1954. **A Stress-Strain Theory for Cohesionless Soil with Applications to Earth Pressures At-Rest and Moving Walls**, Geotechnique, Vol. 4, No. 2, pp. 70–88.

ROWE, P. W., 1969. **Progressive Failure and Strength of a Sand Mass**, Proc. 7th Int'l Conf. SMFE, Mexico City, Vol. 1, pp. 341–349.

RYMSZA, B., 1979. **Pression des Terres au Repos en Conception des Constructions de Soutenement**, Design Parameters in Geotech. Eng., BGS, London, Vol. 1, pp. 247–248.

SCHMIDT, B., 1967. **Lateral Stresses in Uniaxial Strain**, Bulletin No. 23, The Danish Geotechnical Institute, Copenhagen, Denmark, London, Vol. 1, pp. 5–12.

SEED, R. B., 1983. **Soil-Structure Interaction Effects of Compaction-Induced Stresses and Deflections**, PhD Thesis, University of California, Berkely.

SEED, R. B., and DUNCAN, J. M., 1986. **FE Analyses: Compaction-Induced Stresses and Deformations**, Journal of Geotech. Eng., Proc. ASCE, Vol. 112, No. 1, pp. 23–43.

SEEMEL, R. N., and PARE, J.-J., 1979. **Embankment Dams, Interface with Foundations and Adjoining Structures**, 13^{th} International Congress on Large Dams, New Delhi, pp. 125–140.

SHERIF, M. A., ISHIBASHI, I., and LEE, C. D., 1982. **Earth Pressures Against Rigid Retaining Walls**, Journal of Geotech. Eng., Proc. ASCE, Vol. 108, No. GT5, pp. 679–695.

TAYLOR, D. W., 1948. **Fundamentals of Soil-Mechanics**, John-Wiley & Sons.

TERZAGHI, K., 1934 **Large Retaining Wall Tests**, Engineering News Record, Vol. 3, pp. 136–140.

VAUGHAN, P. R., and KENNARD, M. F., 1972. **Earth Pressures at a Junction Between an Embankment Dam and a Concrete Dam**, Proc. 5^{th} European Conf. SMFE, Madrid, Vol. 1, Theme 2, pp. 215–221.

VIOTTI, C. B., and DE AVILA, J. P., 1979. **Some Conceptual Aspects Between Embankment and Concrete Dams and Experimental Data from São Simão Dam**, 13^{th} International Congress on Large Dams, New Delhi, pp. 779–796.

YUDHBIR, V. A., 1974. **Active Earth Pressure Analysis Using Relevant Soil Modulus**, Soils and Foundations, Japanese Soc. of SMFE, Vol. 14, No. 2, pp. 89–95.

ZAMAN, M. M., and DESAI, C. S., 1983. **Models for Sliding and Separation at Interfaces Under Static and Cyclic Loading**, Proc. International Conference on Constitutive Laws for Engineering Materials, Tucson, Arizona, pp. 383–390.

Tables

Cell No.	P_c	Measured Pressures kN/m²				P_{CC}/P_c
		P_{CA}	P_{CB}	P_{CC}	[illegible]	
1	470	364	312	[illegible]	[illegible]	0.72
2	364	266	222	244	[illegible]	0.67
3	259	189	165	179	[illegible]	0.69
4	159	93	123	108	[illegible]	0.68
5	369	133	104	119	78	0.32

Table 2.1: Pressures Measured at the End of Construction at Cow Green Dam. Vaughan & Kennard (1972)

Pressures measured in kN/m².

	End of construction					One year after impounding		
Cell N°	$\gamma \cdot H$	P	u	P′	$P'/\gamma \cdot H$	P	u	P′
1	990	140	15	125	0.14	440	415	25
2	910	320	0	320	0.35	140	4	136
3	1 050	380	27	353	0.34	510	298	212
4	1 050	180	27	153	0.15	390	298	92
5	400	80	0	80	0.20	230	129	101
6	420	100	0	100	0.24	130	13	117
7	360	60	—	60	0.17	120	—	120

(γ) Unit weight of the soil in kN/m³ : γ core = 21, γ gravel = 22, γ sand = 18.	(γ) *Poids spécifique du sol en kN/m³ :* γ *noyau = 21,* γ *gravier = 22,* γ *sable = 18.*
(H) Height of fill over the cell.	(H) *Hauteur du remblai sur la cellule.*
(P) Total pressure.	(P) *Pression totale.*
(u) Pore pressure.	(u) *Pression interstitielle.*
(P′) Effective pressure.	(P′) *Pression effective.*

Table 2.2: Pressures Measured Along Interface at the São Simão Dam After Construction. Viotti & De Avila (1979)

NON-LINEAR K_0-LOADING/UNLOADING MODEL PARAMETERS

Parameter	Name	Recommended Limits	Method of Estimation Based on ϕ'
α	Unloading Coefficient	$0 \le \alpha \le 1$	See Figure 3-6 for relationship between α and $\sin\phi'$
β	Reloading Coefficient	$0 \le \beta \le 1$	Assume $\beta \approx 0.6$
K_0	Coefficient of At-Rest Lateral Earth Pressure for Virgin Loading	$0 \le K_0 \le 1$	$K_0 \approx 1 - \sin\phi'$
$K_{1,\phi'}$	Frictional Component of Limiting Coefficient of At-Rest Lateral Earth Pressure for Unloading	$K_0 \le K_{1,\phi'} \le K_p$	$K_{1,\phi'} \approx \tan^2 (45 + \phi'/2)$
c'	Effective Stress Strength Envelope Cohesion Intercept	--	--

Note: K_1 = Limiting Coefficient of At-Rest Lateral Earth Pressure for Unloading.

$\sigma'_{h,lim} = K_1 \sigma_v'$ and $K_1 = K_{1,\phi'} + \frac{2c'}{\sigma_3'} \sqrt{K_{1,\phi'}}$

K_p = Coefficient of Passive Lateral Earth Pressure

Table 2.3: Non-Linear K_o-Loading/Unloading Model Parameters. Seed R. B. (1983)

Parameter	Name	Function
K, K_{ur}	Modulus number	Relate E_i and E_{ur} to σ_3
n	Modulus exponent	
c	Cohesion intercept	Relate $(\sigma_1-\sigma_3)_f$ to σ_3
ϕ, $\Delta\varphi$	Friction angle parameters	
R_f	Failure ratio	Relates $(\sigma_1-\sigma_3)_{ult}$ to $(\sigma_1-\sigma_3)_f$
K_b	Bulk modulus number	Value of B/P_a at $\sigma_3 = P_a$
m	Bulk modulus exponent	Change in B/P_a for ten-fold increase in σ_3

Table 3.1: Summary of the Hyperbolic Parameters.Duncan et al. (1978)

WALL ANGLE	W1	W2	W3
θ	80	85	90

INTERFACE	I1	I2	I3
	smooth	abrasive	rough
c_a (KN/m^2)	0	25	50
δ	0.1	$1/3\phi$	$2/3\phi$
$\Delta\delta$	0	0	0
K_I	10	40000	75000
K_{Iur}	20	80000	150000
n	0.0	1.0	1.0
R_f	1.0	0.9	0.9

FOUNDATION	F1	F2	F3
	compressible	average	incompressible
γ (KN/m^3)	20	20	20
K	50	200	1000
n	0.5	0.5	0.5
R_f	1.0	1.0	1.0
K_b	100	400	2000
m	0.15	0.25	0.5
c'(KN/m^2)	0	0	0
ϕ'	30	40	50
$\Delta\phi'$	0	0	0
K_o	0.50	0.36	0.23

BACKFILL	B1	B2	B3
	soft	medium	stiff
γ (KN/m^3)	20	20	20
K	50	400	1200
n	0.4	0.5	0.6
R_f	0.7	0.8	0.9
K_b	100	300	600
m	0.20	0.50	0.25
c'(KN/m^2)	5	25	50
ϕ'	30	33	35
$\Delta\phi'$	0	0	0
K_o	0.50	0.45	0.43

Table 3.2: Summary of Material Properties for Parametric Study

RUN TYPE	DEPTH (m)	CENTROID (m)*H	MAGNITUDE (kN)
VARIATION OF WALL ANGLE			
1222	71.226	0.288	66728
2222	74.077	0.259	62592
3222	72.814	0.272	60179
INTERFACE ROUGHNESS			
2122	68.756	0.312	75897
2222	74.077	0.259	62592
2322	73.551	0.264	61342
FOUNDATION COMPRESSIBILITY			
2212	79.875	0.201	65069
2222	74.077	0.259	62592
2232	73.123	0.269	60655
BACKFILL MATERIALS			
2221	70.372	0.296	71817
2222	74.077	0.259	62592
2223	73.501	0.265	54055

Table 5.1: Application of Lateral Thrusts.

	W1 ⇝ W3			I1 ⇝ I3			F1 ⇝ F3			B1 ⇝ B3		
	D	N	I	D	N	I	D	N	I	D	N	I
ALONG INTERFACE												
Normal Stresses	√			√				√		√		
Shear Stresses		√				√*		√				√
Principal Stress Rotation			√			√*		√		√		
Shear Displacements			√	√*			√*					√*
IN SOIL MASS												
Mobilized Shear Stresses		√				√*	√			√		
Settlement		√		√*			√*			√*		
Principal Stress Ratio		√				√	√					√*
Principal Stress Rotation		√				√	√			√		

D	Decreasing Trend
N	Negligible Effect
I	Increasing Trend
*	Major Influence

Table 5.2: Summary of Parametric Study.

Figures

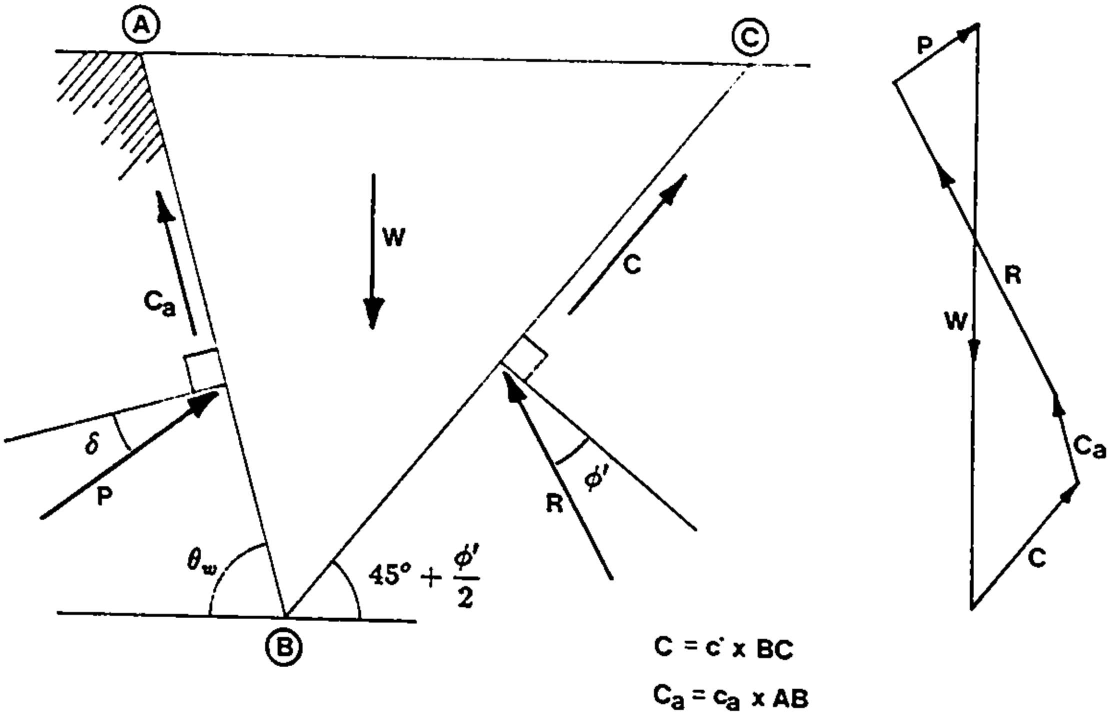

Figure 2.1: Active Soil Wedge Behind Retaining Wall and Force Polygon Diagram.

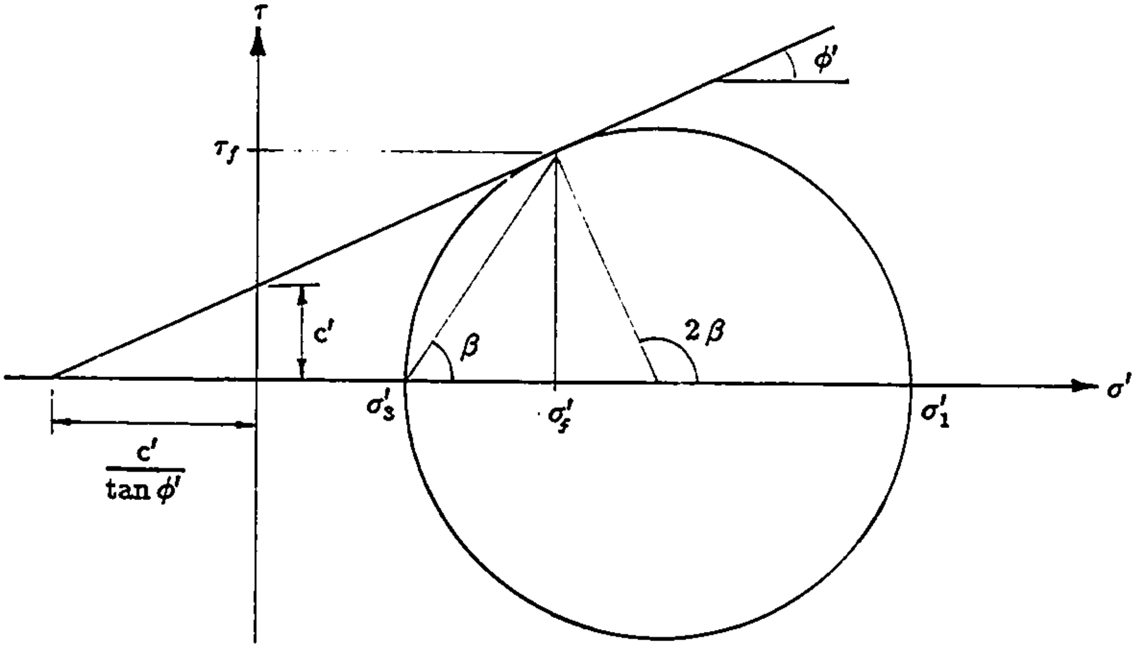

Figure 2.2: Typical Mohr-Coulomb Failure Envelope.

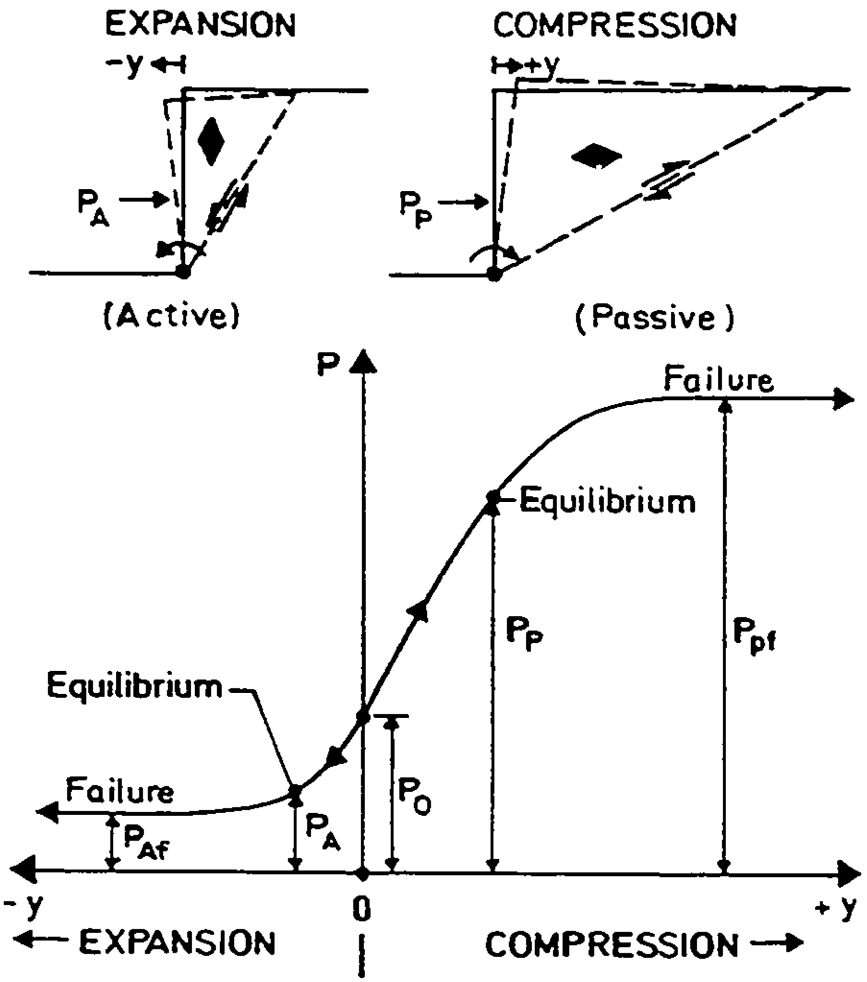

Figure 2.3: Definition of Earth Pressures at Equilibrium and At-Rest. Janbu (1972)

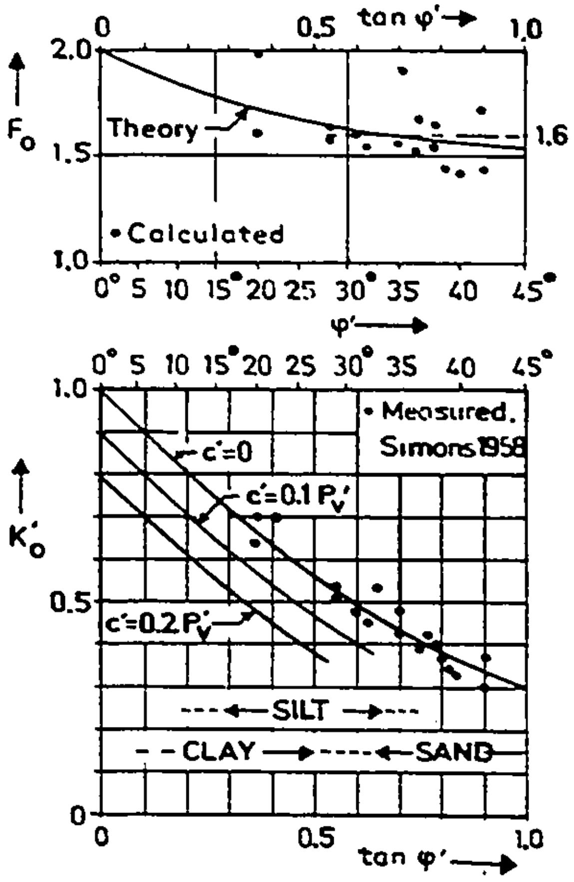

Figure 2.4: Coefficient of Earth Pressure At-Rest, for NC Soils. Janbu (1972)

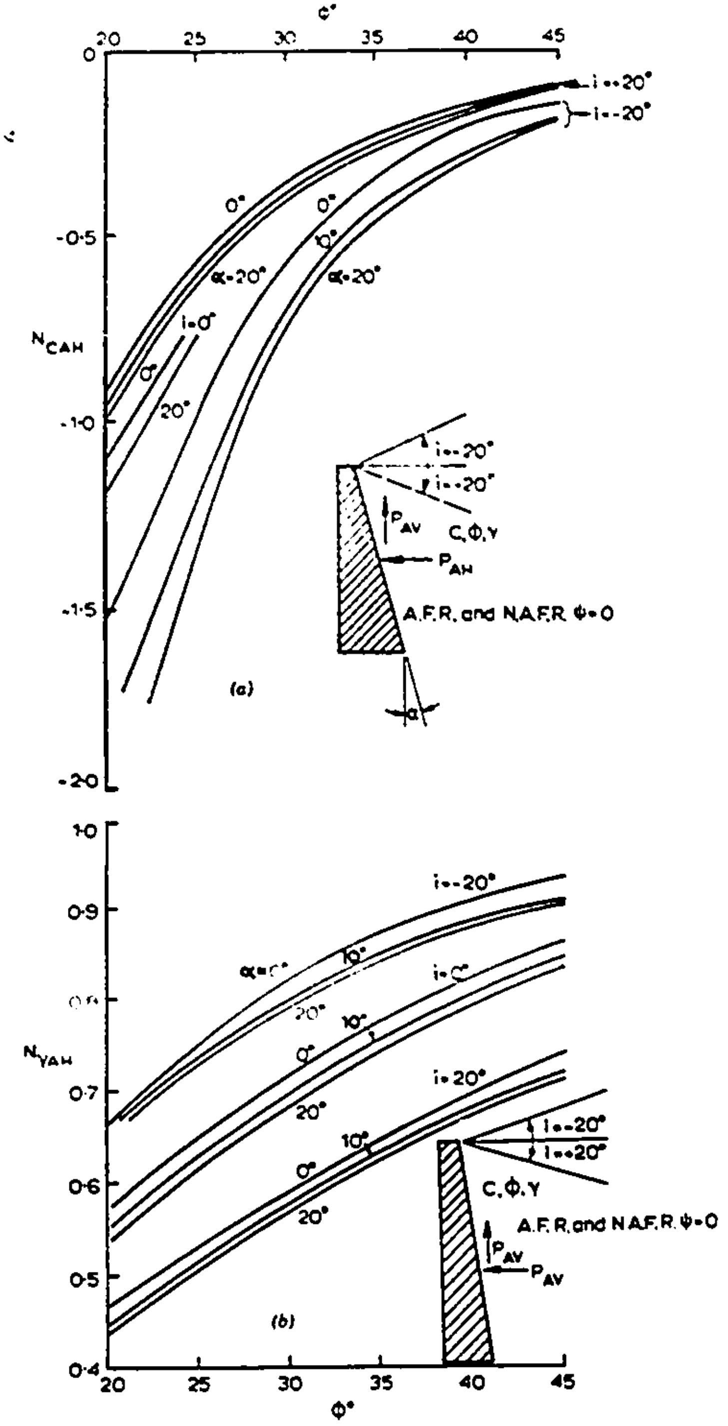

Figure 2.5: Values of Active Thrust Factors N_{cAH} and $N_{\gamma AH}$. Lee & Herington (1972)

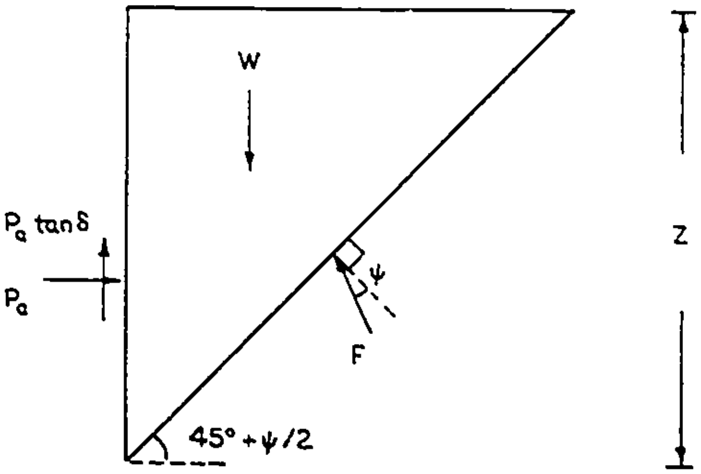

Figure 2.6: Free Body Diagram of an Active Soil Wedge. Bang (1985)

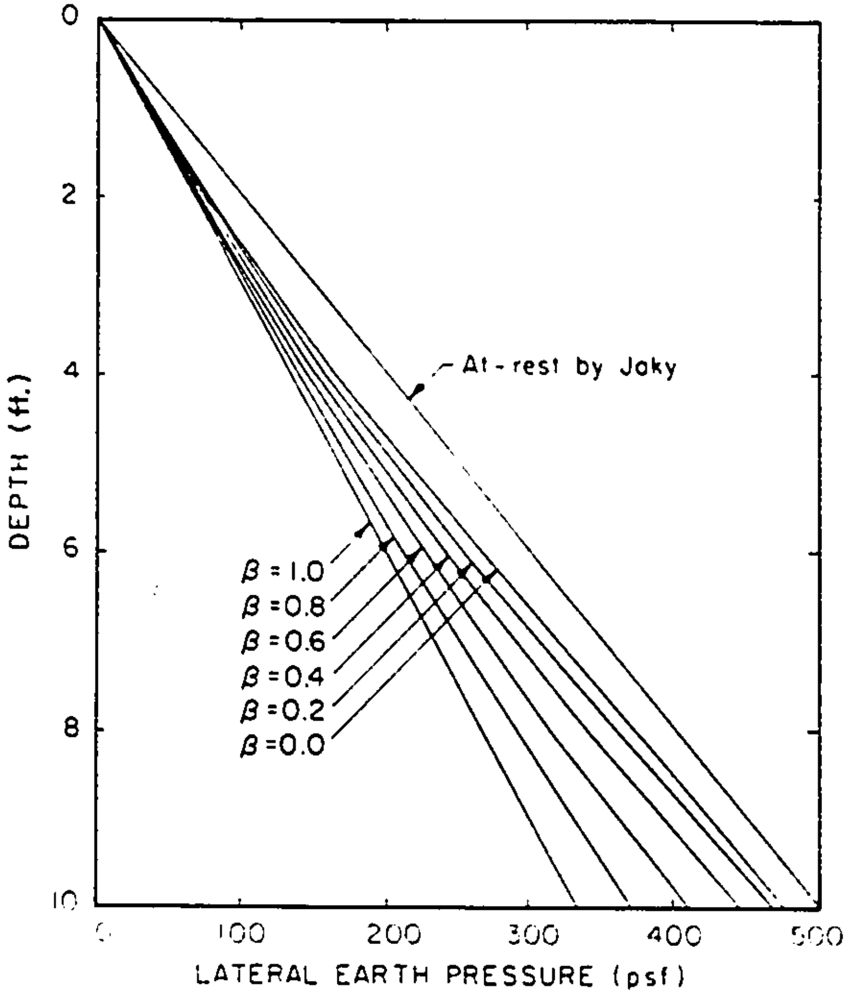

Figure 2.7: Variation of Lateral Earth Pressures. Bang (1985)

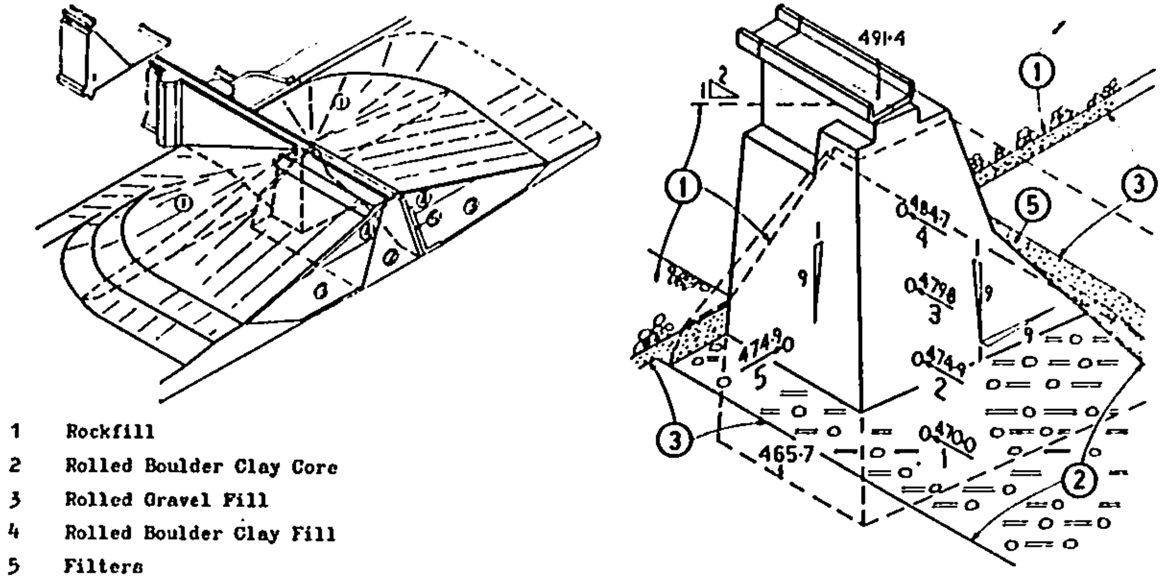

Figure 2.8: Arrangement of the Cow Green Junction and the Location of the Instruments. Vaughan & Kennard (1972)

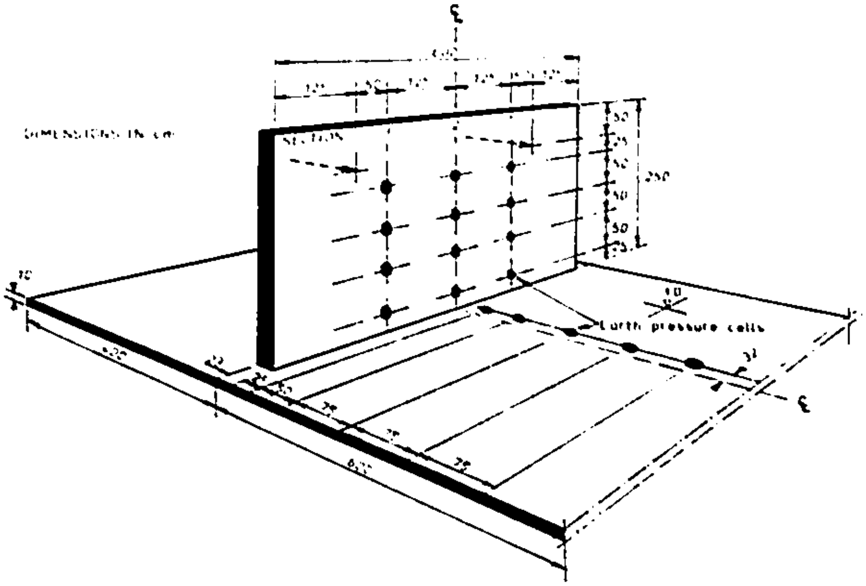

Figure 2.9: Dimensions of Experimental Wall and Location of Earth Pressure Cells. Rehnman & Broms (1972)

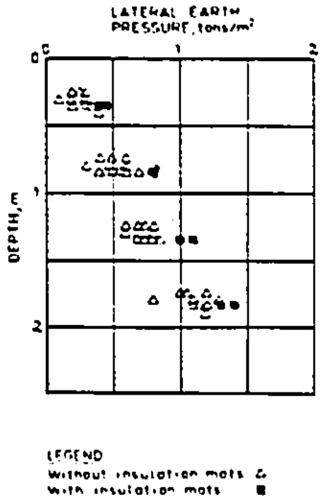

Figure 2.10: Measured Earth Pressure Distribution in a Loosely Placed Backfill of Gravelly Sand. Rehnman & Broms (1972)

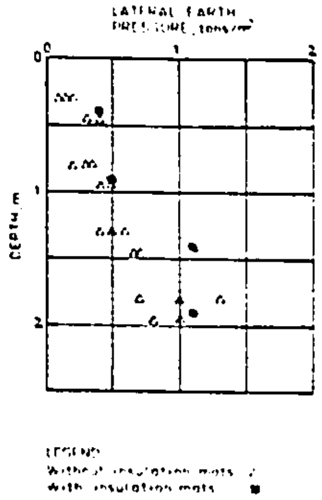

Figure 2.11: Measured Earth Pressure Distribution in a Loosely Placed Backfill of Silty Fine Sand. Rehnman & Broms (1972)

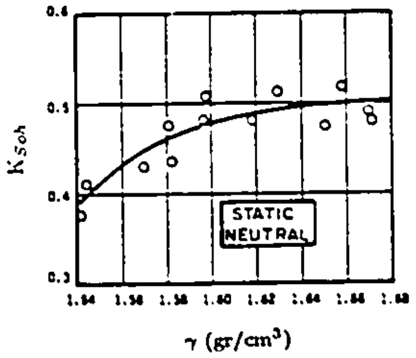

Figure 2.12: Variation of Earth Pressure Coefficient with Soil Densification. Sherif et al. (1982)

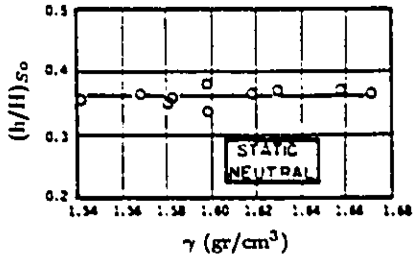

Figure 2.13: Experimental $(h/H)_{so}$ Values versus Soil Density. Sherif et al. (1982)

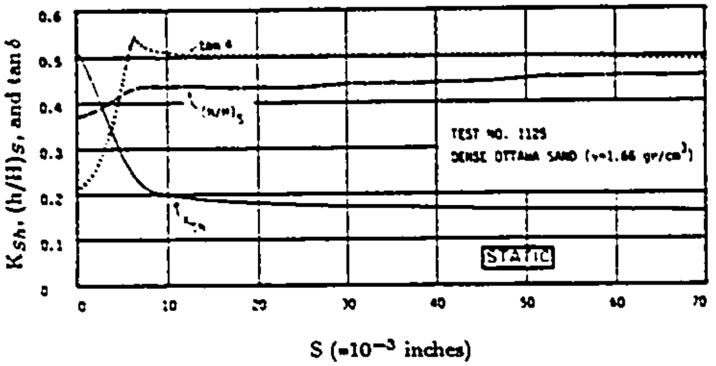

Figure 2.14: Lateral Earth Pressure Coefficient K_{sh}, Height of Resultant Pressure Application $(h/H)_s$, and Coefficient of Wall Friction $\tan\delta$ versus Wall Displacements S. Sherif et al. (1982)

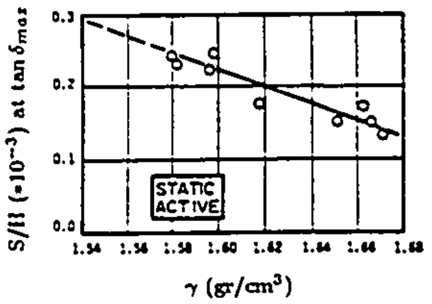

Figure 2.15: Wall Displacements at $\tan\delta_{max}$ versus Soil Density. Sherif et al. (1982)

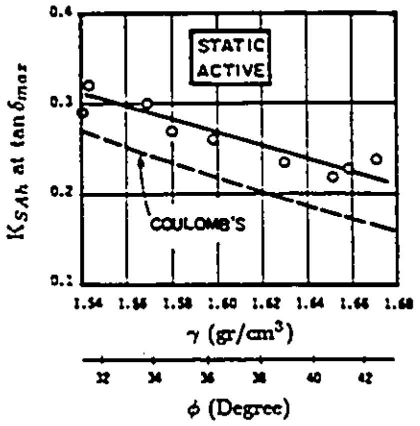

Figure 2.16: Experimental K_{SAh} Values at $\tan\delta_{max}$ versus Soil Density and Angle of Internal Friction. Sherif et al. (1982)

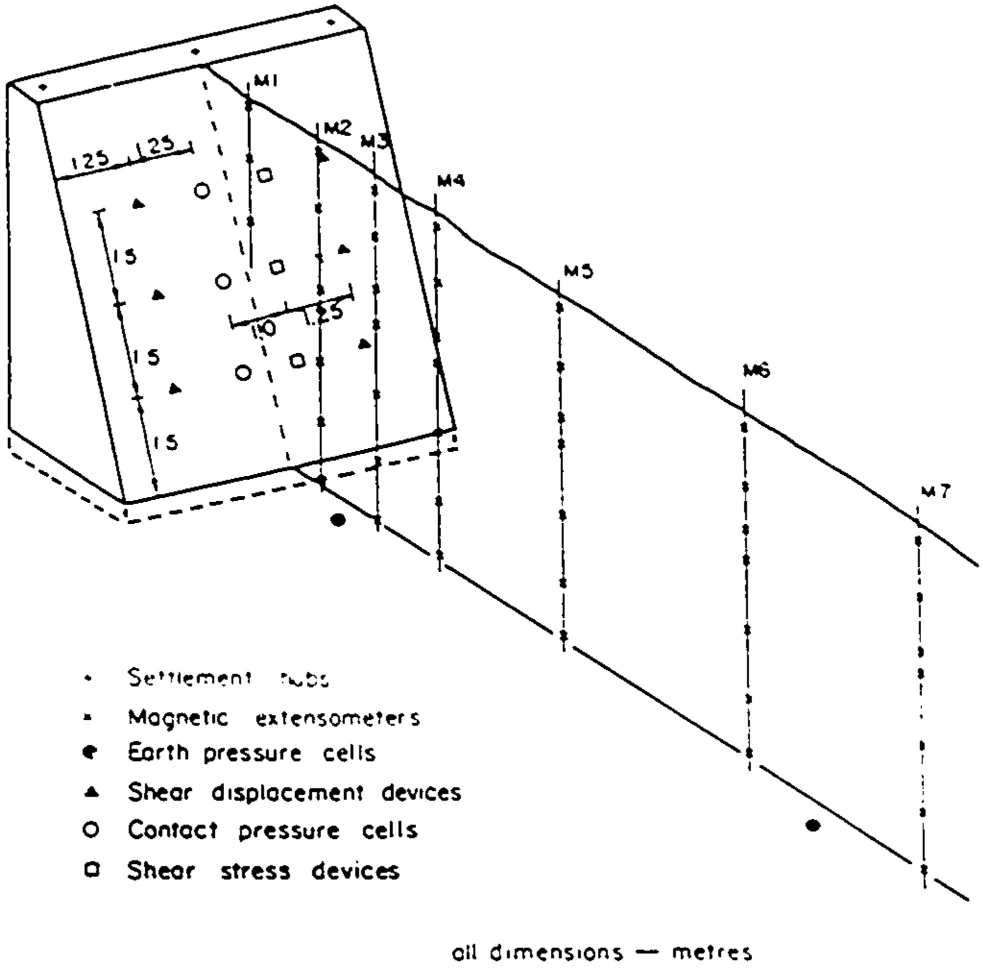

Figure 2.17: General View of Wall Instrumentation at Dickson Dam. Brandt (1985)

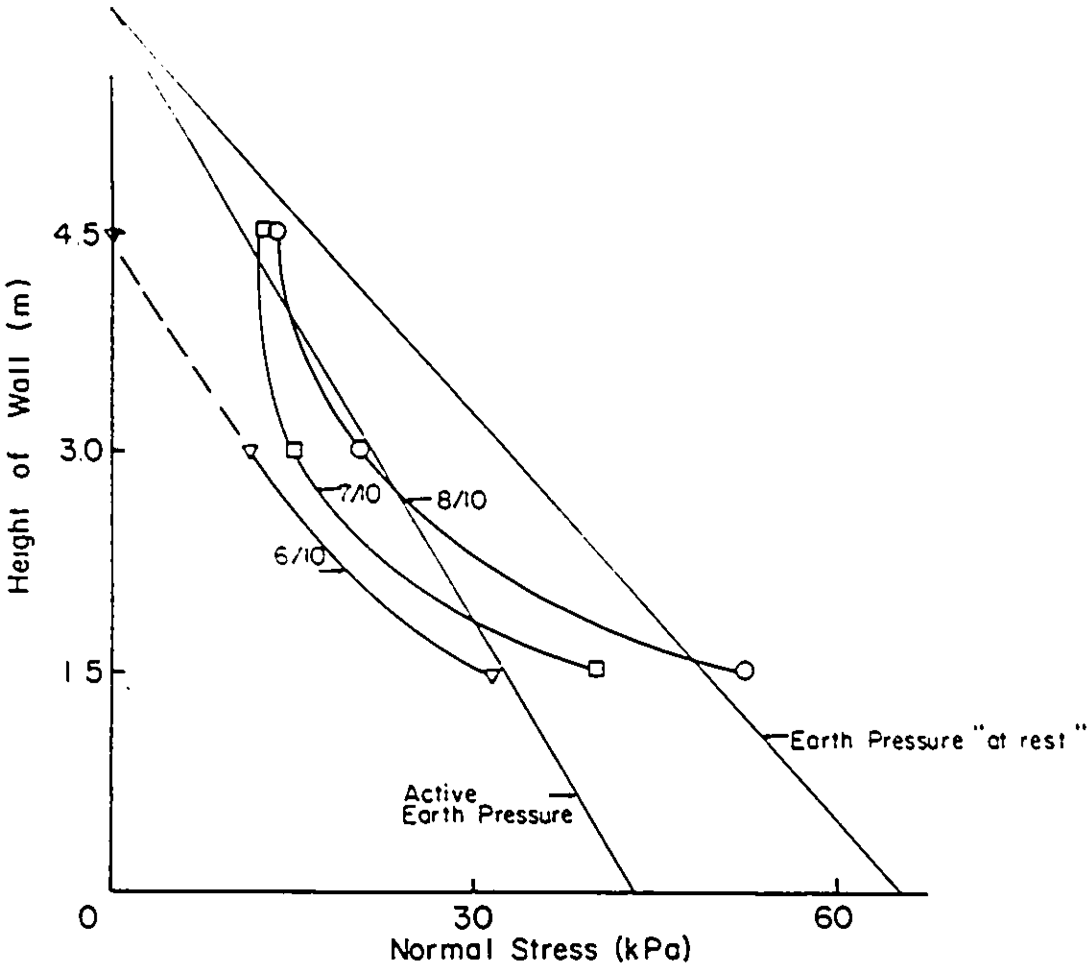

Figure 2.18: Normal Stress versus Height of Wall. Brandt (1985)

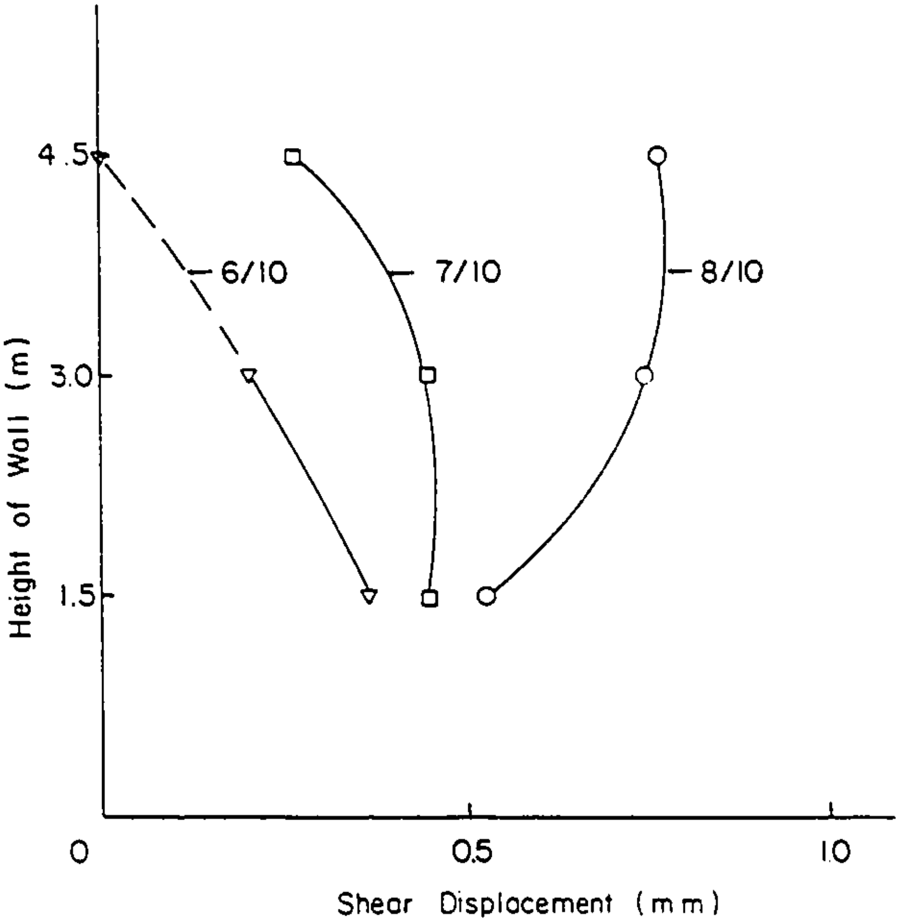

Figure 2.19: Shear Displacement versus Height of Wall. Brandt (1985)

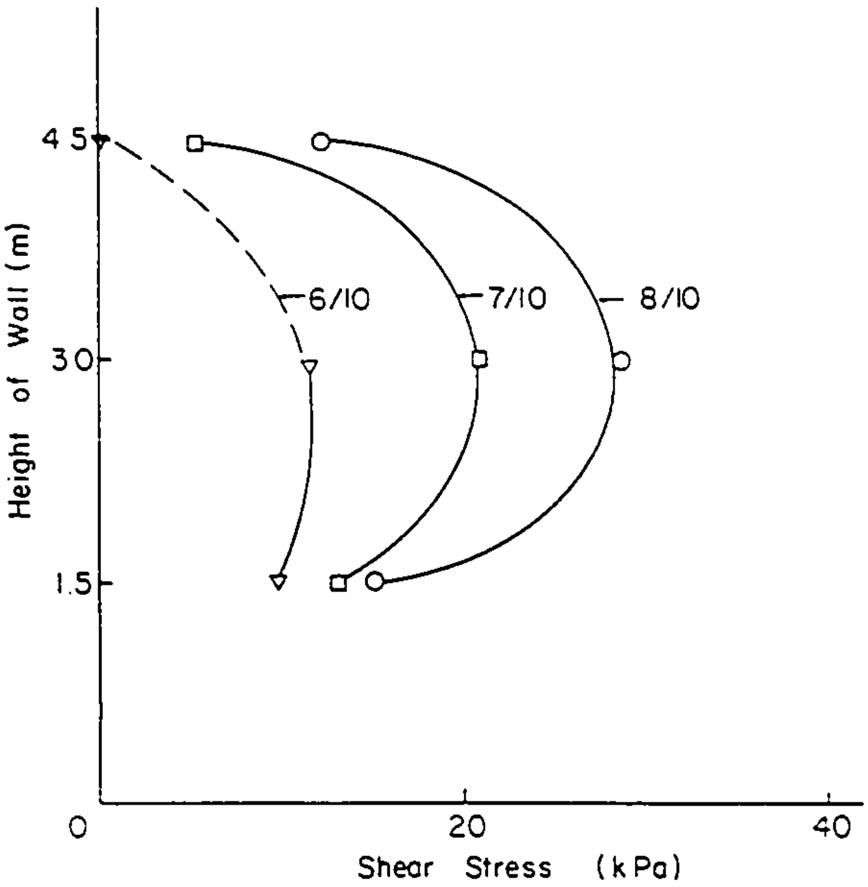

Figure 2.20: Shear Stress versus Height of Wall. Brandt (1985)

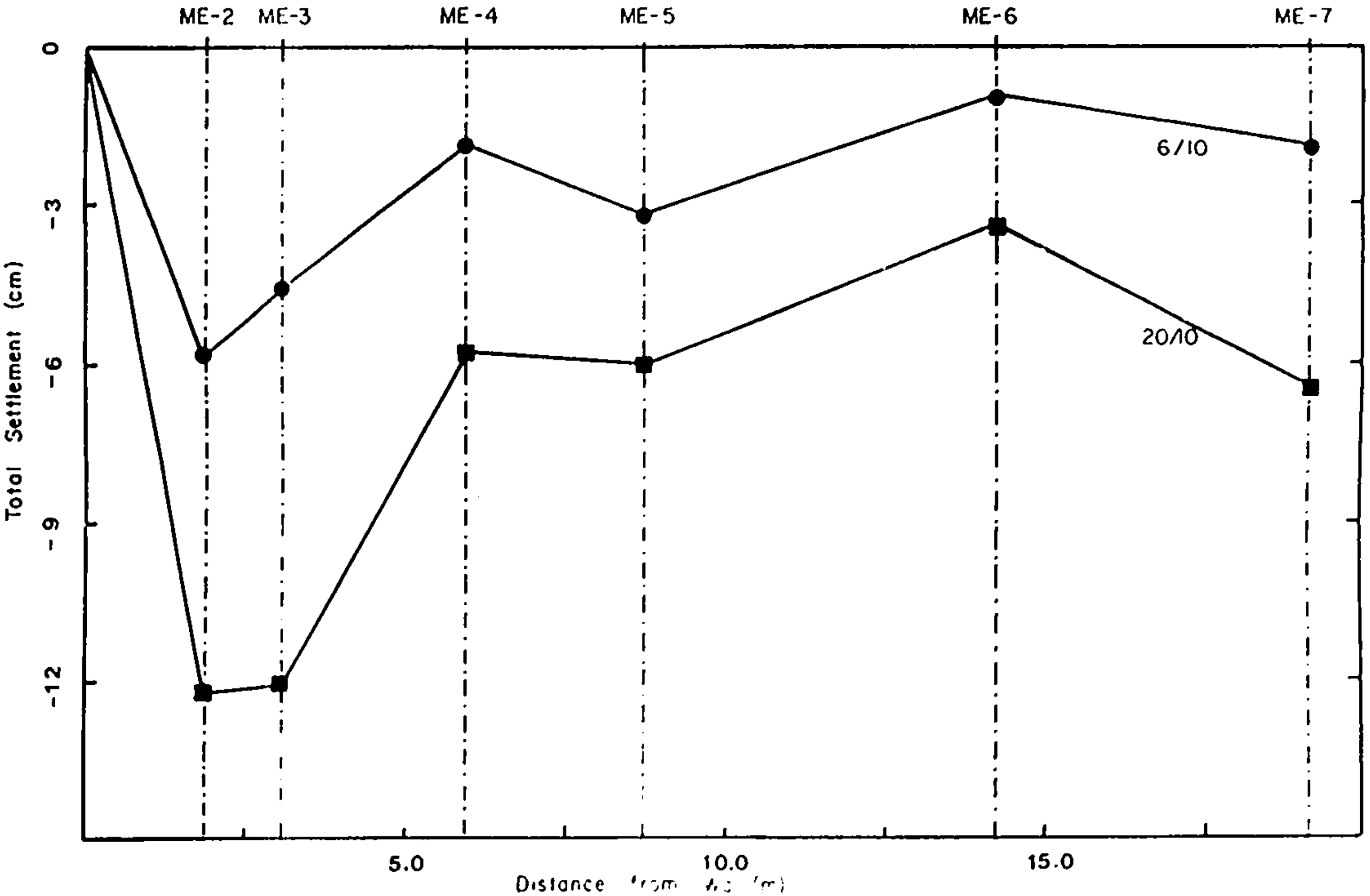

Figure 2.21: Total Settlement versus Distance from Wall. Brandt (1985)

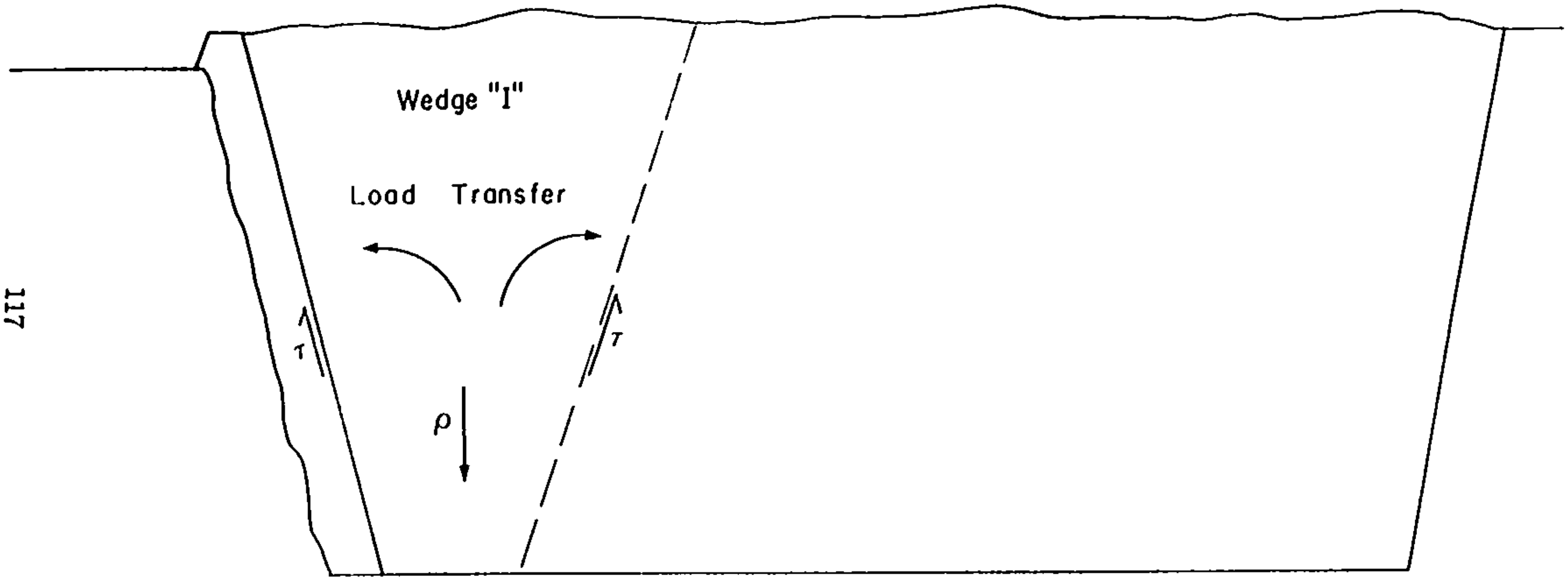

Figure 2.22: Sketch for Proposed Load Transfer Mechanism. Brandt (1985)

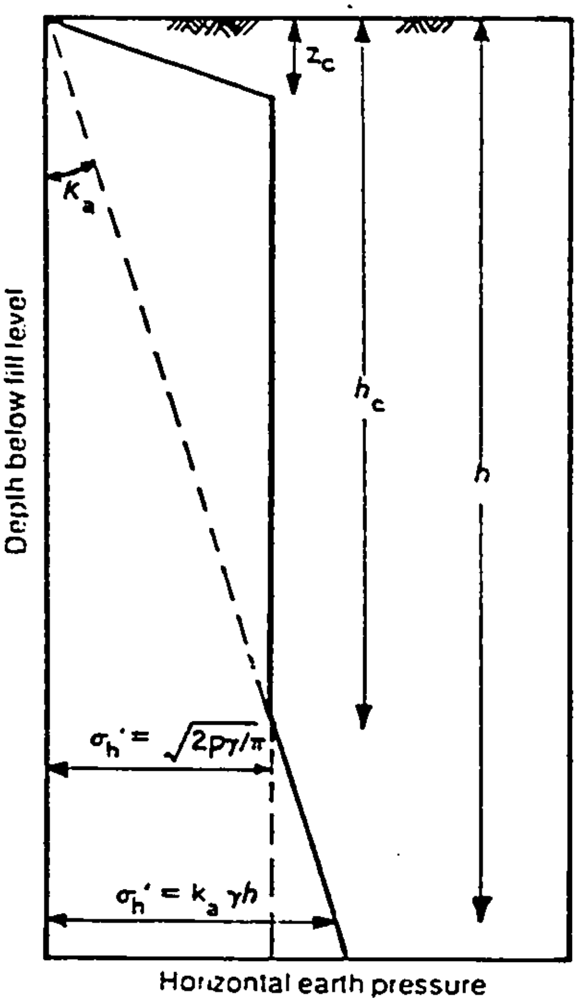

Figure 2.23: Horizontal Pressure Distribution due to Compaction-Induced Stresses. Ingold (1979)

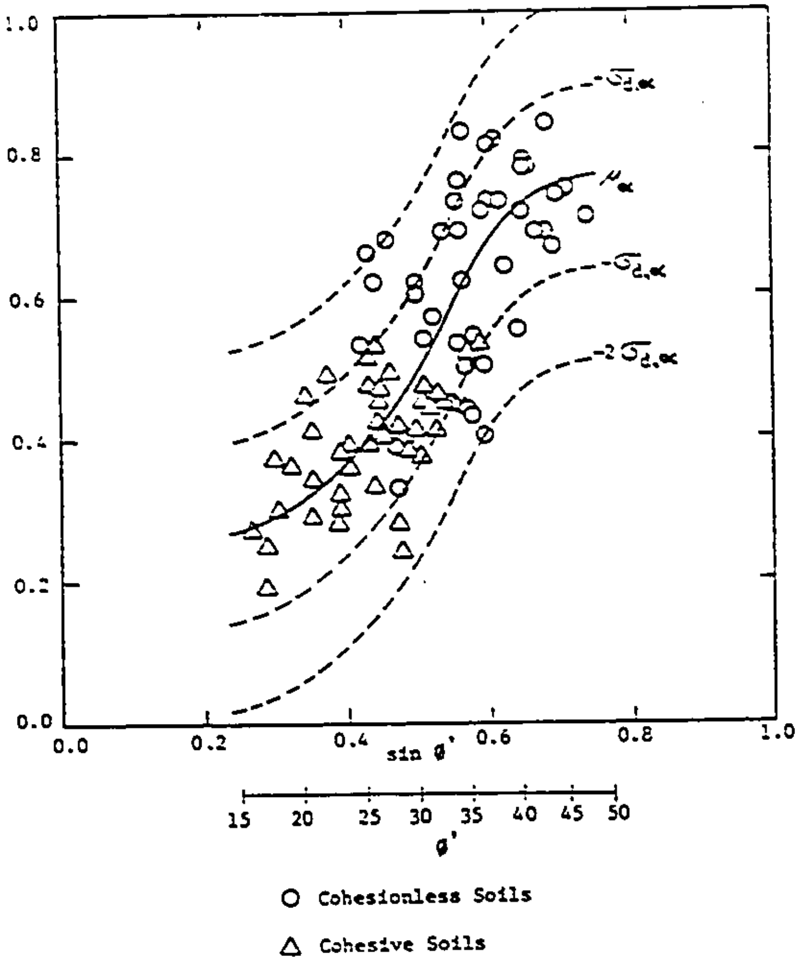

Figure 2.24: Suggested Relationship Between $\sin \phi'$ and α.
Seed R. B. (1983)

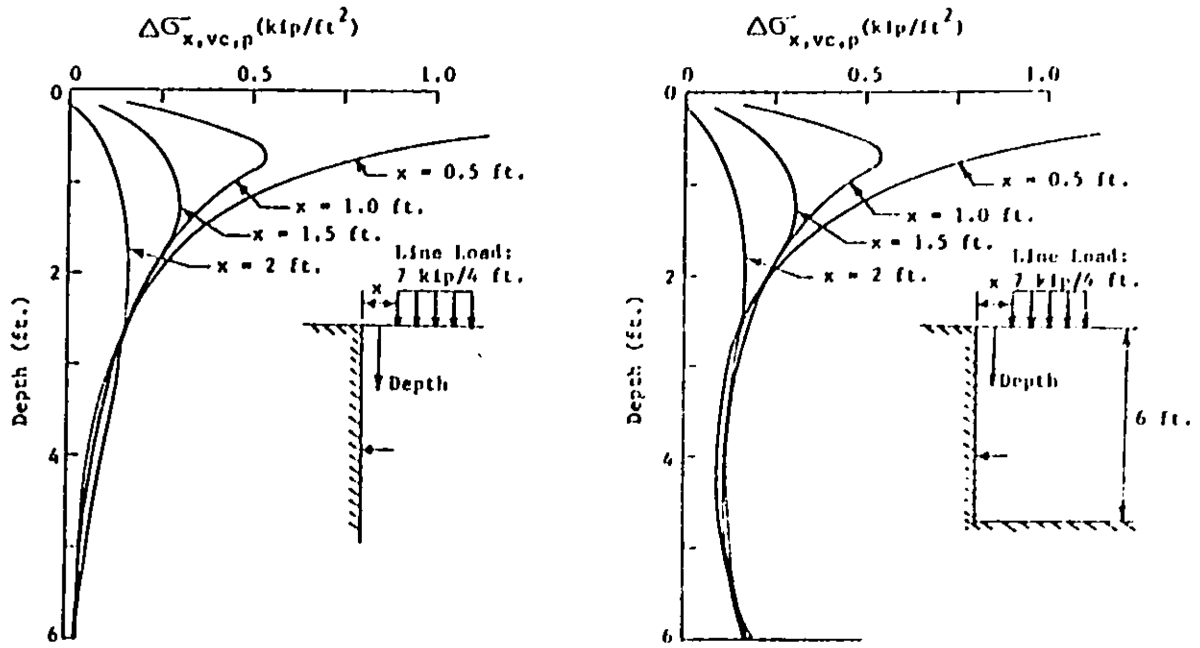

Figure 2.25: Profiles of $\Delta\sigma_{h,vc,p}$ against a Vertical Wall for a Single Drum Roller. Seed R. B. (1983)

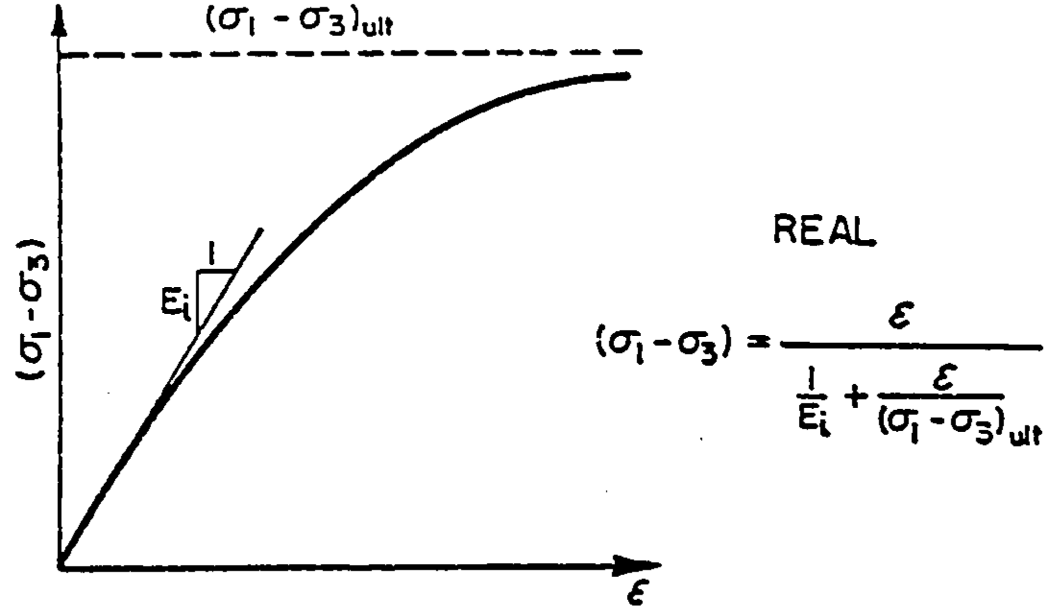

Figure 3.1: Hyperbolic Representation of Nonlinear Stress-Strain Curve. Duncan et al. (1978)

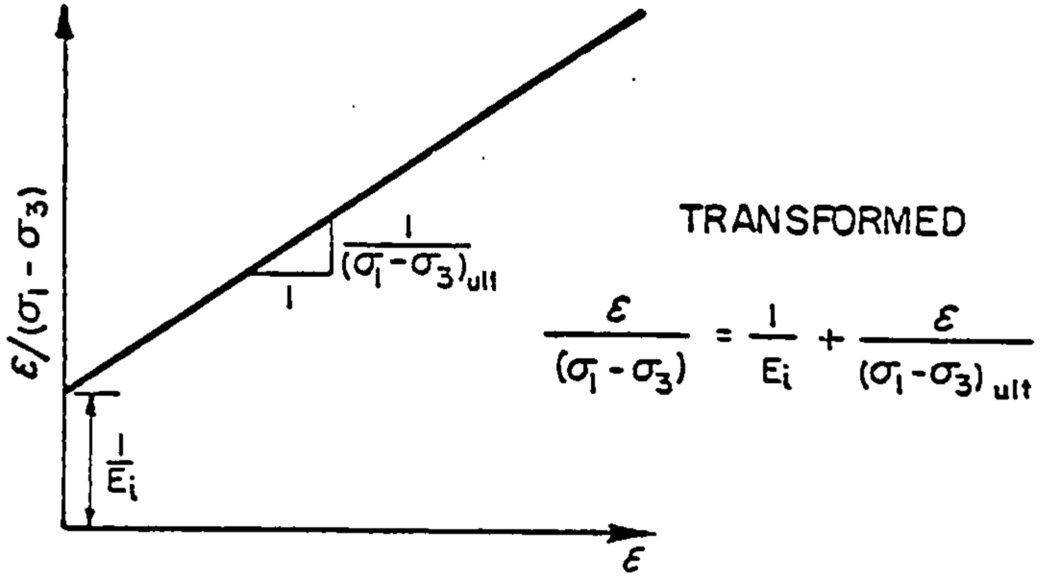

Figure 3.2: Hyperbolic Equation Transformed into Linear Relationship. Duncan et al. (1978)

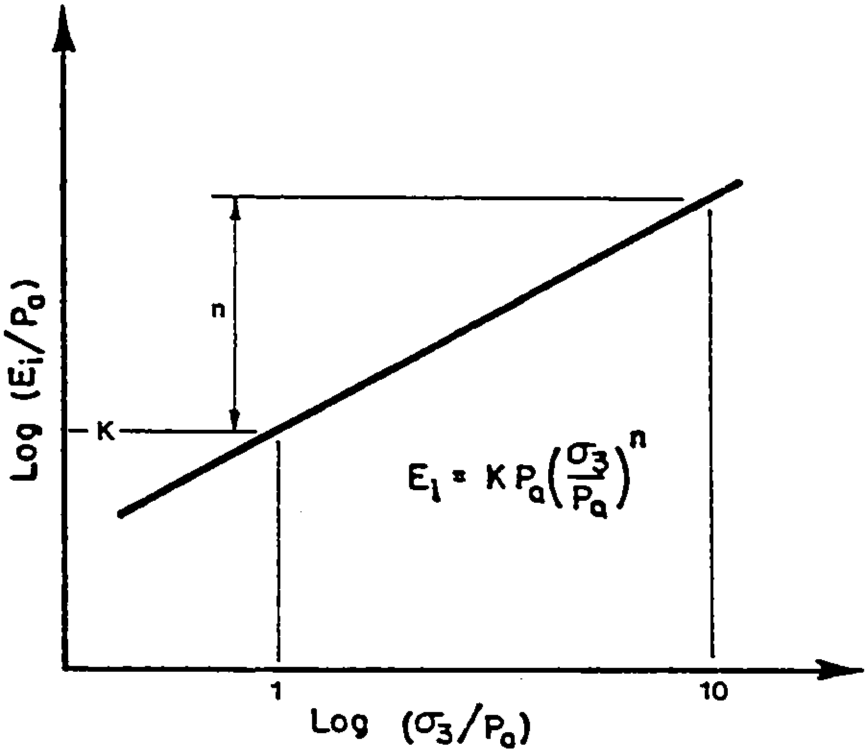

Figure 3.3: Variation of Initial Tangent Modulus with Confining Pressure. Duncan et al. (1978)

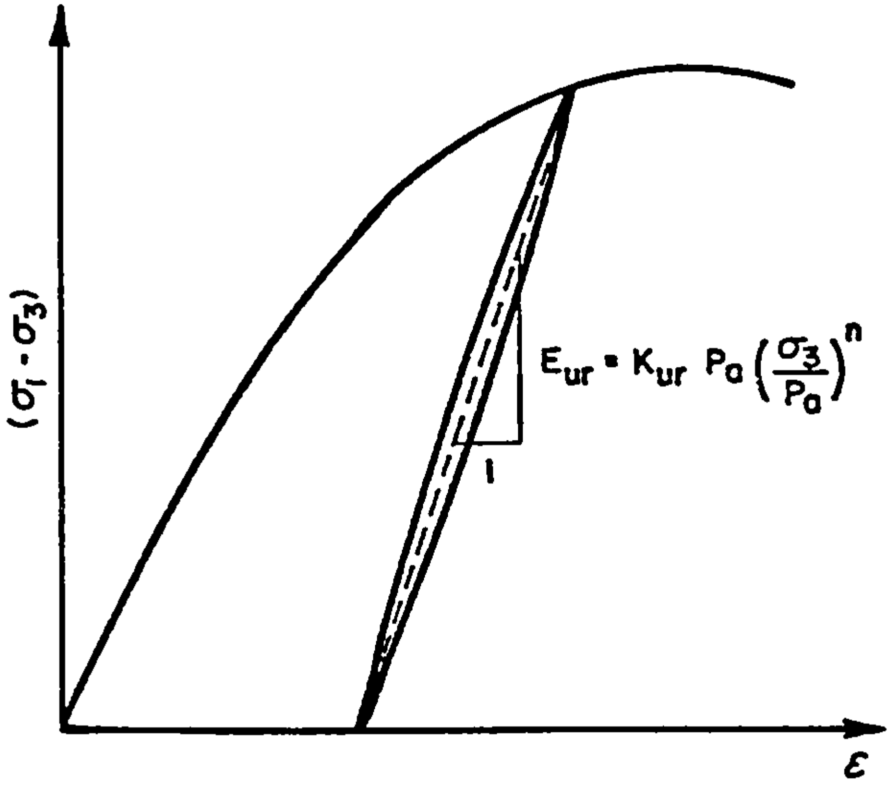

Figure 3.4: Unloading-Reloading Modulus. Duncan et al. (1978)

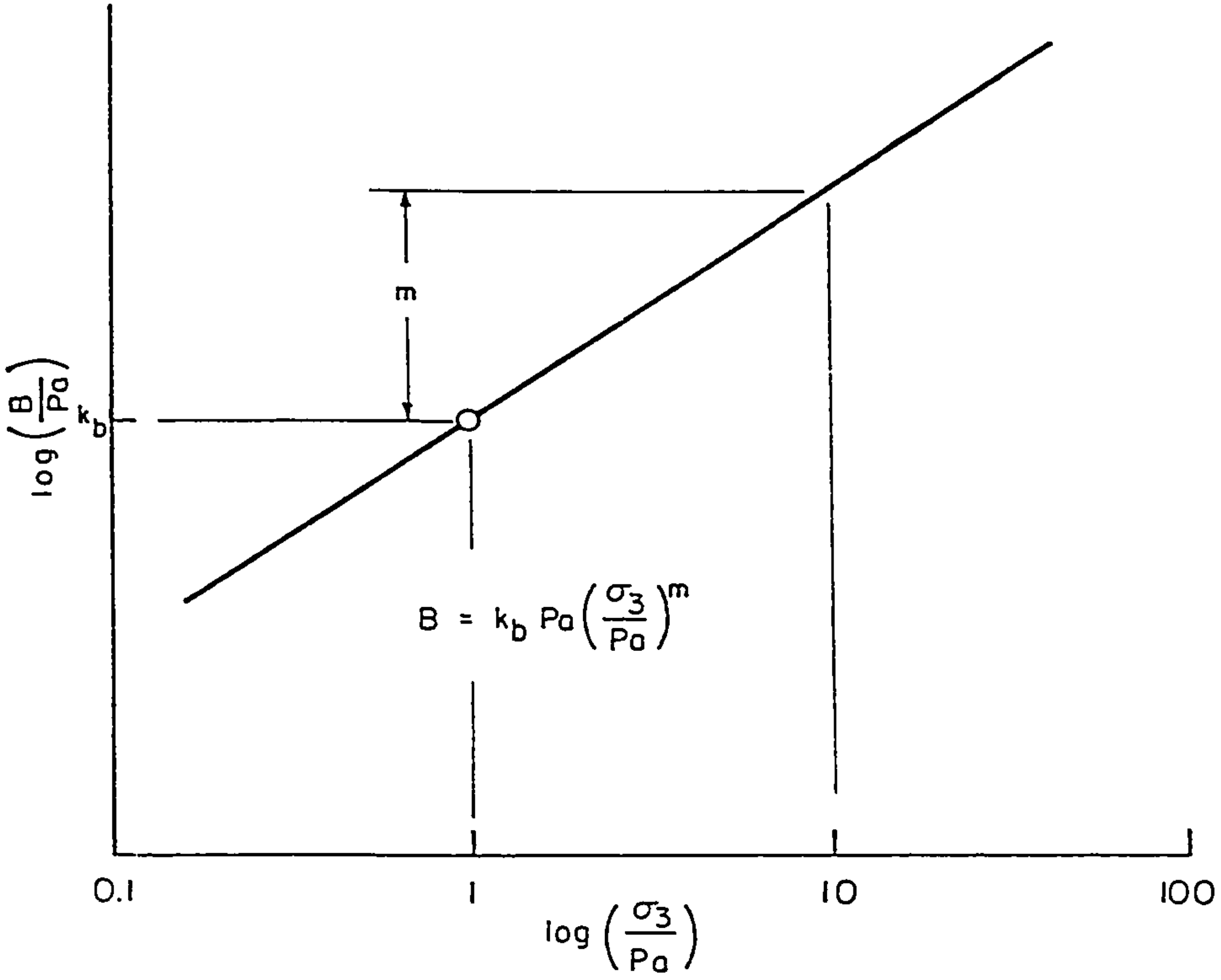

Figure 3.5: Variation of Bulk Modulus with Confining Pressure. Duncan et al. (1978)

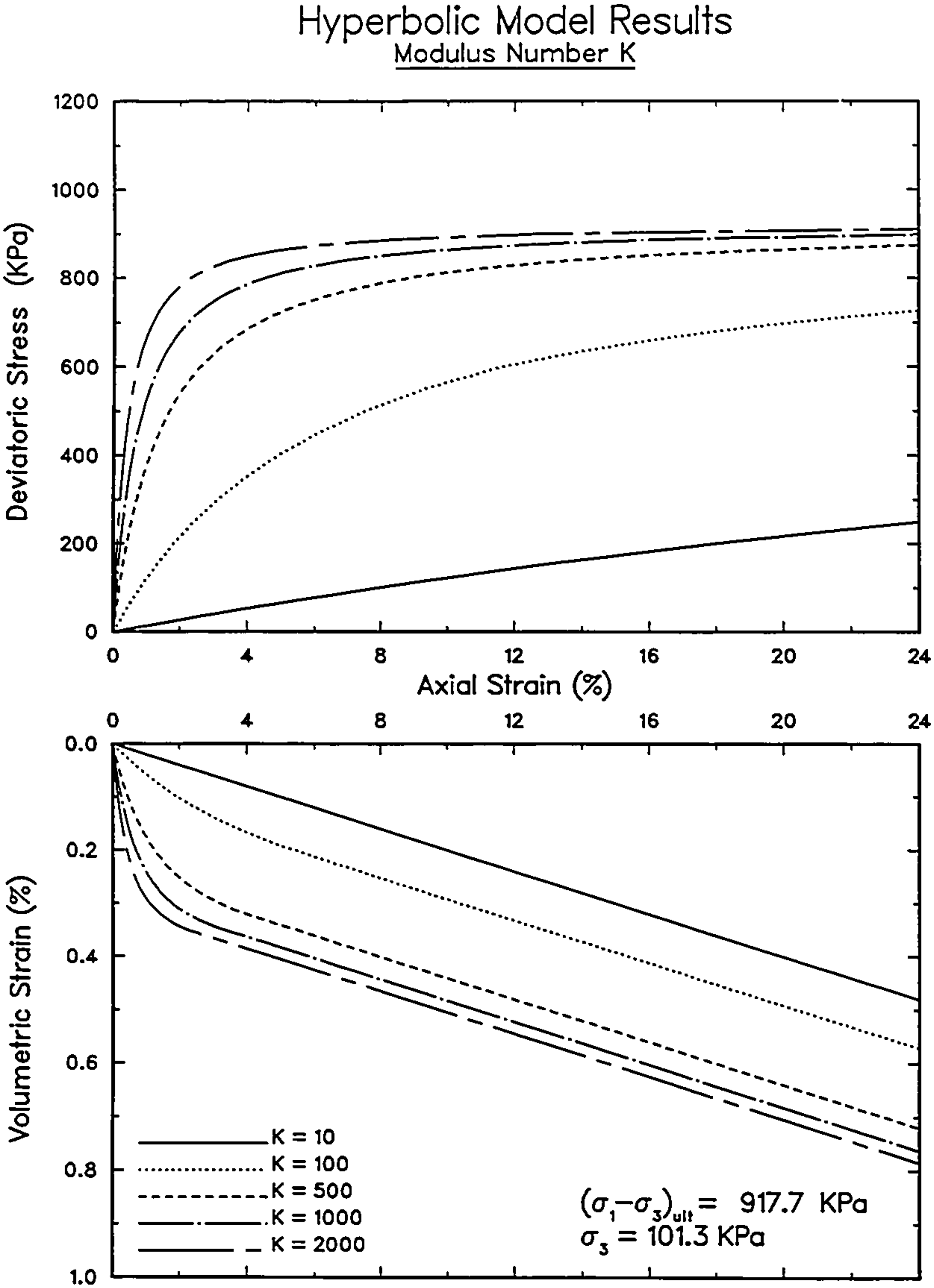

Figure 3.6: Sensitivity Analysis on Modulus Number K

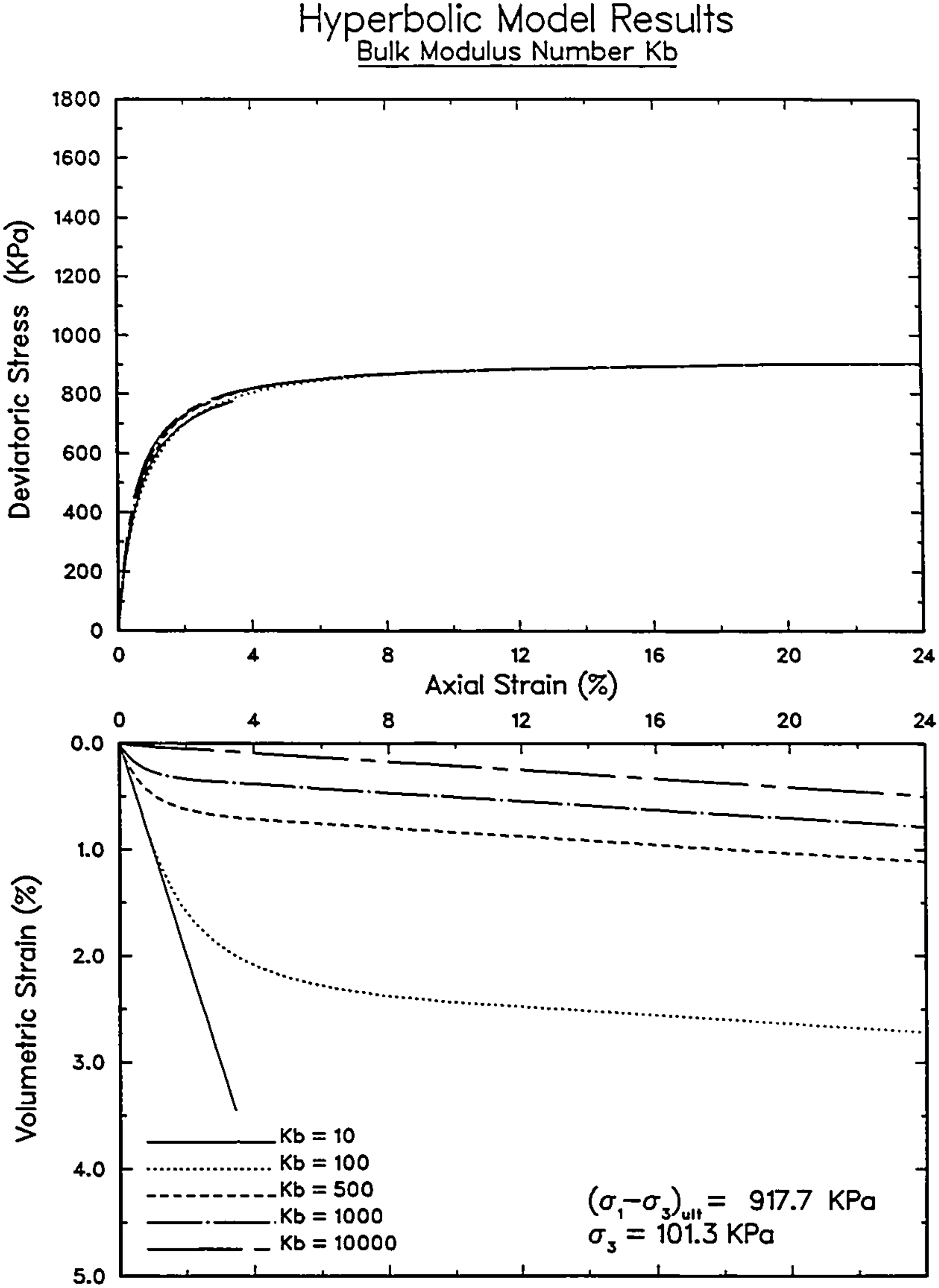

Figure 3.7: Sensitivity Analysis on Bulk Modulus Number K_b

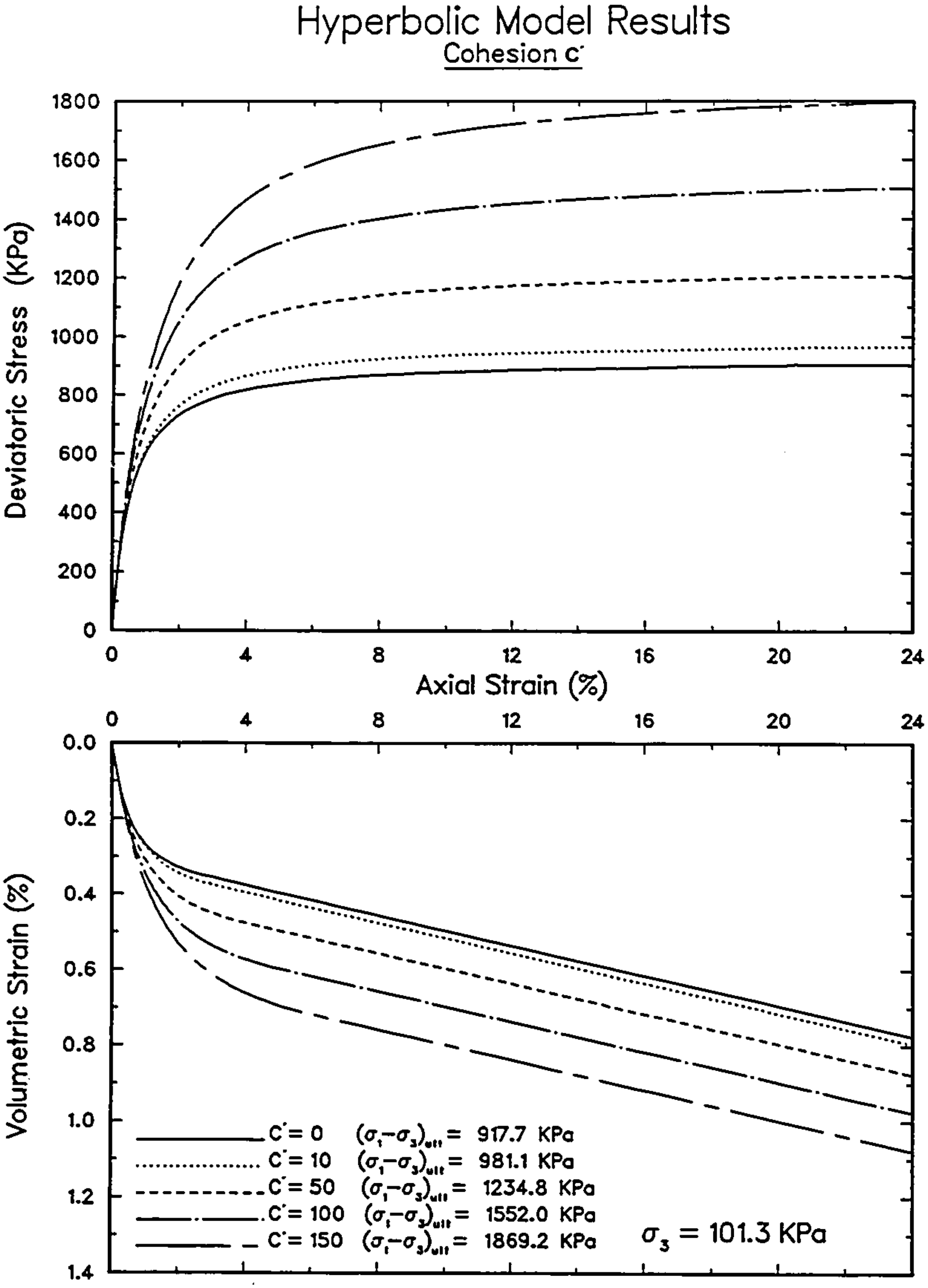

Figure 3.8: Sensitivity Analysis on Cohesion c'

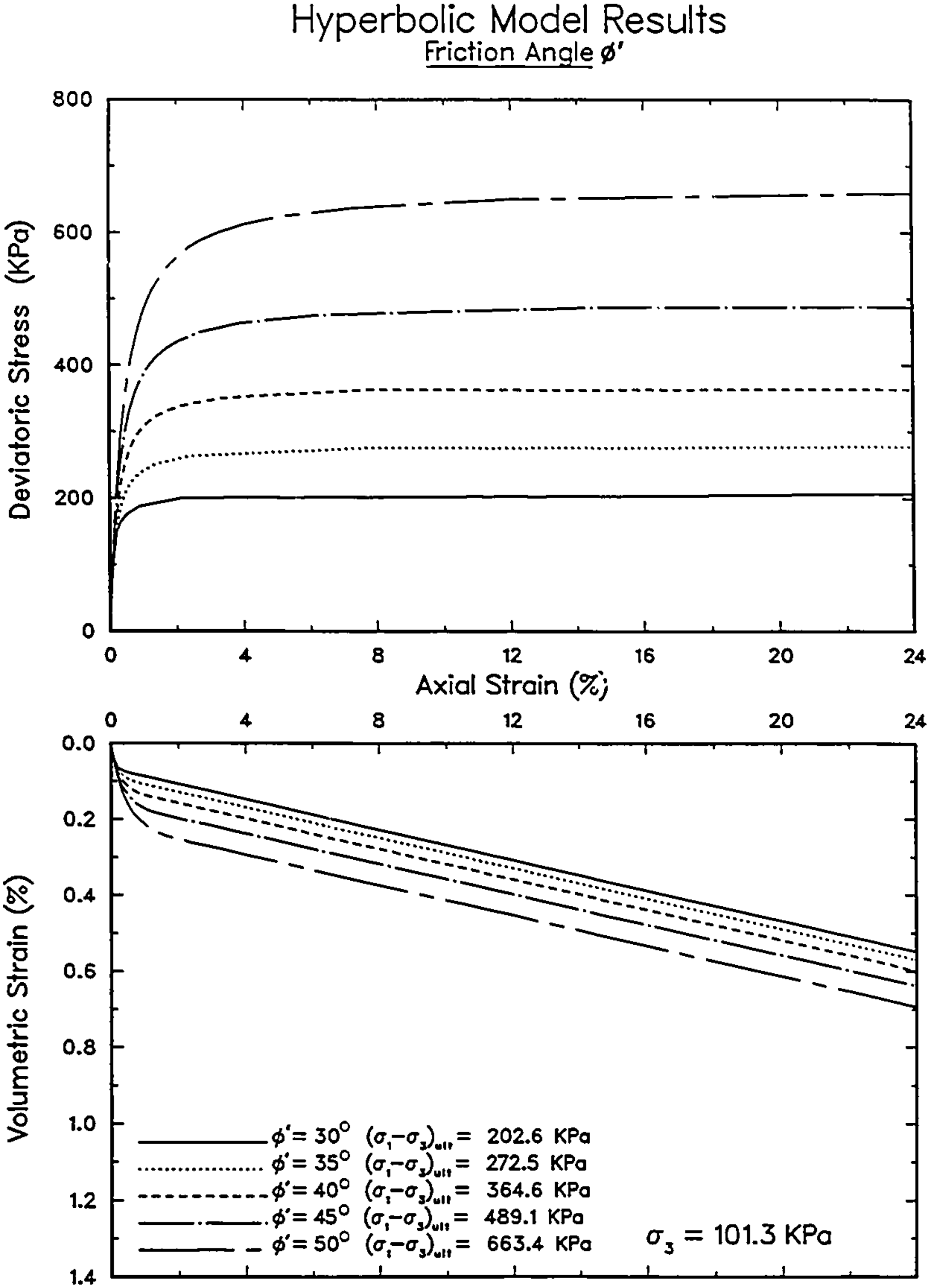

Figure 3.9: Sensitivity Analysis on Friction Angle ϕ'

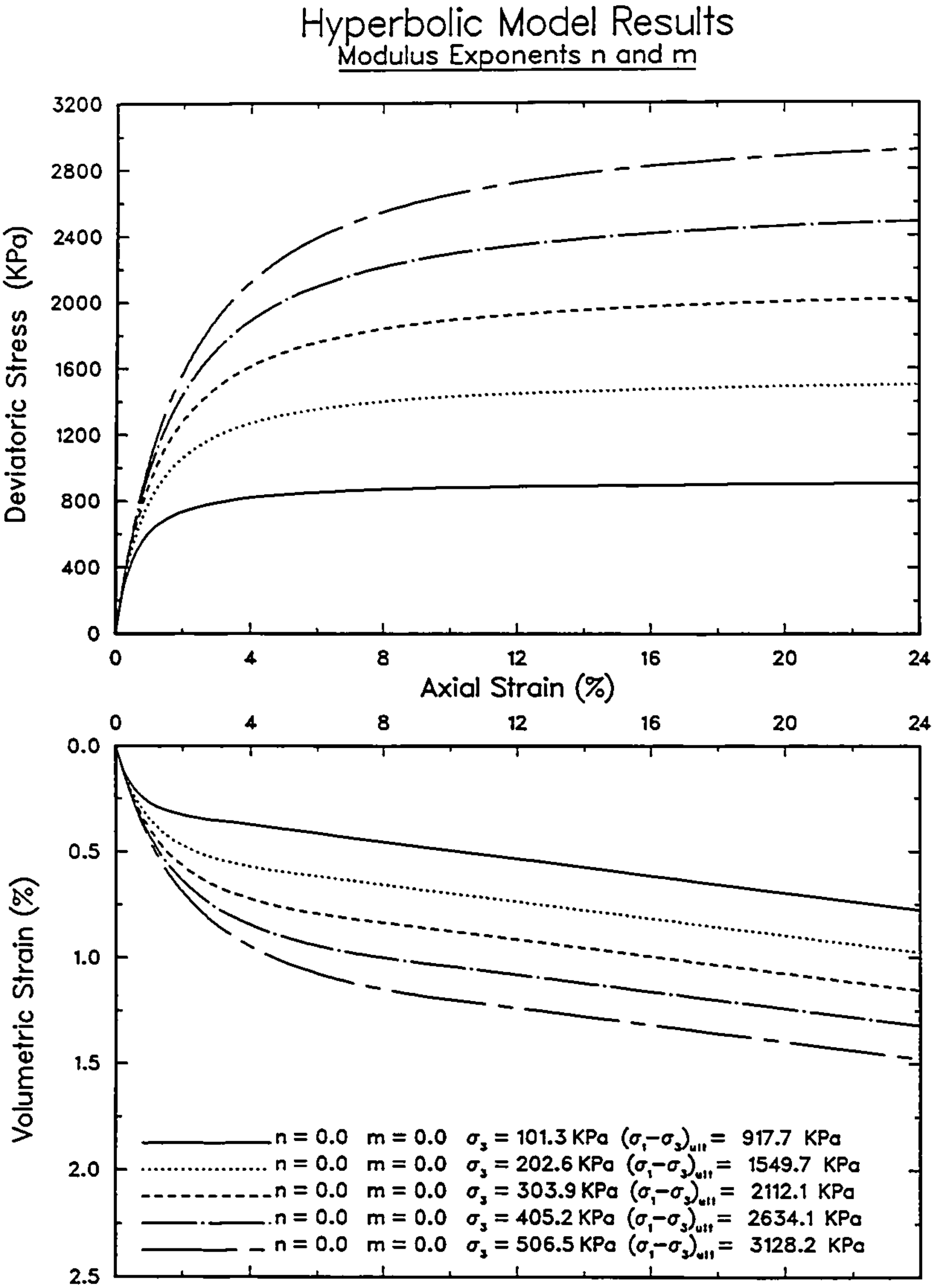

Figure 3.10: Sensitivity Analysis on Modulus Exponents n and m with n=0.0 and m=0.0

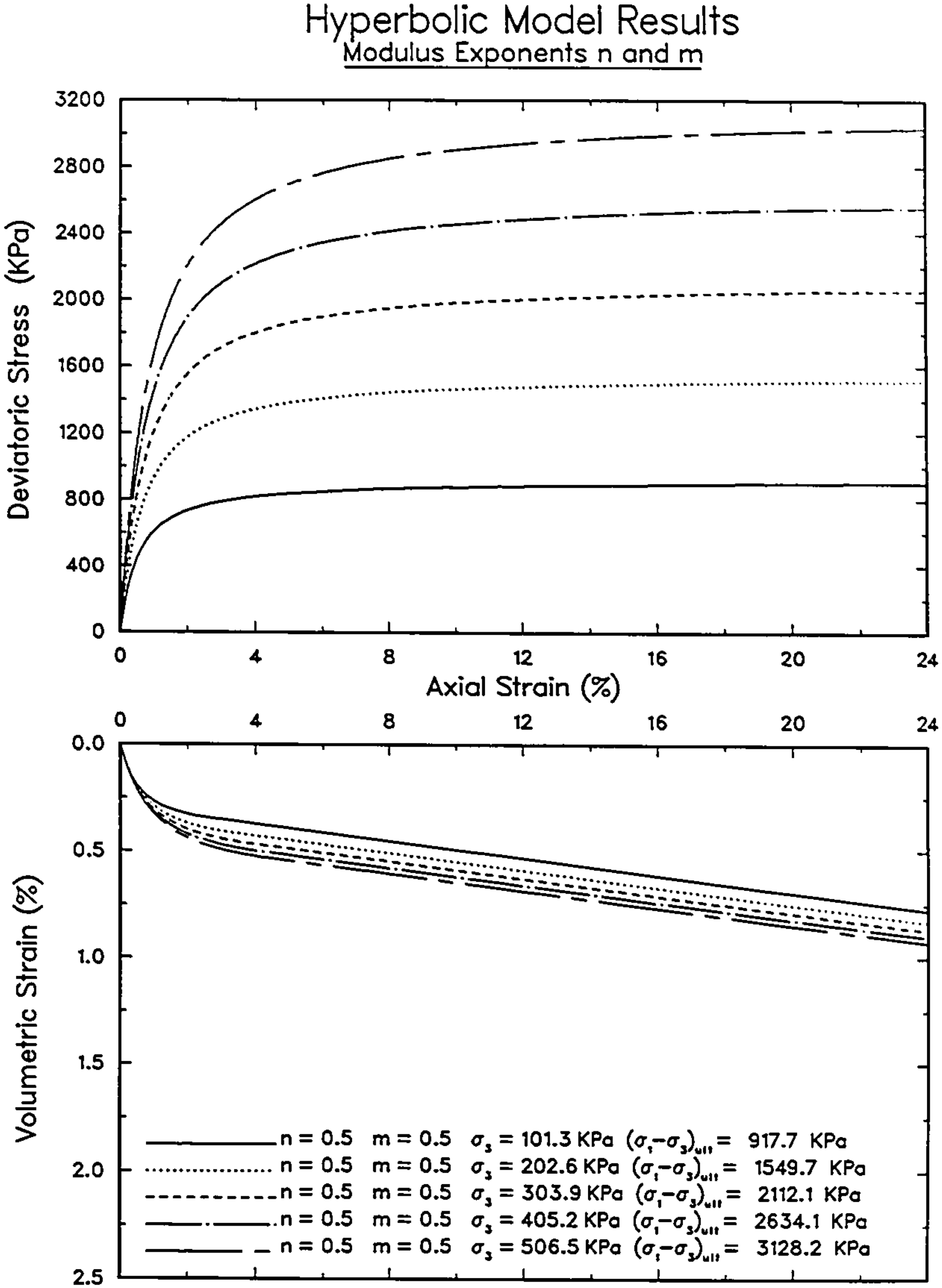

Figure 3.11: Sensitivity Analysis on Modulus Exponents n and m with n=0.5 and m=0.5

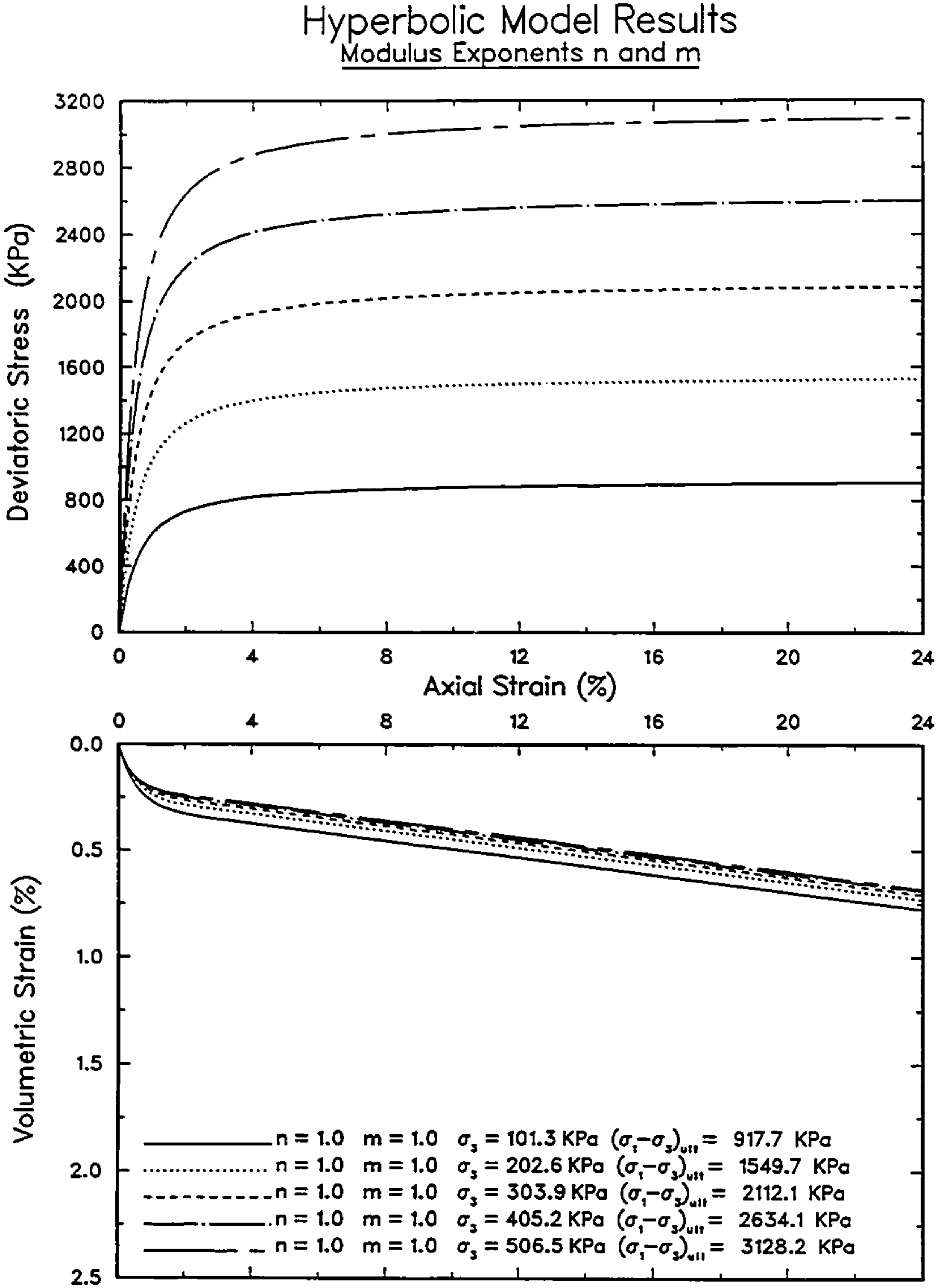

Figure 3.12: Sensitivity Analysis on Modulus Exponents n and m with n=1.0 and m=1.0

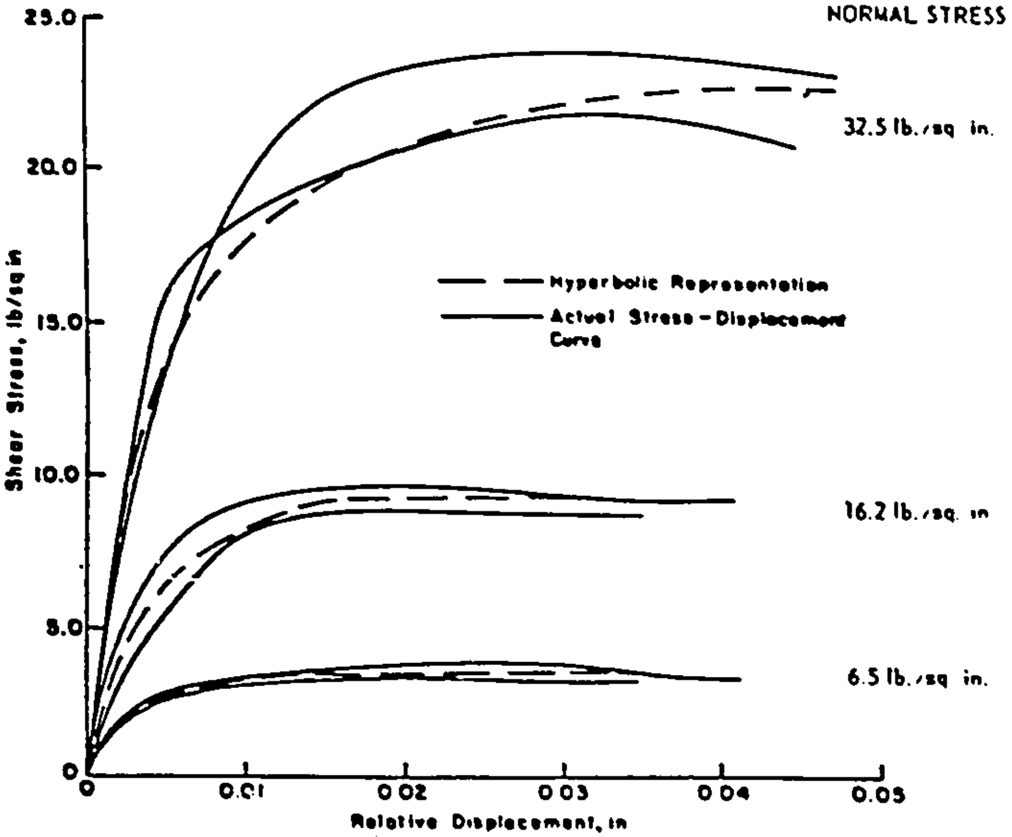

Figure 3.13: Comparison of Hyperbolic and Actual Stress-Strain Curves. Duncan et al. (1978)

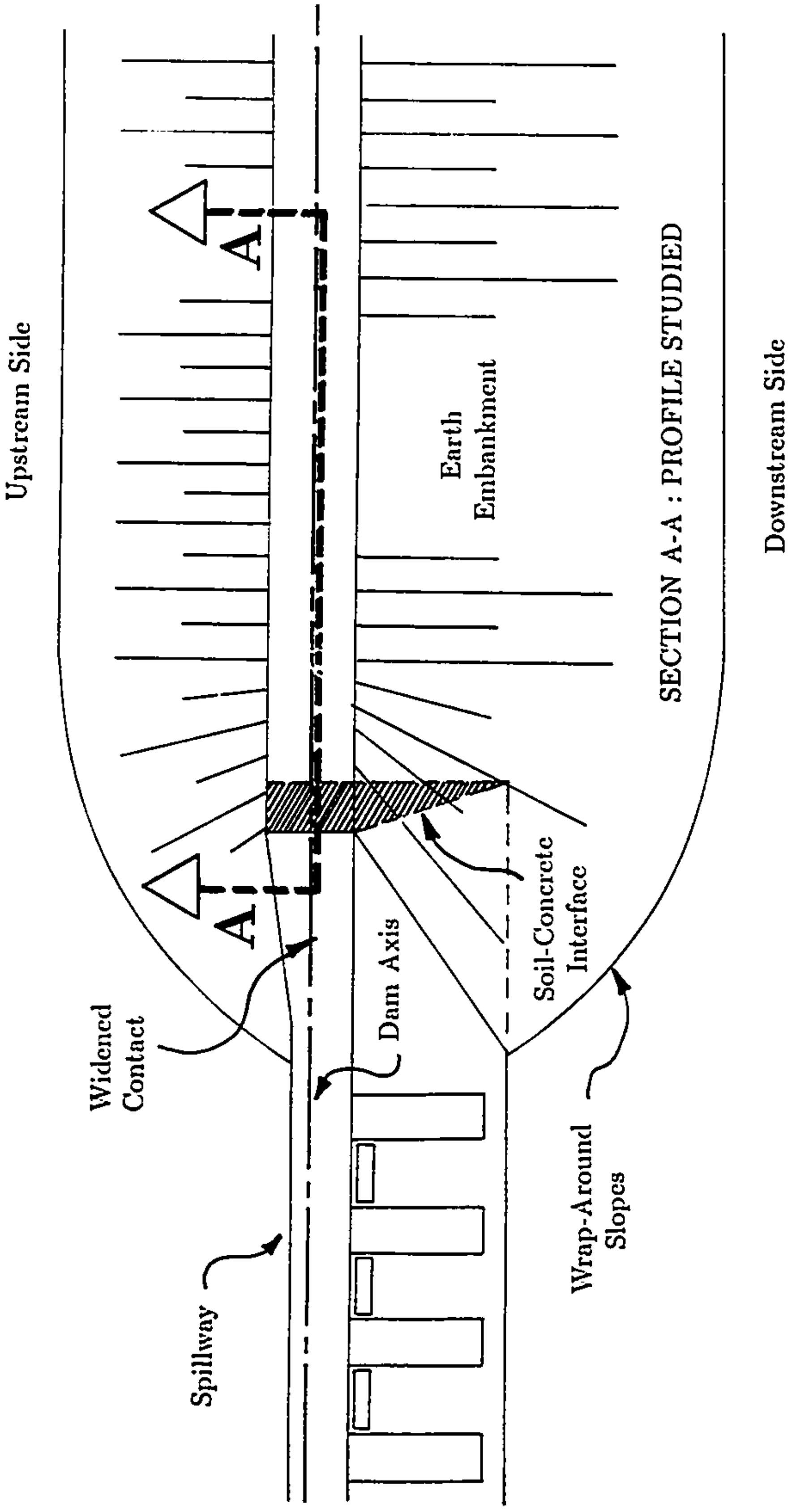

Figure 3.14: Plan View of Proposed Finite Element Mesh Profile.

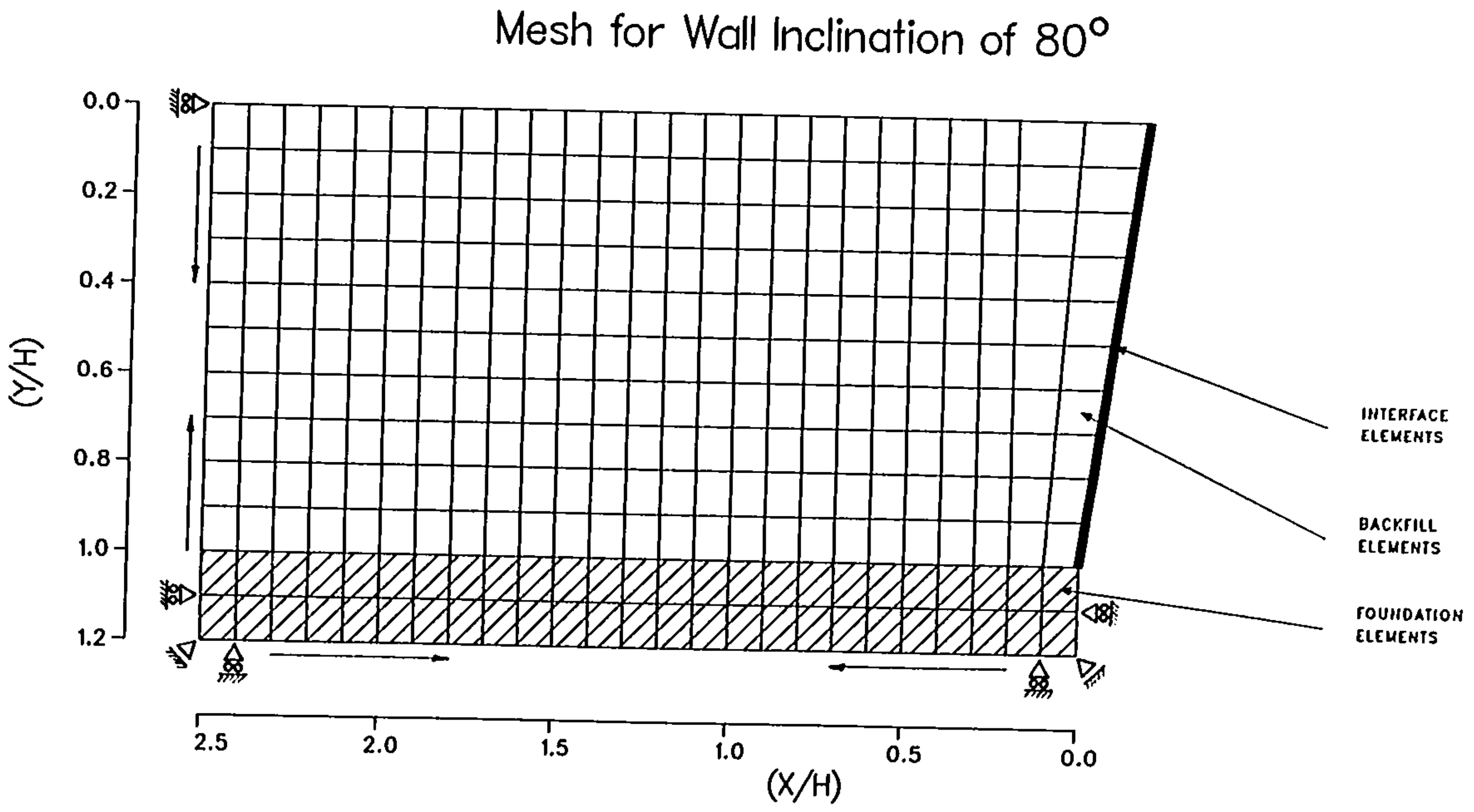

Figure 3.15: Finite Element Mesh for Wall W1

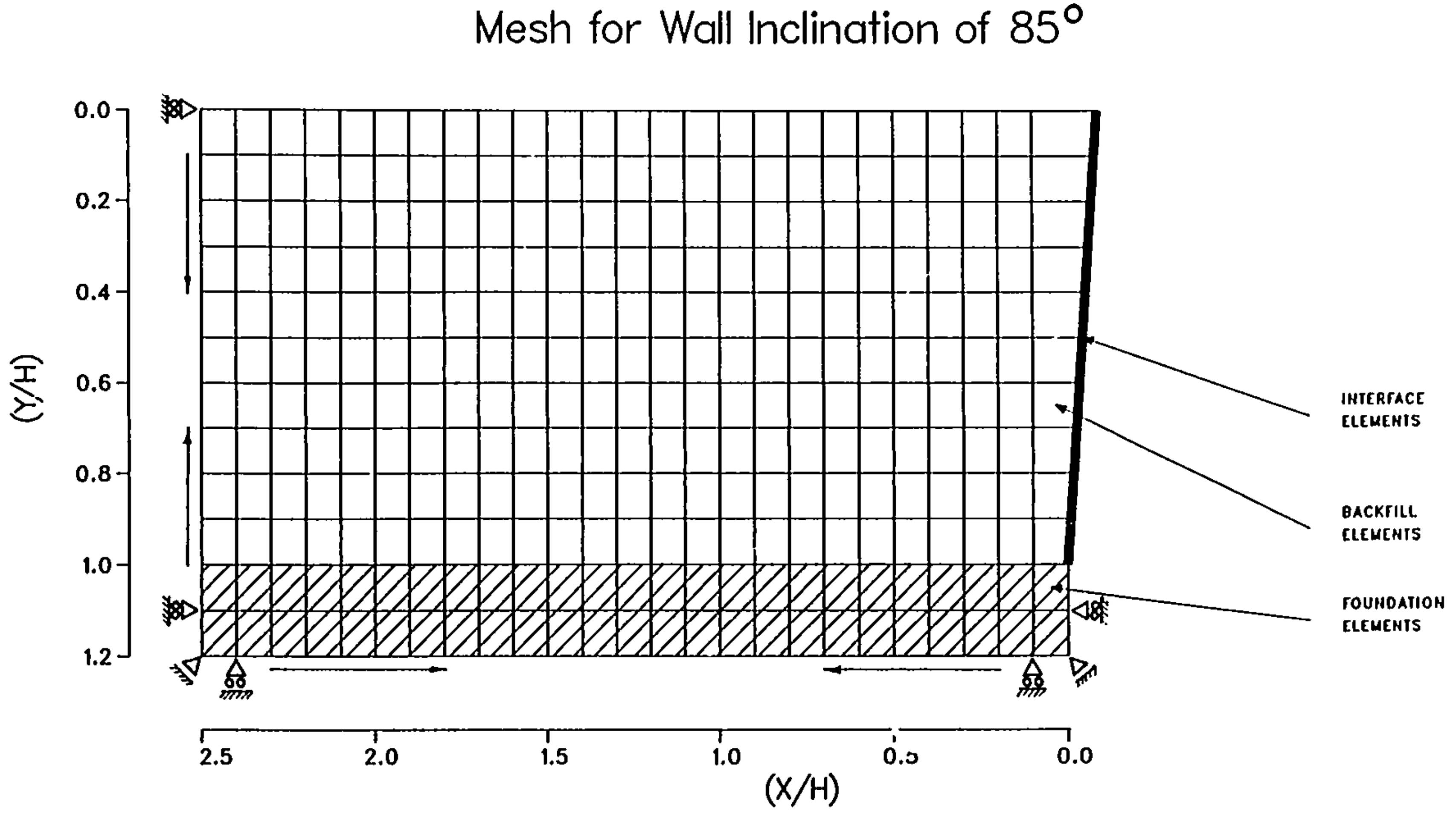

Figure 3.16: Finite Element Mesh for Wall W2

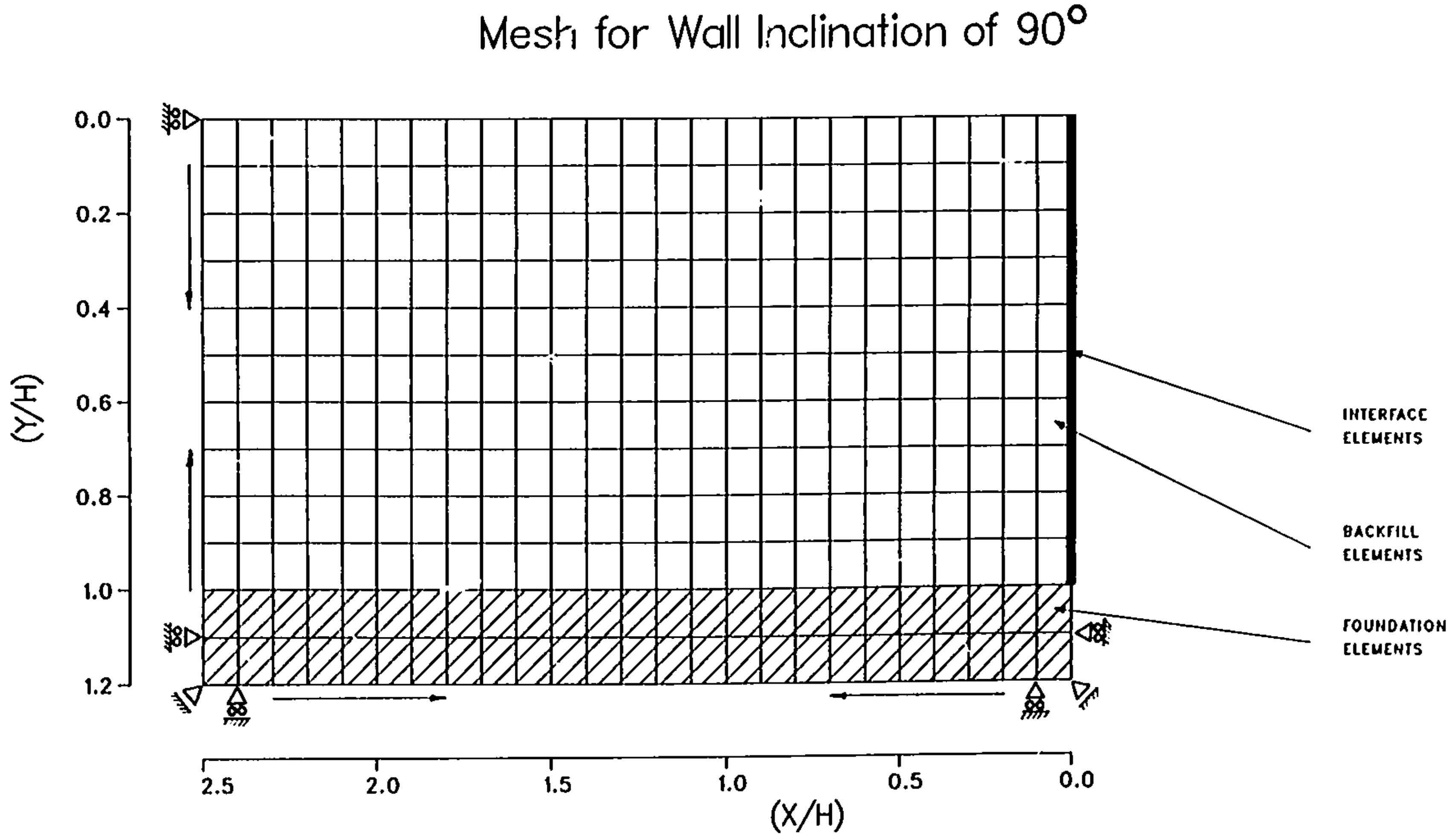

Figure 3.17: Finite Element Mesh for Wall W3

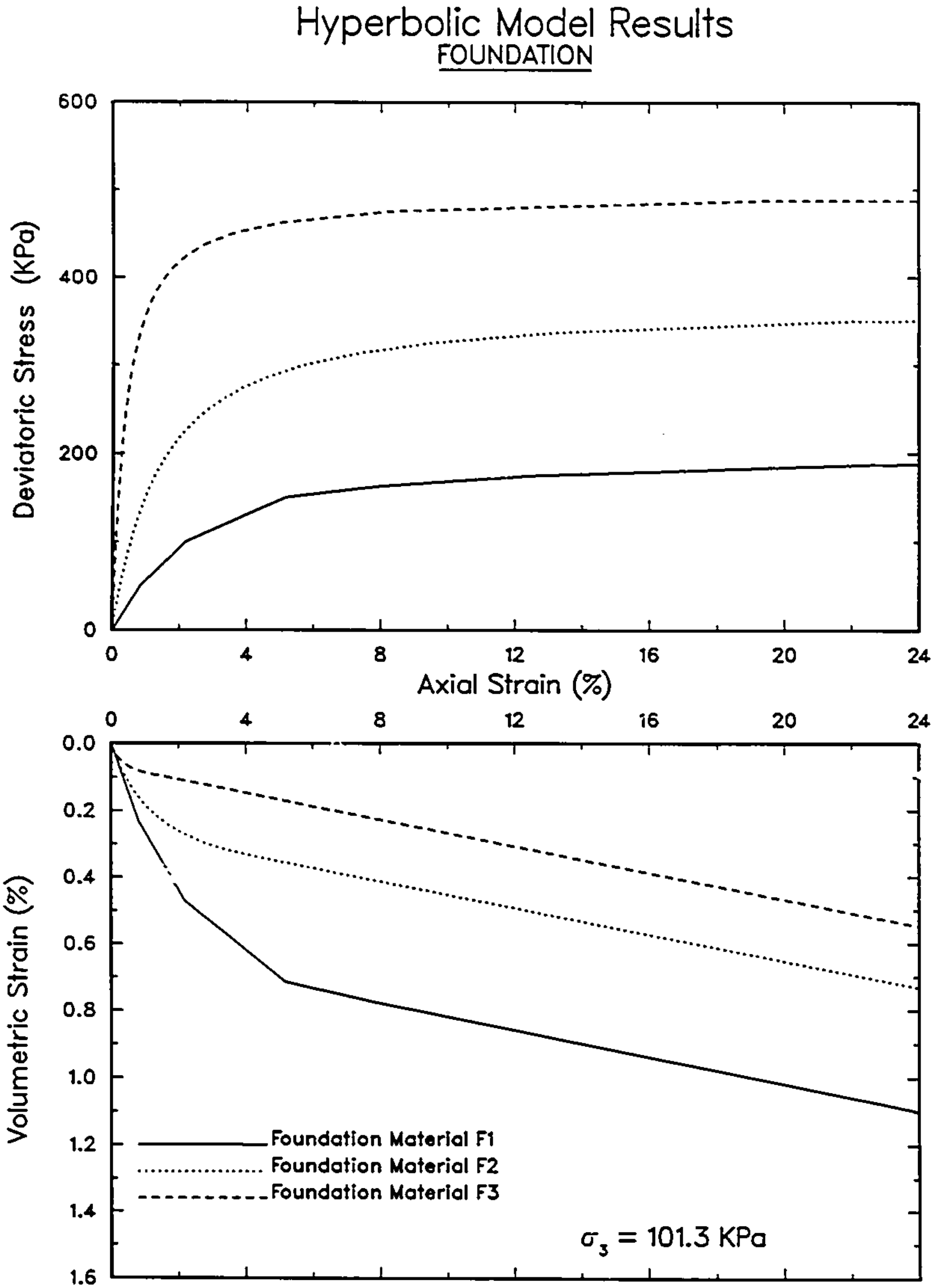

Figure 3.18: Deviatoric Stress, Axial Strain and Volumetric Strain Curves for Foundation Materials F1–F2–F3.

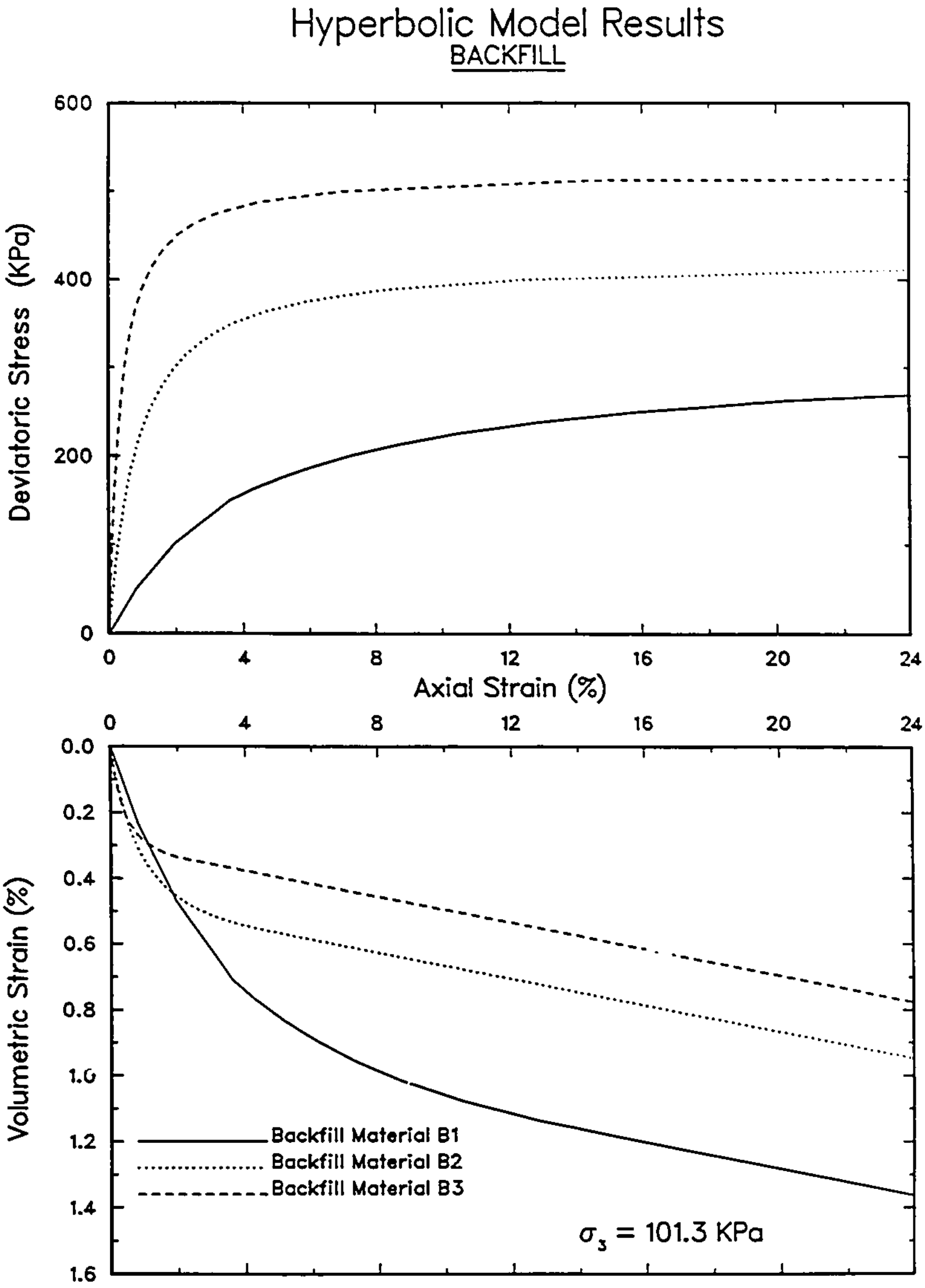

Figure 3.19: Deviatoric Stress, Axial Strain and Volumetric Strain Curves for Backfill Materials B1–B2–B3.

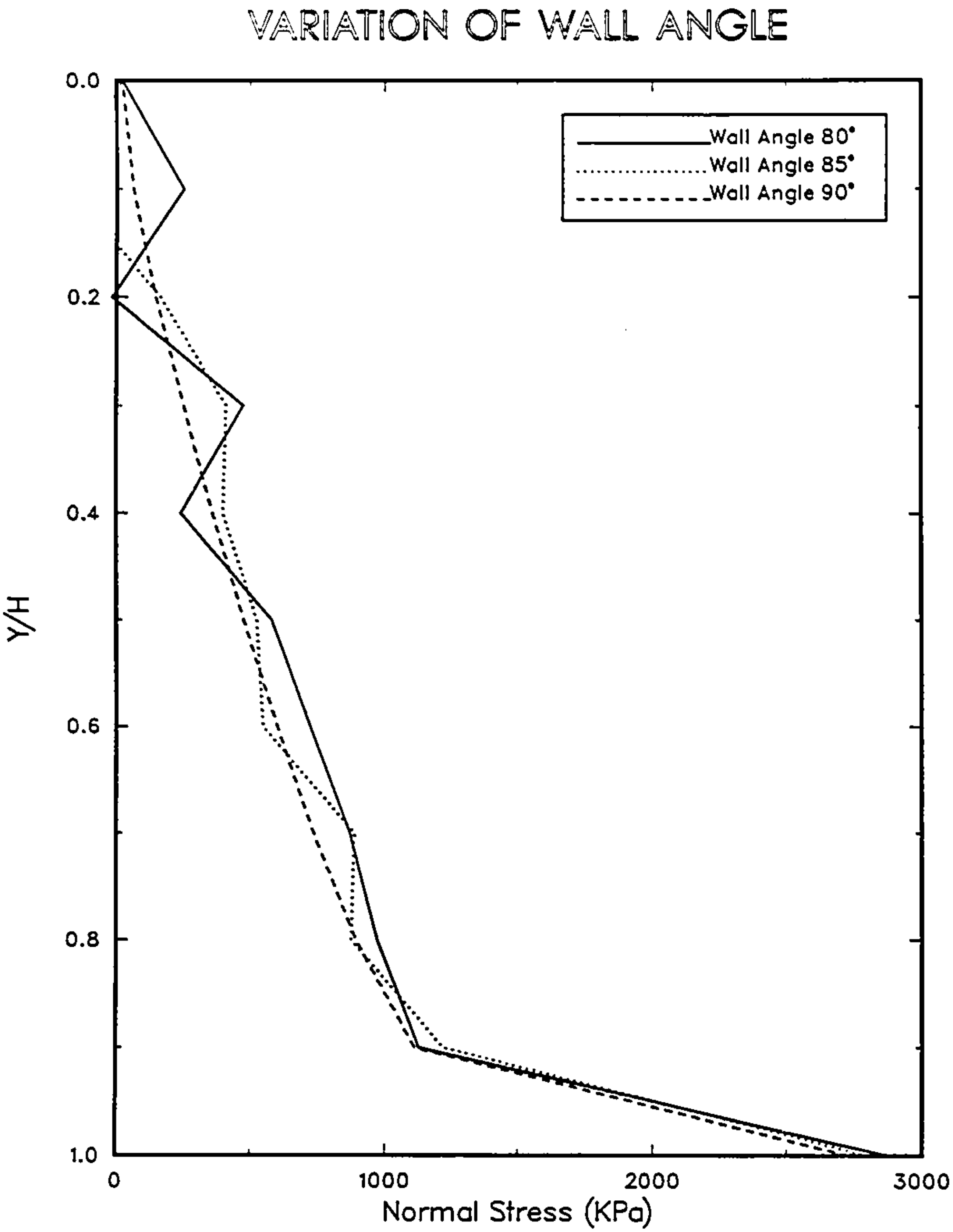

Figure 4.1: Normal Stresses Along Interface
for Run Types 1222–2222–3222

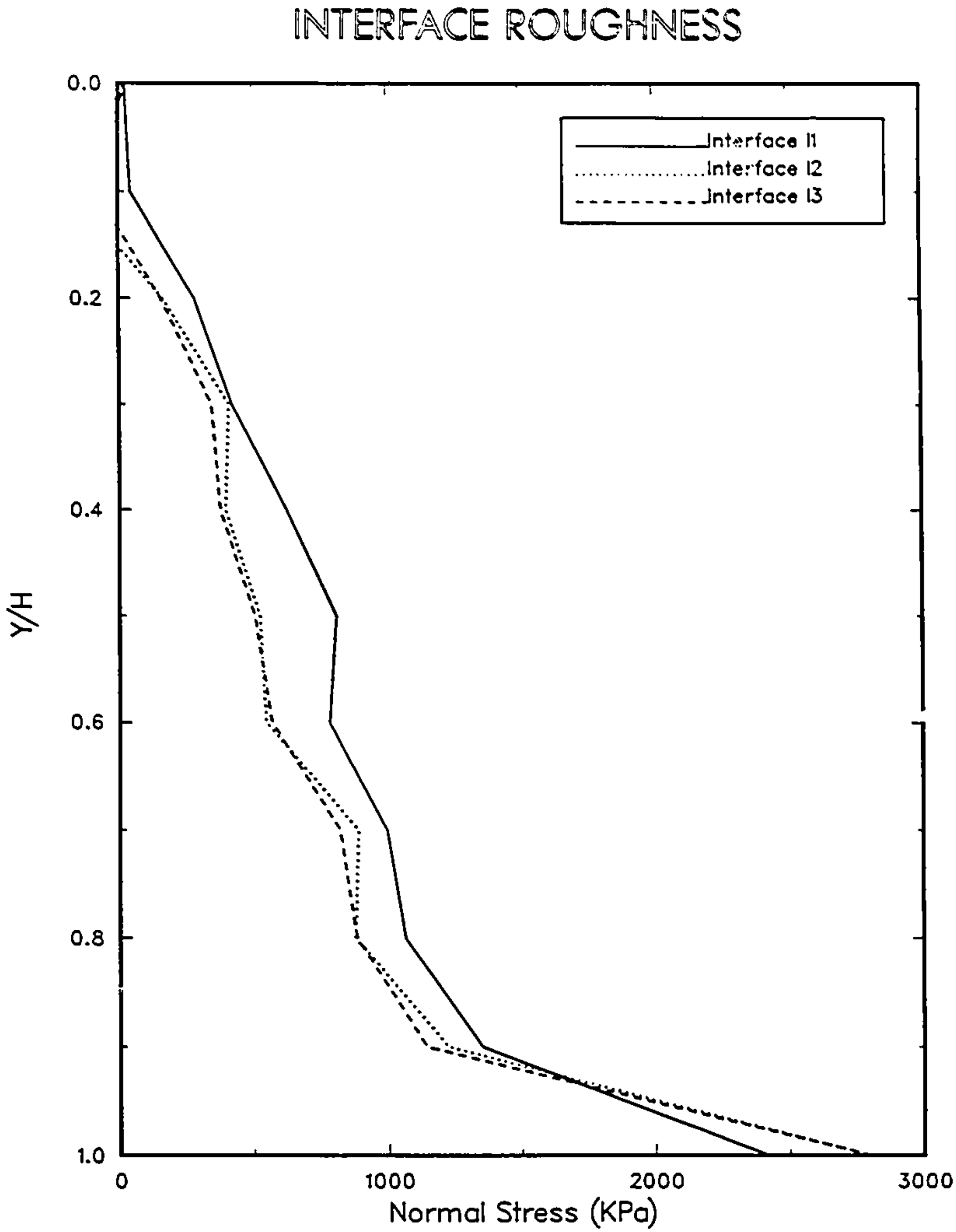

Figure 4.2: Normal Stresses Along Interface
for Run Types 2122–2222–2322

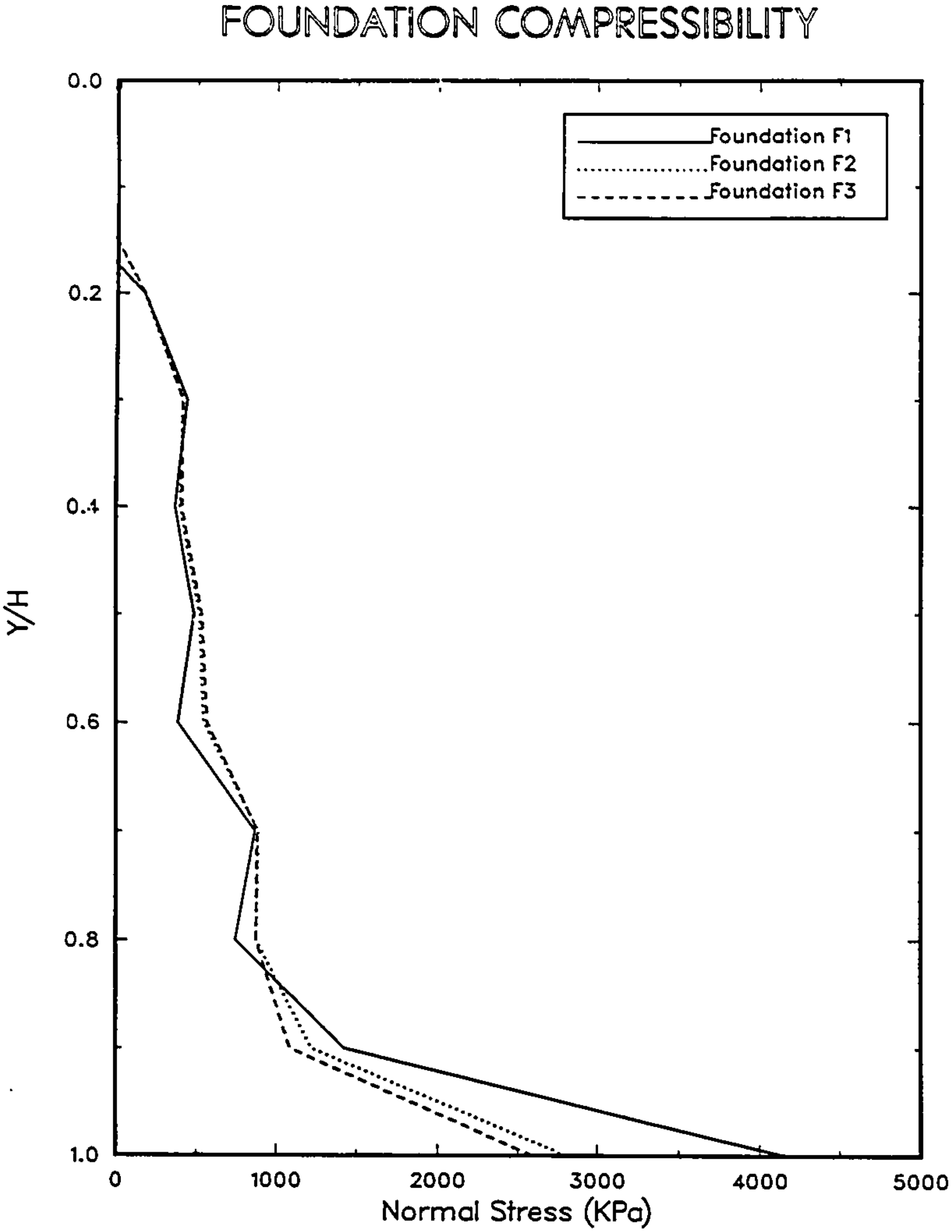

Figure 4.3: Normal Stresses Along Interface
for Run Types 2212–2222–2232

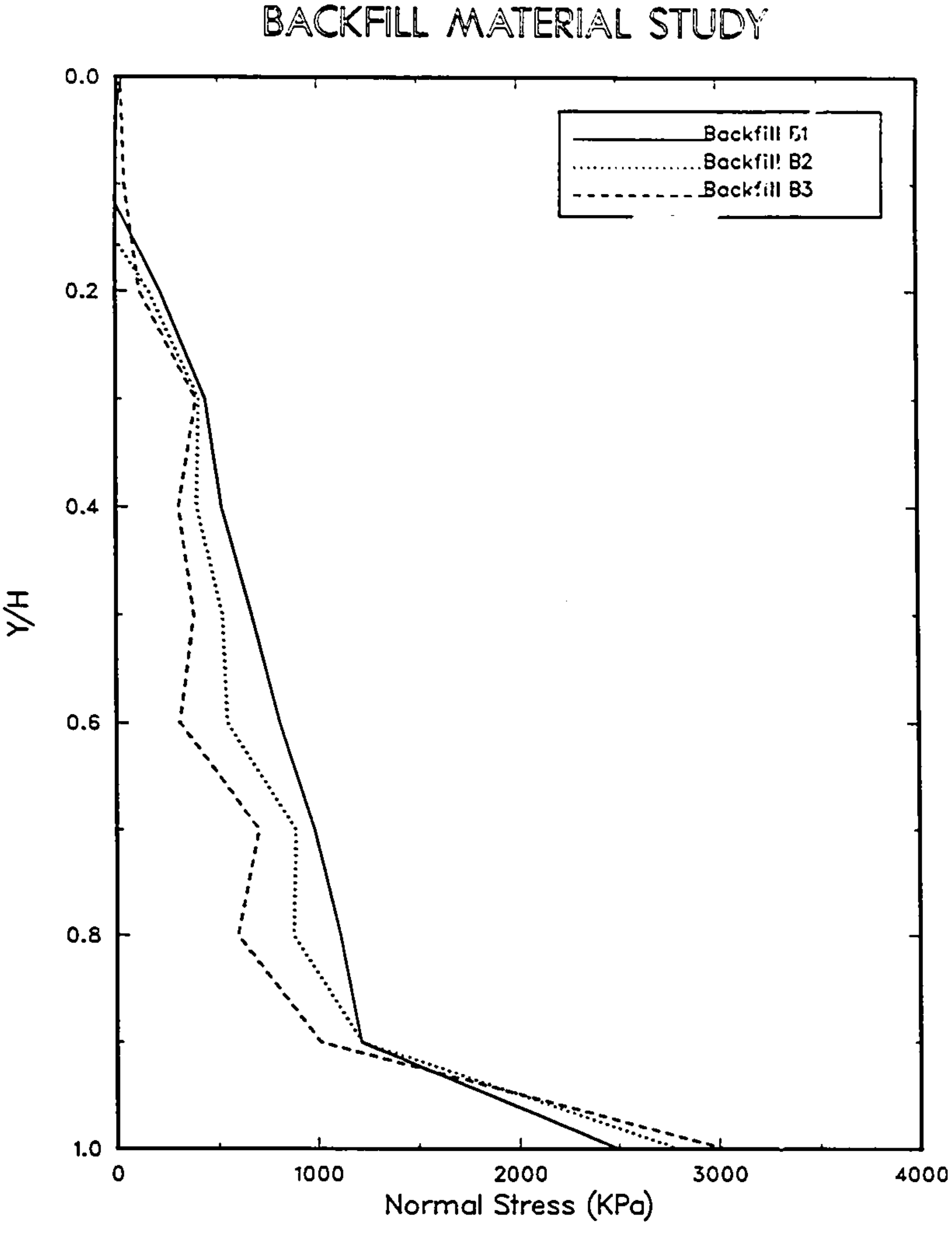

Figure 4.4: Normal Stresses Along Interface for Run Types 2221-2222-2223

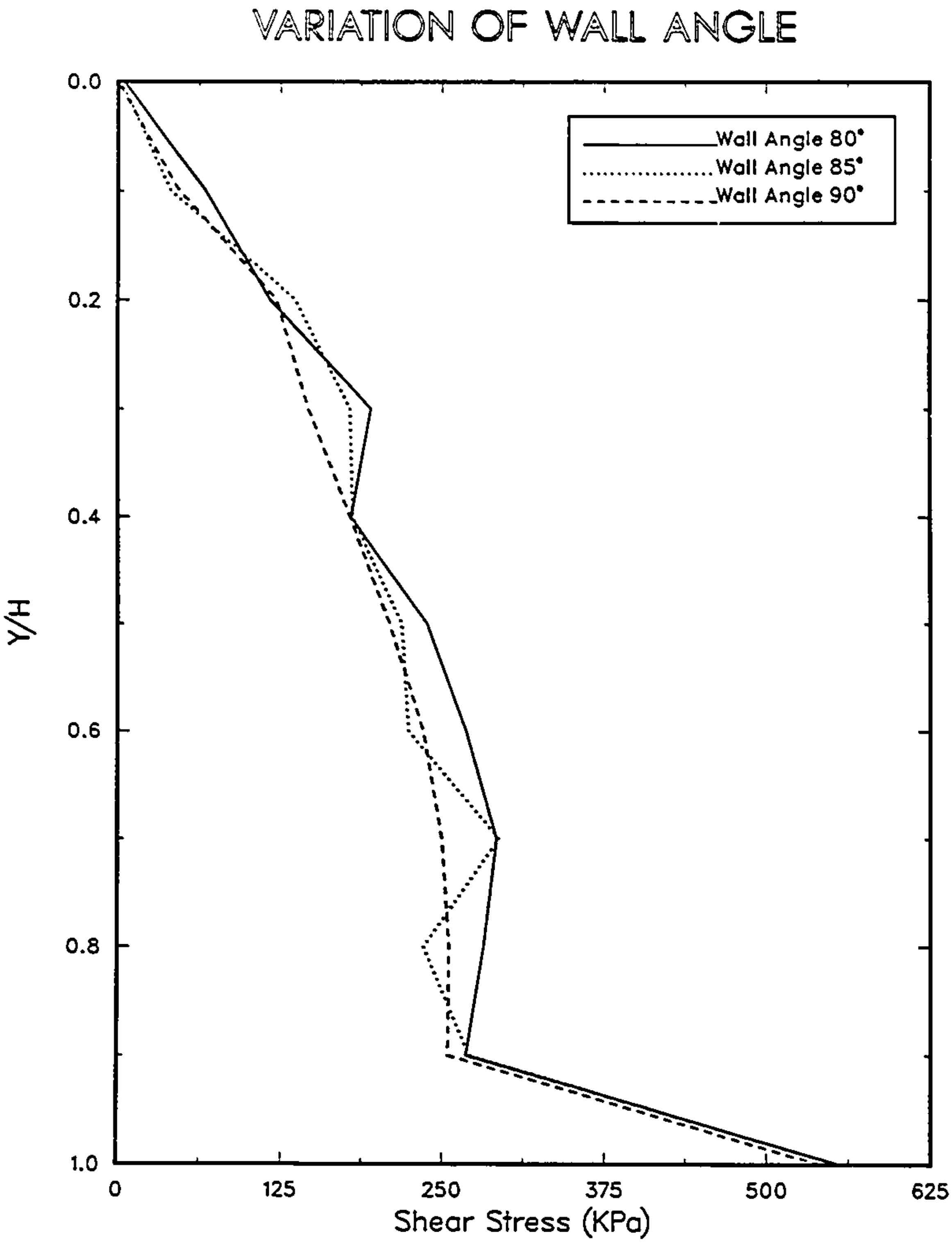

Figure 4.5: Shear Stresses Along Interface
for Run Types 1222–2222–3222

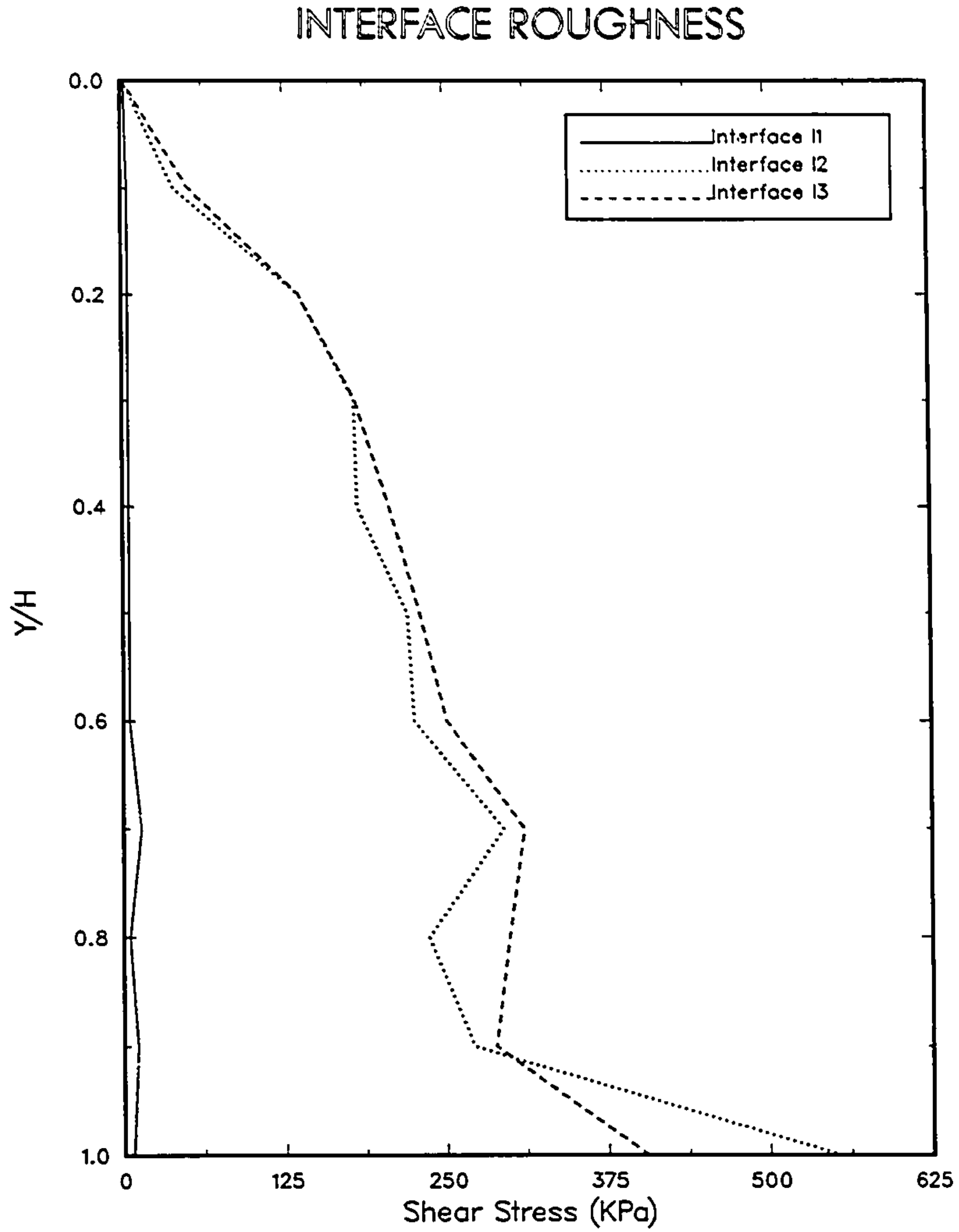

Figure 4.6: Shear Stresses Along Interface for Run Types 2122–2222–2322

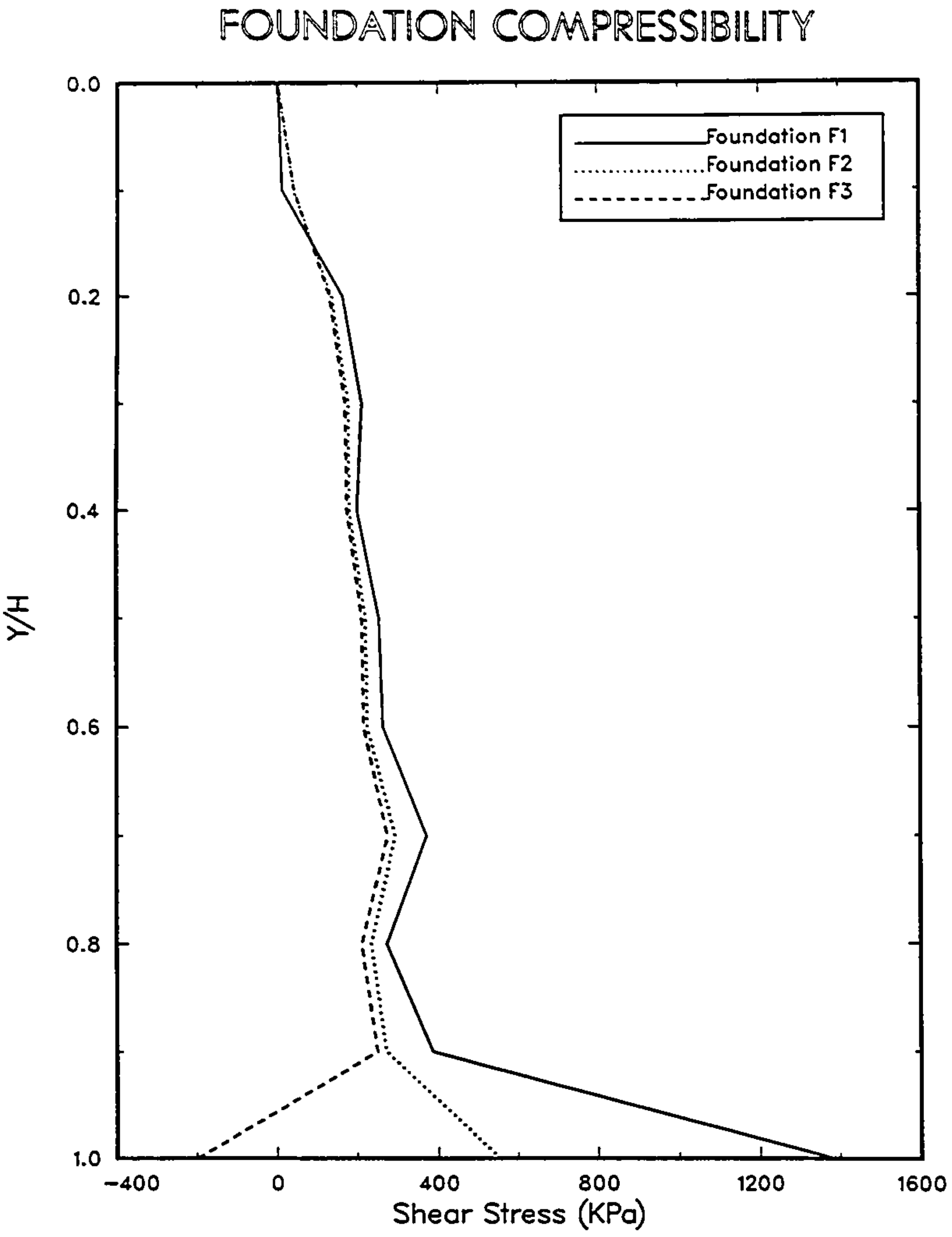

Figure 4.7: Shear Stresses Along Interface for Run Types 2212–2222–2232

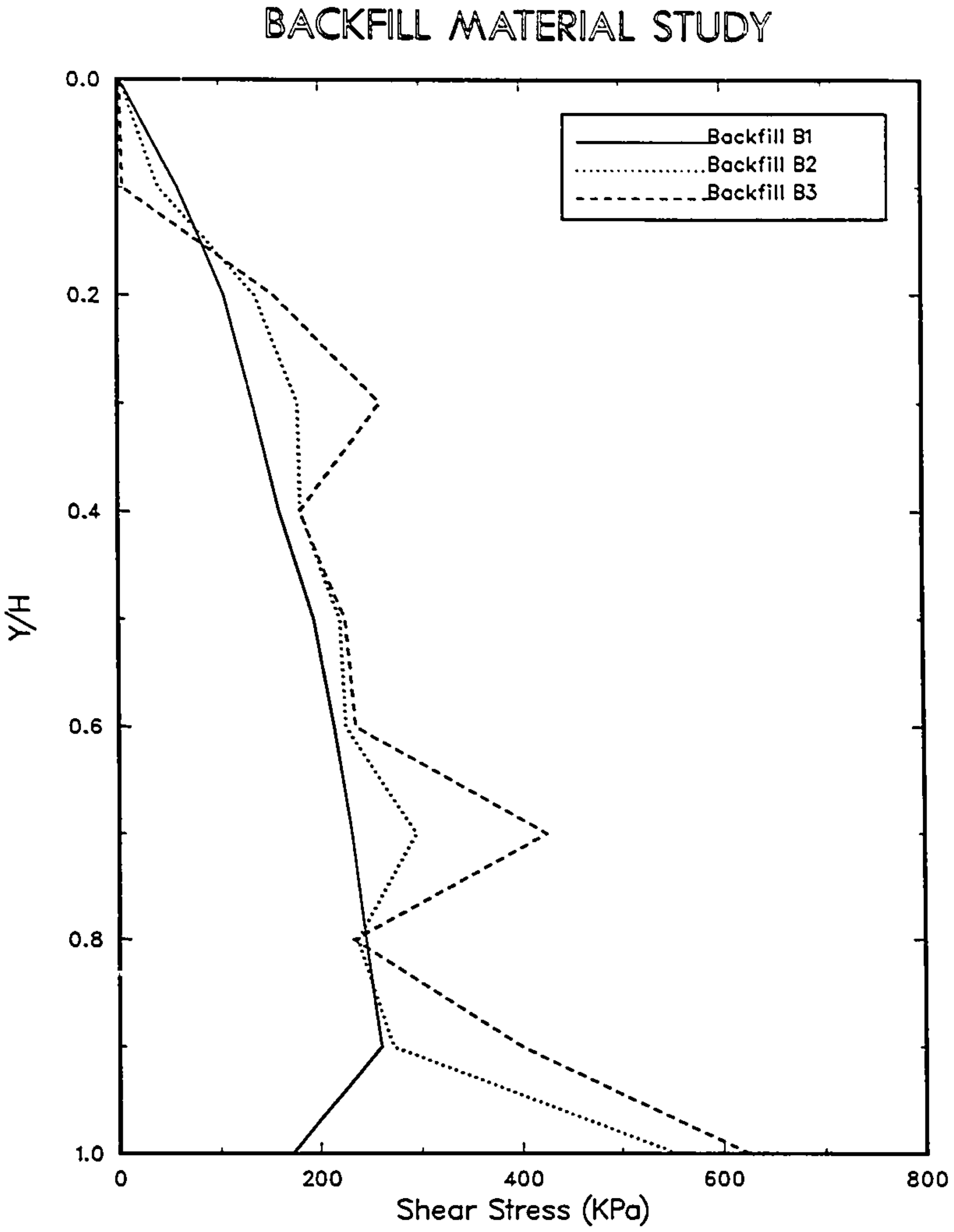

Figure 4.8: Shear Stresses Along Interface
for Run Types 2221–2222–2223

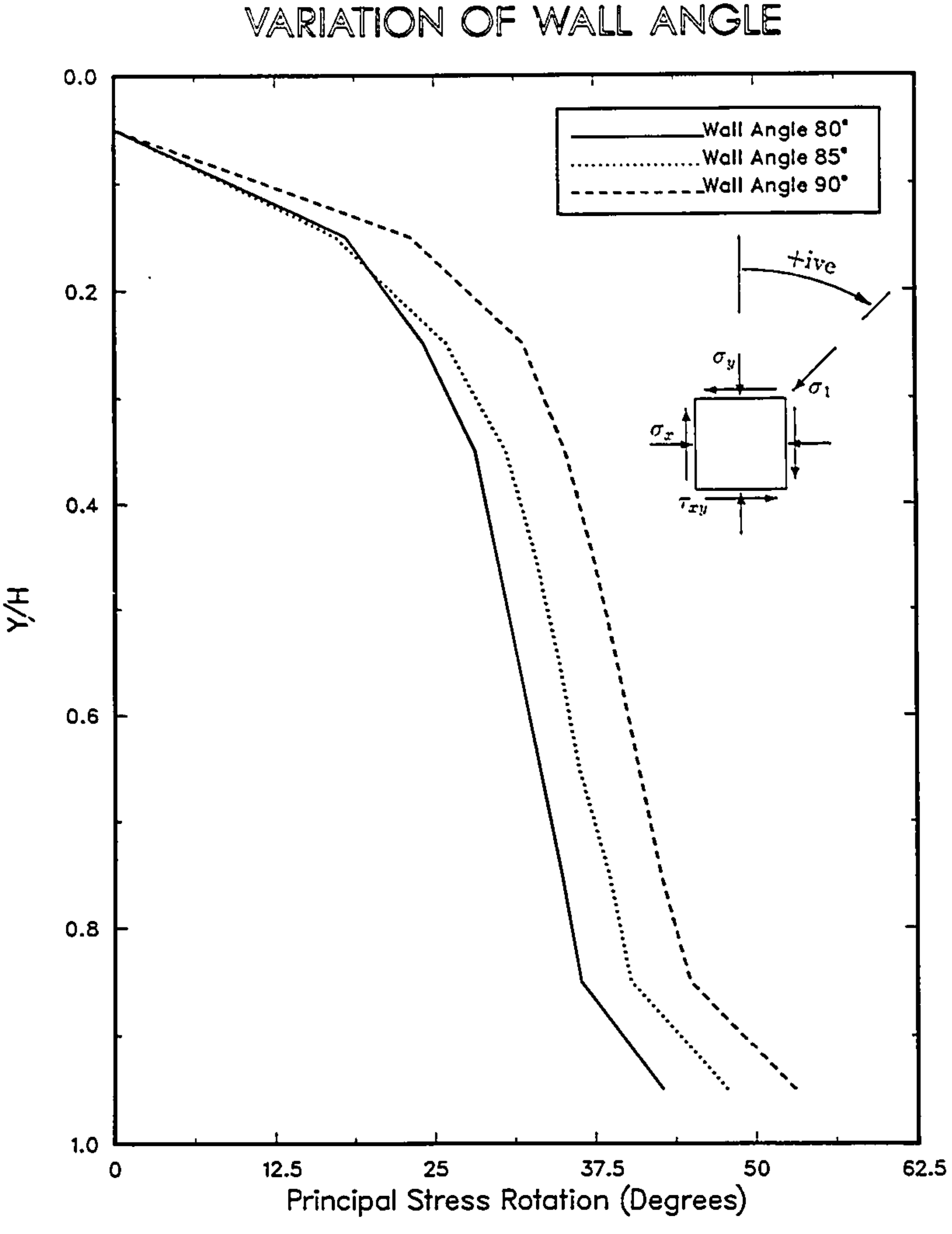

Figure 4.9: Principal Stress Rotations Along Interface for Run Types 1222–2222–3222

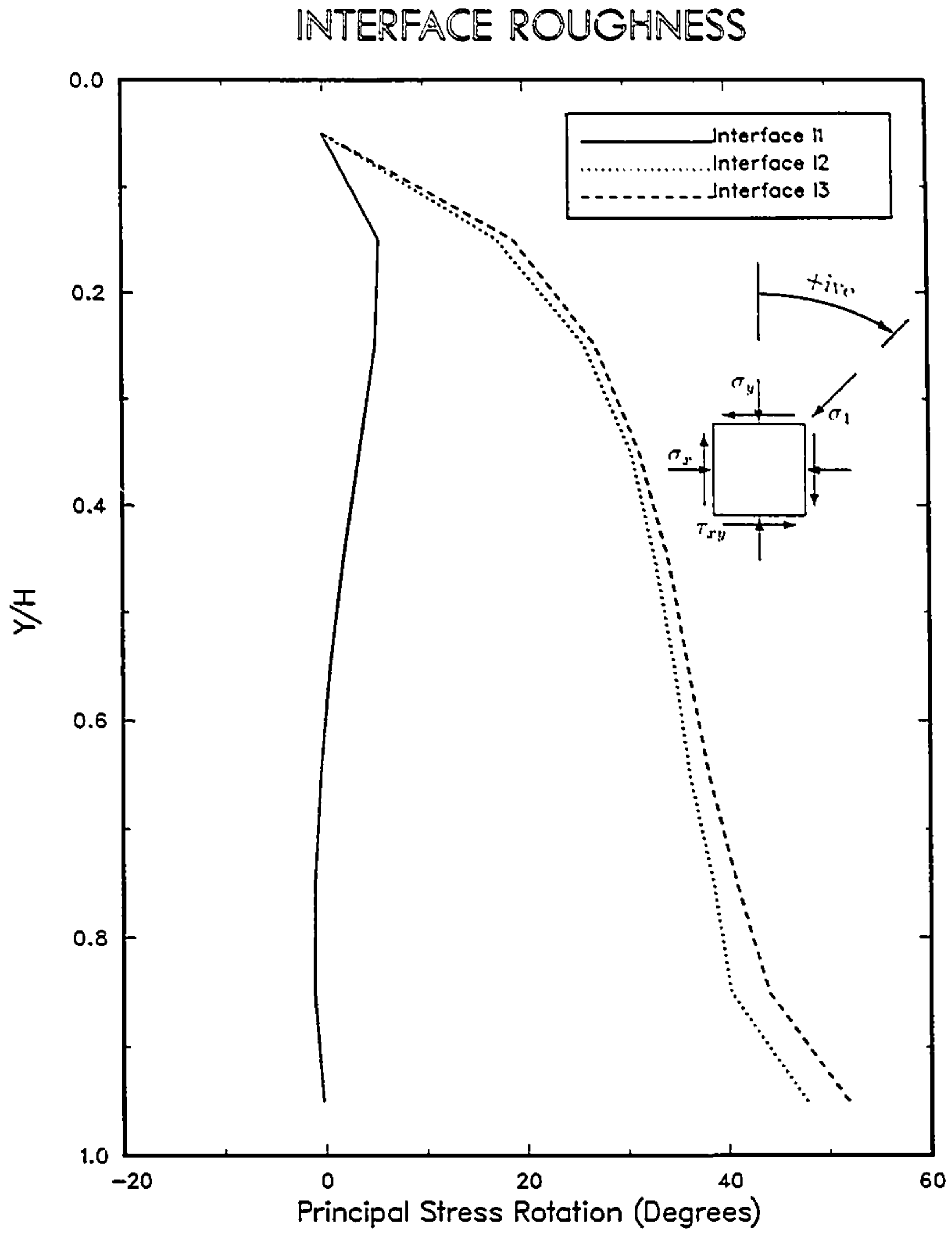

Figure 4.10: Principal Stress Rotations Along Interface for Run Types 2122–2222–2322

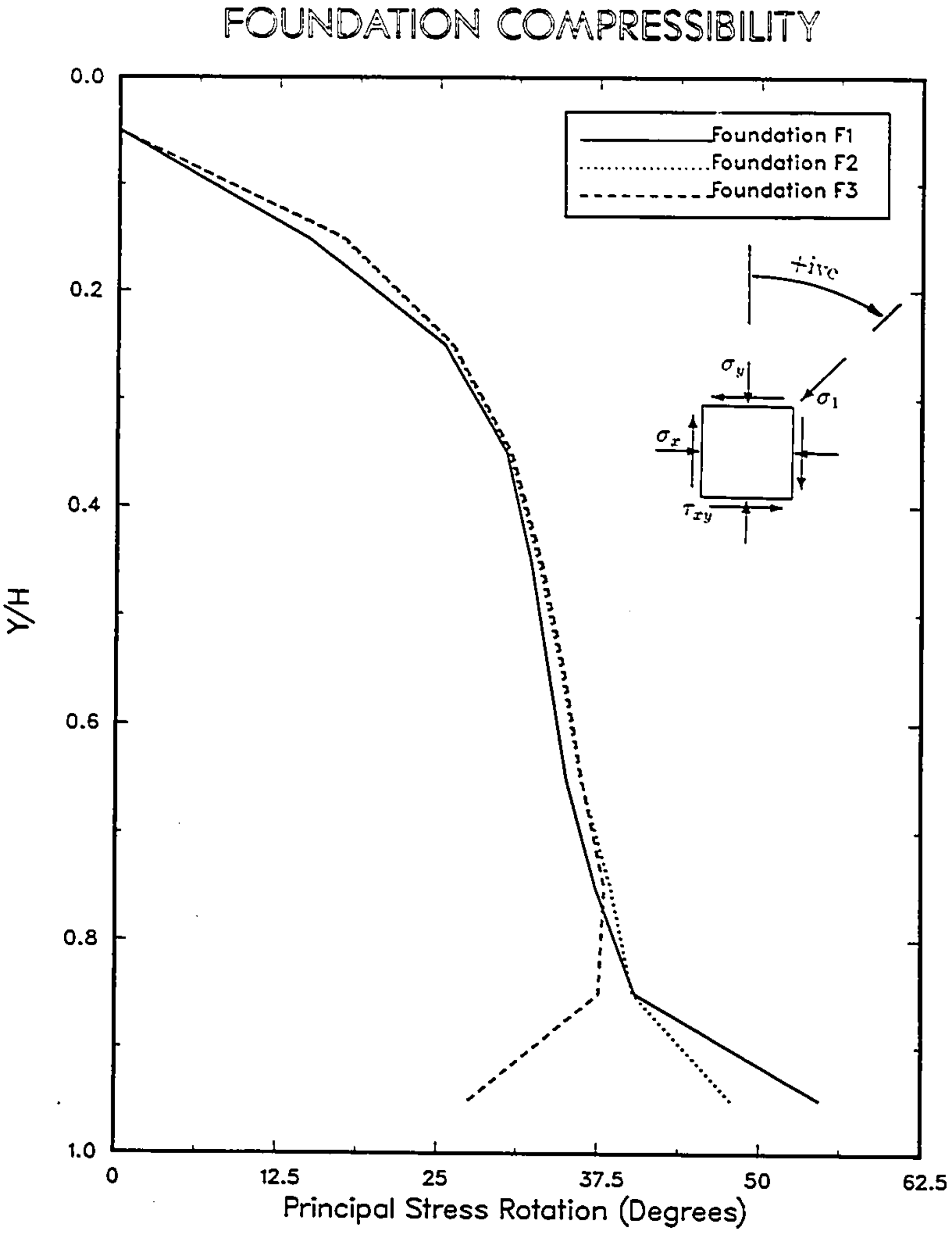

Figure 4.11: Principal Stress Rotations Along Interface for Run Types 2212–2222–2232

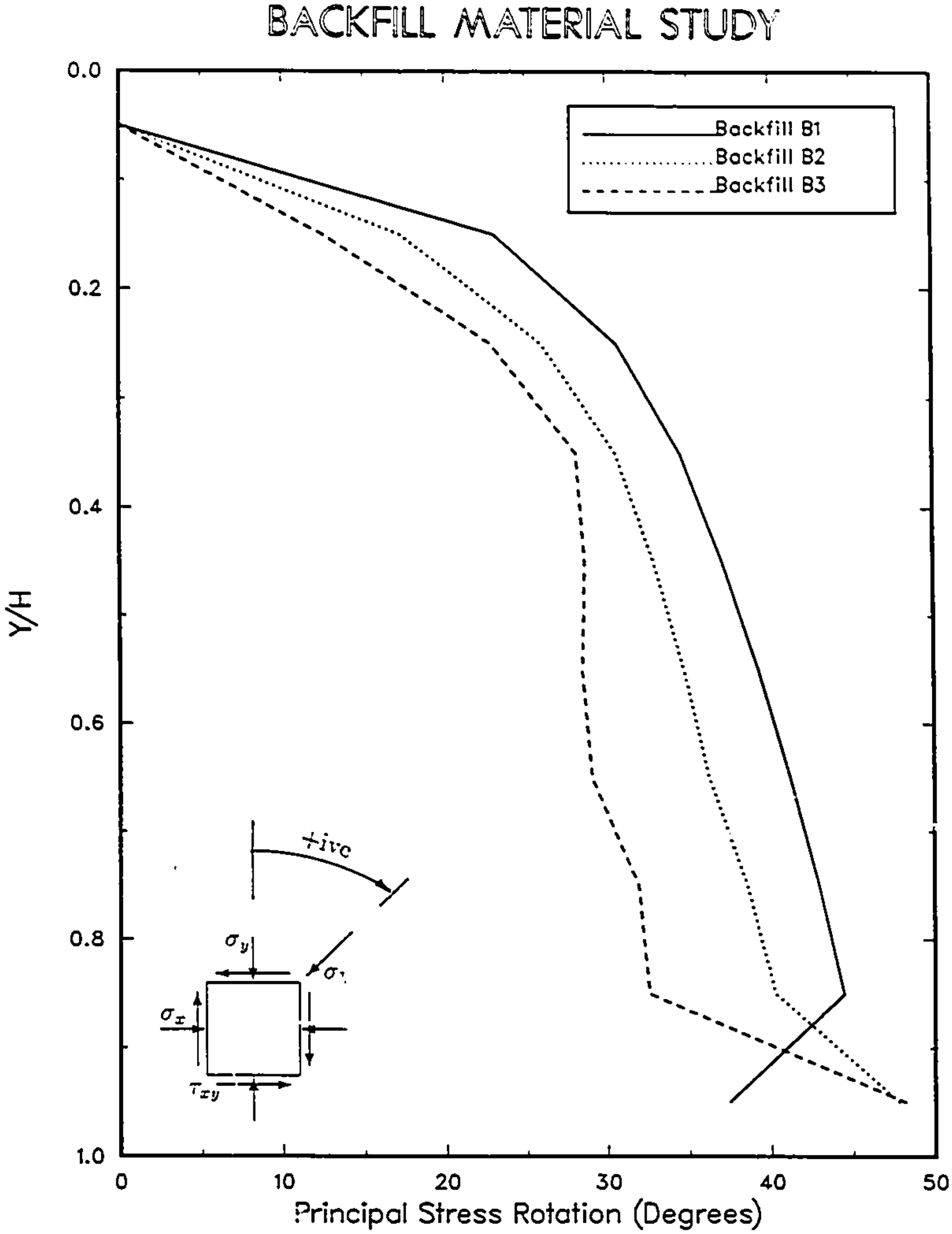

Figure 4.12: Principal Stress Rotations Along Interface for Run Types 2221–2222–2223

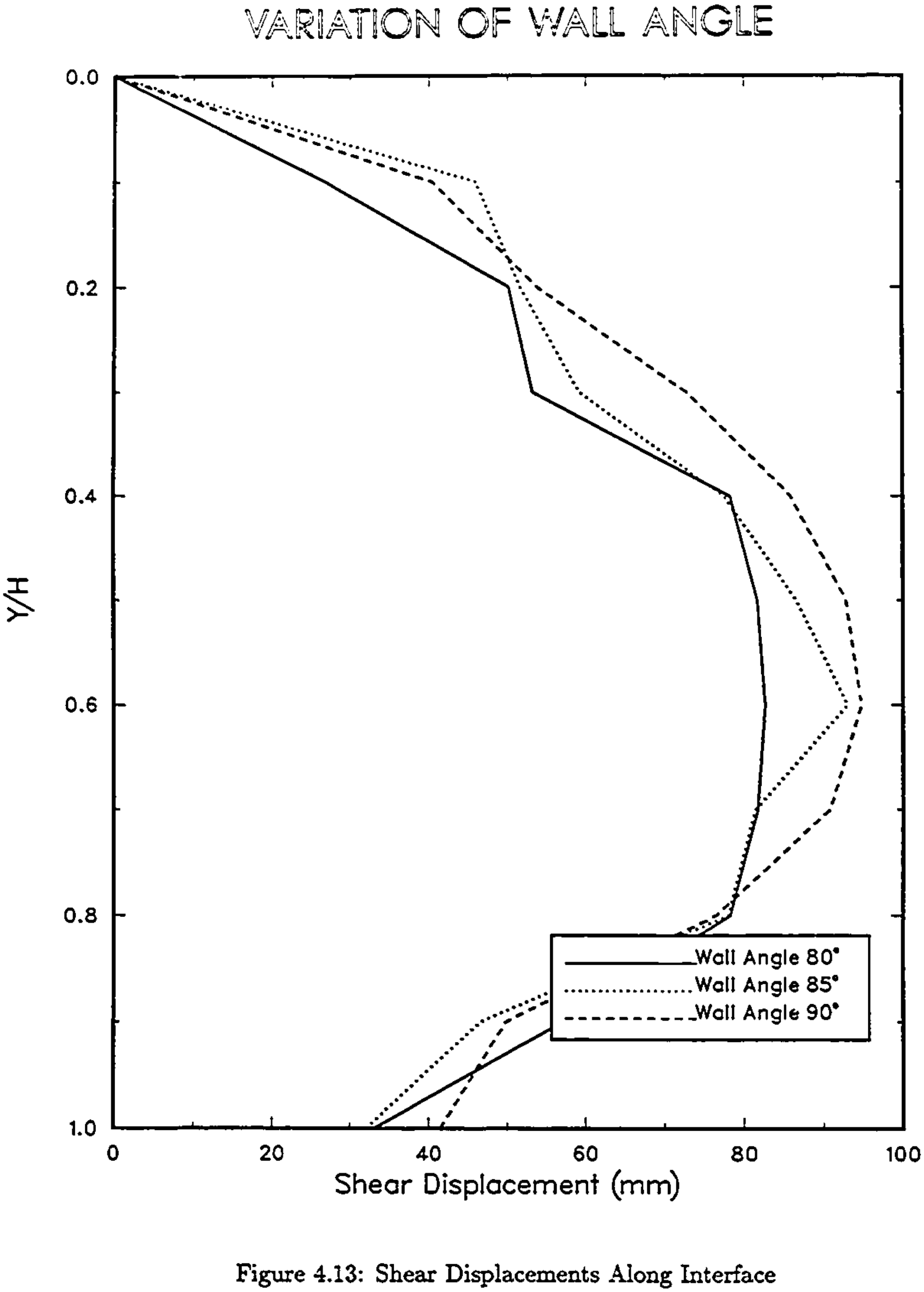

Figure 4.13: Shear Displacements Along Interface for Run Types 1222–2222–3222

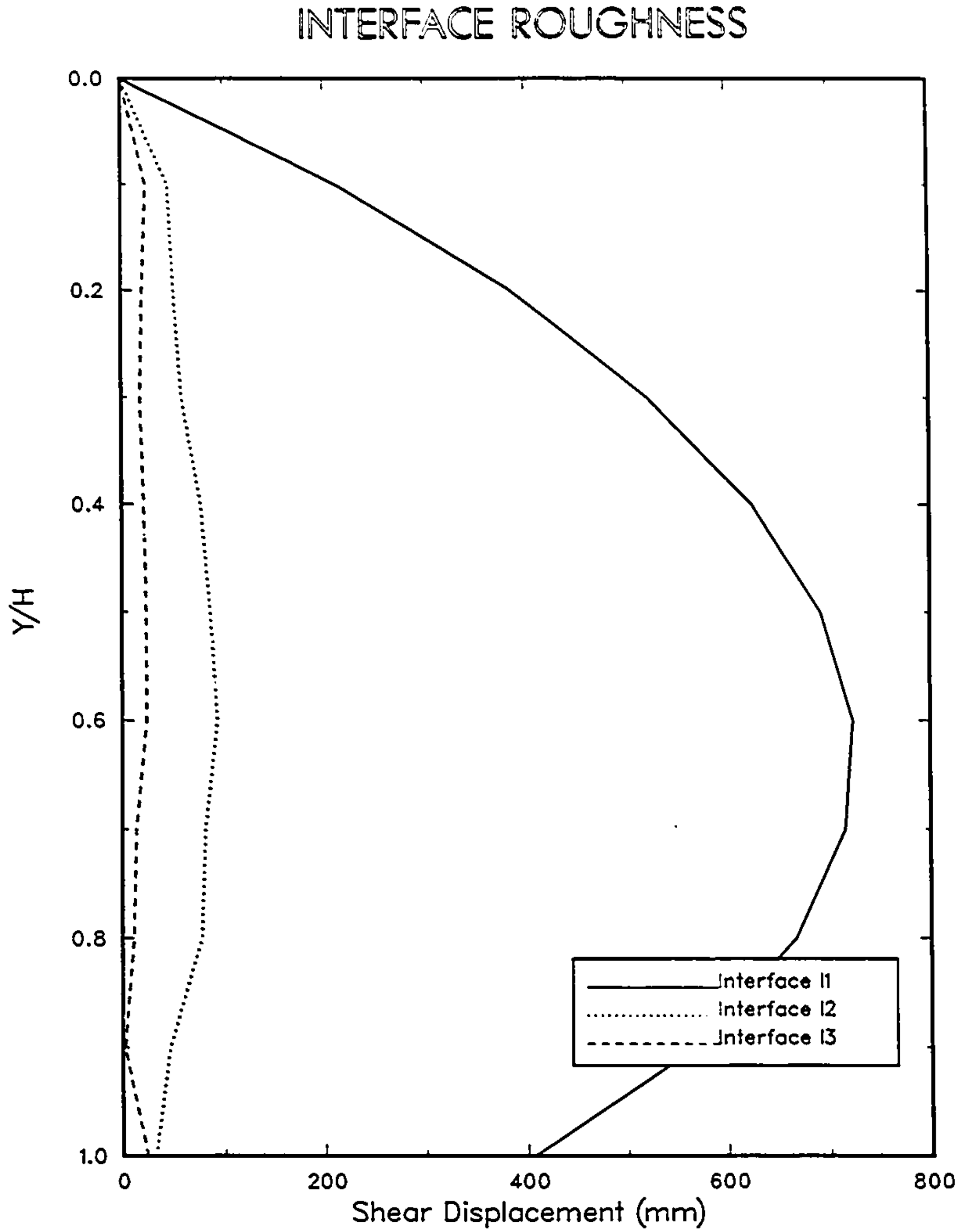

Figure 4.14: Shear Displacements Along Interface
for Run Types 2122–2222–2322

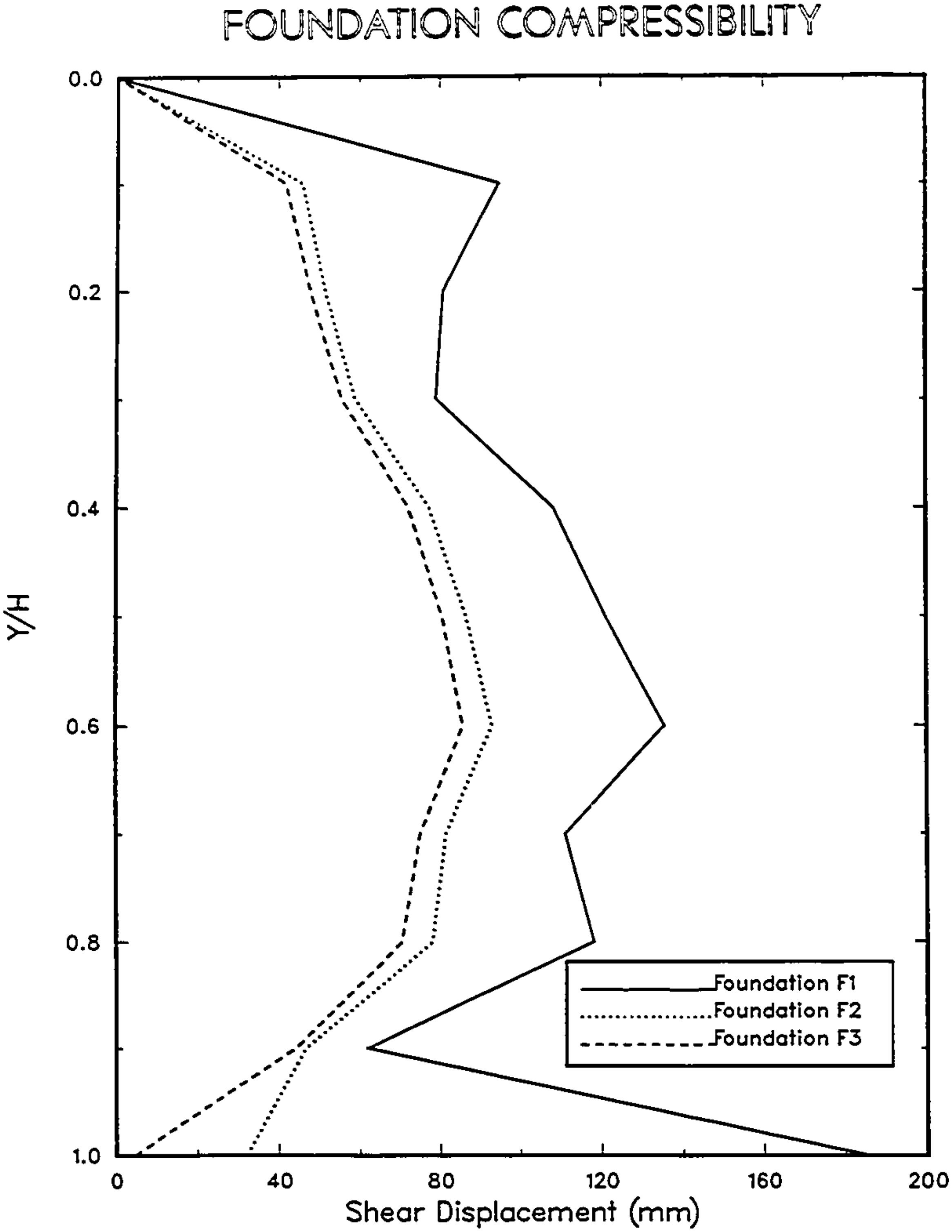

Figure 4.15: Shear Displacements Along Interface for Run Types 2212–2222–2232

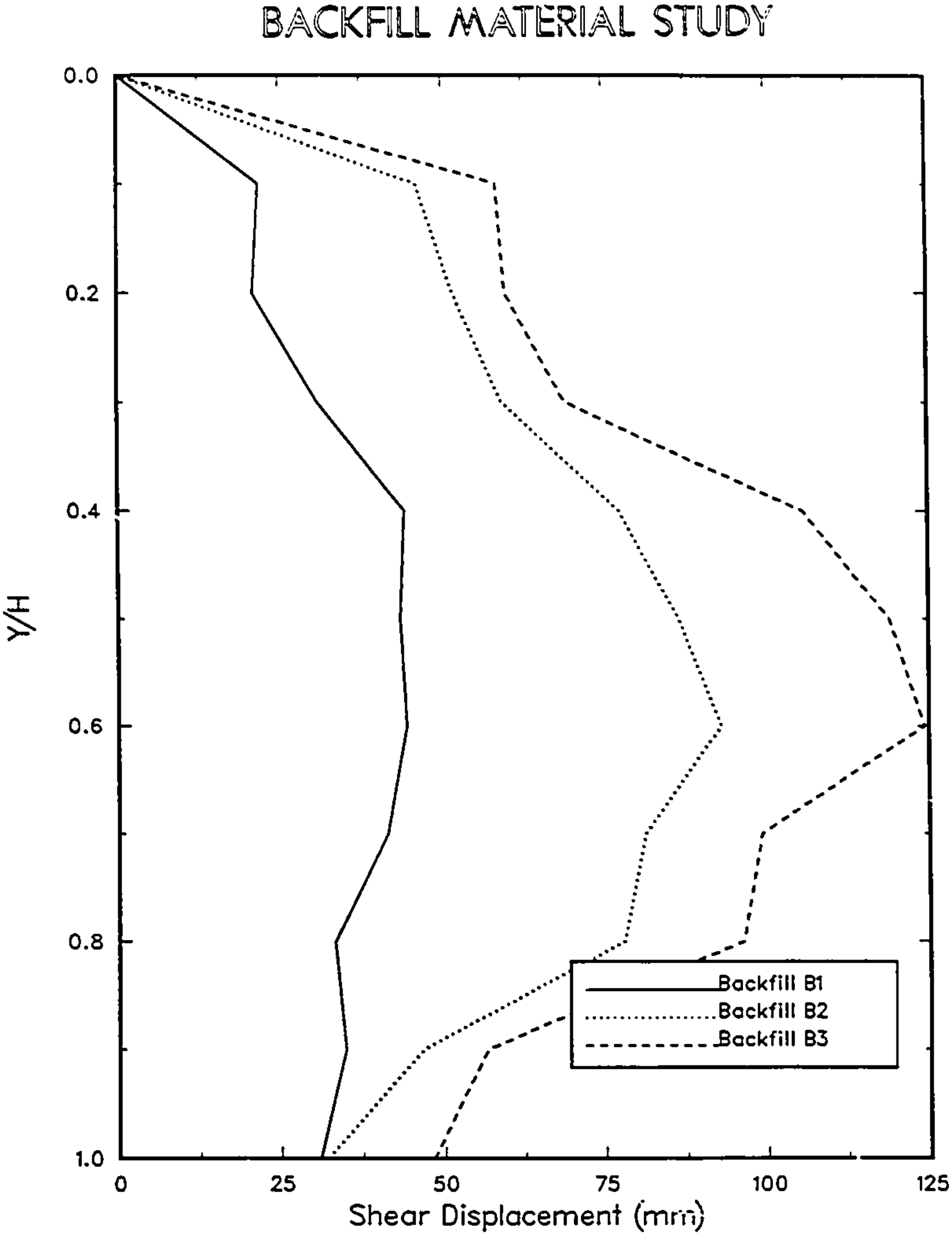

Figure 4.16: Shear Displacements Along Interface
for Run Types 2221–2222–2223

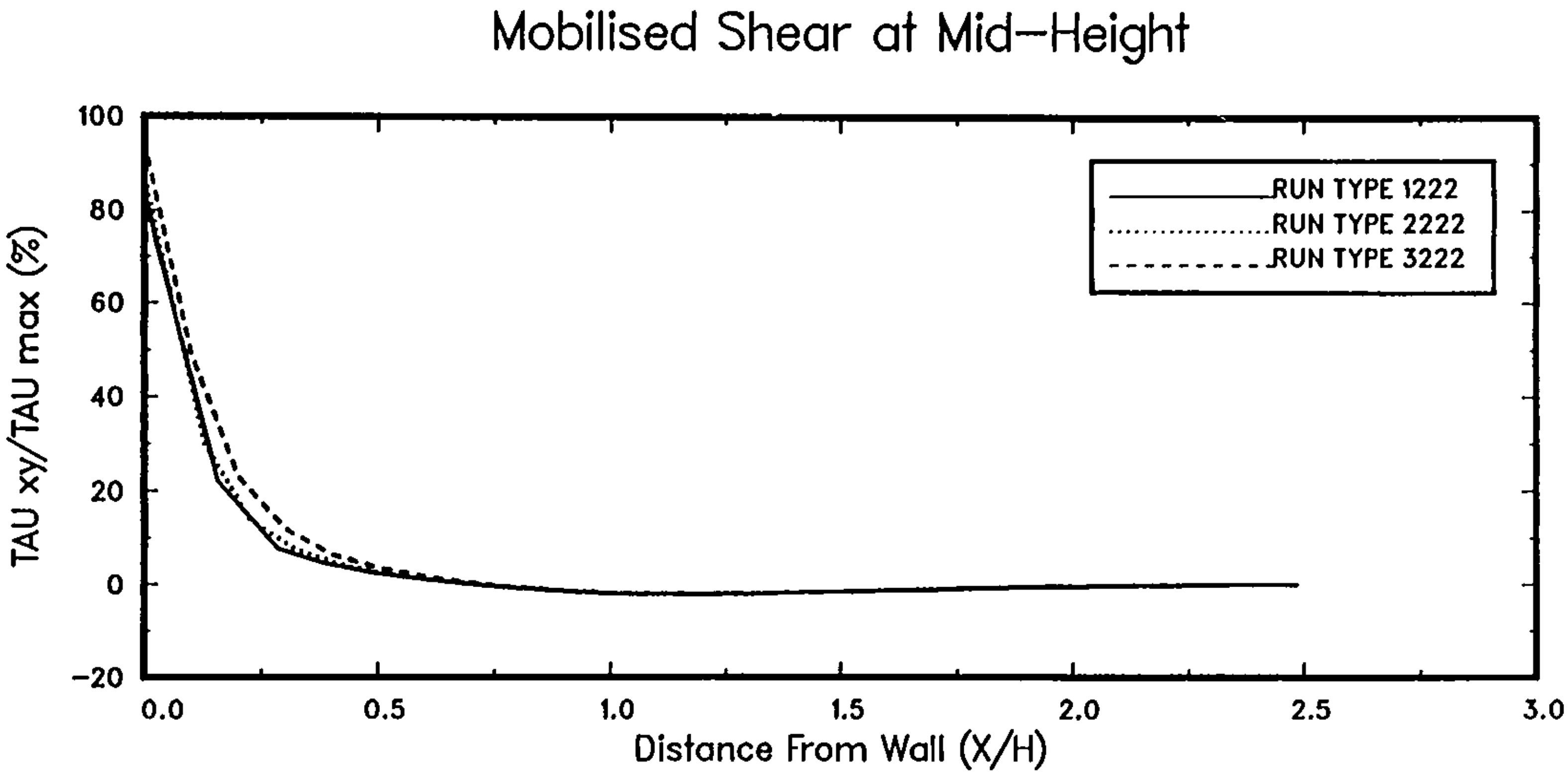

Figure 4.17: Variations of τ_{mob} in Soil Mass for Wall Angles W1–W2–W3

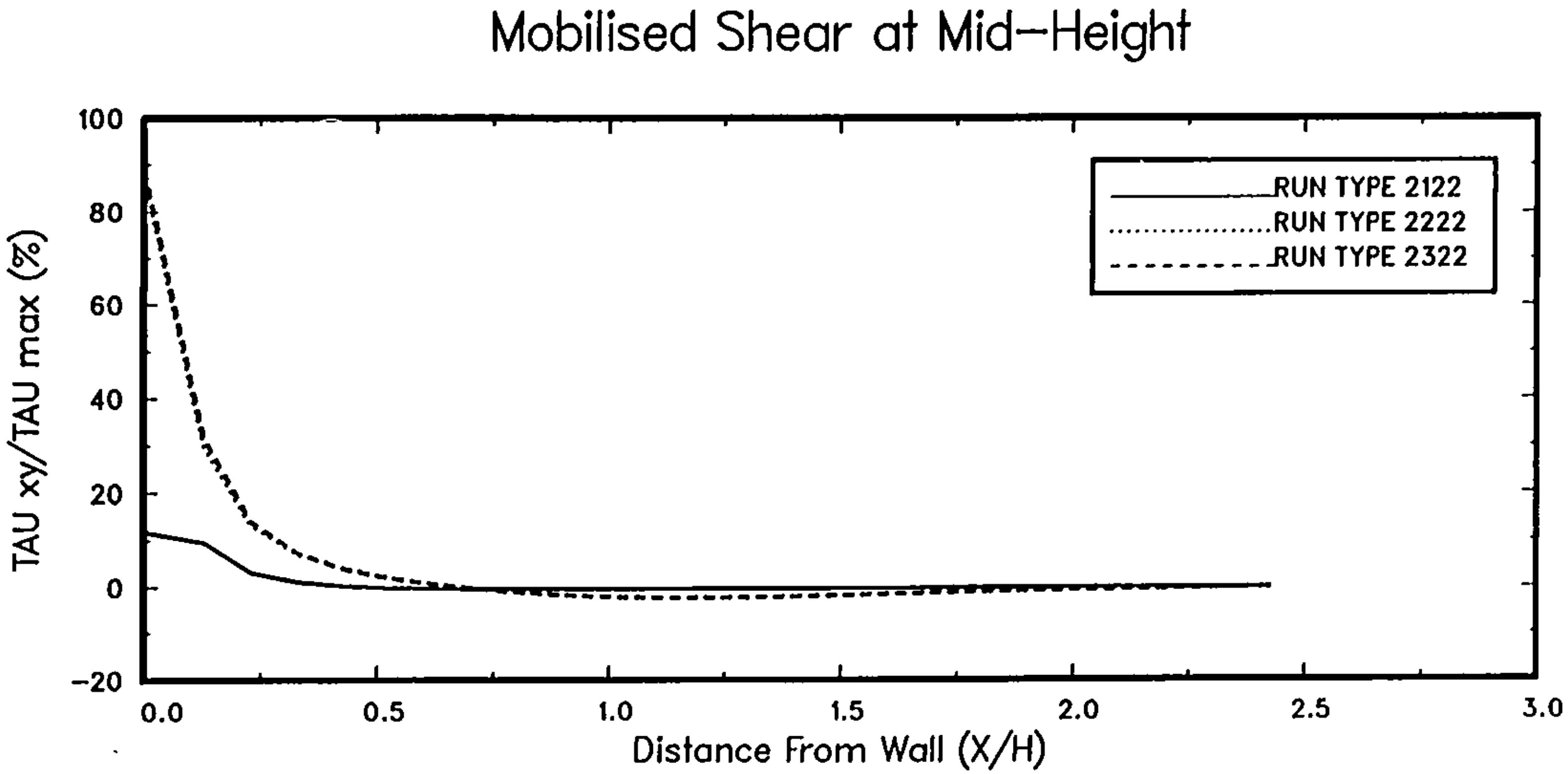

Figure 4.18: Variations of τ_{mob} in Soil Mass for Interfaces I1–I2–I3

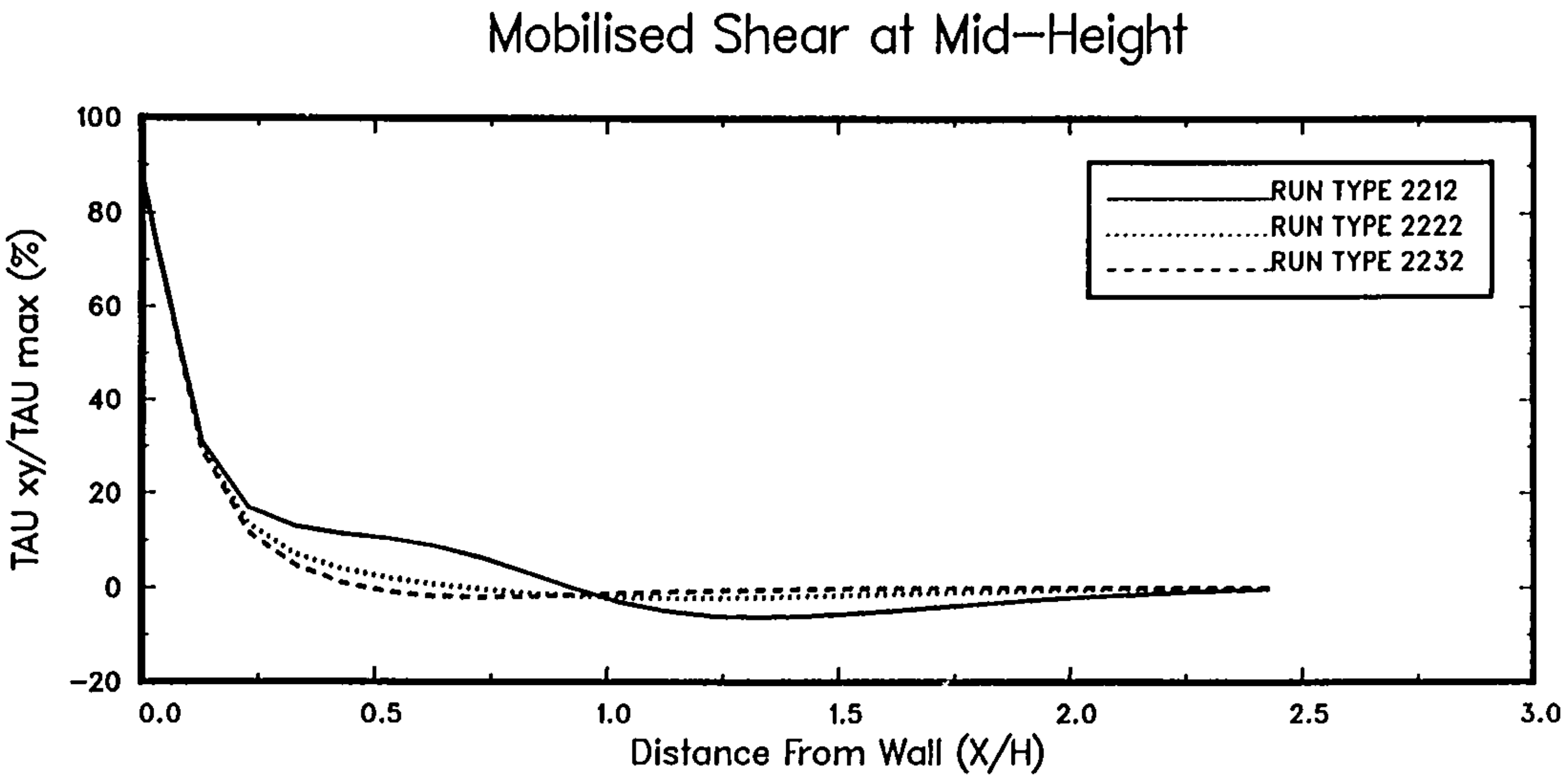

Figure 4.19: Variations of τ_{mob} in Soil Mass
for Foundation Materials F1–F2–F3

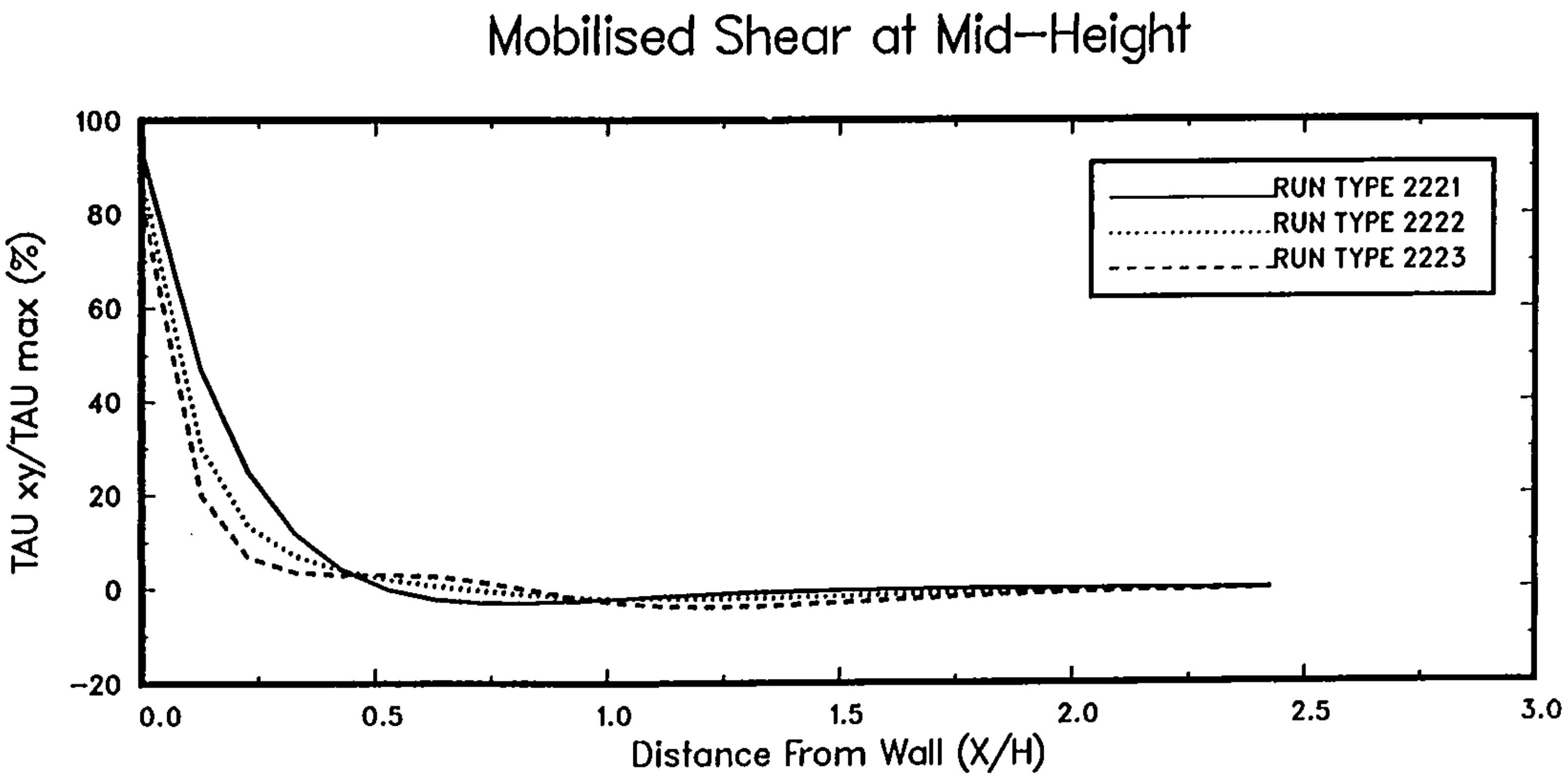

Figure 4.20: Variations of τ_{mob} in Soil Mass for Backfill Materials B1–B2–B3

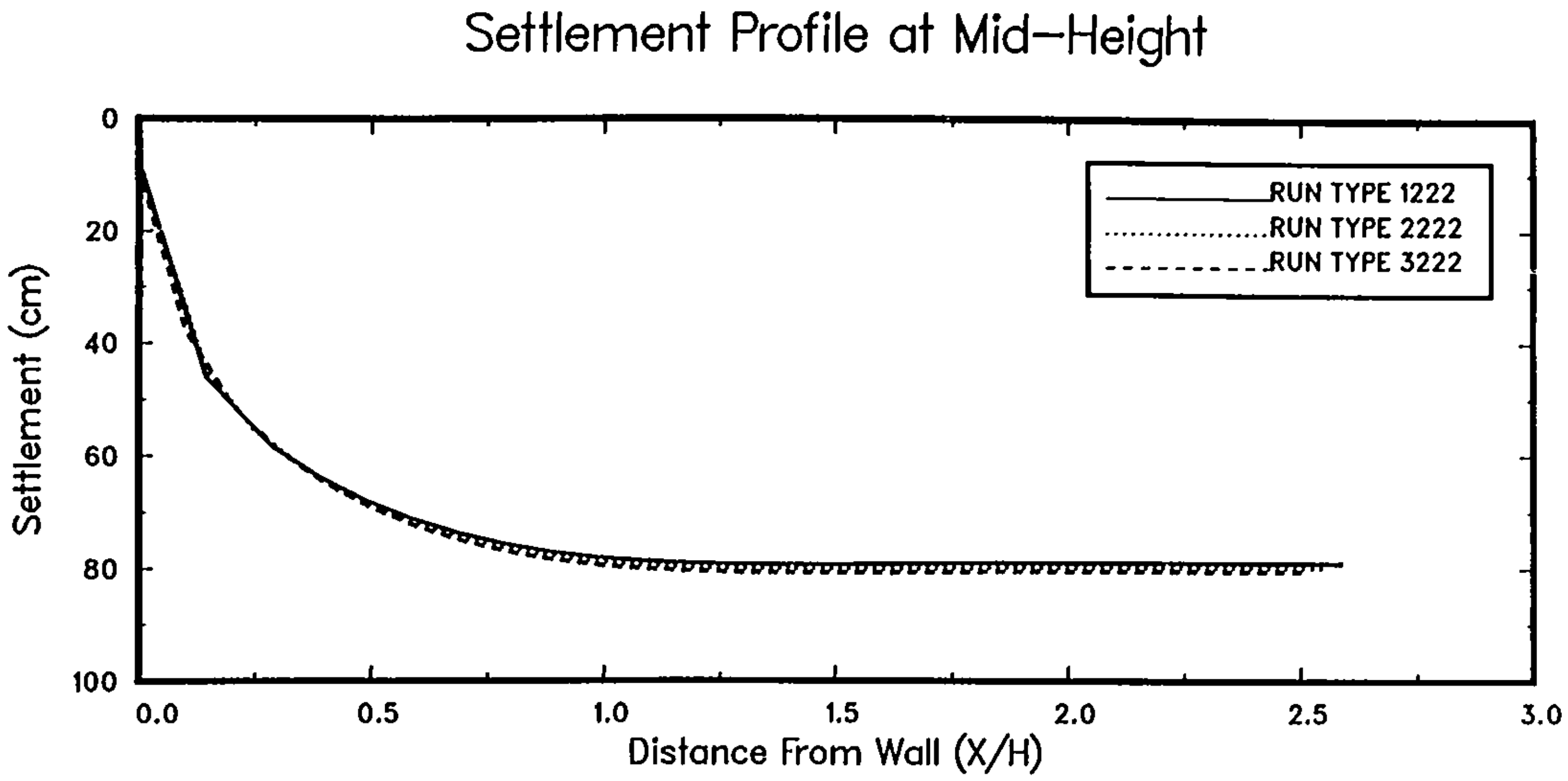

Figure 4.21: Typical Settlement Curves in Soil Mass for Wall Angles W1–W2–W3

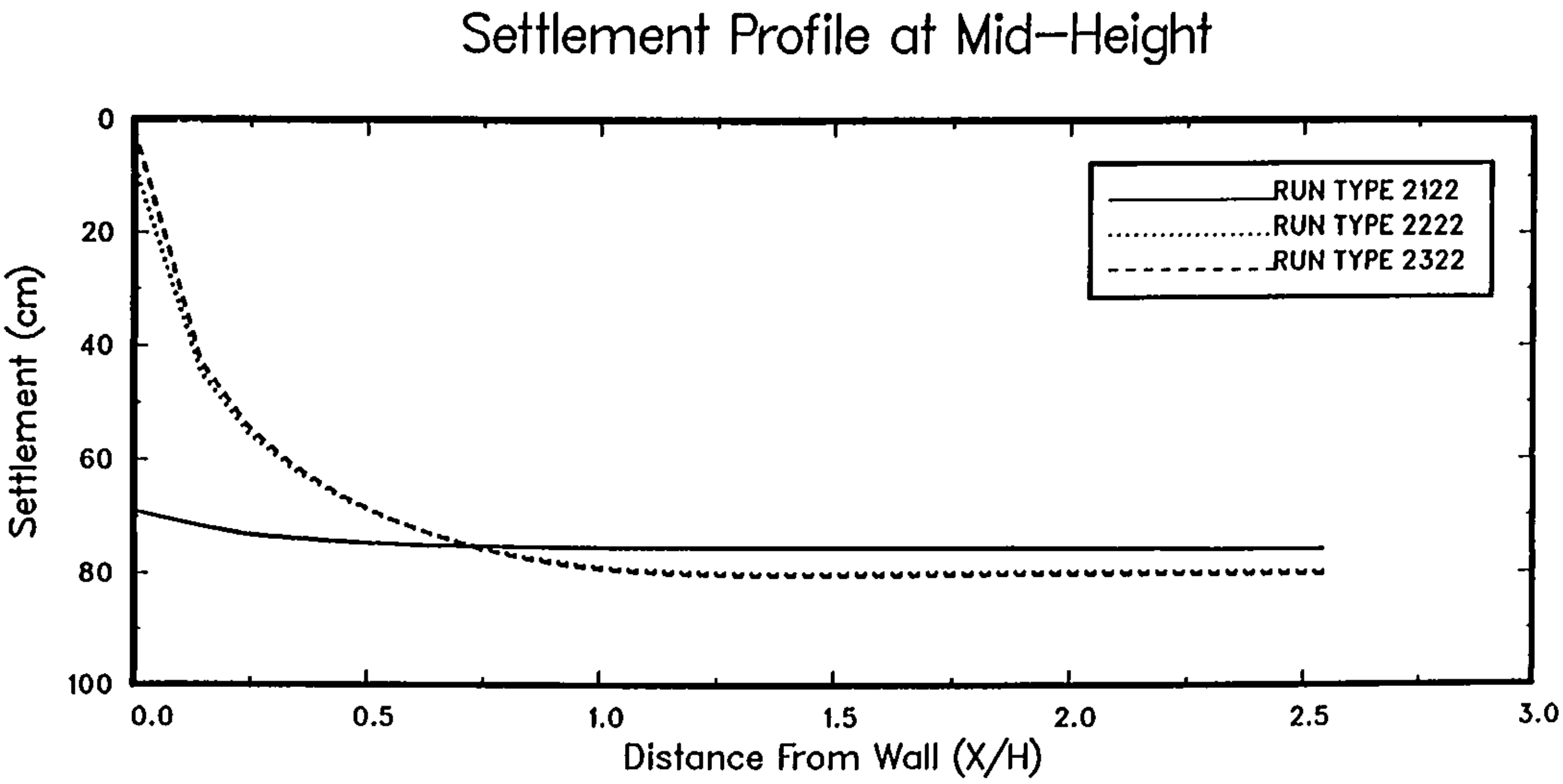

Figure 4.22: Typical Settlement Curves in Soil Mass for Interfaces I1-I2-I3

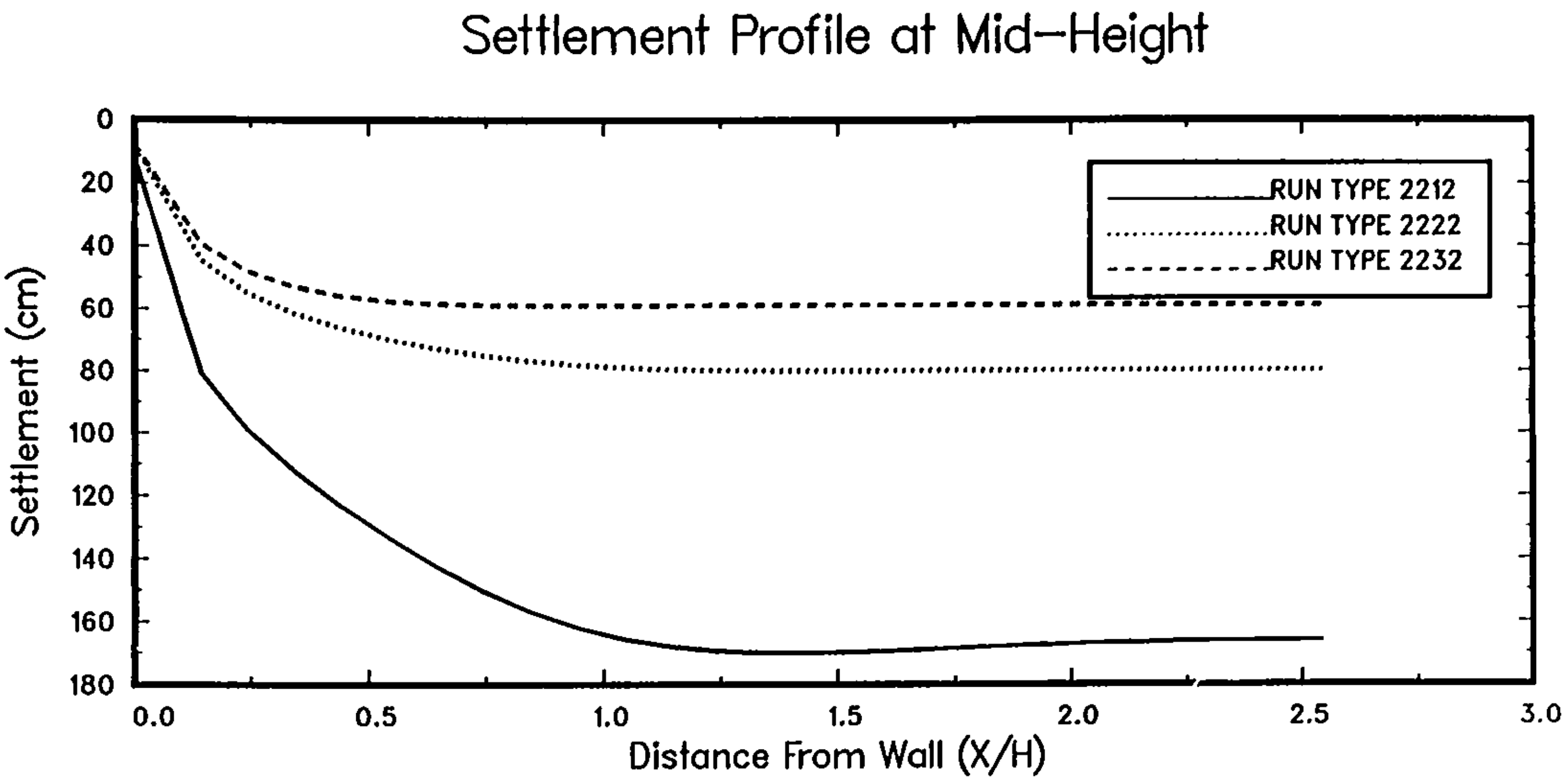

Figure 4.23: Typical Settlement Curves in Soil Mass for Foundation Materials F1–F2–F3

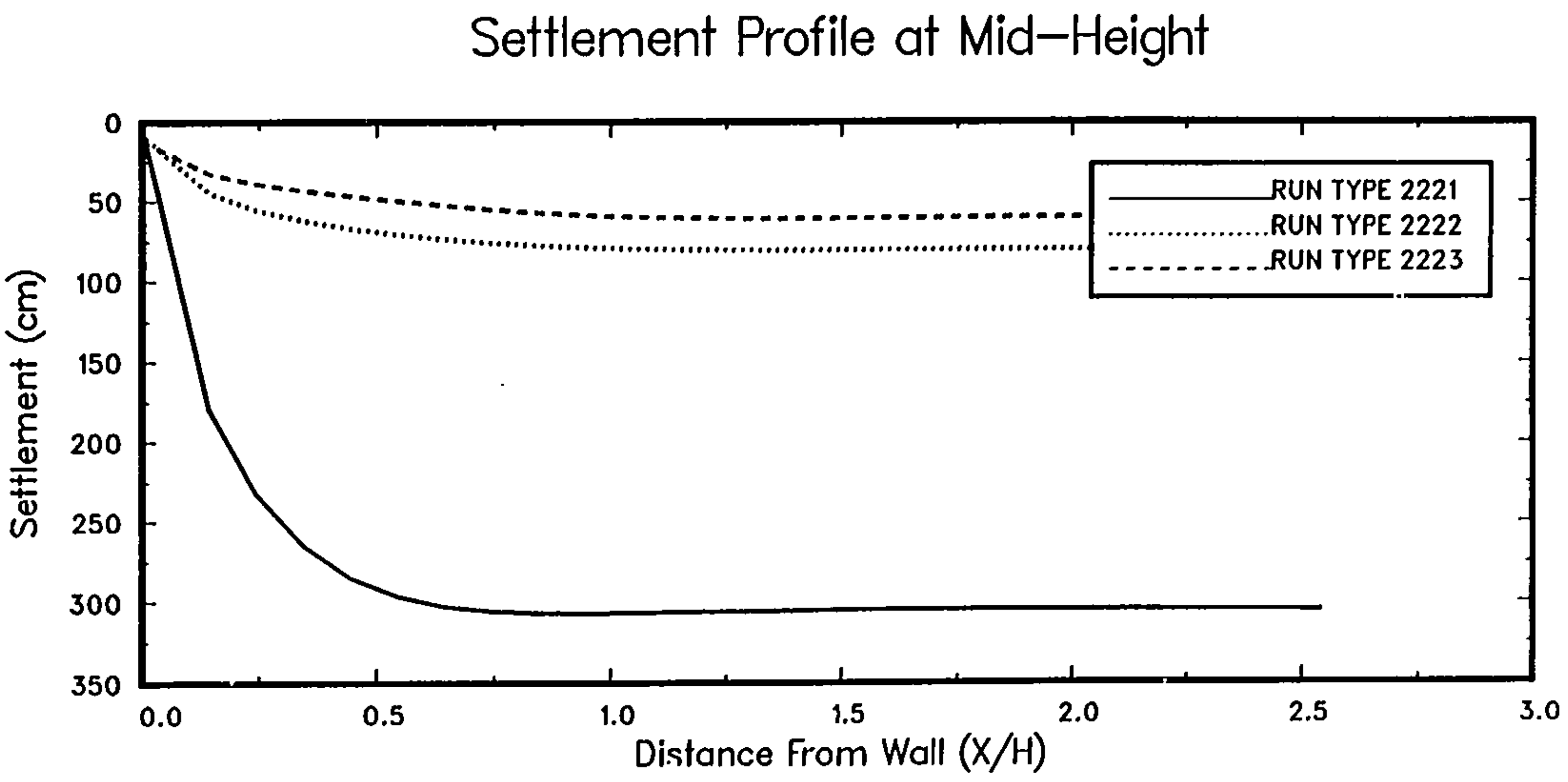

Figure 4.24: Typical Settlement Curves in Soil Mass
for Backfill Materials B1-B2-B3

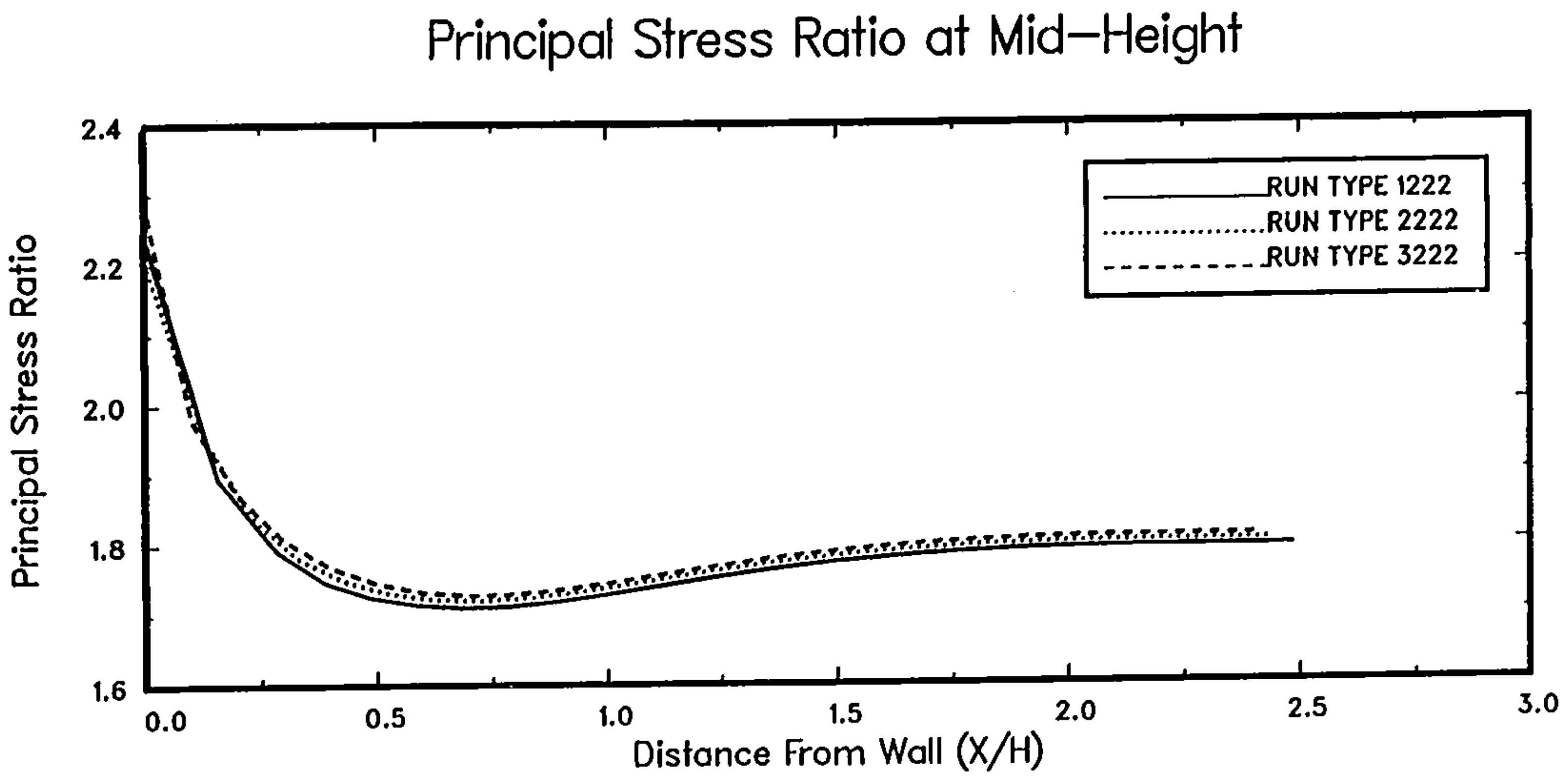

Figure 4.25: Principal Stress Ratio Values in Soil Mass for Wall Angles W1–W2–W3

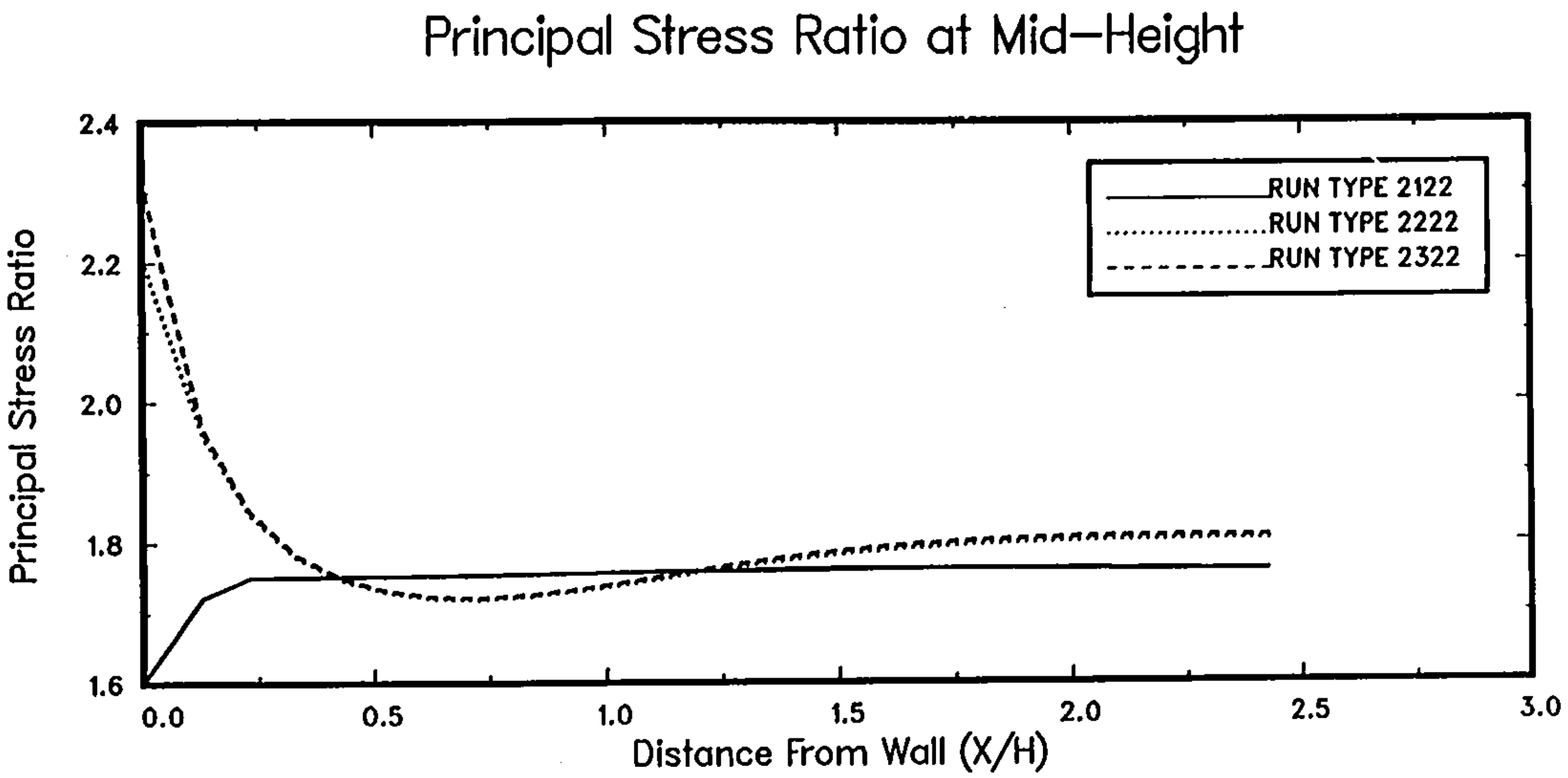
Principal Stress Ratio at Mid–Height

Figure 4.26: Principal Stress Ratio Values in Soil Mass for Interfaces I1–I2–I3

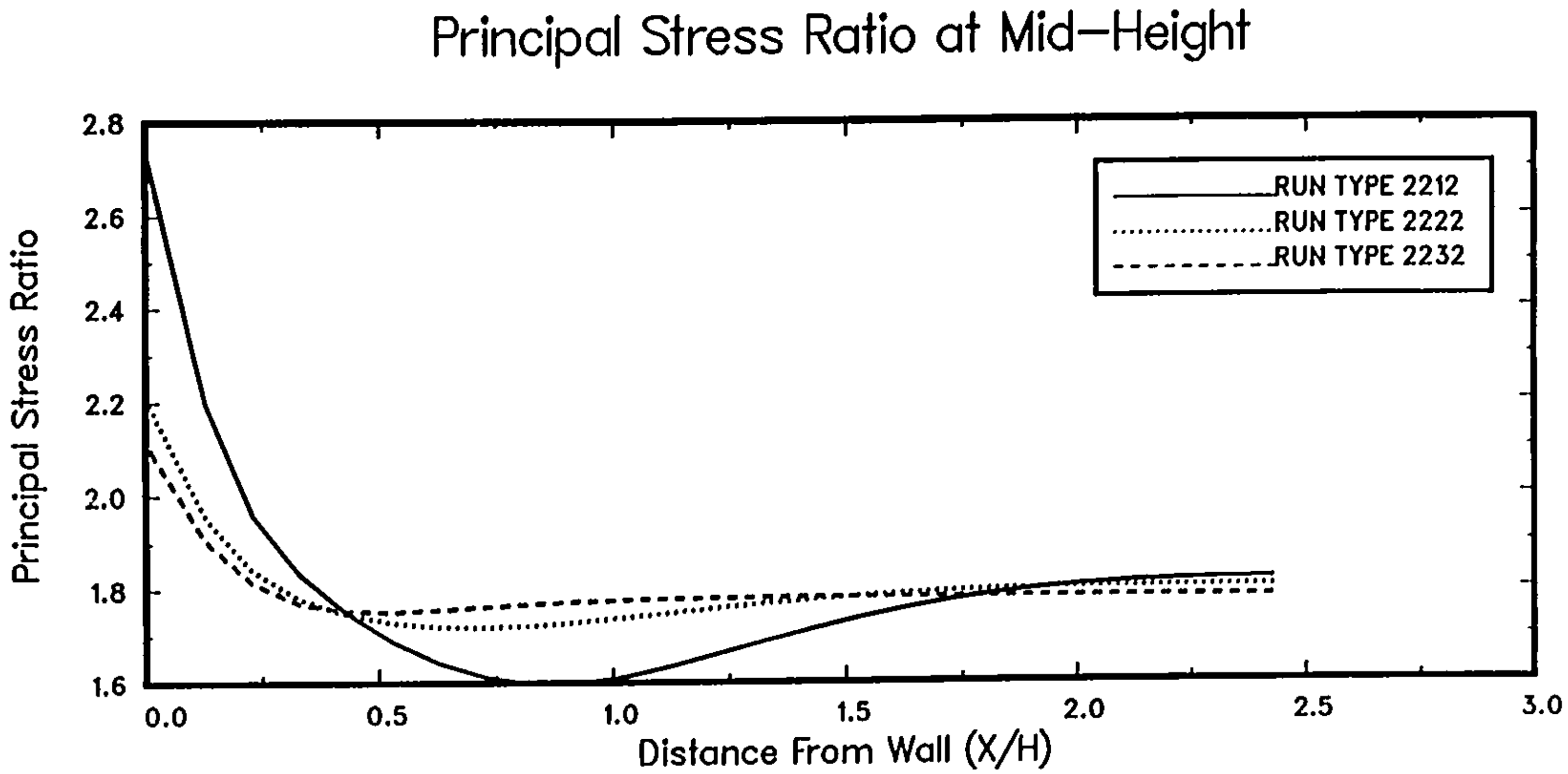

Figure 4.27: Principal Stress Ratio Values in Soil Mass
for Foundation Materials F1-F2-F3

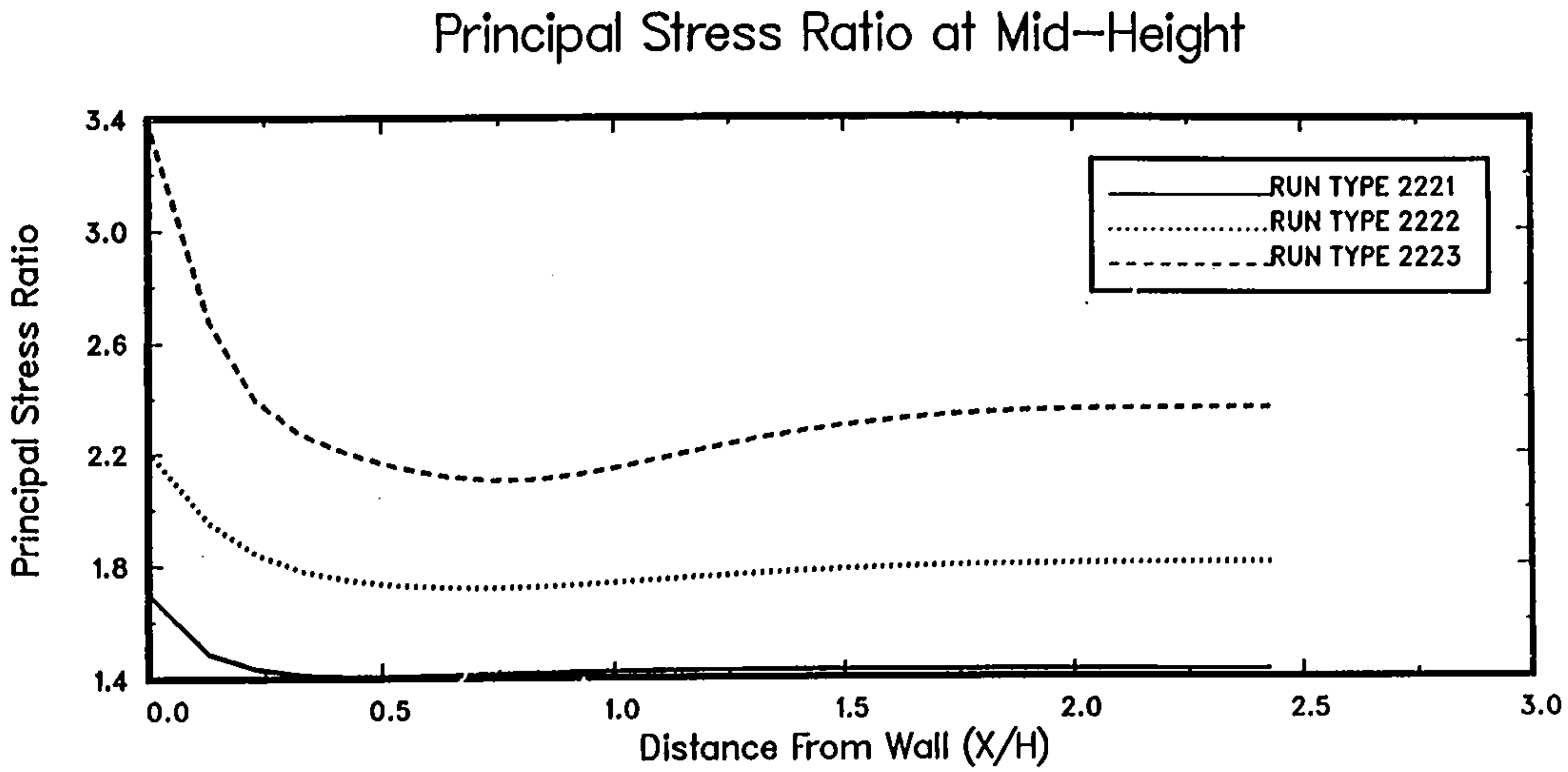

Figure 4.28: Principal Stress Ratio Values in Soil Mass for Backfill Materials B1–B2–B3

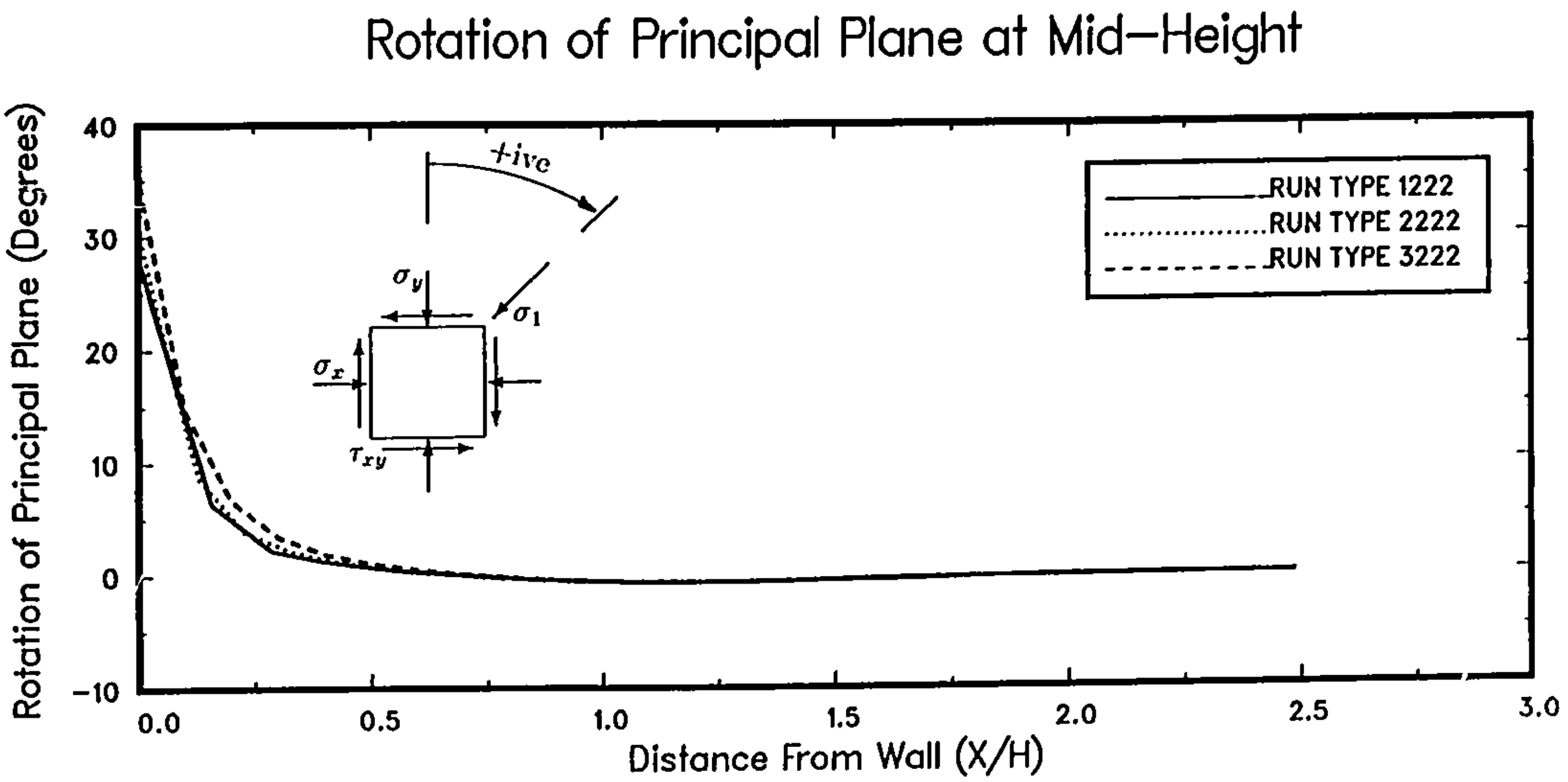

Figure 4.29: Rotation of Principal Planes in Soil Mass for Wall Angles W1–W2–W3

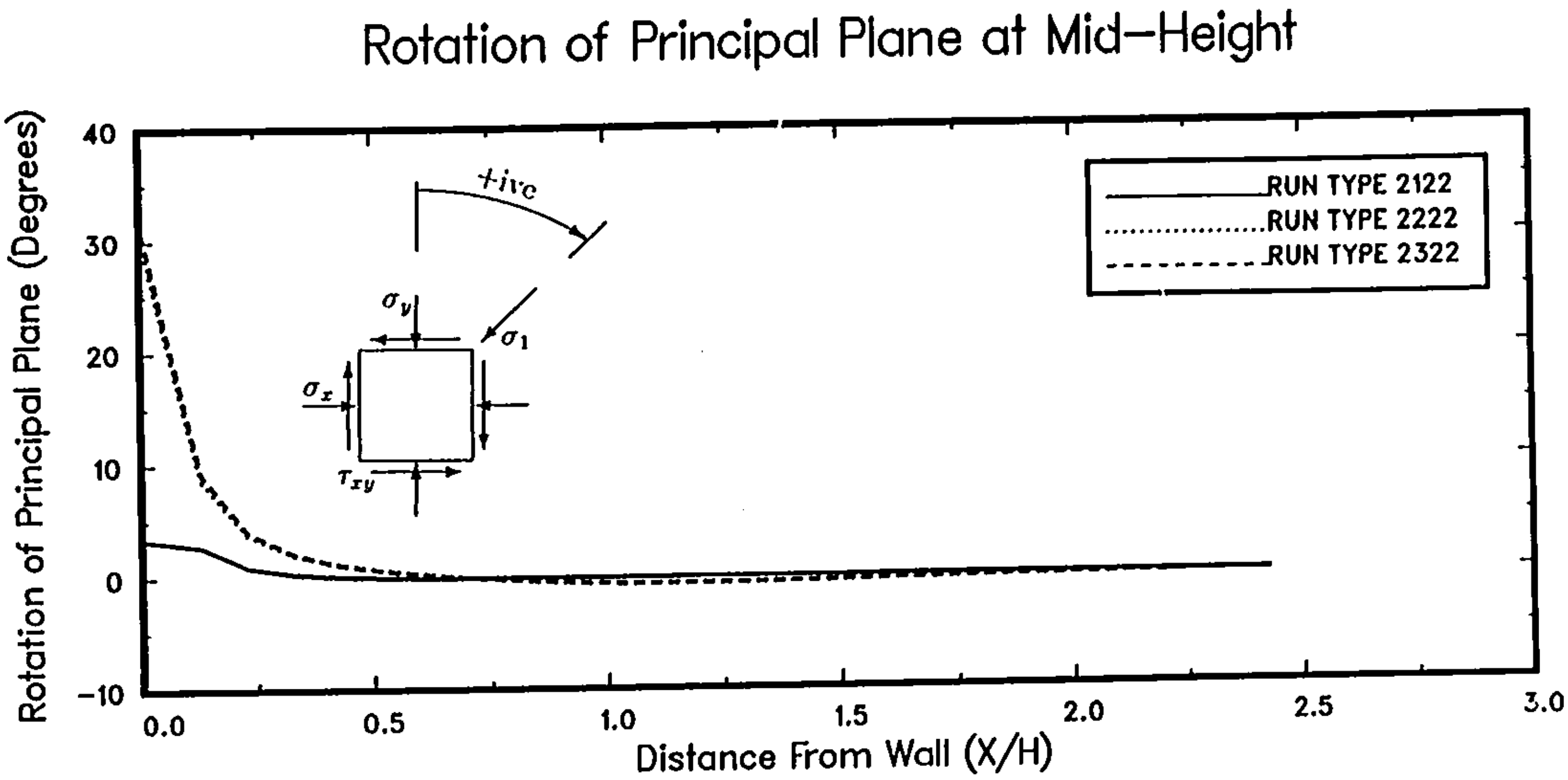

Figure 4.30: Rotation of Principal Planes in Soil Mass for Interfaces I1–I2–I3

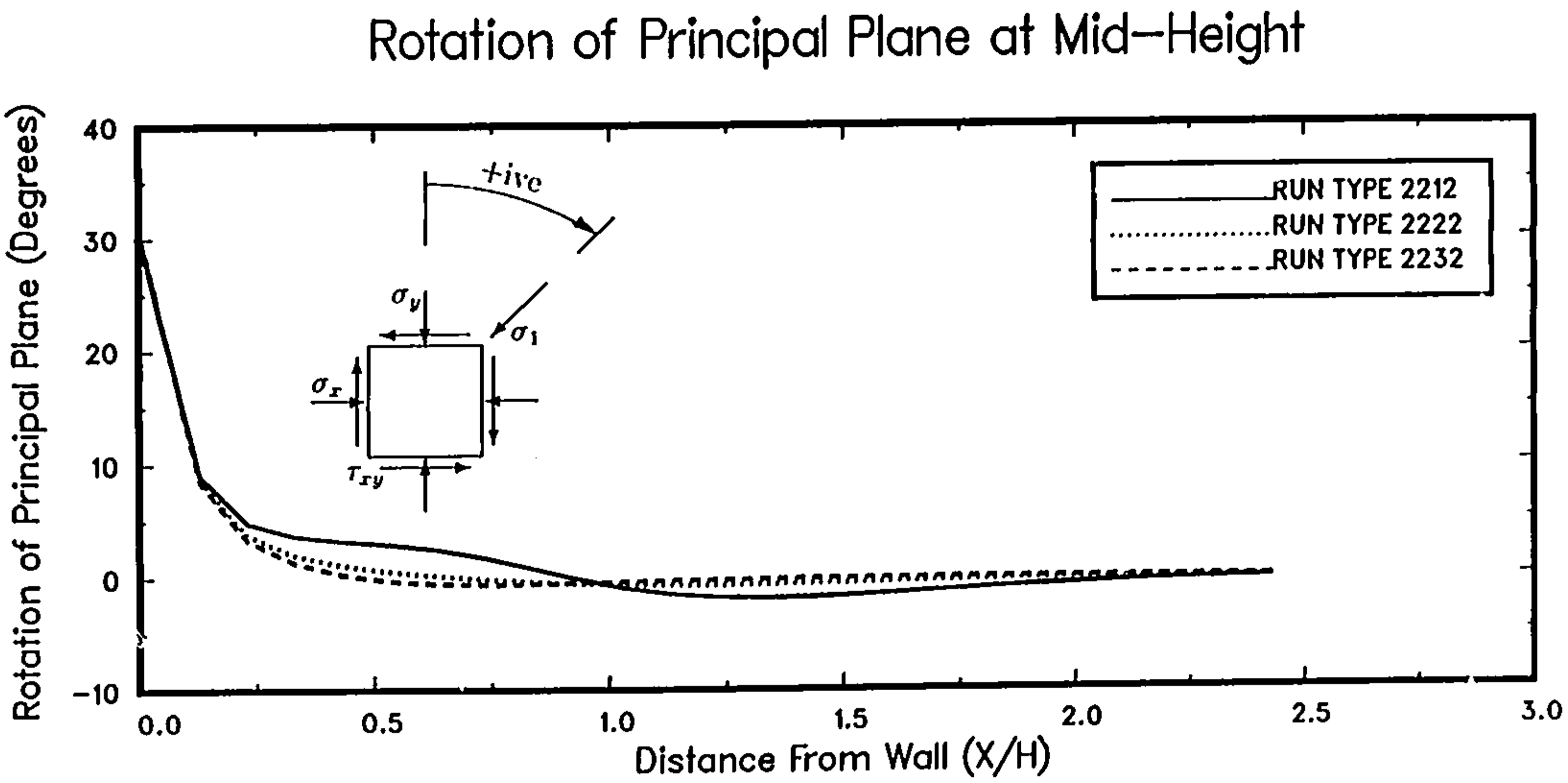

Figure 4.31: Rotation of Principal Planes in Soil Mass
for Foundation Materials F1–F2–F3

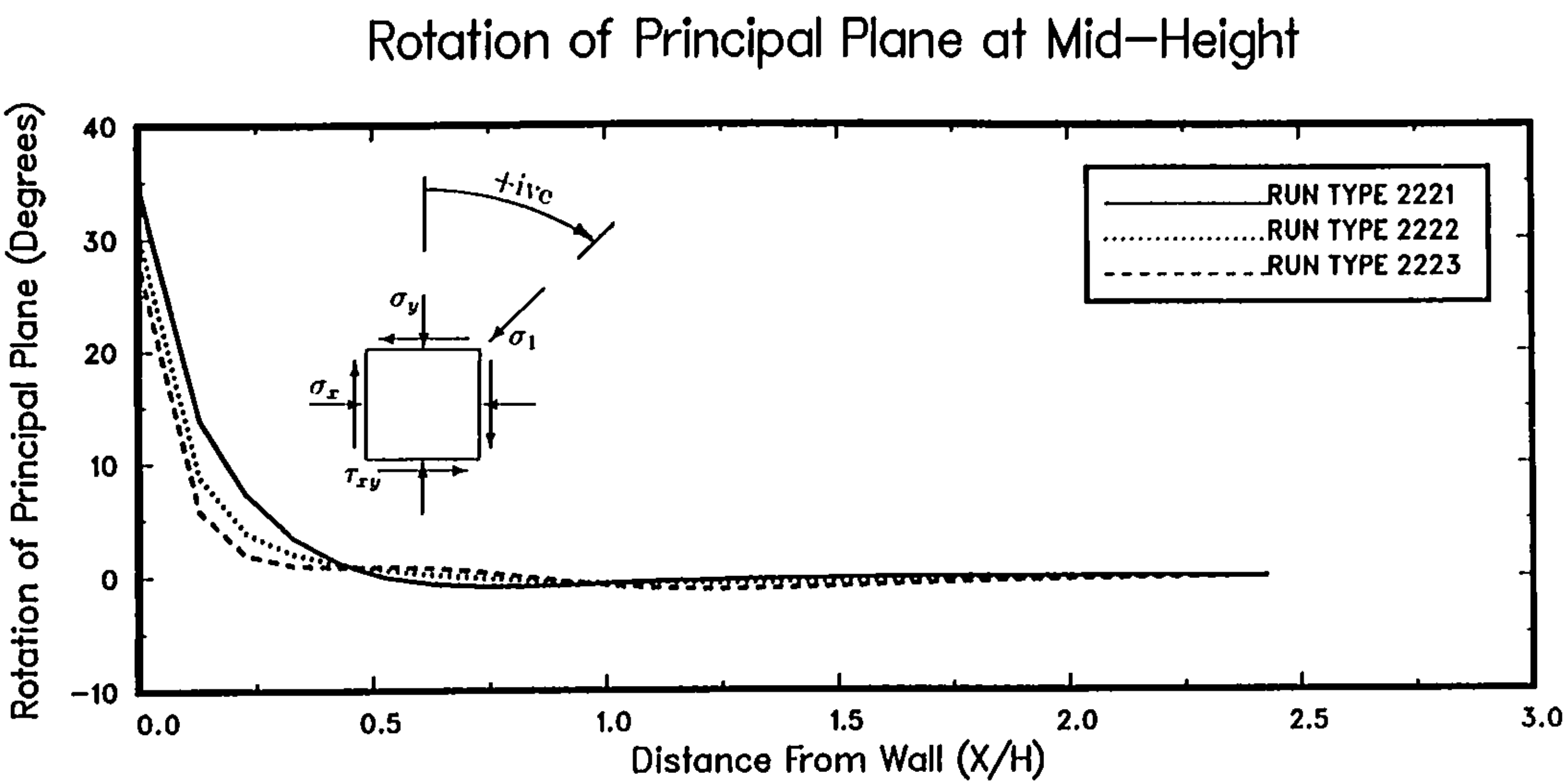

Figure 4.32: Rotation of Principal Planes in Soil Mass for Backfill Materials B1–B2–B3

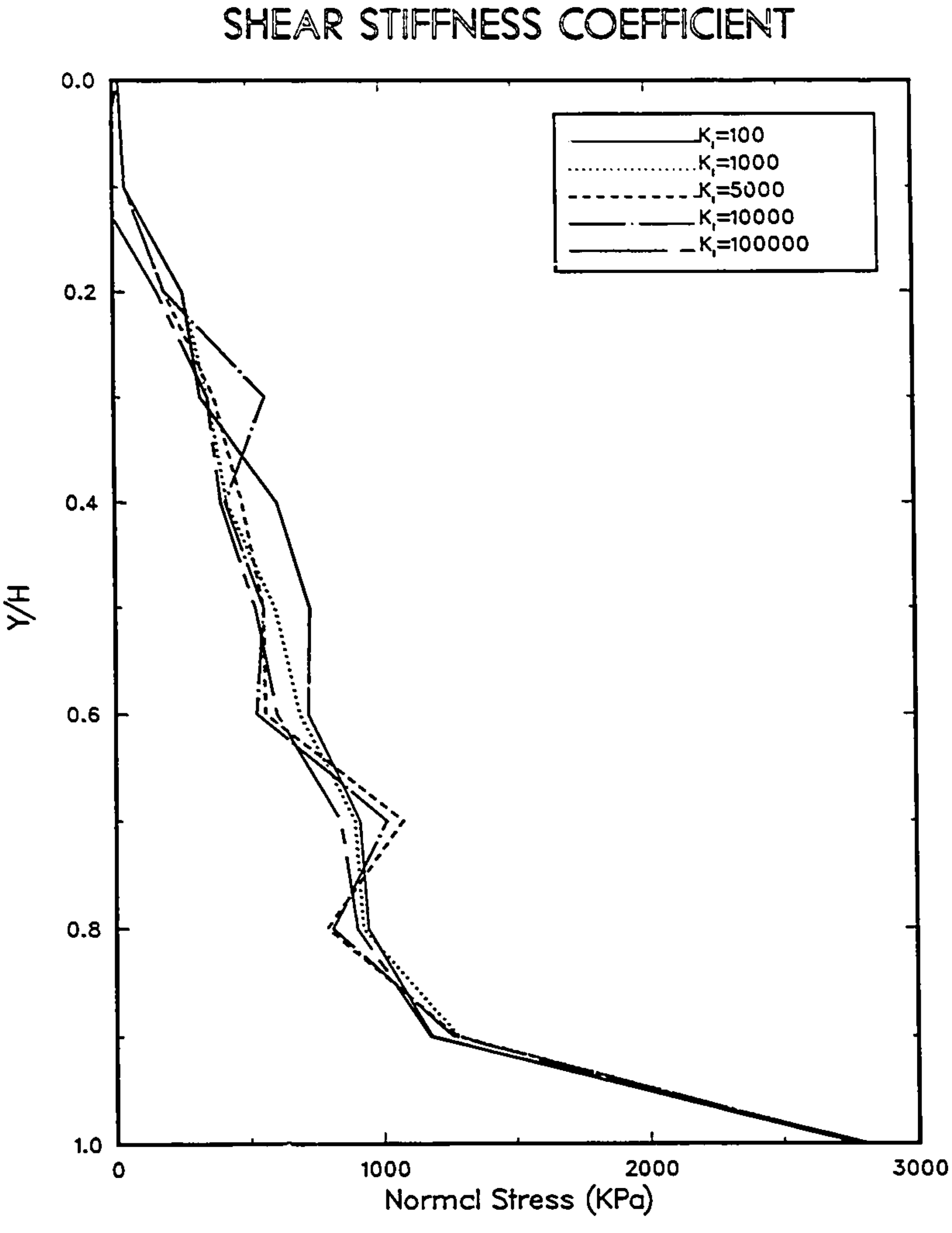

Figure 5.1: Normal Stresses Along Interface for Shear Stiffness Coefficient K_I Sensitivity Study.

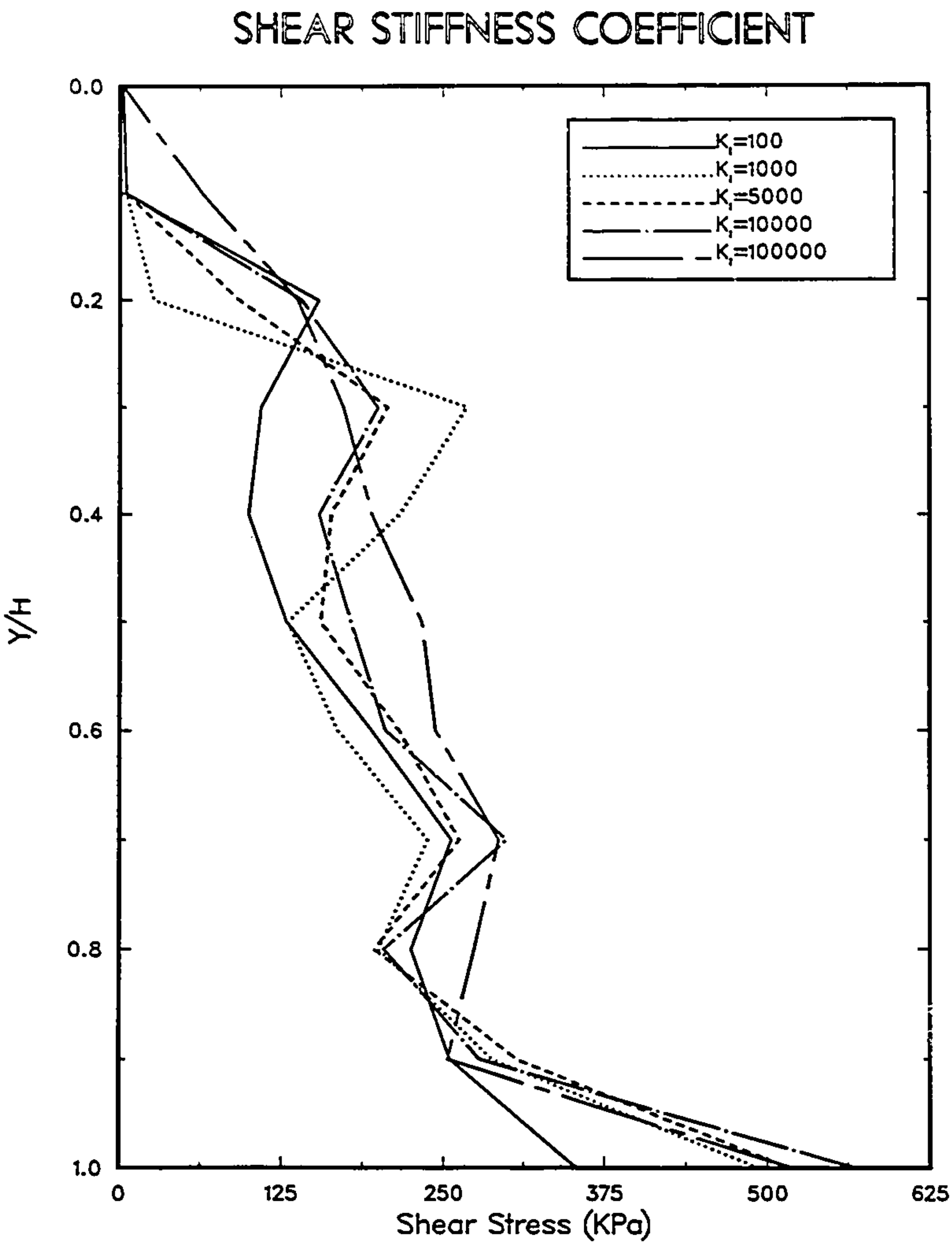

Figure 5.2: Shear Stresses Along Interface for Shear Stiffness Coefficient K_t Sensitivity Study.

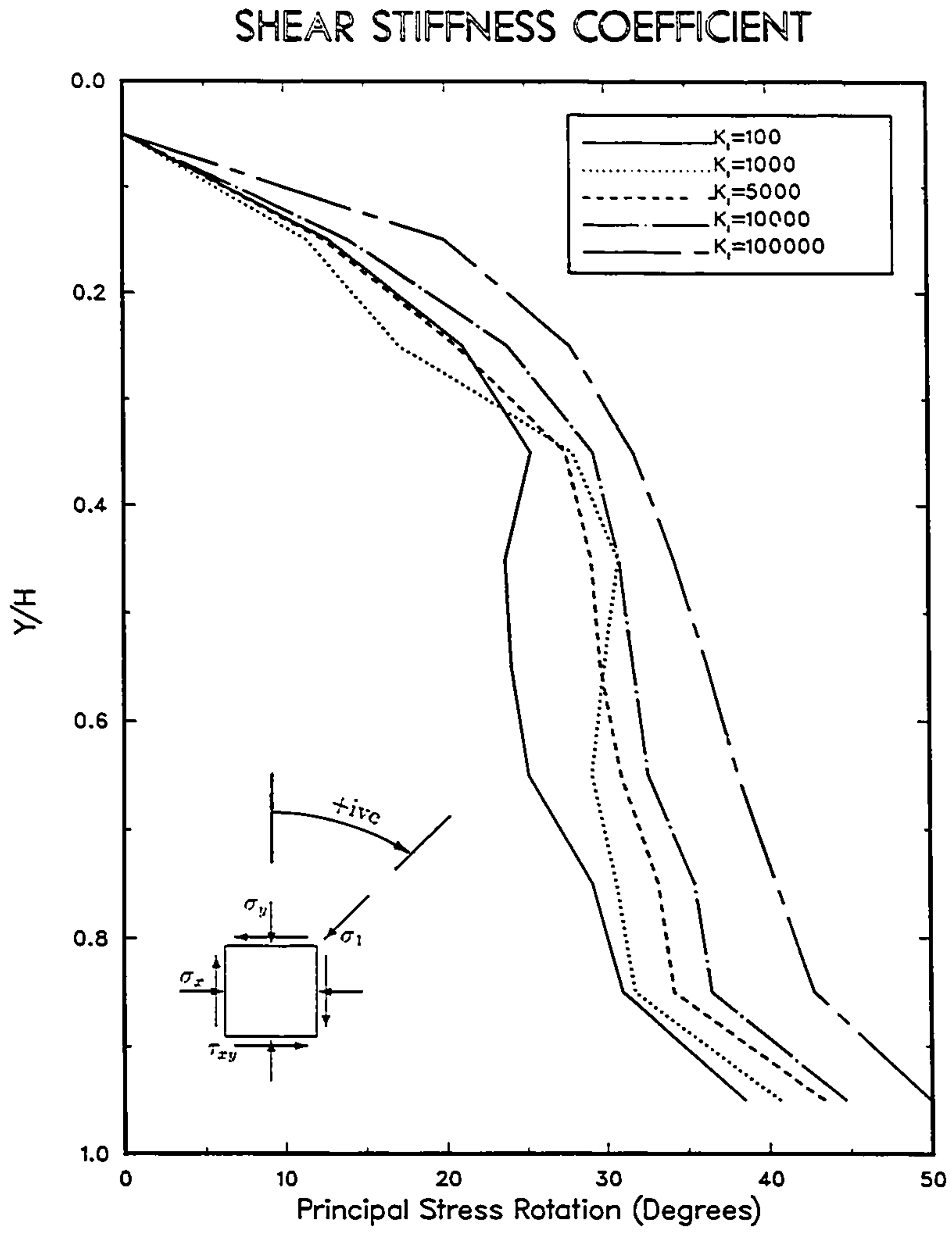
SHEAR STIFFNESS COEFFICIENT

Figure 5.3: Principal Stress Rotations Along Interface for Shear Stiffness Coefficient K_f Sensitivity Study.

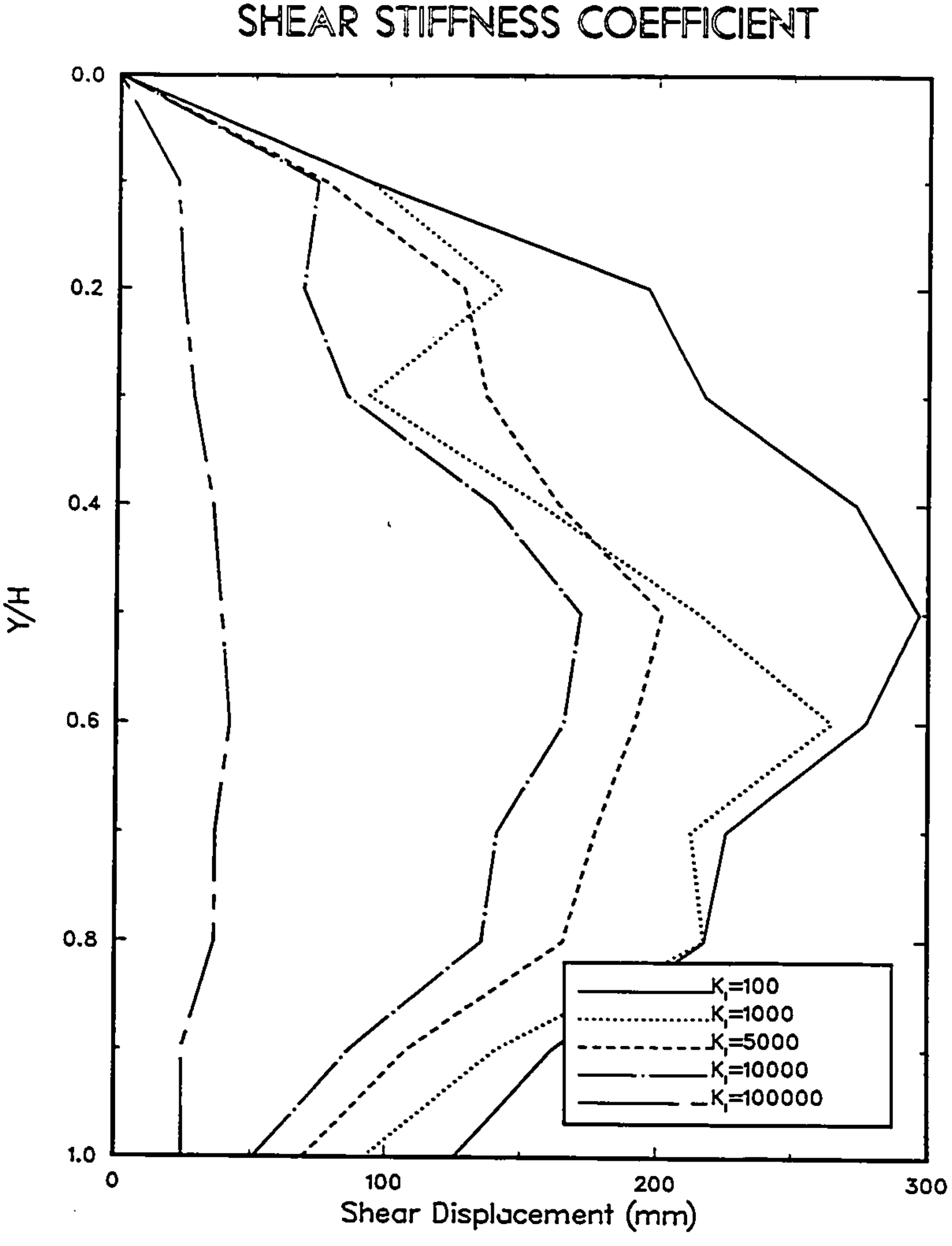

Figure 5.4: Shear Displacements Along Interface for Shear Stiffness Coefficient K_I Sensitivity Study.

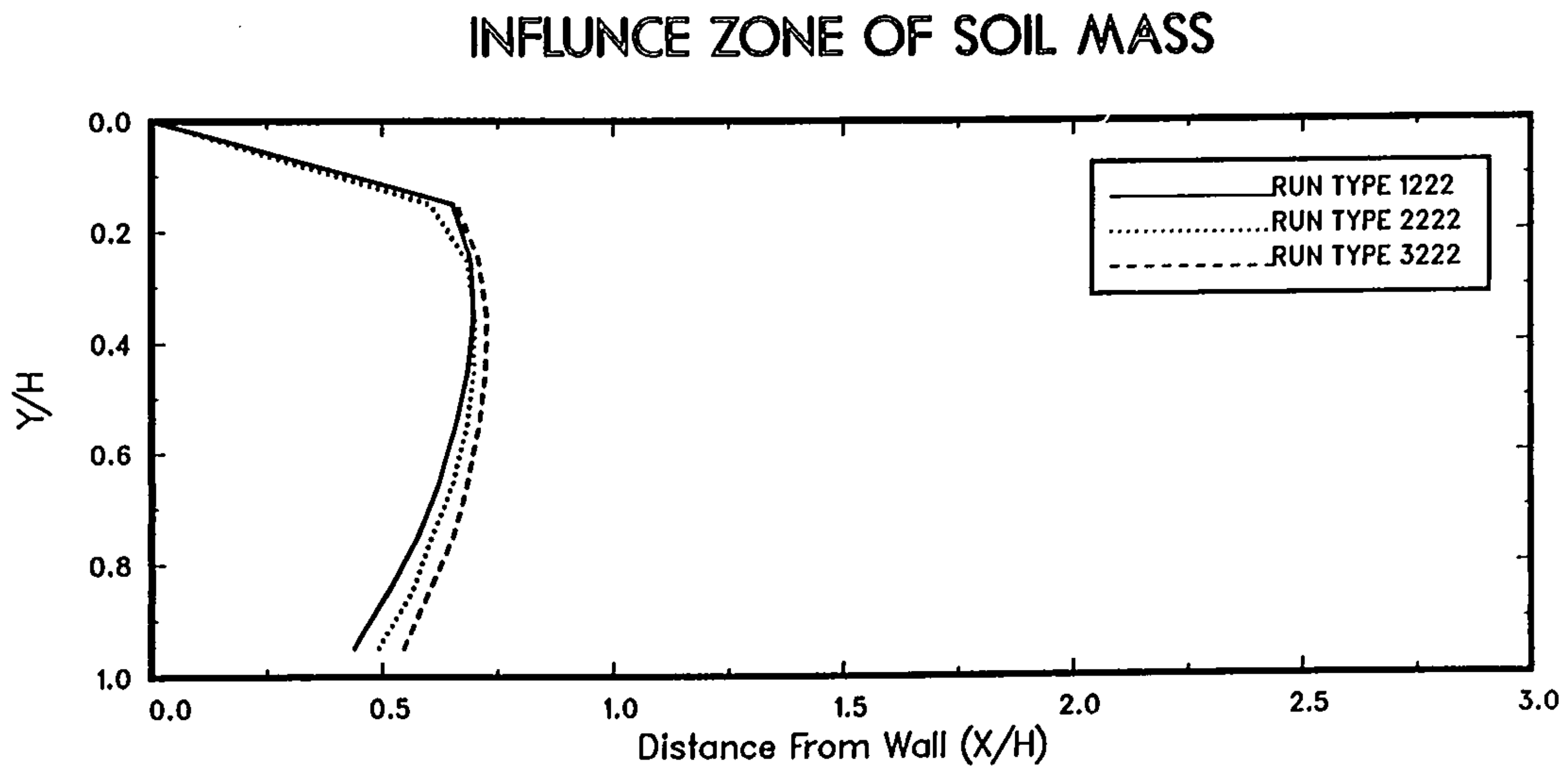

Figure 5.5: Influence Zone for Wall Angles W1-W2-W3.

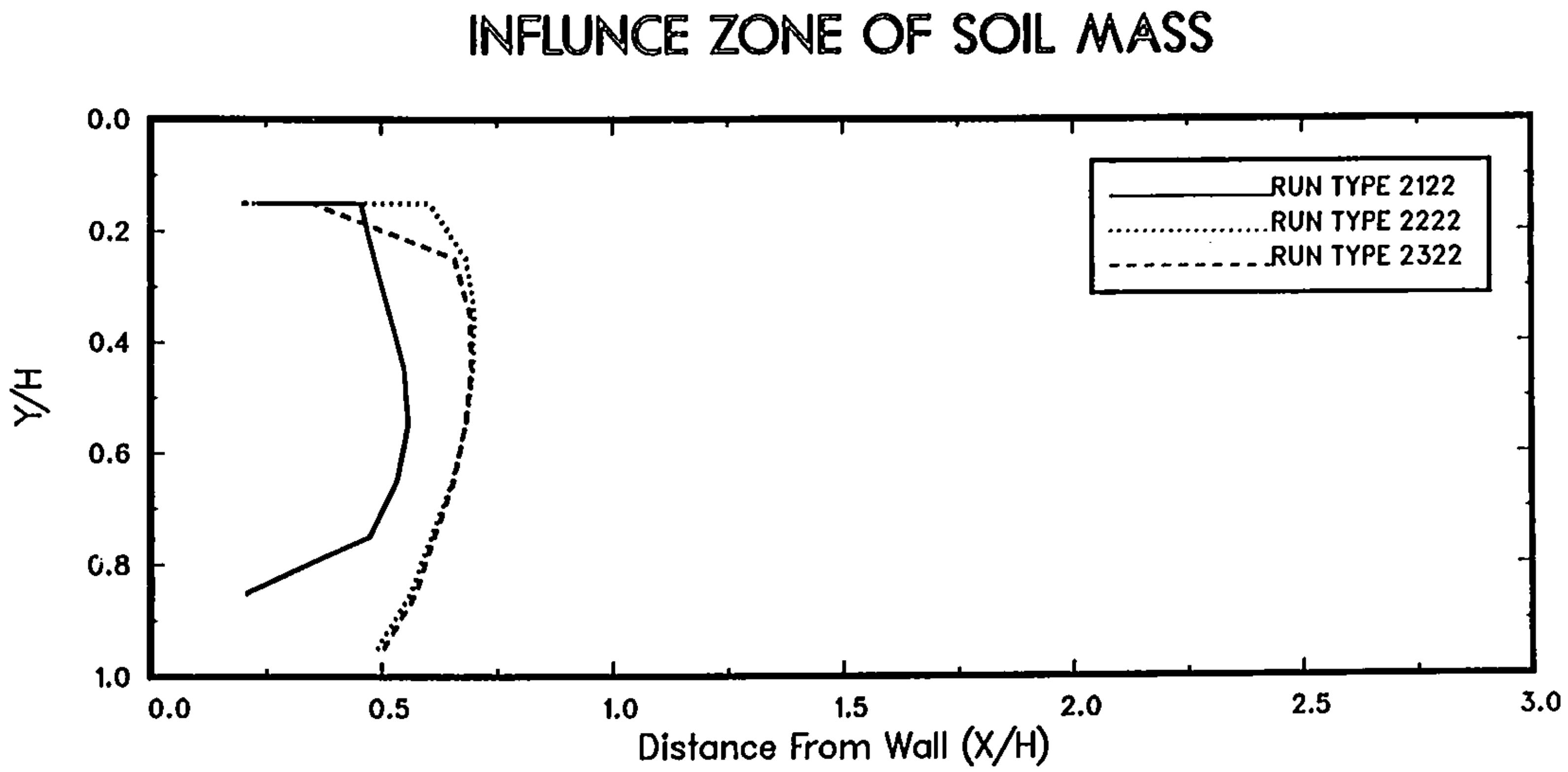

Figure 5.6: Influence Zone for Interfaces I1–I2–I3.

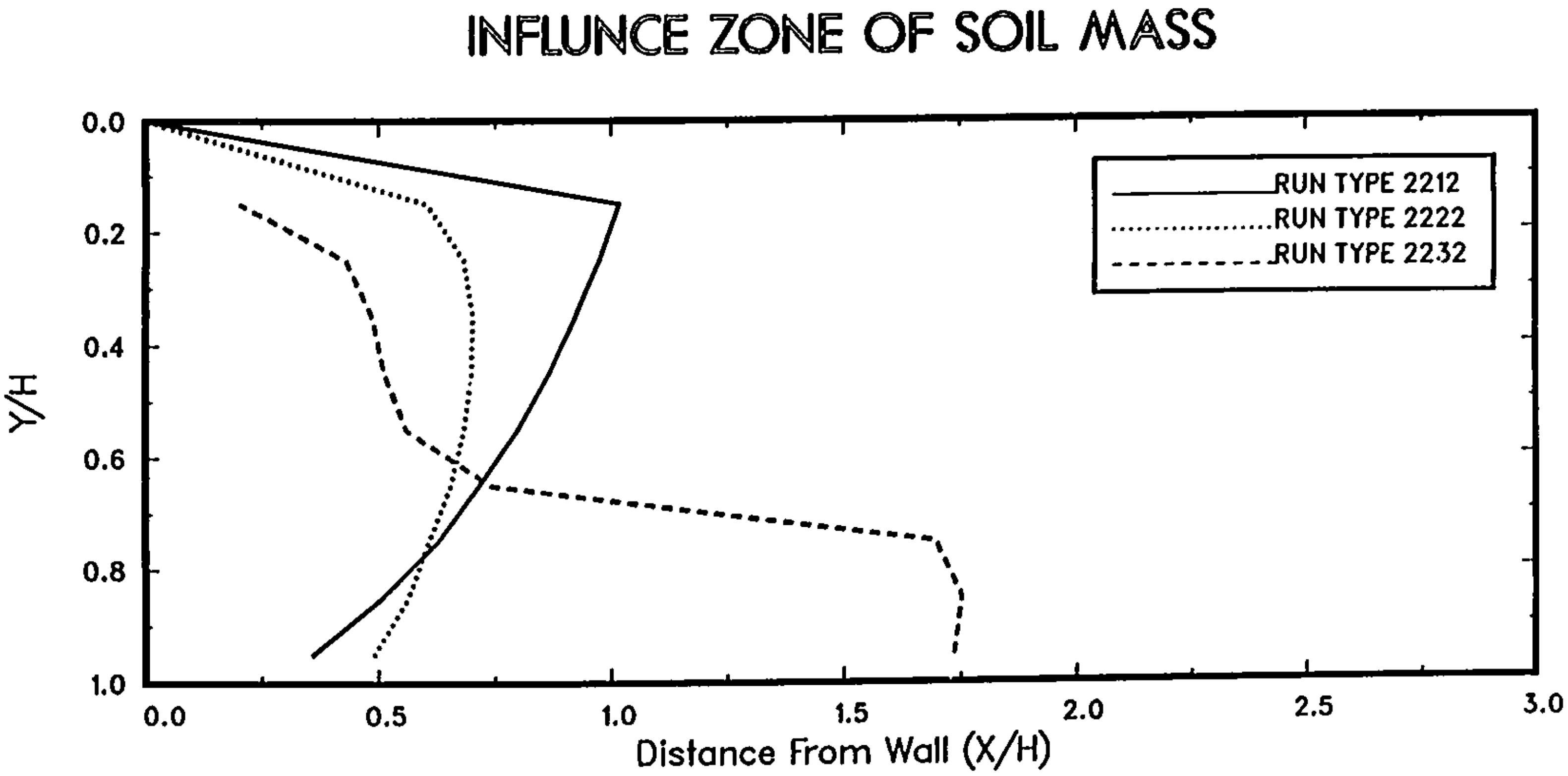

Figure 5.7: Influence Zone for Foundation Materials F1-F2-F3.

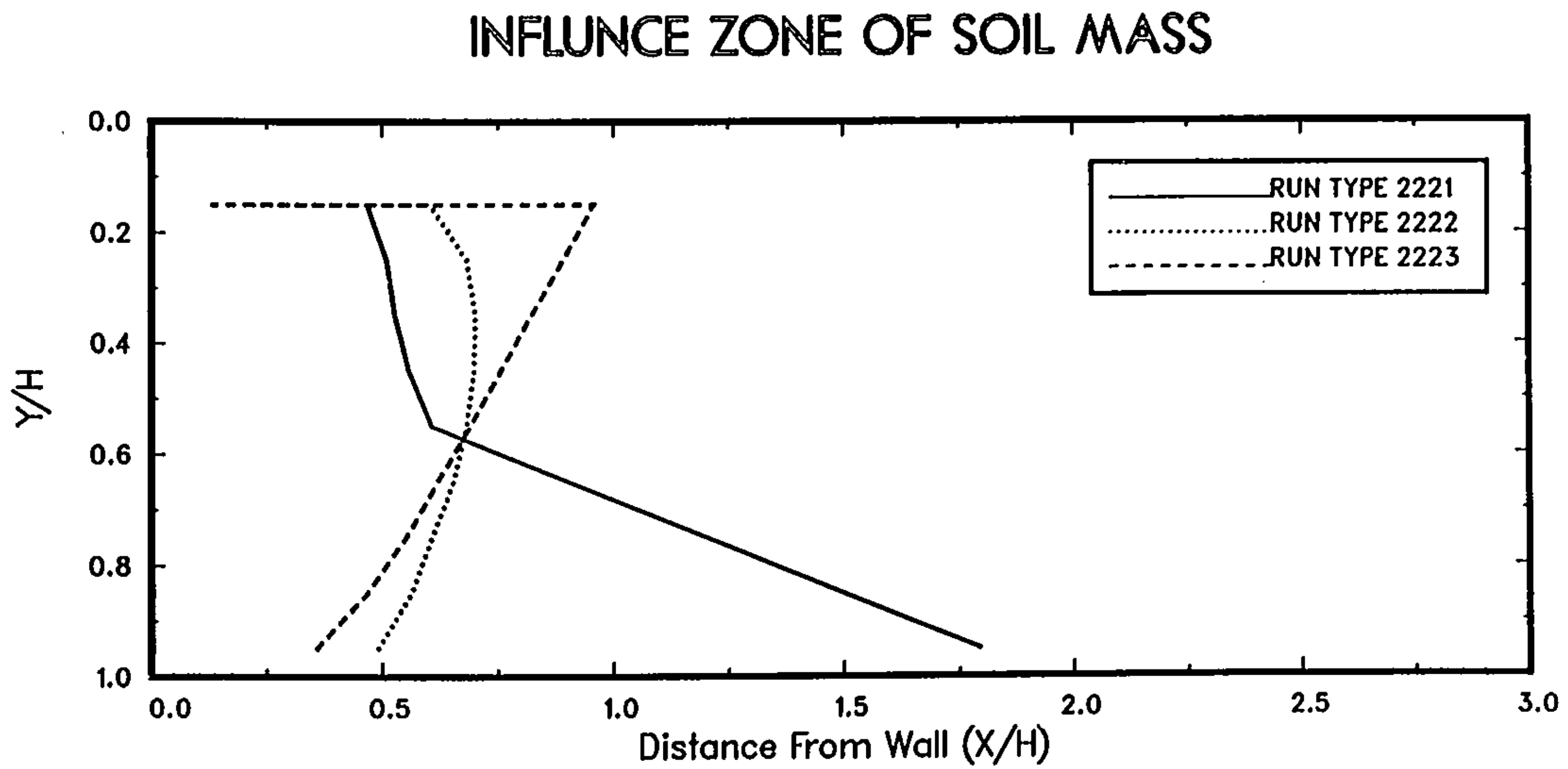

Figure 5.8: Influence Zone for Backfill Materials B1–B2–B3.

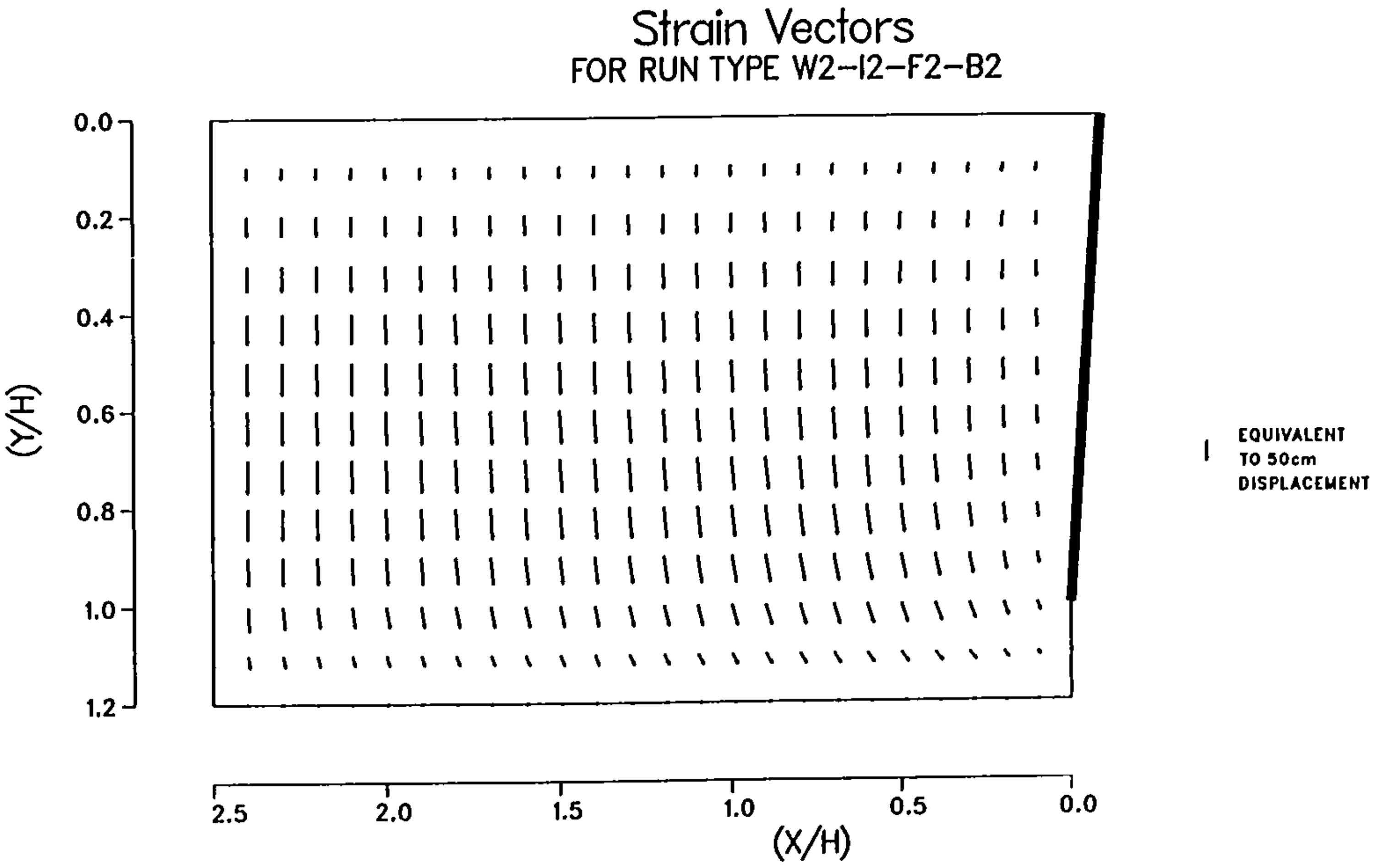

Figure 5.9: Typical Strain Vectors of Node Displacements in Soil Mass.

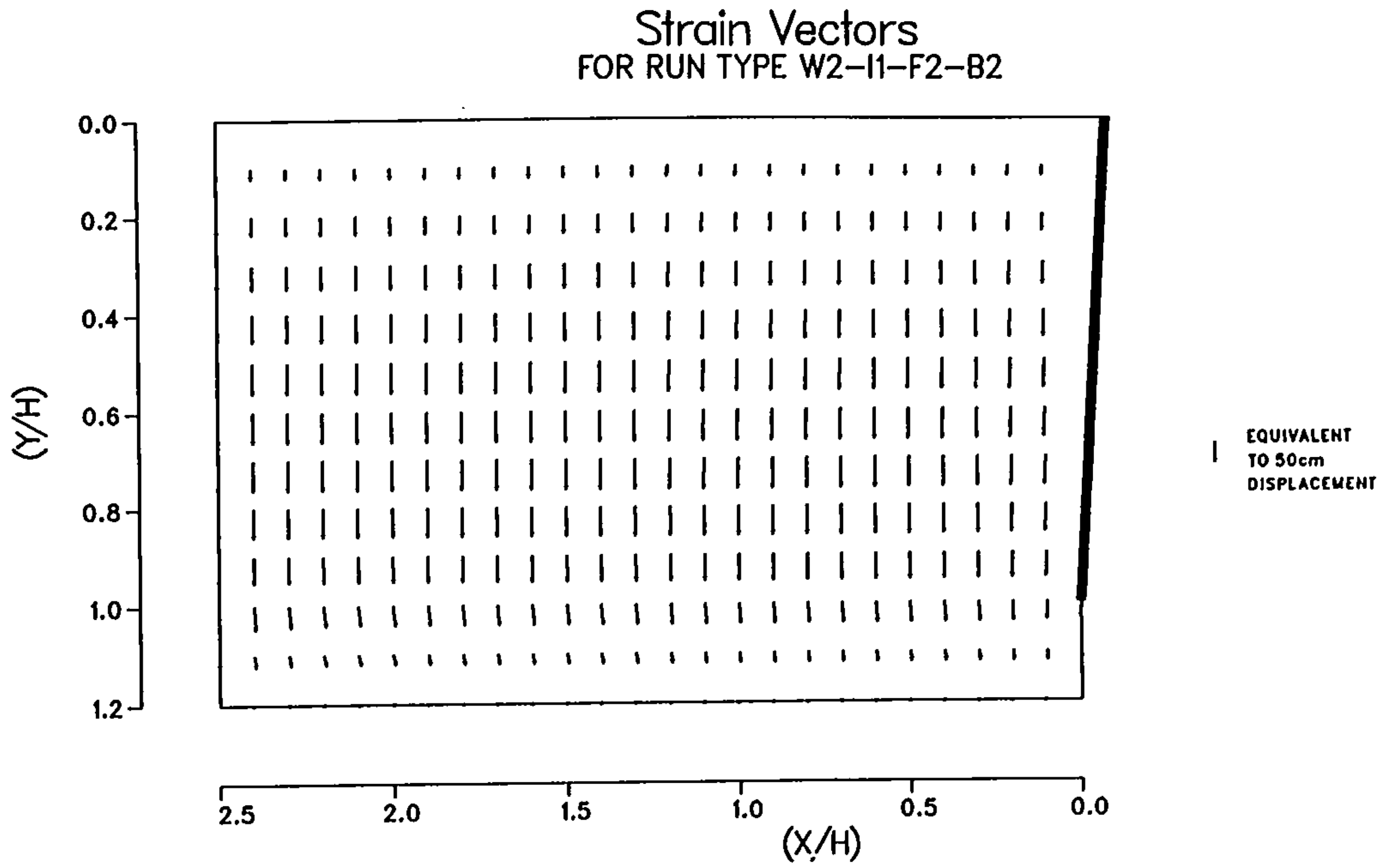

Figure 5.10: Strain Vectors for Smooth Interface I1.

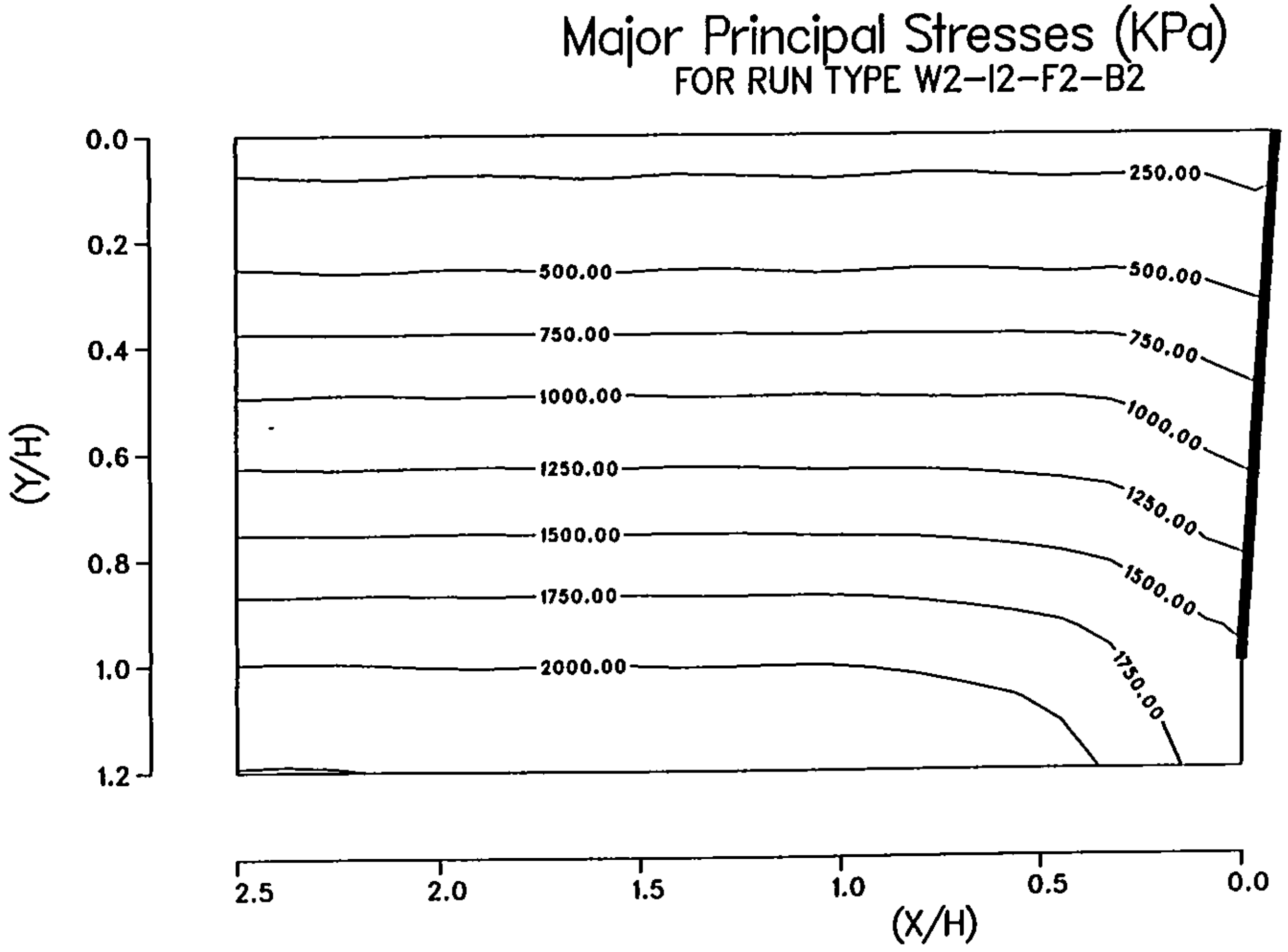

Figure 5.11: Typical Major Principal Stresses σ_1 in Soil Mass.

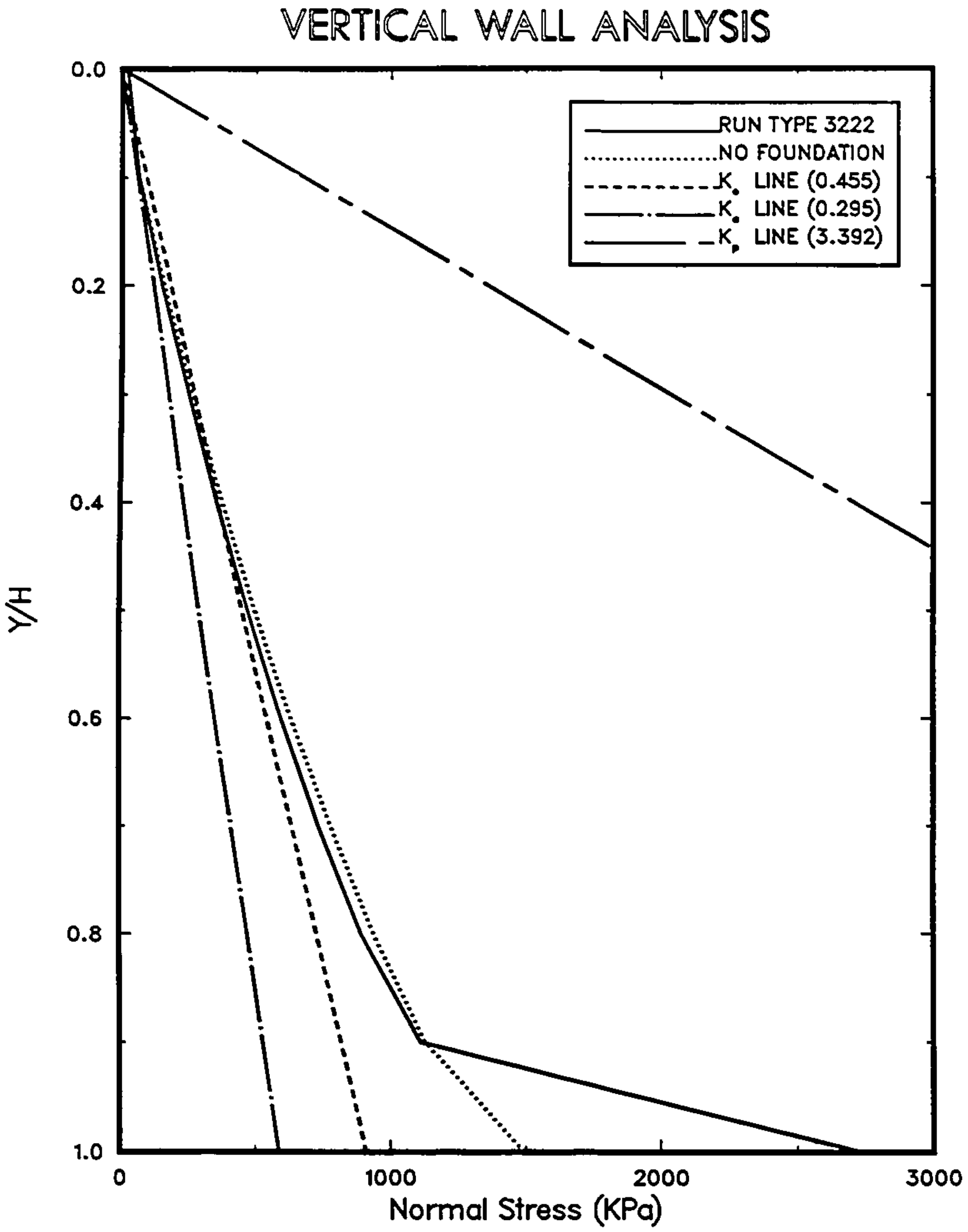

Figure 5.12: Lateral Earth Pressure Coefficients for 90° Wall.

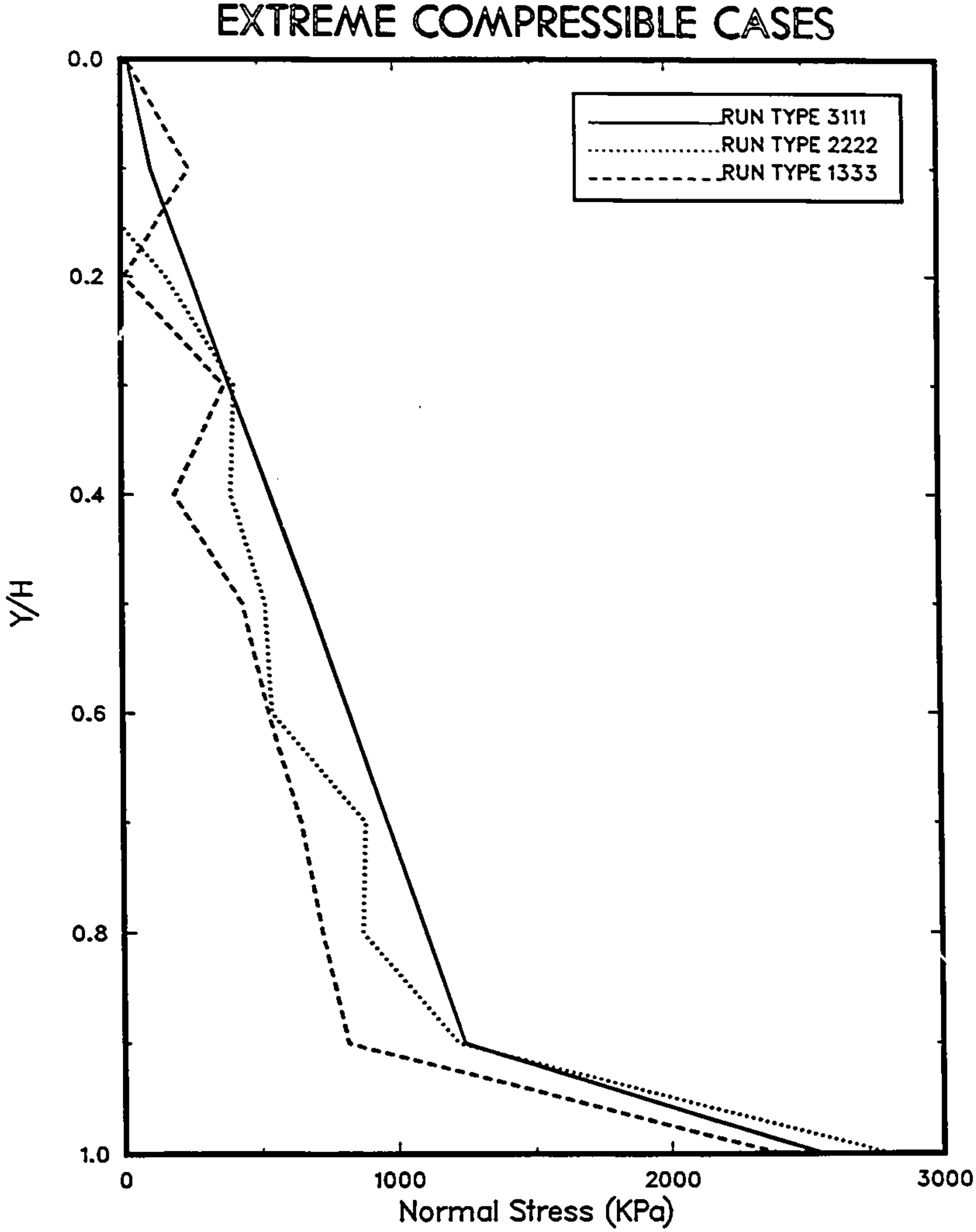

Figure 5.13: Normal Stresses Along Interface for Extreme Compressible Cases.

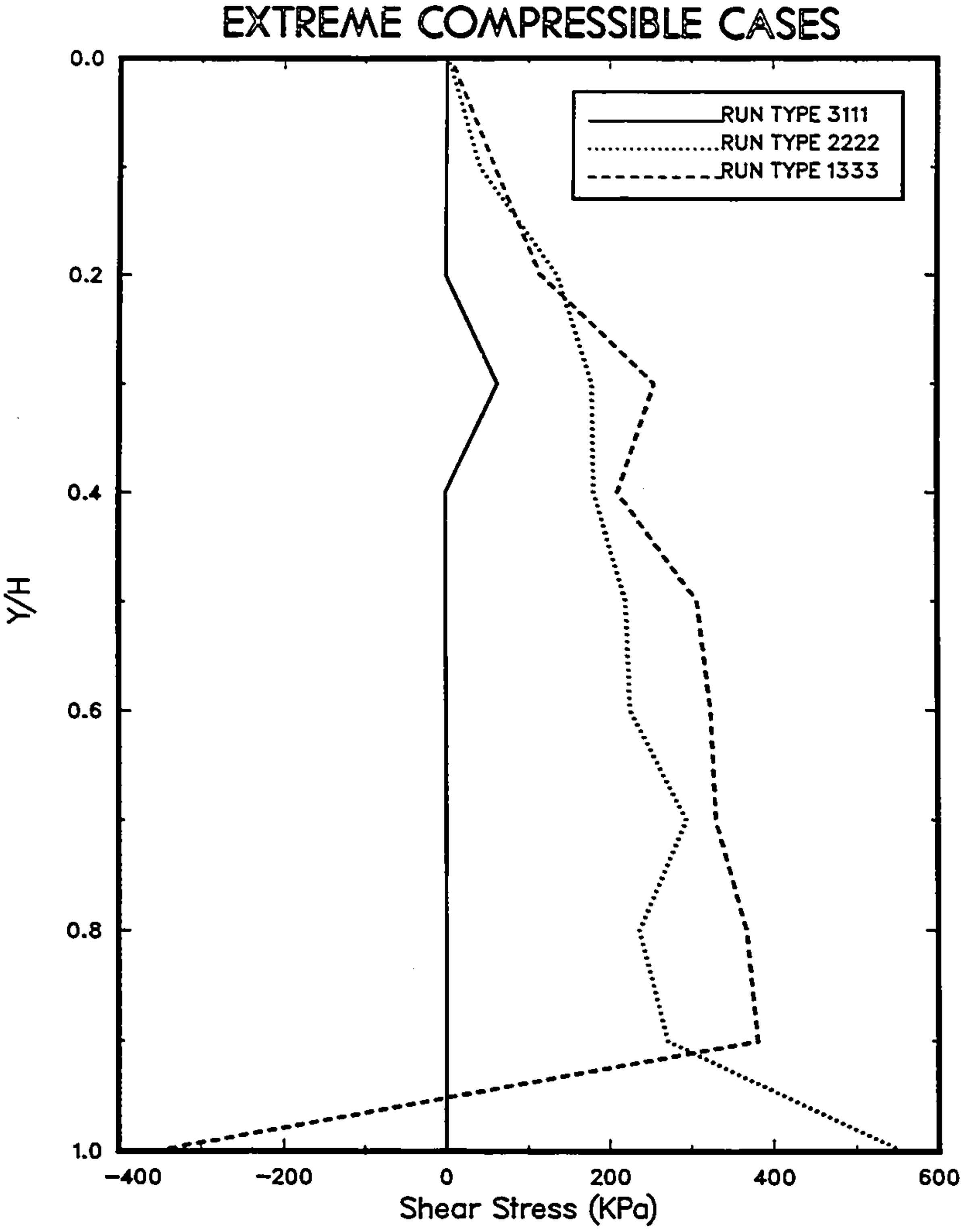

Figure 5.14: Shear Stresses Along Interface for Extreme Compressible Cases.

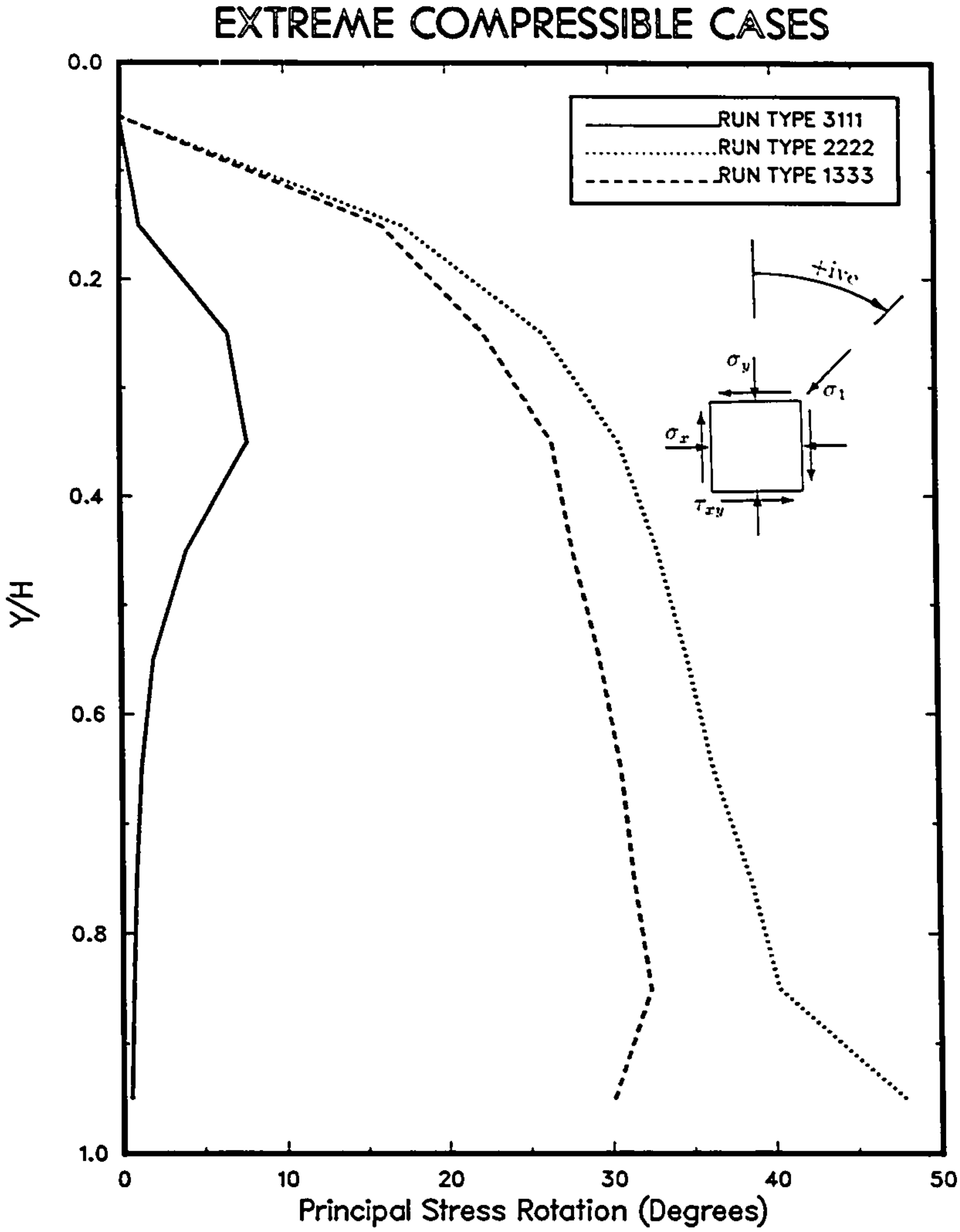

Figure 5.15: Principal Stress Rotations Along Interface for Extreme Compressible Cases.

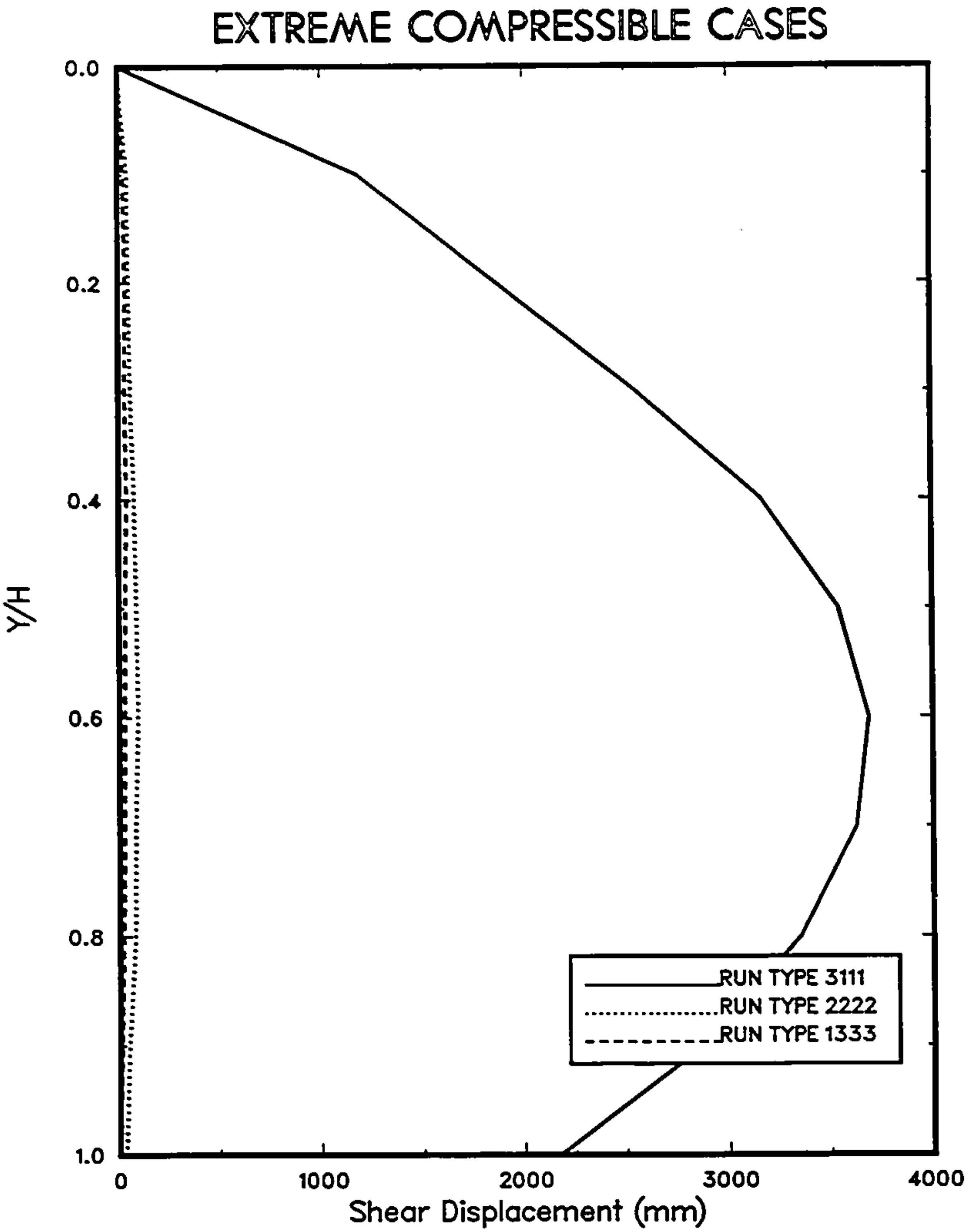

Figure 5.16: Shear Displacements Along Interface for Extreme Compressible Cases.

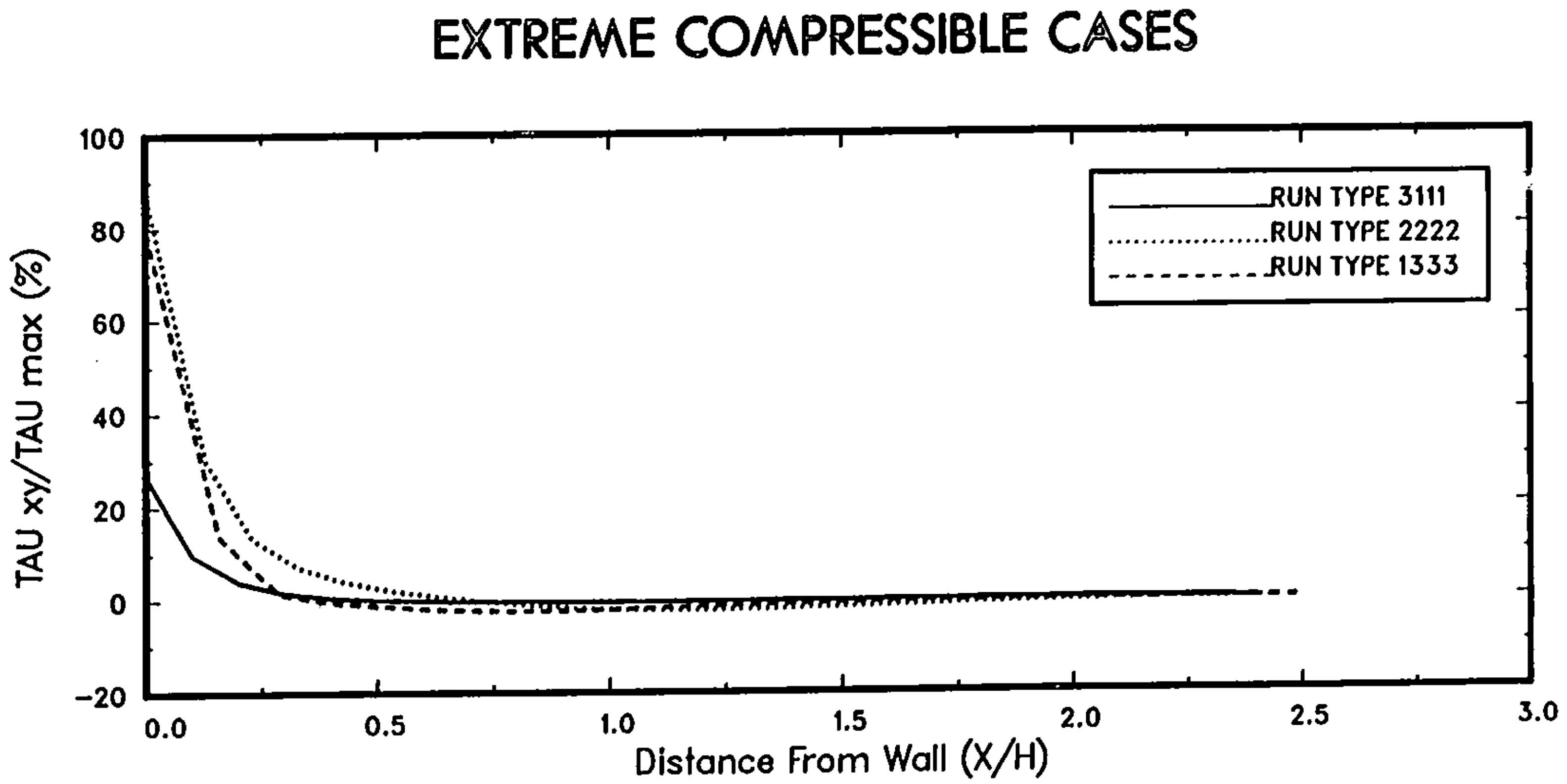

Figure 5.17: Variations of τ_{mob} in Soil Mass for Extreme Compressible Cases.

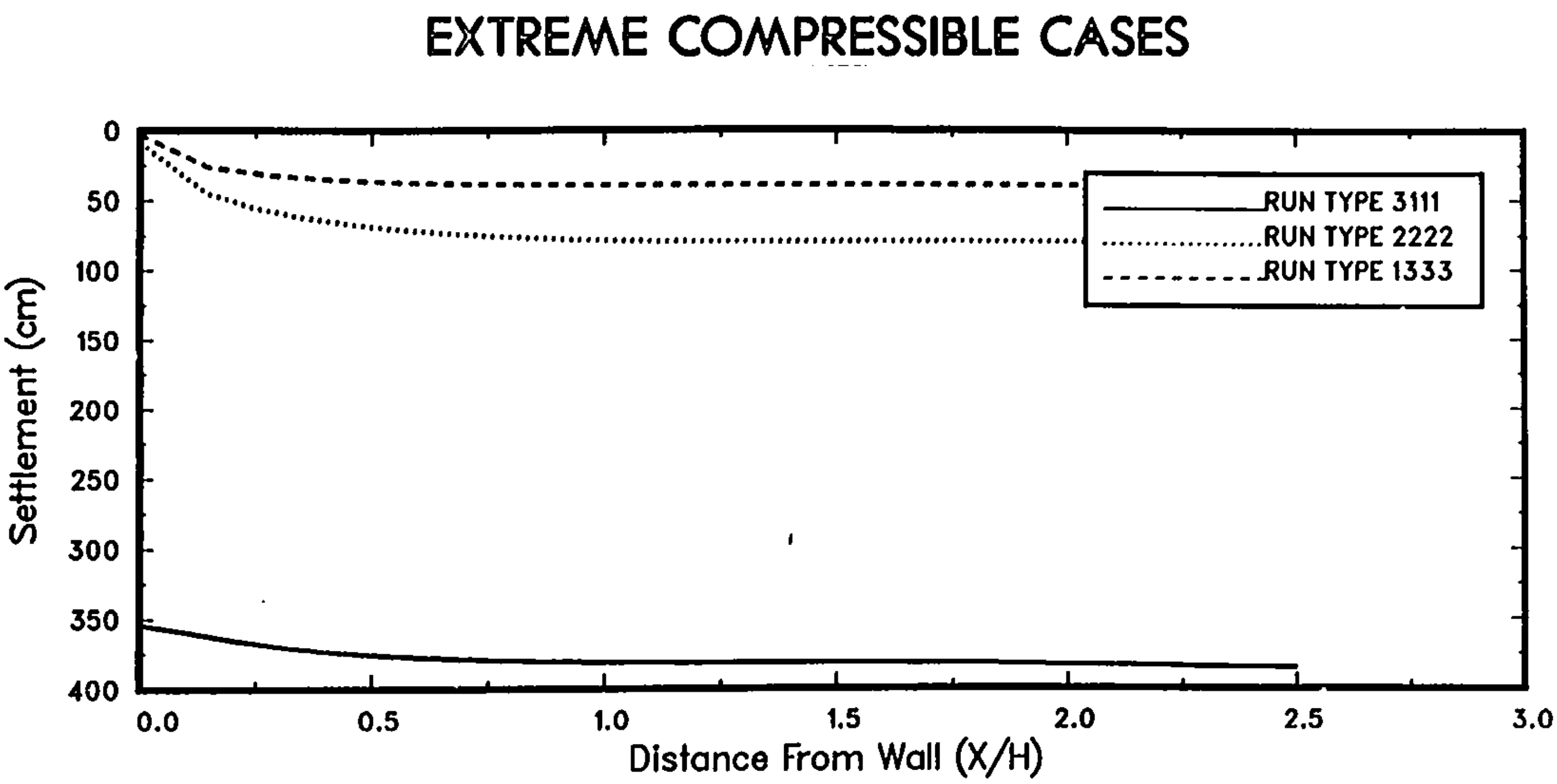

Figure 5.18: Typical Settlement Curves in Soil Mass for Extreme Compressible Cases.

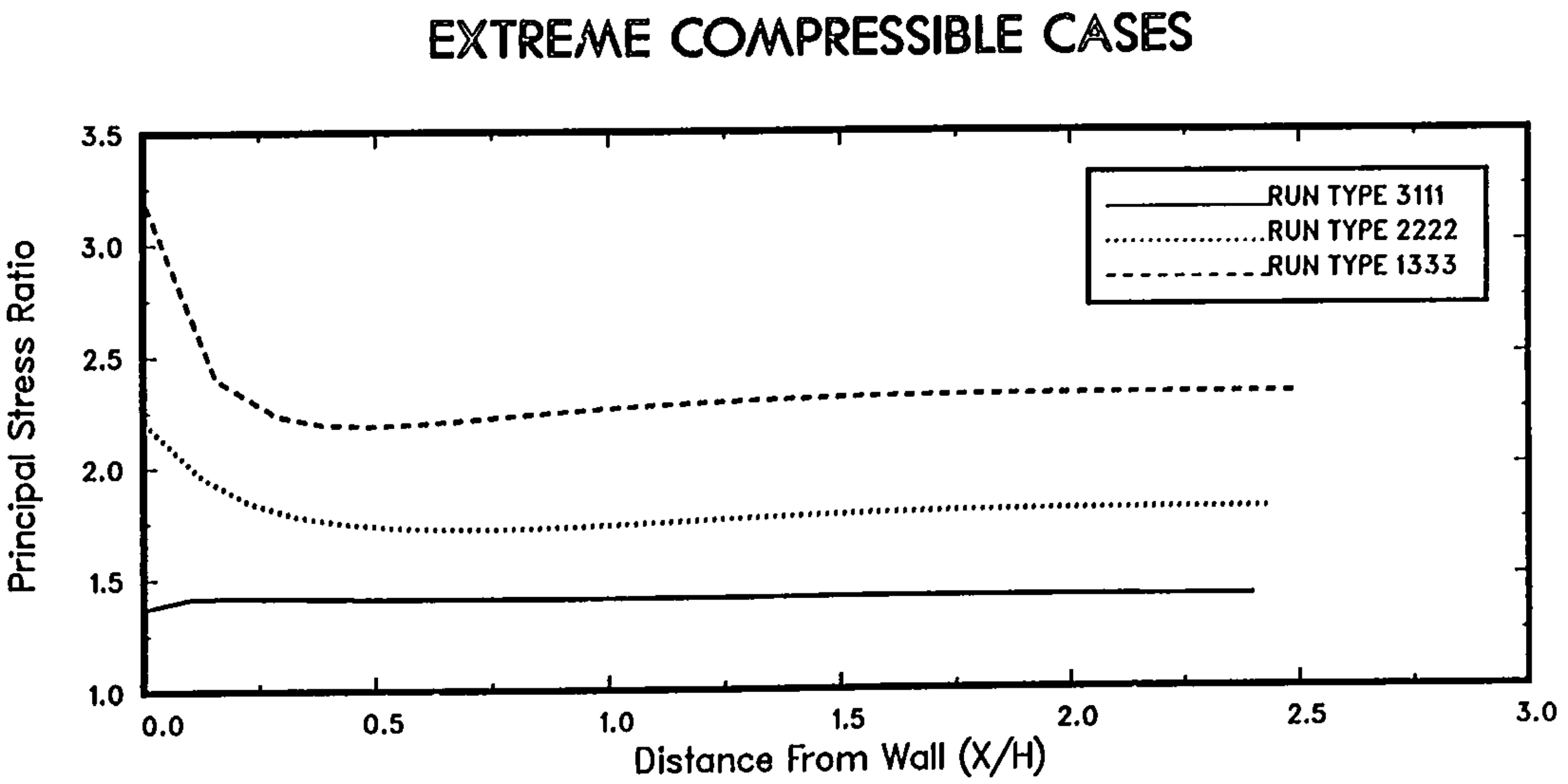

Figure 5.19: Principal Stress Ratio Values in Soil Mass for Extreme Compressible Cases.

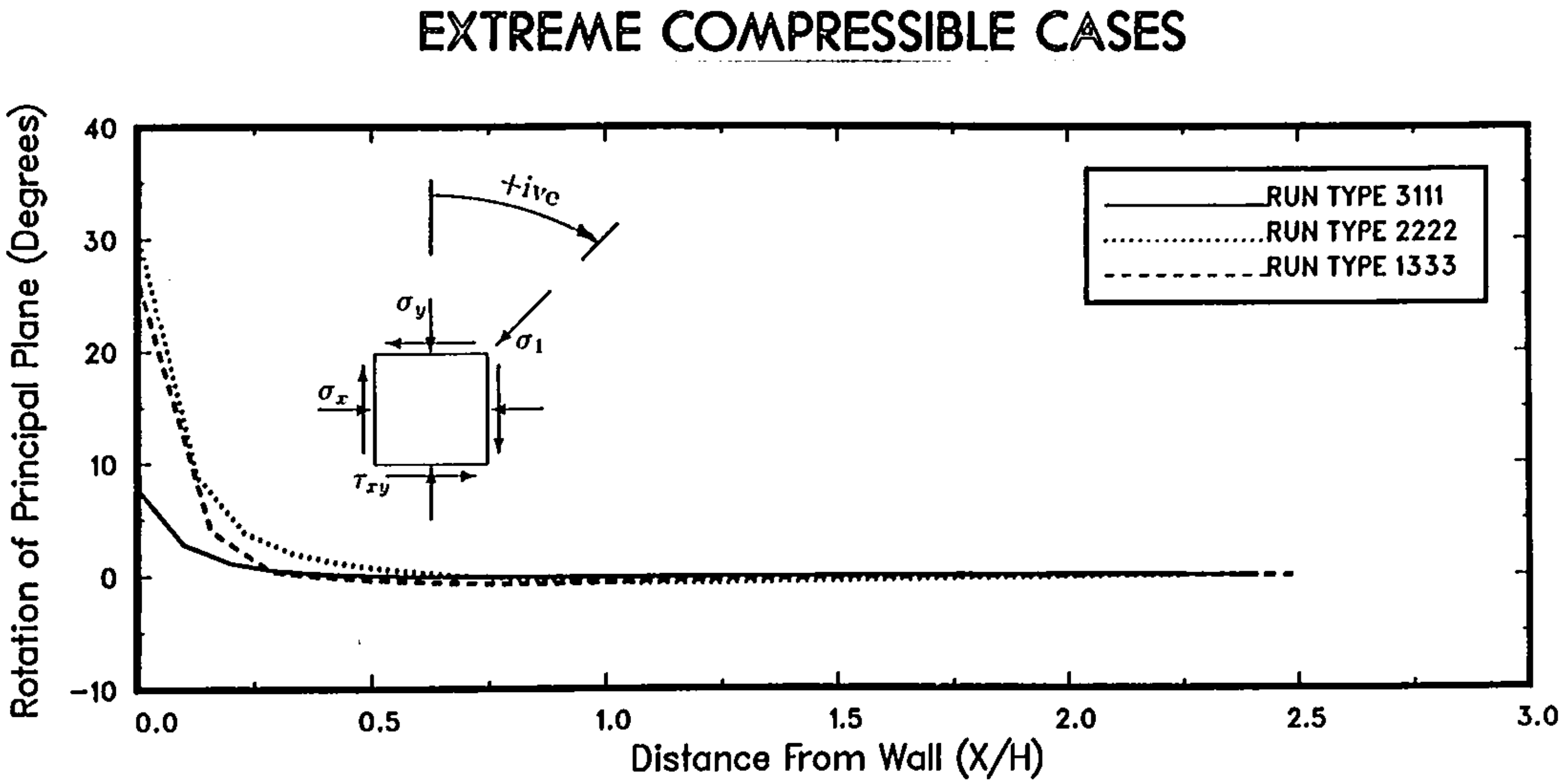

Figure 5.20: Rotation of Principal Planes in Soil Mass for Extreme Compressible Cases.

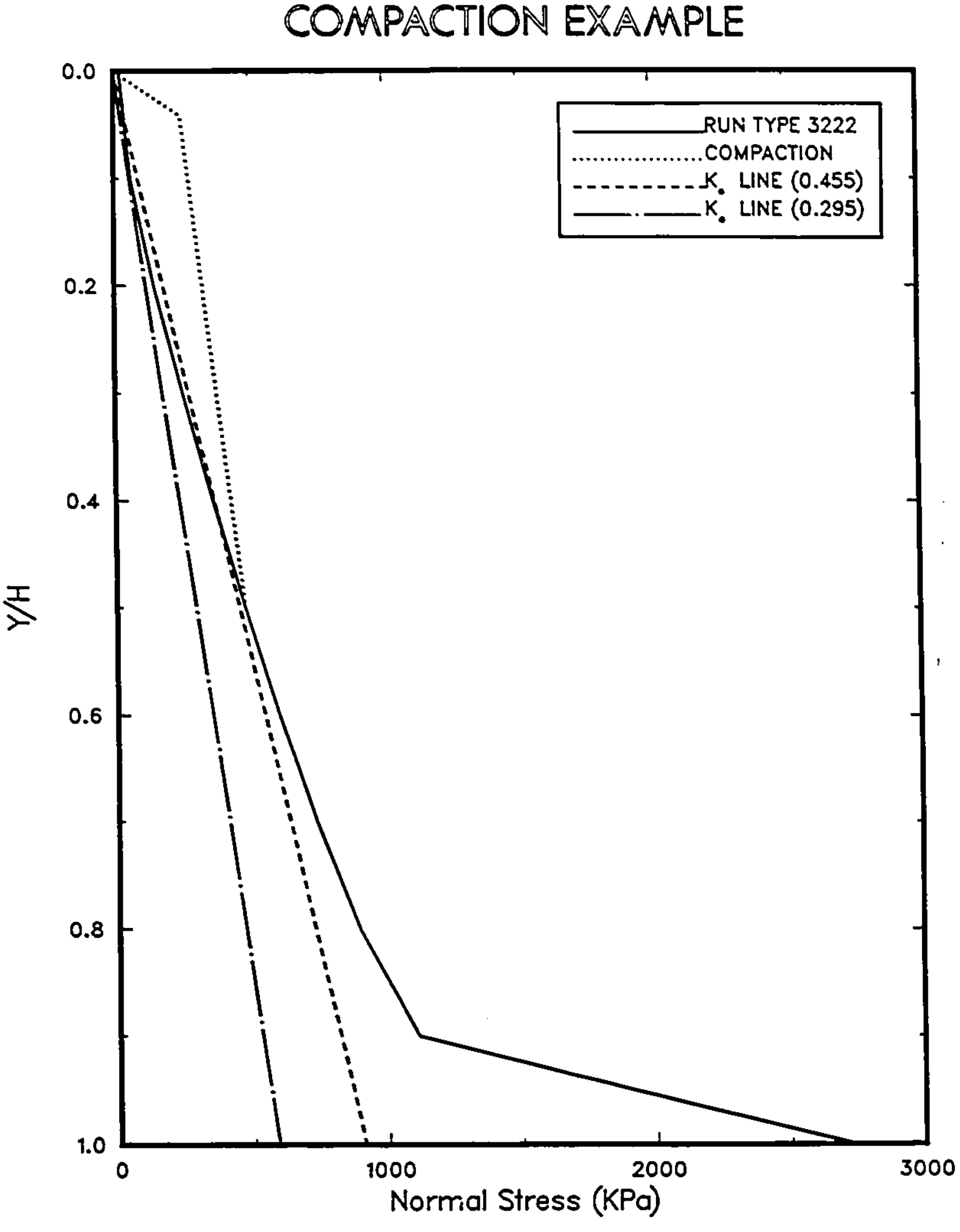

Figure 5.21: Example of Compaction-Induced Stresses.

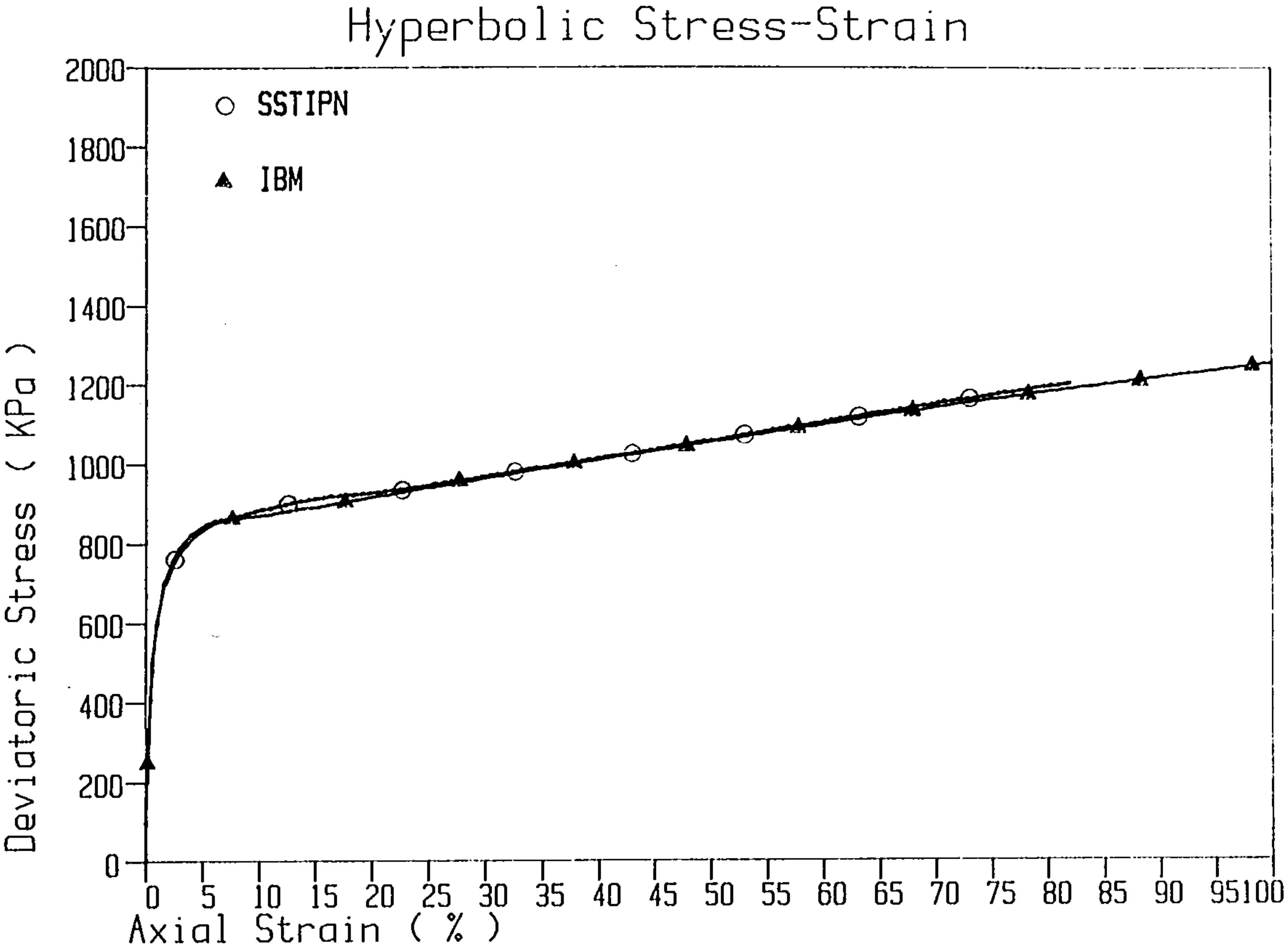

Figure 5.22: Comparison Between SSTIPN and Hyperbolic Model on IBM Micro Computer.

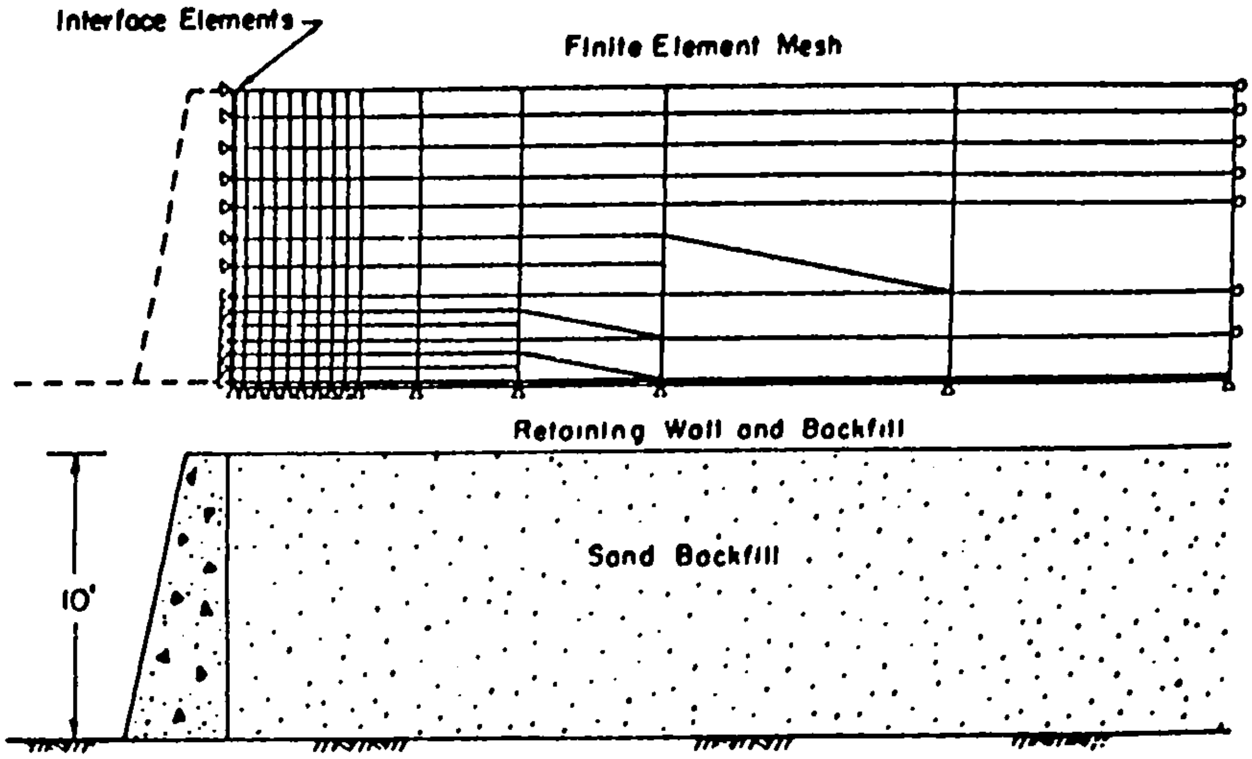

Figure 5.23: Finite Element Mesh. Clough & Duncan (1971).

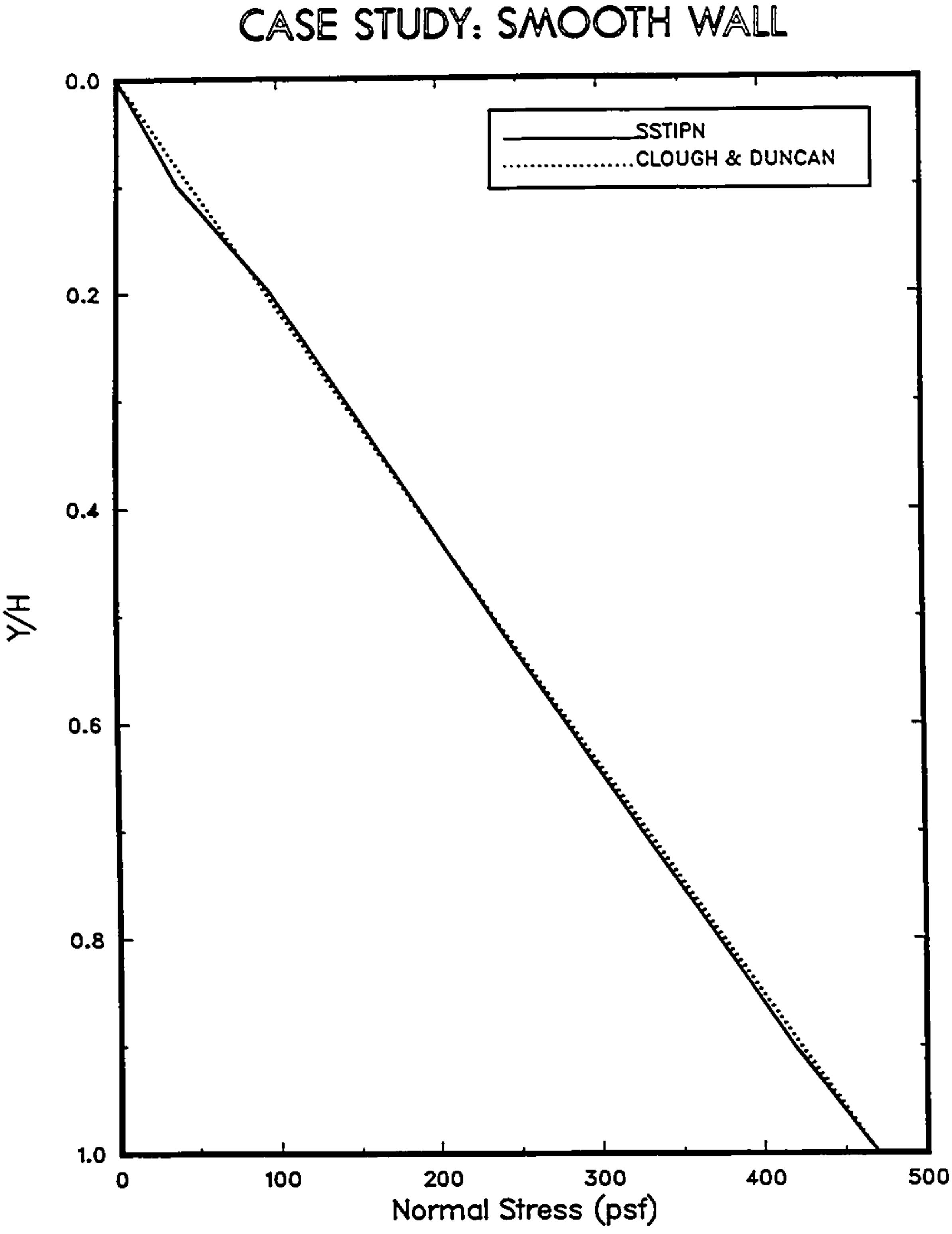

Figure 5.24: Case Study: Smooth Wall

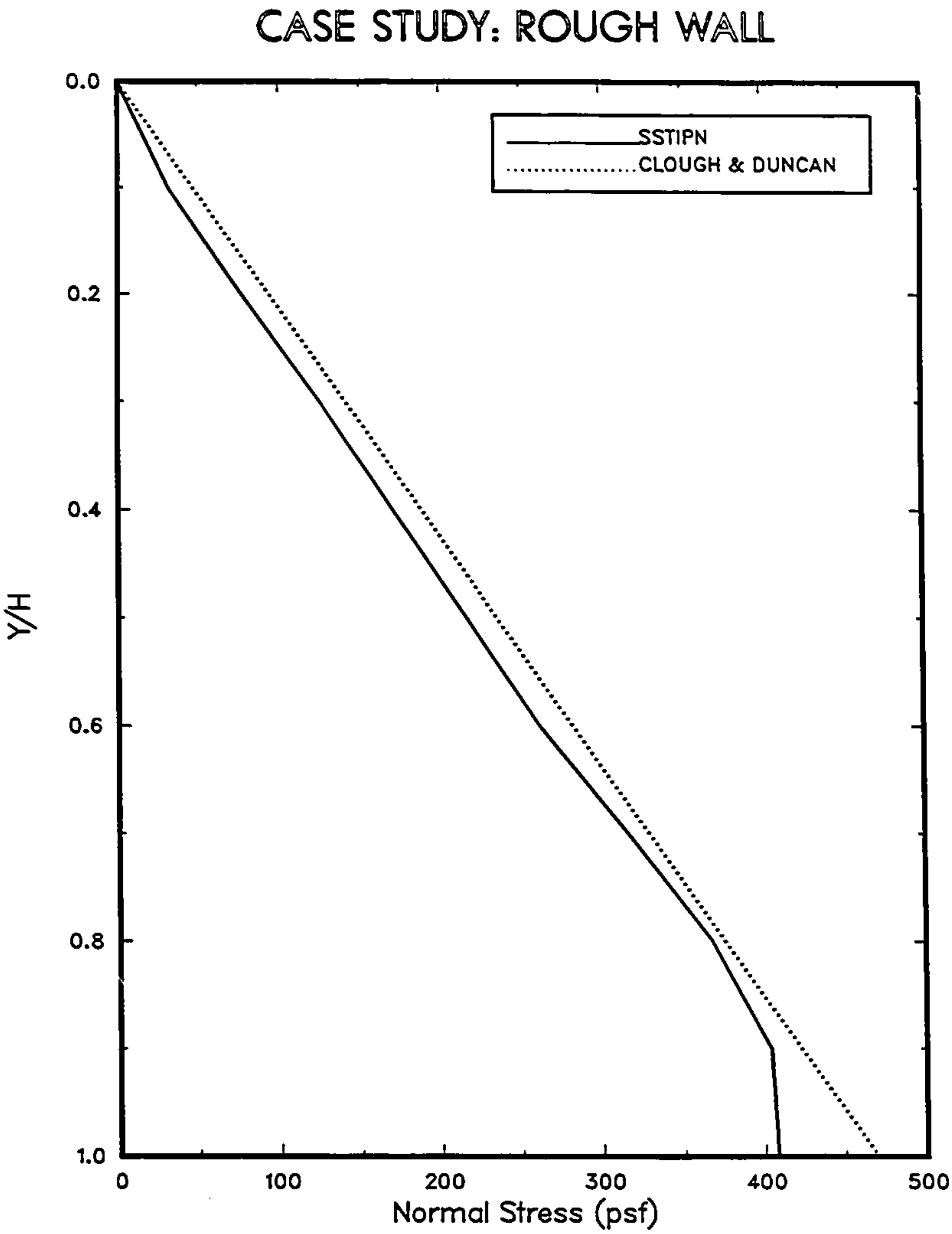

Figure 5.25: Case Study: Rough Wall

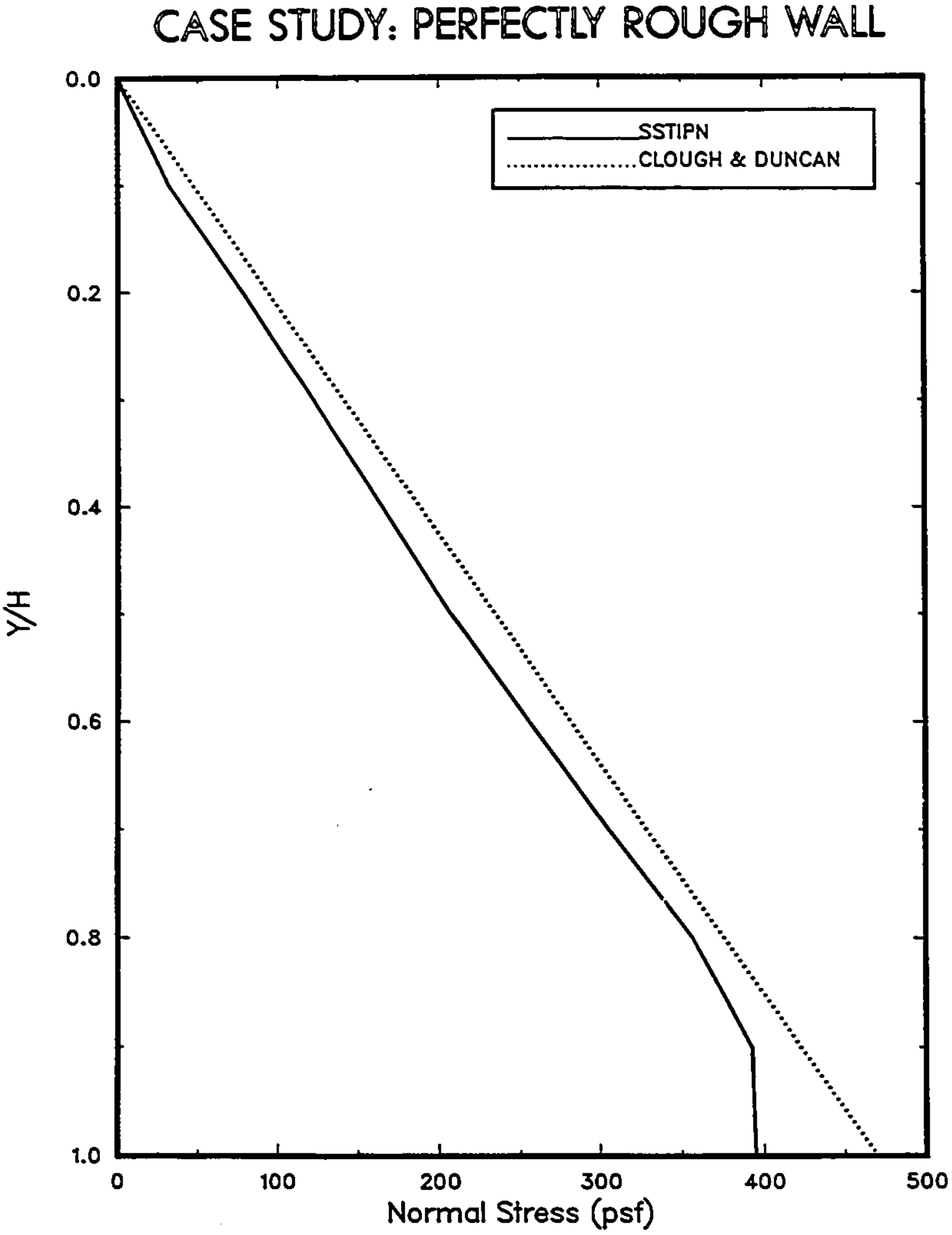

Figure 5.26: Case Study: Perfectly Rough Wall